JAZAN UNIVERSITY

The Saudi Journal of Applied Sciences and Technology

المجلة السعودية للعلوم التطبيقية والتقنية

Volume 1 April 2025


بسم الله الرحمن الرحيم

KINGDOM OF SAUDI ARABA
Ministry of Education
Jazan University

The Saudi Journal of Applied Sciences and Technology

Volume: 1

Issue: 1

Message from

Jazan University President

In the Name of Allah, the Most Gracious, the Most Merciful,

I am proud to present the first volume of the Saudi Journal of Applied Science and Technology. This journal reflects Jazan University's commitment to advancing research, innovation, and scientific excellence. At Jazan University, we recognize that applied and technical sciences are vital for driving national progress and supporting the ambitious goals of Saudi Vision 2030. This journal aims to provide a platform for researchers, academics, and industry experts to share their valuable contributions, fostering a culture of knowledge exchange and scientific development.

I commend the efforts of the editorial board, the contributing authors, and the reviewers who have dedicated their time and expertise to uphold the highest academic and ethical standards. Their commitment embodies our shared vision of making meaningful contributions to the global research community while addressing the challenges and opportunities relevant to the Kingdom of Saudi Arabia and beyond. I encourage all researchers and scholars to engage with this journal by submitting their research, collaborating on innovative projects, or applying the findings to real-world challenges. Together, we can enhance the impact of applied sciences and technology on society, industry, and economic growth.

Professor Mohammed Aburasain

President, Jazan University

Message from

Vice President for Postgraduate and Research Affairs

In the Name of Allah, the Most Gracious, the Most Merciful,

Scientific research is vital for progress and innovation. I proudly introduce the first volume of the Saudi Journal of Applied Science and Technology, which aims to promote research excellence in applied and technical sciences. At Jazan University, we foster an environment encouraging curiosity and collaboration, allowing researchers to share their work and tackle real-world challenges.

The journal's success relies on the dedication of authors, reviewers, and the editorial team, who ensure high-quality publications. I invite scholars from various disciplines to contribute research and collaborate across fields. We can further advance science and technology through ongoing research and knowledge exchange. I look forward to witnessing the contributions this journal will make in supporting research and innovation, and I am confident it will play a key role in shaping the scientific landscape of the future.

Dr. Abdulkarim Muraea

Vice President for Postgraduate and Research Affairs, Jazan University

Editorial Team

Editorial Office Manager

Mr. Bassem Alkaabi

Tel: 0173295000-1915

Email: balkabi@jazanu.edu.sa

Editorial Office Secretary

Mr. Bandar Ali Wasli

SJAST@jazanu.edu.sa

Foreword Editorial

With great enthusiasm, we introduce the first volume of the Saudi Journal of Applied Science and Technology. This journal represents a significant step in Jazan University's commitment to fostering research, innovation, and academic excellence in applied and technical sciences. We aim to provide a distinguished platform for researchers, academicians, and industry professionals to share their knowledge, insights, and discoveries. Scientific and technological advancements are crucial in addressing modern challenges and driving economic and industrial development. This journal aims to contribute to the advancement of knowledge and the practical application of scientific findings by publishing high-quality, peer-reviewed research. The articles in this volume cover diverse topics, reflecting the multidisciplinary nature of applied sciences and their impact on various sectors.

This milestone would not have been possible without many individuals' dedication and hard work. We sincerely thank the contributing authors for their valuable research, the reviewers for their rigorous evaluation and constructive feedback, and the editorial team for their relentless efforts in ensuring the journal meets the highest academic and ethical standards. Their collective contributions have helped shape a publication that we hope will serve as a valuable resource for researchers and practitioners. As we launch this first volume, we invite researchers from across disciplines to engage with the journal by submitting their work, collaborating with fellow scholars, or applying the research findings to real-world challenges. We are confident this journal will catalyze knowledge exchange, innovation, and scientific progress in Jazan, the Kingdom of Saudi Arabia, and the broader global research community.

We look forward to the Saudi Journal of Applied Science and Technology's continued growth and role in advancing applied sciences for society's benefit.

Dr. Zuhair Alaas
Editor-in-Chief
Saudi Journal of Applied Science and Technology
Jazan University

Aim of the journal

The Saudi Journal of Applied Sciences and Technology (SJAST) is a platform that aims to develop science and technology not only in the Kingdom of Saudi Arabia but also outside its borders. It is a peer-reviewed journal available to everyone that supports Saudi Vision 2030, which seeks to make the Kingdom of Saudi Arabia a leader in knowledge and improve the quality of life by promoting scientific and technological development. The journal is a knowledge platform accessible to individuals from academic and research communities to share their innovative ideas across geographical borders. The Saudi Journal of Applied Sciences and Technology seeks to create an effective communication channel between policymakers, government agencies, academic and research institutions, and individuals interested in basic sciences and their applications.

Scope of the Journal

The Saudi Journal of Applied Sciences and Technology is a respected journal looking to publish the latest developments in applied science, technology, and computer research. The journal is a resource for academics, researchers, and professionals seeking to keep up-to-date with the latest developments in engineering, non-health applied sciences, and computer science. The journal is committed to publishing only innovative and valuable research that is theoretically important and practically applicable, and all submissions are subject to peer review to ensure that published articles meet the highest standards of scientific quality and technical relevance. The journal accepts both original and recent review articles. Submitted work must be in English and not previously published or submitted elsewhere to be eligible for publication. In addition, authors must address any ethical questions regarding the content or data collection.

Open access

The Saudi Journal of Applied Sciences & Technology is a peer-reviewed, open-access journal published twice yearly. It allows public access to accepted articles and promotes knowledge exchange. All published manuscripts are available on the journal's website for immediate reading, downloading, and sharing, with no printed copies. We believe our journal will support your professional advancement.

For more information, visit the journal's website at:
https://journals.jazanu.edu.sa/ojs/index.php/SJAST/index

Table of Contents

Contents

Date of publication: April 24, 2025.

Evaluating the Sensitivity of Air Infiltration Rates on Envelope Thermal Insulation Performance

Azzam H. Alosaimi[1]
[1]Civil and Architectural Engineering Department, Engineering and Computer Science College, Jazan University, Jazan, KSA
Corresponding author: Azzam H. Alosaimi (e-mail: aalosaimi@ jazanu.edu.sa).

ABSTRACT High energy demands and greenhouse gas emissions have increased globally, prompting the development of energy-efficiency frameworks, legislation, and housing approvals. Due to extremely hot climatic conditions, Saudi Arabia is a primary energy producer and consumer. According to the Saudi Efficiency Center, cooling energy accounts for about 70% of the residential sector's energy demands. Although the government has issued building codes to improve overall energy efficiency and mandated the building envelope's thermal insulation, insulation performance may vary significantly when infiltration rates are not adequately evaluated. The effect of the air infiltration rate on thermal insulation performance in building envelopes is a critical factor in reducing energy demands and carbon emissions. Therefore, this study evaluates the effect of the air infiltration rate on the performance of various types of thermal building insulation using the EnergyPlus simulation tool. The findings indicate that an increased infiltration rate lowers thermal insulation efficiency and raises the indoor air temperature. Positive linear correlations were detected between an increased infiltration rate and insulation efficiency in the Jazan region, regardless of the season and insulation type. This research emphasizes the need to apply effective air sealing and waterproofing to reduce heat gains and mitigate the effect of the infiltration rate on thermal insulation performance.

INDEX TERMS Airflow Rate, Energy Efficiency, Infiltration Rate, Sensitivity Analysis, Thermal Insulation.

I. INTRODUCTION

Its vast petroleum reserves heavily influence Saudi Arabia's (SA) economy, positioning it as a world-leading oil producer and exporter. This dominance in oil production has played a central role in shaping the nation's energy policy and economic developments. As a significant player in the Organization of the Petroleum Exporting Countries (OPEC), SA holds substantial sway over global oil markets. Moreover, SA's economy and energy infrastructure rely heavily on oil, constituting 65% of the nation's total energy output, with natural gas comprising 35% [1].

The kingdom's heavy reliance on oil as a significant source of energy production and consumption has contributed immensely to massively rising carbon emissions, such as carbon dioxide (CO_2). According to data from the International Energy Agency, SA was the sixth largest emitter of CO_2 from fossil fuel combustion in 2019, at approximately 582.5 million metric tons. These increased emissions released large volumes of CO_2 and greenhouse gases into the atmosphere, significantly contributing to global warming. The upward trend in greenhouse gases has intensified the pressure on natural resources.

The reliance on oil in SA is apparent in many sectors, including buildings, transportation, industry, and electricity generation. The country's substantial oil refining capacity and petrochemical industries reinforce its dependence on oil-based energy (International Statistics and Analysis, 2019). Fig. 1 presents the primary energy production and consumption trends of the Middle Eastern nations, highlighting the position of SA as a leading producer and consumer since 2009.

In SA, buildings account for about 36% of the country's total electricity energy use [1], with the residential housing sector representing about 50% [2]. Population growth, a hot climate, and extensive air conditioning have driven this excessive energy consumption. The 36% energy demand from buildings primarily comprises cooling energy. In the residential sector, cooling energy accounts for nearly 70% of total energy consumption [3].

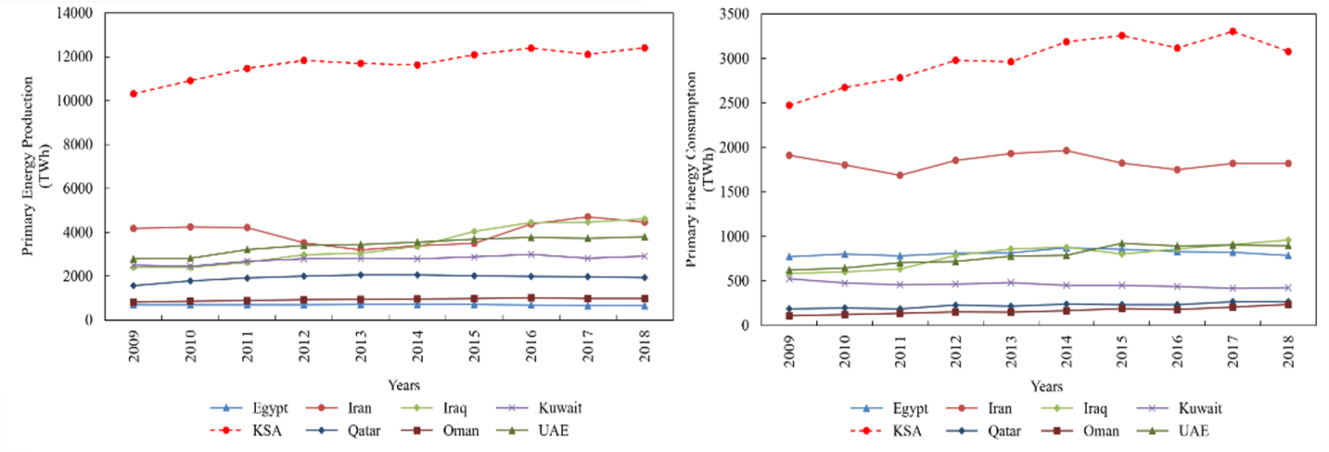

FIGURE 1. **Primary energy production and consumption of Middle Eastern countries (chart from [5]).**

In addition, SA is interested in diversifying its energy portfolio to progress toward energy-efficiency targets. Further, SA is committed to reducing its CO_2 by 2030 to meet the international minimum requirements set by the Paris Agreement in 2014, documented by the National Determined Contributions of the United Nations Framework Convention on Climate Change [4]. Hence, SA has addressed energy efficiency in various sectors to reduce energy demands and transition to a diverse and sustainable economic future.

In 2016, the Saudi Vision 2030 initiative was declared to diversify the nation's dependence on petroleum by promoting alternative energy sources, including renewable energy, such as solar and wind. These efforts align with global trends toward sustainability and environmental responsibility, highlighting the importance of energy-efficiency measures (e.g., effective insulation) in reducing the electricity energy demands of buildings.

A critical strategy for reducing the energy demands of buildings is to enhance the thermal insulation of their envelopes by creating a more effective barrier between indoor and outdoor environments. Improved insulation diminishes heat transfer and reduces energy demands on cooling systems. The improvement in insulation contributes to improved energy efficiency, enhances indoor comfort, and reduces energy costs [5].

Air infiltration significantly contributes to increased heat transfer and energy demand from the unintentional flow of hot air into buildings through cracks, gaps, and other openings in the building envelope [6]. Air infiltration remains an unexplored factor that necessitates further research. Neglecting the infiltration rate is concerning because it is crucial in determining a building's energy efficiency and overall performance. It also influences the performance of thermal insulation and may lower its efficiency.

Thermal insulation efficiency may perform differently for various infiltration rates, and the payback periods could be inaccurate. Despite its importance, the lack of research on air infiltration in SA is notable. Studies have suggested that air infiltration contributes significant heat gains in building energy use, CO_2, and electrical costs [5]. Thus, a research gap exists, particularly concerning Jazan City.

II. LOCATION AND CLIMATE

Jazan City in southwestern SA spans approximately 13500 km² and includes 29 historic districts and approximately 4000 villages. Fig. 2 shows a map of the Jazan region. Jazan's port is the third largest SA by capacity, a central entry point for imports to the southwestern region, and a significant transit hub.

Jazan's climate is strongly influenced by its proximity to the Red Sea, with high humidity levels averaging 68% throughout the year, peaking at 74% in January and dropping to 66% in August. The average high temperature reaches 38.5°C in summer and 30°C in winter, whereas the average low is 29°C in summer and 21°C in winter. Prevailing winds come from the west to the south at an average speed of 12 km/h [7].

FIGURE 2. **Jazan City, Saudi Arabia [7].**

The unique climatic conditions of the Jazan region affect the performance of standard thermal insulation and air-sealing measures that reduce building energy demands. This problem requires region-specific specialized solutions to address these climatic conditions. Despite implementing building codes and rapidly expanding Jazan's infrastructure, energy-efficient retrofitting measures are necessary to reduce building energy demands and lower CO_2 emissions.

III. THERMAL INSULATION

Thermal insulation of the envelope refers to materials and techniques that reduce or prevent heat transfer through the building envelope. Thermal insulation of buildings has become increasingly important in SA due to its hot climate and growing energy demands. Recent research on thermal insulation in building envelopes has focused on optimizing its type, thickness, and placement to maximize energy efficiency. A standard method for calculating insulation thickness in these studies is the degree-day analysis, measuring the energy required to maintain a consistent indoor temperature based on outdoor temperature fluctuations [8].

[9] explored critical factors influencing the energy demand of the residential sector, such as weather conditions, dwelling types, building envelopes, and air conditioning systems. They [9] analyzed monthly electricity consumption for 115 dwellings in Dhahran in the eastern province of SA in 2012. The dwellings included 62 apartments, 28 villas, and 25 traditional houses. The study found that 50% of apartments and over 75% of traditional houses did not have thermal insulation. This finding is significant because SA has used insulation for over 20 years. However, uncertainties remain regarding the influence of infiltration rates on the most effective insulation types.

[10] applied the EnergyPlus simulation tool to evaluate the effect of building envelope designs on the energy efficiency of residential buildings in SA. Their findings indicated energy savings ranging from 22.7% to 39.5% in distinct climatic regions. The study highlighted that the wall's thermal mass was particularly effective in Abha's temperate climate, whereas the least energy savings were observed in Jeddah. Jeddah has extremely hot and humid environmental conditions that may have altered thermal insulation performance due to the higher moisture content in the air. Substantial diurnal temperature fluctuations significantly enhanced the insulation efficiency.

[11] and [12] identified that over 65% of the annual energy consumption in non-insulated villas in hot and arid regions (e.g., Qassim) could be attributed to air conditioning, representing a significant portion of the electricity usage in SA households. Considering that the residential sector consumes 50% of the total energy in the building sector, improving its energy efficiency is imperative. Although previous efforts have primarily concentrated on enhancing the efficiency of electrical appliances, an increasing need exists to evaluate potential improvements in thermal performance and building envelope design.

Other studies have emphasized the importance of climate-specific strategies for improving building energy efficiency. For instance, [13] demonstrated that integrating thermal insulation in the building envelope significantly reduces cooling loads in hot climates. Similarly, [14] found that using reflective materials and proper shading devices promotes substantial energy savings in arid regions. These studies and the research by [10] highlight the critical role of tailored building envelope solutions in optimizing energy performance across diverse climatic conditions.

[15] highlighted the requirement of controlling condensation in building envelopes in SA's hot-humid environment. They observed that condensation concerns could substantially affect the longevity and thermal performance of wall materials because accumulated moisture in building materials reduces insulation effectiveness and increases cooling loads. The study indicated that moisture control measures (e.g., vapor barriers and permeable materials) are critical to preserving energy efficiency and interior thermal comfort in these settings.

Given the limited data on condensation in building envelopes in the Jazan region, studies from comparable locations with similar environmental conditions were reviewed. For instance, [16] explored condensation effects in building envelopes in hot and humid climates. They [16] studied wall assemblies in the humid tropical islands of the South China Sea and observed a significant reduction in thermal insulation efficiency due to increased moisture content. Furthermore, [17] identified a direct correlation between elevated moisture levels and wall materials' decreased thermal resistance (i.e., the R-value). These findings support the importance of moisture control strategies in building design to maintain indoor comfort and energy efficiency in humid regions.

The literature review highlights increasing evidence supporting the need for thermal insulation in buildings across SA to enhance energy efficiency. However, a notable gap in the research concerns the Jazan region, which is particularly important given its unique climatic conditions. These conditions significantly differ from those of other SA regions and may influence the effectiveness of thermal insulation.

Moreover, the latest version of the Saudi Building Code (SBC) mandates the application of thermal insulation to building envelopes to lower thermal conductivity and reduce heat transfer [18]. While this regulation is promising, further investigation is required to understand how varying infiltration rates affect the performance of insulation materials in various climates.

The most common thermal insulation types in the local Saudi market include board, batt, cellular glass (CG), fiberglass (FG), and polyurethane (PO), which are summarized and compared. These insulating materials were selected because they are widely available and commonly used in the Saudi market. Each material had specific benefits consistent with local construction methods and climatic

circumstances, making them suitable for assessing building energy performance in SA [5]. The insulation thicknesses applied in this study (i.e., 25, 50, 75, and 100 mm) were determined based on practical considerations in SA's building sector because typical insulation thicknesses for various building types are generally within this range. The specified thicknesses enabled a variety of energy performance outcomes, including cost-effective and high-performance scenarios [19].

Fig. 3 represents a comparative analysis of thermal insulation types. The board and poly materials had the lowest thermal conductivity (0.03 W/mK) and the highest R-values (43 and 35 m²·K/W, respectively), with superior insulating properties. The board had a 40 kg/m³ density and a heat capacity of 1400 J/kg·K, so it was lightweight yet effective. In contrast, batt had the highest conductivity (0.05 W/m·K) and the lowest R-value (19 m²·K/W), so it was the least effective insulator among the compared materials. The CG and FG materials exhibit moderate conductivity, material resistance (R-value), density, and heat capacity values, so their performance falls between the board and batt materials. Although insulation significantly reduces the infiltration rate and heat transfer between a building's interior and exterior environments and makes buildings more airtight, its thermal performance may be compromised.

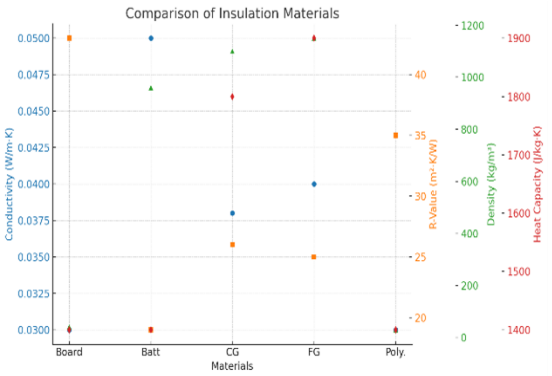

FIGURE 3. **Insulation material details and comparison (Data collected from multiple sources [5], [9], and [10]).**

IV. INFILTRATION RATE

The infiltration rate refers to the air-leakage rate at which outside air (unconditioned) enters a building through unintended openings (e.g., cracks, gaps, and other penetrations) in the building envelope. It measures how much air can be changed in 1 h and is expressed by the air changes per hour (ACH). The building infiltration rate is critical for evaluating indoor conditions to promote energy efficiency, indoor air quality, and thermal comfort [20].

The envelope cracks create an air-leakage area, allowing unconditioned air to flow from outdoor to indoor environments and mix with conditioned air. Therefore, high infiltration rates can lead to increased energy consumption, as cooling systems work harder to maintain the desired indoor temperature. Additionally, infiltration can influence occupant comfort and health by introducing pollutants, allergens, and humidity into the indoor environment [20].

Infiltration arises due to a pressure difference ($\triangle P$) across the envelope caused by geometrical, physical, and environmental variables. Geometrical variables include the building design, area, shape, and volume. Physical variables are the physical properties of the constitution materials, such as thermal conductivity and thickness. Environmental variables include weather variations, such as the dry bulb temperature, wind speed and angle, and sky cover. Infiltration can also result from construction defects, poor sealing, or aging materials, per [5].

Building air leakage is closely correlated with construction methods. According to [20] and [21], the wall construction type is a critical factor in the energy efficiency of retrofitting approaches. The UK commonly uses load-bearing walls with timber framing. When plasterboard is mounted using adhesive dabs, it can create interconnected air-leakage pathways throughout the building, making it difficult to achieve adequate air sealing. A wet-plastered masonry wall can be significantly more airtight than a dry-plastered one [21].

In contrast, timber-framed walls are prevalent in northern Europe and North America. [20] analyzed data from the Building Research Establishment database, a UK-based organization, and indicated that timber-framed buildings are generally more airtight than masonry buildings. However, this difference was less significant when considering the age of the houses because most UK timber-framed homes are relatively new constructions.

In SA, residential buildings typically employ concrete, blocks, clay bricks, and stone construction materials, while Portland cement is the predominant building construction material. Concrete is made by mixing cement, water, coarse aggregate, and sand, providing a robust and durable solution for building structures, foundations, and other construction elements. The prevalence of these materials reflects the need for sturdy and resilient construction in the region's challenging climate and environmental conditions. Generally, concrete has a low infiltration rate due to its dense structure, providing an effective barrier against air leakage [22]. However, concrete buildings can still be infiltrated by air leaks in joints, cracks, and improperly sealed connections with other building components (e.g., doors, windows, and utility penetrations).

Despite the increasing research on energy efficiency in buildings in SA, a significant knowledge gap remains regarding infiltration rates in residential buildings. Infiltration critically affects heat gains, particularly in hot climates. Uncontrolled air leakage can significantly increase cooling loads and lower indoor thermal comfort.

The current literature has identified several common sources of air leakage, including building materials [20], thermal insulation [23], insulated concrete [24], windows and doors [25], air barriers [26], and garages [27]. However, specific studies on quantifying and mitigating infiltration rates in Saudi residential buildings are limited. Therefore,

considering the extreme temperatures and heavy dependence on air conditioning for thermal comfort, understanding and addressing infiltration to optimize energy use is imperative.

Air infiltration substantially influences insulation performance due to air leakage through building envelopes. Air leakage may compromise the thermal conductivity of insulation materials. According to [28], air infiltration raises heating and cooling demands and changes moisture levels, leading to material deterioration and poor building efficiency. For example, airtight construction, such as passive house standard buildings, highlights the necessity of reducing air infiltration to achieve optimal energy efficiency and thermal comfort [29].

Furthermore, climate-specific models reveal that differences in the air infiltration rate considerably influence energy demand. For example, increased air infiltration in lightweight and heavyweight construction emphasizes the importance of effective air-tightness techniques [29].

A few studies have evaluated the air infiltration rate in SA, such as those conducted by [30], [31], and [5]. For instance, [30] analyzed air-leakage patterns and behaviors in single-family homes with central air conditioning. They identified sources and rates of air leakage, assessed their effects on energy performance, and provided insight to improve the efficiency of central air conditioning systems. The findings offered strategies for enhancing air tightness in buildings and energy efficiency in similar residential settings. However, the study contributions could have been more significant if they had considered a larger sample size and included energy simulation to allow for more generalizable results and a better understanding of the implications of air leakage on energy performance across a broader range of homes.

[31] studied air infiltration rates in residences in SA, finding substantial disparities due to differences in architectural designs, climates, and construction processes. In Jeddah, infiltration rates have frequently been estimated to be 1 ACH for simulation purposes, with some studies reporting 0.32 and 0.35 ACH values due to exfiltration from central heating, ventilation, and air conditioning (HVAC) systems. Moreover, [31] revealed diverse values in several types of buildings and conditions and highlighted the prospect of energy savings when achieving SBC's stricter guidelines of 0.2 ACH. These findings indicated the need to consider air infiltration elements in insulation construction and energy modeling to increase overall building efficiency.

[5] developed a model to predict the infiltration rate and associated heat loss for the residential sector in SA using MATLAB software. The model predicts airflow rate values more consistent with the SBC standard of 0.2/h, as opposed to the higher values of 0.8/h commonly reported in the literature. [5] demonstrated that heat loss in Saudi homes could reach up to 37.3 MW·h, with a median value of 1.97 MW·h. However, the study did not explore the relationship between infiltration rates and the performance of envelope thermal insulation. While the study provided valuable insight into energy retrofitting measures and infiltration rate values for the housing sector, it did not explore the effect of the infiltration rate on thermal insulation performance in the Jazan region. Hence, this clear research gap indicates the need for further investigation.

A. *INFILTRATION RATE MEASUREMENTS*

Infiltration rates in buildings can be evaluated via actual measurements or modeling techniques. The most common approach is applying actual measurements using the blower door test, which installs a specialized frame and fan at the main entrance of a building with all internal openings sealed. The fan creates a pressure difference between the indoor and outdoor environments by extracting air from the interior, and the resulting pressure differential (ΔP) is measured to determine the infiltration rate [32].

The University of Nottingham developed a more recent accurate measuring tool, the pulse test, to measure air leakage. Unlike the blower door test, typically installed at the main entrance, the pulse test is a portable device placed in the center of a dwelling. After sealing all openings, the device calculates the airflow rate via a dynamic measuring process to provide additional data on the interior temperature, humidity, and pressure differences [33]. As it operates in a single pulse, the pulse test does not require blocking building doorways to create a continuous airflow (using a fan). Thus, the pulse test method is less intrusive, simpler, and faster. The UK government recently accepted it for measuring air tightness in buildings because it simplifies and accelerates air-tightness testing. However, the pulse test cannot identify specific air-leakage paths due to its general dynamic measurement technique, unlike the blower door test, which can locate areas of significant air leakage.

Both approaches have been widely employed to measure building air leakage, each with advantages and disadvantages. The blower door test has been frequently used for precise, quantitative assessments of air tightness in buildings by pressurizing and depressurizing a structure to measure the airflow to maintain a constant pressure. Nonetheless, variations in temperature, building volume, and pressure boundary conditions can affect the test when they are not adequately considered. In contrast, the pulse test is a more straightforward, quicker alternative that measures pressure decay in a building over time, with quick leakage rate estimations. Although less intrusive and effective for recognizing significant leaks, some variables (e.g., building configurations) may reduce the accuracy of the pulse test. It is also less reliable for tight structures and minor leaks demanding greater precision [33].

B. *INFILTRATION RATE MODELING*

Modeling building infiltration rates is critical for evaluating energy efficiency, indoor air quality, and thermal comfort by assessing air leakage through the building envelope due to gaps, cracks, and other openings. Energy simulation software packages, such as Department of Energy (DOE-2)

and EnergyPlus, include features for modeling infiltration rates. These simulation tools allow users to set values based on blower door test results, building details, and other data sources [34].

These tools can simulate how infiltration affects the thermal insulation performance by considering pressure differentials, environmental conditions, and other factors. Thus, users can model various scenarios and evaluate the effects of infiltration on indoor air temperature (IAT) and indoor contamination. These simulation tools also support informed decisions on optimizing energy efficiency and improving thermal comfort, making infiltration rate modeling an essential component in designing and retrofitting buildings for better performance [5].

The two energy-building simulation types are *active* and *free-run* simulations. Active simulations consider building system operations (e.g., heating and cooling), whereas free-run simulations refer to energy modeling without active building systems, such as heating and cooling units. The free-run simulation approach assesses how a building behaves under natural conditions without artificial climate control, providing insight into the passive design, thermal mass effects, and influence of building envelope characteristics on indoor thermal comfort [35].

Energy simulation software can be instrumental in guiding building design, retrofitting projects, and energy-efficiency measures. With the ability to simulate the influence of infiltration, users can identify critical areas for improvement, such as sealing gaps, enhancing insulation, and implementing controlled ventilation systems. This approach reduces energy consumption and creates a more comfortable and healthier indoor environment.

Evaluating air infiltration rates with actual measurements is the most accurate approach and typically involves specialized equipment, such as blower door tests or pulse tests. However, modeling techniques offer a practical alternative when direct measurement is impossible due to a lack of data or limited access to these tools.

V. METHOD

This study developed a free-run simplified building model to assess the effect of varying infiltration rates on the performance of various thermal insulation types used in building envelopes. This research employed a one-parameter-at-a-time approach to analyze IAT using EnergyPlus simulation software. EnergyPlus was employed for this study due to its robust capabilities for building energy performance analysis. This software offers a comprehensive insight into the envelope heat transfer performance. It supports the dynamic modeling of air infiltration by calculating the heat-transfer time lag and damping effects to reflect real-world conditions, accounting for the outdoor air temperature, wind speed and angle, and ΔP [34].

A. BUILDING MODEL

The energy model was developed to simulate the passive behavior of the actual building space, allowing for a concentrated analysis of how infiltration rates affect the performance of thermal insulation types in the Jazan region. The modeling approach assesses the fundamental influence of air infiltration to provide a clear understanding of the passive performance of thermal insulation types. The study objective was to determine how variations in the infiltration rate influence thermal insulation performance. Therefore, the model eliminated building systems (e.g., cooling, lighting, and equipment) to isolate the effects of the infiltration rate on insulation performance.

The selected building model was a villa with a total floor area of 525 m^2. The walls were constructed with 20-mm plaster on the interior and exterior surfaces, with a 150-mm concrete hollow block. The roof consisted of 10-mm built-up roofing, a 200-mm concrete roof slab, and 13-mm plaster on the inside. The floor comprised ceramic tile with a 100-mm concrete slab on the grade. The windows included single-clear glazing with wood frames, and the window-to-wall ratio was 13%. The air infiltration rate was 0.8 ACH [12]. Table I summarizes the building model details.

TABLE I
BUILDING DETAILS FROM [12]

Building model	Villa details
Floor area	525 m^2
Wall construction	20-mm plaster outside and inside, 150-mm concrete hollow block
Roof construction	10-mm built-up roofing, 200-mm concrete roof slab, 13-mm plaster inside
Floor construction	Ceramic tile, 100-mm concrete slab on grade
Glazing	Single clear (wood frame)
Window-to-wall ratio	13%
Air infiltration	0.8 ACH

The infiltration rate set by [12] was derived from the minimum cooling requirements of the American Society of Heating, Refrigerating, and Air Conditioning Engineers (ASHRAE). However, this value might not be sufficiently precise for predictive modeling. [5] evaluated the sensitivity of infiltration rates on energy modeling outcomes, finding that it substantially influences heat-transfer calculations for uninsulated building envelopes. However, the broader effects of infiltration rates on building envelope configurations with various thermal insulation materials remain unexplored. Consequently, this study investigated the impact of infiltration rates on envelope thermal insulation in a hot and humid region.

All exterior surfaces, including solar radiation and wind, were exposed to weather variations. The weather data for the Jazan region were obtained from EnergyPlus weather data

(i.e., from the .epw files). The data were selected over other types because they represent the actual context.

The study investigated five types of thermal insulation: board, batt, FG, CG, and PO. The insulation thicknesses were systematically increased to 25, 50, 75, and 100 cm, labeled 1, 2, 3, and 4, respectively. For instance, board insulation with a thickness of 50 cm was denoted as Board 2. The insulation was applied to the exterior surface because it performed better than interior surface applications [5]Air infiltration rates were incrementally increased (i.e., 0, 0.25, 0.50, 0.75, and 1 ACH) for each insulation type to examine the effect on the IAT.

The simulation was conducted on two highly different days to observe the differences in thermal insulation performance: January 1, representing the coldest day in winter, and August 1, representing the hottest day in summer. This selection was critical to capture the hourly effects on the IAT by varying the thermal insulation type and thickness. These two days were selected to reflect the extremes of seasonal environmental conditions using data from the typical meteorological year for the researched region. This approach was similar to a recent research [7] approach that sought to decrease computational requirements while concentrating on border circumstances, where building performance is most challenging. The simulation approach to developing the base model required a validation stage of the outer surface temperature and IAT to ensure it behaved similarly to the original model.

VI. VALIDATION

A. OUTSIDE TEMPERATURE VALIDATION

The mean outside surface face temperature (OSFT) is an essential metric for evaluating the insulation performance of a building envelope in an energy model. This measure indicates how much heat the outer surface receives from solar radiation and the ability of the surface to store, resist, and transfer heat. The OSFT was selected for the validation because it directly reflects the heat influence from solar radiation on the external surfaces of the thermal envelope.

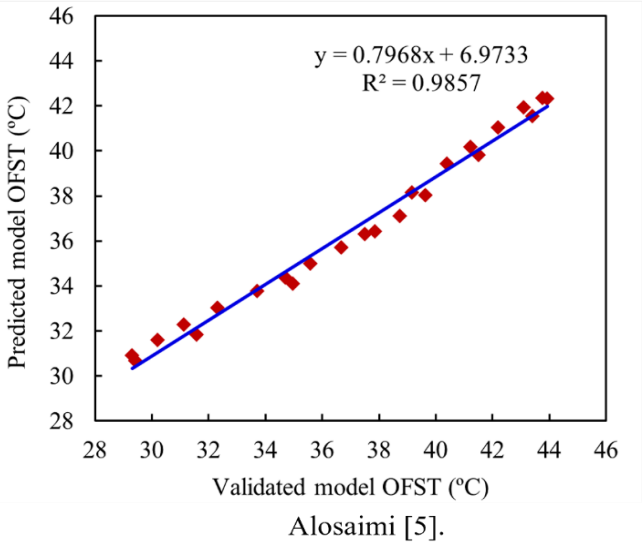

FIGURE 4. **The outside surface face temperature of the proposed model and [5] energy model.**

The model was simulated hourly on July 1 to examine the thermal envelope performance during an extremely hot day. The mean OSFT from the proposed base model was compared with a previously validated model by [10], [12], and, more recently, [5]. Fig. 4 indicates a strong agreement with a performance coefficient (R2) of 0.98, suggesting that the proposed model effectively captures the critical aspects of the building envelope's thermal behavior. This measure indicates the reliability of the heat transfer and insulation performance simulation.

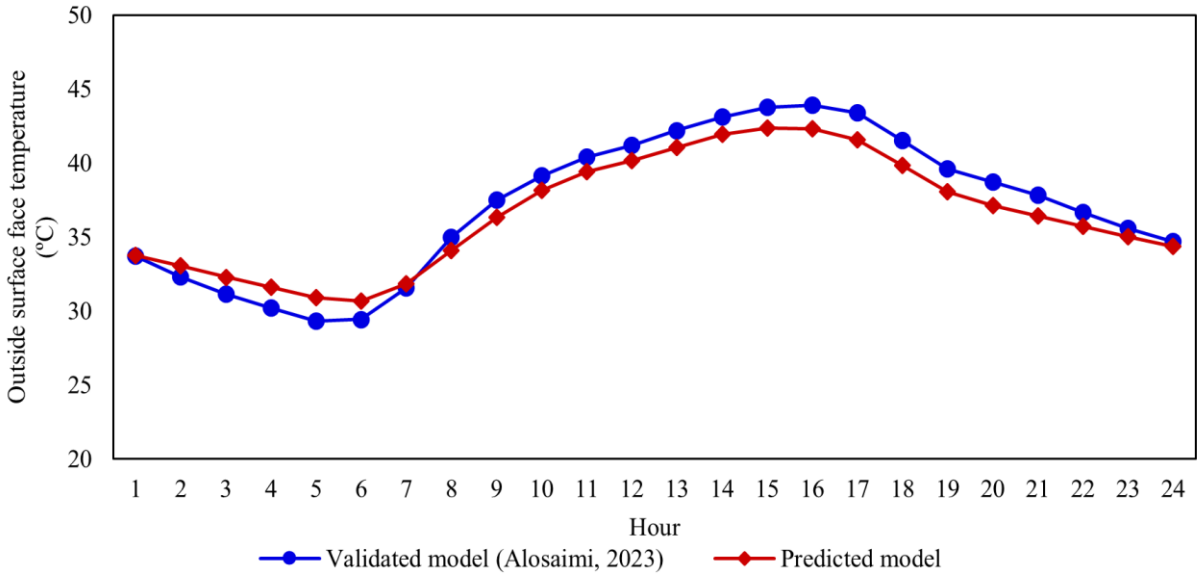

FIGURE 5. **Hourly outer surface face temperature for the proposed and [5] energy models.**

Fig. 5 describes an hourly OSFT comparison of both models, which performed similarly with similar peak hours. The peak OSFT of the proposed model was 42.3°C at 16:00, whereas the [5] model indicated a peak of 43.9°C. The lowest OSFT of the proposed model was 30.6°C at 18:00, compared to 29.3°C at 17:00 in the [5] model. Table II summarizes both models' descriptive statistics.

TABLE II
DESCRIPTIVE STATISTICS OF THE ENERGY MODELS

Building model	[5]	Proposed model
Mean	37.2	36.6
SE	1.0	0.8
Median	37.7	36.4
SD	4.8	3.9
Variance	23.2	15.0
Kurtosis	-1.2	-1.3
Skewness	-0.2	0.1
Range	14.6	11.7
Minimum	29.3	30.7
Maximum	43.9	42.4
Sum	891.9	878.0
Count	24.0	24.0
Confidence level (95.0%)	2.0	1.6

B. *INDOOR AIR TEMPERATURE VALIDATION*

The IAT calibration displayed similar trends between the proposed model in this study and [5] previously validated model. Fig. 6 highlights the correlation between the models with an R^2 value of 0.98. This finding is significant because it indicates that the model predicts values similar to actual

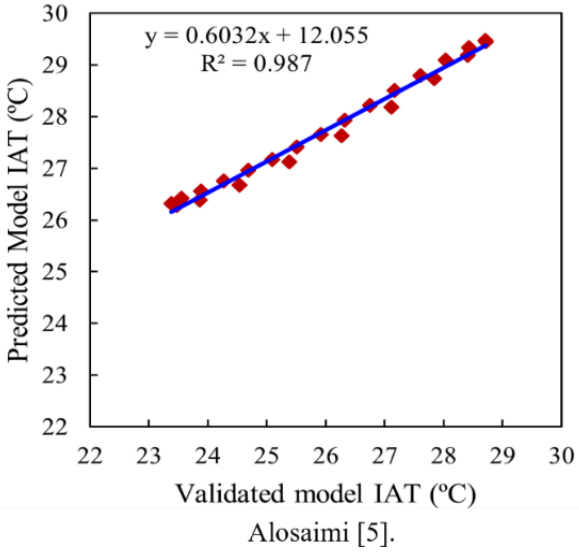

FIGURE 6. **Indoor air temperature of the proposed model and [5] energy model.**

building values. Fig. 7 highlights the hourly IAT of both models, indicating similar trends and behaviors during the hourly simulations. Both models have identical IAT peak hours at 18:00 before sunset, which is explained by the high thermal mass of the building and the time delay of heat transfer from the exterior to interior surfaces. The IAT validation exhibited a similar IAT between the previously validated and proposed models. This finding reveals that the proposed model in this study can produce similar IAT values or outputs as the validated model and allows for evaluating the influence of the infiltration rate on the thermal insulation performance of the envelope.

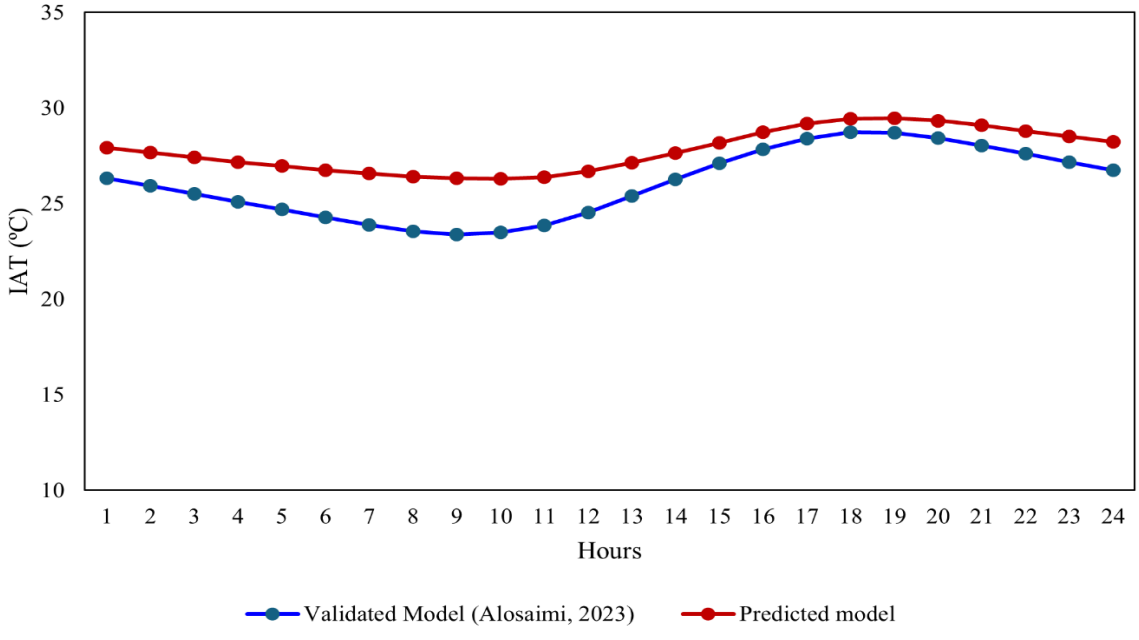

FIGURE 7. **Hourly indoor air temperature (IAT) of the proposed model vs. the validated model by [5].**

VII. RESULTS

This study aims to determine how variations in the infiltration rate influence thermal insulation performance in the hot and humid region of Jazan.

A. THERMAL INSULATION

Applying distinctive types of thermal insulation to the building envelopes exhibited varying effects on the IAT of the proposed base model during winter and summer. The predictions indicated that January 1 had a lower IAT, whereas August 1 required more cooling energy due to higher heat loads. Fig. 8 describes the performance and effects of the insulation type and thickness on the IAT. The dashed orange line presents the mean IAT in winter of the base model (without thermal insulation), whereas the dashed blue line indicates the mean IAT during summer of the base model. Most insulation types increased the heat transfer from the exterior to interior environments, resulting in a higher IAT. This unexpected effect was likely due to the high humidity levels and extreme weather conditions in SA. However, 50-cm thick CG insulation (i.e., CG2) lowered the mean IAT from 23.2°C to 23°C in January and from 23.5°C to 23.2°C in July due to its impermeability to water and water vapor. Hence, certain insulation types effectively mitigate heat transfer despite challenging climatic conditions. In contrast, applying 100-cm polyurethane insulation (i.e., PO4) maintained the IAT of the base model at 23.2°C in January and 23.5°C in July. These results suggest that various insulation materials and thicknesses significantly influence the IAT and building energy demand for cooling.

B. INFILTRATION RATE

Infiltration rate variations and the thickness of five types of thermal insulation significantly influenced the IAT. Fig. 9 indicates that the mean IAT rises across all insulation types as the infiltration rate systematically increases. This trend occurs because a higher infiltration rate allows more hot and humid outdoor air to enter the building, raising the IAT. The effects were most pronounced in environments where temperature differentials between indoor and outdoor spaces were significant, which is often in SA's climate.

[12] assumed an identical air infiltration rate for three residence types (i.e., villas, apartments, and traditional houses) of 0.8 ACH. However, this assumption might have led to inaccurate results, especially considering the various building types and construction materials.

[31] revealed that the infiltration rates of Saudi residences could be 1 ACH for modeling and simulation evaluations. In contrast, other studies have demonstrated that infiltration rates could be 0.32 to 0.35 ACH. However, they did not capture the effects of varied infiltration rates on energy performance in the Jazan region. [5] predicted housing infiltration rates of the total housing stock in Saudi in various regions and revealed that the mean air infiltration rates were 0.02 and 0.24 ACH for apartments and villas, respectively. Moreover, [5] found a mean infiltration rate in Jazan dwellings of 0.05 ACH. This research has applied a range of infiltration rate values to capture the effects on the IAT.

The results indicate that controlling infiltration rates is critical to maintaining optimal IAT and energy efficiency, even with varying thermal insulation thicknesses. The

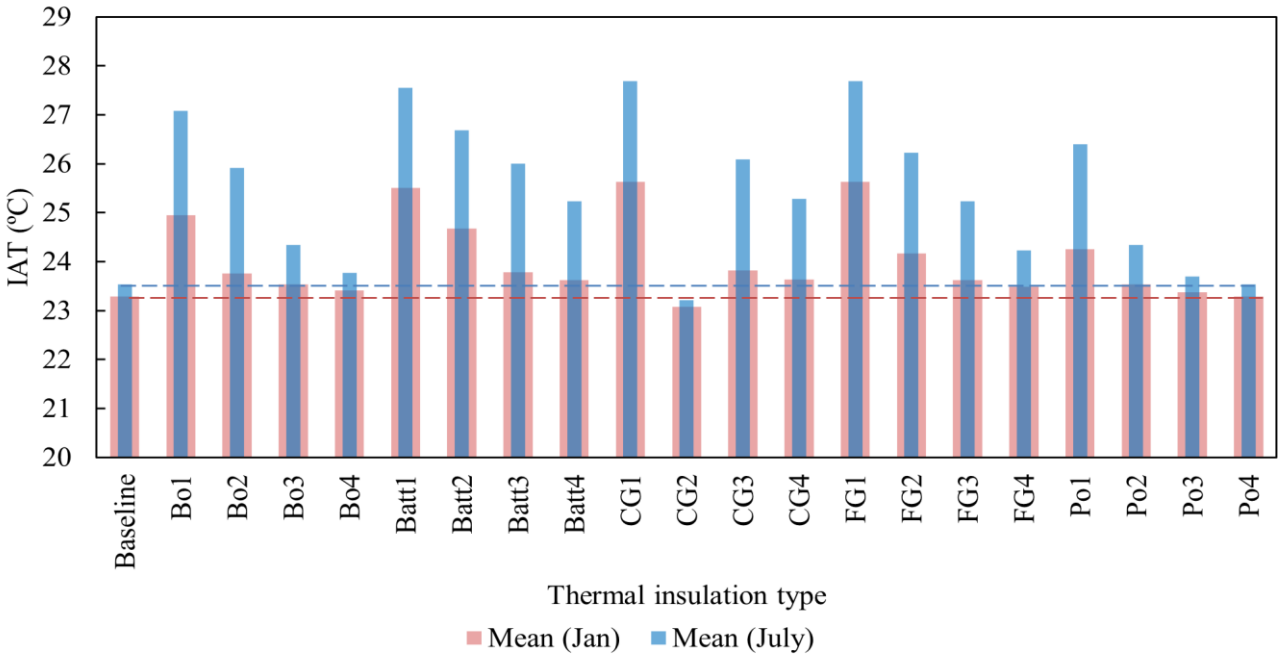

FIGURE 8. **Indoor air temperature of a building with differing thermal insulation types and thicknesses.**

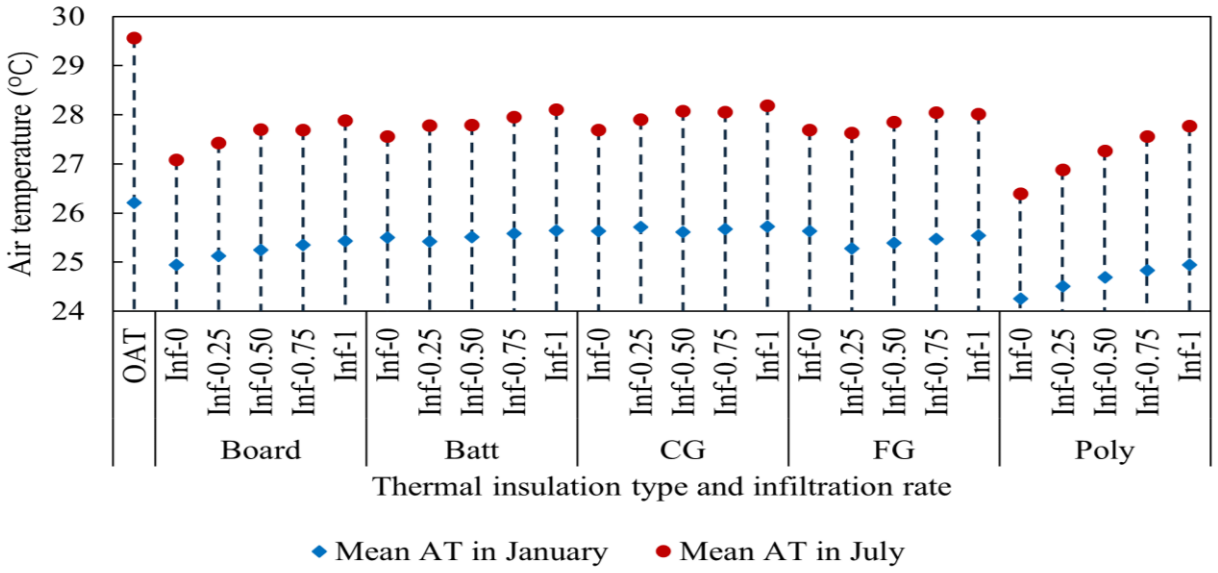

FIGURE 9. **Indoor air temperature of the building with differing thermal insulation types and thicknesses.**

findings highlight the importance of performing a sensitivity analysis to identify the correlation between the air infiltration rate and thermal insulation type and thickness.

C. *SENSITIVITY ANALYSIS*

A sensitivity analysis was conducted to identify the relationship between the infiltration rate, insulation type and thickness, and influence on the IAT. The study revealed that higher infiltration rates lead to a higher IAT, particularly under extreme weather conditions. This finding identified the complex relationship between insulation and infiltration in determining indoor thermal stability. The study highlights that, during extremely hot and humid weather, the effect of a high air infiltration rate is more severe and results in drafts, uncomfortable temperature swings, and increased energy consumption to maintain indoor thermal comfort.

Fig. 10 reveals a positive linear relationship between the mean IAT and the thermal insulation thickness. Hence, the insulation thickness increases as the mean IAT increases. Therefore, thicker insulation may retain more heat. The analysis also demonstrated that a higher air infiltration rate increases the IAT during both seasons. This effect was attributed to the greater air exchange between indoor and outdoor environments, introducing hot and humid air in summer and cooler air in winter. This process alters the thermal stability of the building, the insulation material performance, and the overall energy efficiency. The findings indicate that, as the outdoor air temperature increases, the OSFT of the building rises due to heat absorption.

VIII. DISCUSSION

This study assessed variations in air infiltration in the SA climate, enduring incredibly high temperatures, especially during summer, with notable variations between day and night. Air infiltration significantly strains cooling systems and leads to increased energy demands. This challenge is exacerbated by the critical need for effective insulation to maintain energy efficiency. Thermal insulation can lose effectiveness if air infiltration rates are high, as the ability of the insulation to stabilize indoor temperatures is compromised.

The Jazan region has a distinct climate characterized by high temperatures and humidity in summer and lower, colder temperatures in winter, with substantial seasonal change and humidity levels compared with other regions in SA. These environmental variables are significant when assessing how air infiltration and insulation effectiveness vary by region. For example, although northern regions may experience severe variations in temperature, the greater degree of humidity on the coast of Jazan can lead to unique insulation performance outcomes, particularly with moisture accumulation and material degradation. Nonetheless, regions with more arid climates, such as Riyadh, may display different infiltration characteristics.

Additionally, condensation considerably influences thermal performance, particularly in humid locations like Jazan. Condensation can raise moisture levels in building materials, reducing the insulating efficacy and accelerating material deterioration. Thus, condensation is significant in building design and insulation material selection for high-humidity locations, so condensation management is critical for preserving building envelope durability and energy efficiency over time [15] and [16].

The effect of air infiltration on thermal insulation is a significant concern because it affects energy efficiency, indoor comfort, and sustainability. Uncontrolled hot air entering buildings can undermine the effectiveness of insulation while raising energy demands and increasing the cooling system workload. Thus, studies on the air tightness of buildings and infiltration rates should be conducted with greater depth and larger building samples in diverse climate conditions in SA.

Field studies and actual measurements of infiltration rates are necessary to obtain a comprehensive understanding of the problem. Collecting data from a large sample of buildings could provide a reliable basis for future studies and assist in informed decision-making processes. This data-driven approach could help create influential measures for reducing air infiltration to enhance thermal insulation performance and improve energy efficiency.

This study found that the most suitable thermal insulation for buildings in the Jazan region is CG1. However, [5] suggested that PO4 is the optimal insulation. This discrepancy is attributed to the varying locations with higher humidity and moisture levels. A high infiltration rate allows hot air and moisture to bypass insulation layers, leading to condensation problems. Condensation is a significant problem that considerably influences the building structure, indoor air quality, thermal comfort, and energy performance. Increased condensation reduces insulation performance and introduces health concerns. Therefore, studies on condensation in buildings in the Jazan region are necessary to provide insight into how buildings can be insulated. Studies should focus on thermal bridges and areas where condensation occurs most.

The sensitivity of infiltration rates reveals the critical importance of implementing air-sealing and weather-proofing measures in building envelopes. Architects and engineers are vital in prioritizing strategies to minimize infiltration, reduce the burden on cooling systems, and enhance overall energy efficiency. Critical measures include applying air barriers, sealing gaps and cracks, and specifying insulation materials with low air permeability.

This study highlights the need for more comprehensive investigations to assess infiltration rates in building types across SA's climatic regions. These investigations should aim to identify the primary sources of air leakage, evaluate the effectiveness of existing mitigation measures, and develop guidelines for improving building airtightness.

These research findings can inform future construction regulations in SA, where energy efficiency is becoming increasingly crucial. Regulations should be applied to building commissioning to obtain a maximum infiltration rate value and ensure efficient energy use. Robust and varied values for infiltration rates should be considered according to the building type and location. The climate significantly influences the infiltration rate, so it should be considered in the building code rather than assuming the value of 0.2 ACH for all housing types and locations in SA.

IX. LIMITATIONS

Research on infiltration rates in SA faces several limitations hindering a comprehensive understanding of this problem across its diverse climates. The scope of existing studies is limited, with small sample sizes reducing their generalizability. Most research has focused on residential buildings, neglecting commercial and industrial sectors. Moreover, short-term studies have failed to capture seasonal variations in infiltration rates. Differences in construction materials, techniques, and standards across regions have further complicated the generalizability of findings. Technological and methodological constraints (e.g., inconsistent measurement techniques and limited advanced modeling tools) have also impeded accurate assessments.

Additionally, no studies have explored the interaction between infiltration rates and thermal insulation performance, which is crucial to understanding building energy efficiency. This omission highlights the importance of the current research in filling this significant gap. Addressing these limitations through more comprehensive, diverse, and technologically advanced research is essential to developing effective strategies to optimize energy efficiency in buildings across SA. Although this research adopted a one-parameter-at-a-time approach to investigate the concentrated effect of selected parameters on the IAT, a multivariate sensitivity analysis should be considered to understand how other parameters influence the IAT.

The simplified model, which eliminated active HVAC systems, lighting, and equipment, was limited because these variables significantly affect real-world energy use. Thus, the lack of these systems could limit the application of these findings to actual building settings. Future studies should include precise models of HVAC systems and other energy-consuming components to offer a more comprehensive understanding of the energy performance of a building. A dynamic model accounting for these systems would increase the accuracy and usefulness of the findings. Furthermore, it would be helpful to investigate the relationship between air infiltration, insulation, and HVAC system performance in real-world scenarios.

Furthermore, the dependence on predictions for two days (i.e., winter and summer extremes) restricted the generalizability of the findings throughout the year. During spring and fall, transitional months may have different infiltration and insulation interactions due to changing temperatures and wind conditions. Expanding the analysis to include simulations from more typical months or using an annual hourly weather dataset to enhance the findings would be promising. This upgrade could provide a more thorough understanding of the building's year-round performance and improve the generalizability of the findings, as advocated in [36].

A more thorough seasonal study incorporating actual weather data from different months or a yearly cycle would offer more detailed information on how air infiltration and insulation perform over the year. Experimental validation with actual data from buildings would assist in corroborating the simulation output to bridge the gap between theoretical modeling and practical application. Future research could include field investigations that monitor actual infiltration rates and energy performance in buildings and allow simulation models to be calibrated for improved comprehension of the influence of insulation materials and thicknesses in real-world scenarios.

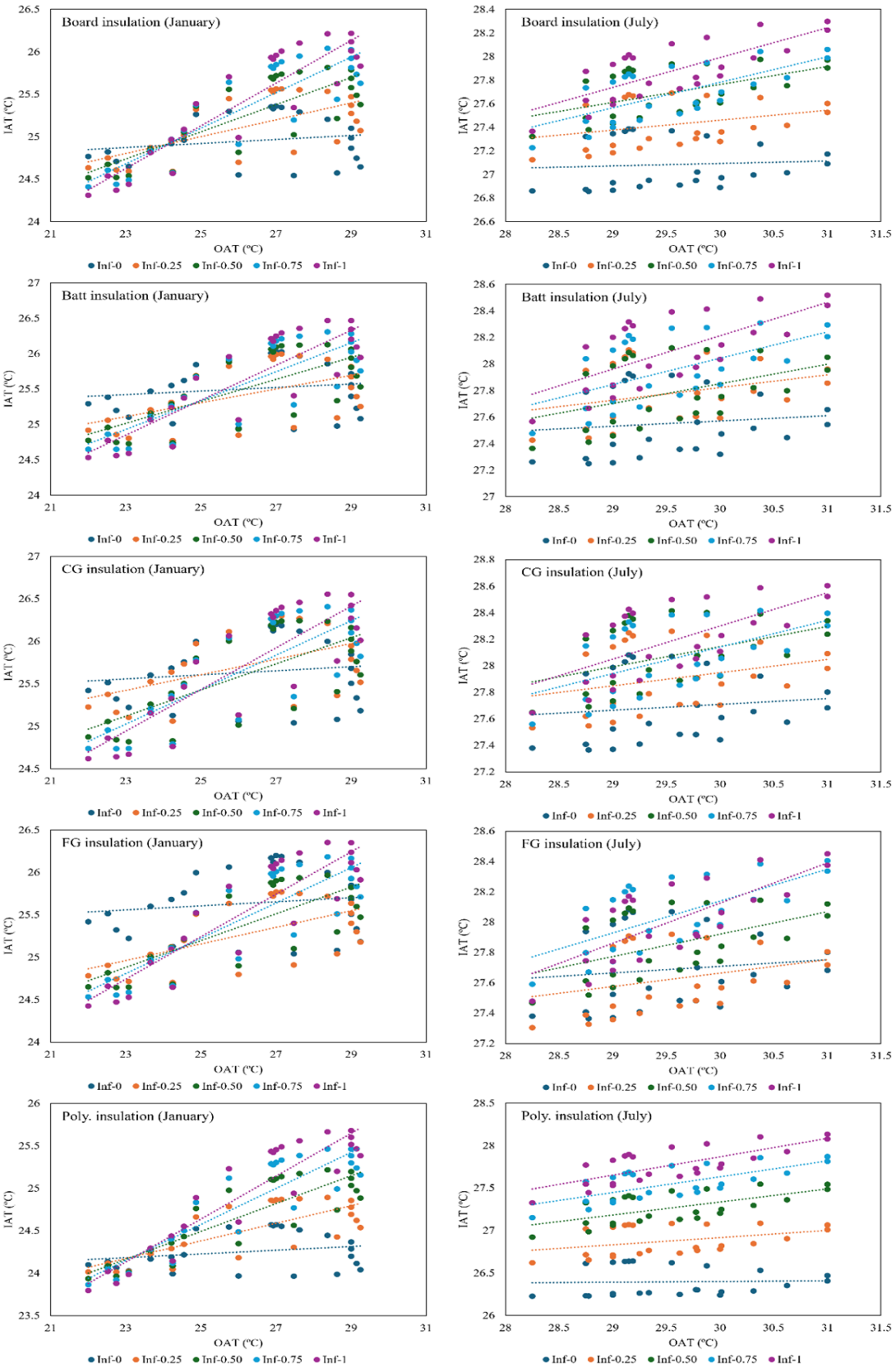

FIGURE 10. **Sensitivity analysis of the infiltration rate and insulation type and thickness on indoor air temperature.**

X. CONCLUSION

Air infiltration rates significantly affect the thermal insulation performance in building envelopes, influencing energy efficiency and indoor air quality. This study analyzed various insulation types—board, batt, FG, CG, and PO—using the EnergyPlus simulation tool. The study applied a one-parameter-at-a-time approach to explore the sensitivity to changing air infiltration rates on thermal insulation performance.

This study examined how various insulation types responded to air leakage by systematically varying infiltration rates, particularly in the hot and humid climate of Jazan. The results indicate that higher air infiltration rates reduce thermal insulation performance and increase energy demand for cooling. These findings highlight the importance of effective air sealing and airtight construction to maximize insulation material efficiency. Proper insulation and reduced air infiltration can enhance energy efficiency and indoor comfort. Air infiltration rates significantly influence thermal insulation performance in building envelopes, affecting energy efficiency, indoor comfort, and indoor air quality. The findings revealed that the Jazan region should apply more region-specific requirements for air tightness to reduce infiltration rates, lower energy demand, and mitigate envelope condensation.

Moreover, this research has important implications for national policy and economic development goals. As a significant member of OPEC and the International Energy Agency, SA is committed to adopting more energy-efficient practices. Enhancing building performance aligns with the country's efforts to reduce energy consumption while maintaining economic competitiveness. With SA's Vision 2030, prioritizing a reduced carbon footprint of the built environment, the study findings can inform policy frameworks that encourage adopting sustainable building technology and airtight construction practices.

The economic benefits of improving insulation performance and reducing energy demand for cooling are substantial to meet SA developmental visions, especially in a region with significant energy costs. Moreover, SA can make meaningful energy conservation and sustainability progress by addressing building air infiltration and insulation to ensure long-term economic gains while fulfilling its global commitments in the energy and environmental sectors.

REFERENCES

[1] M. S. Al-Homoud and M. Krarti, "Energy efficiency of residential buildings in the kingdom of Saudi Arabia: Review of status and future roadmap," J. Build. Eng, vol. 36, p. 102143, 2021.
[2] M. Aldubyan, M. Krarti, and E. Williams, "Residential energy model for evaluating energy demand and energy efficiency programs in Saudi residential buildings," Energy, vol. 195, p. 116980, Mar. 2020.
[3] A., Felimban, A. Prieto, U, Knaack, T. Klein, and Y. Qaffas, "Assessment of current energy consumption in residential buildings in Jeddah, Saudi Arabia," Buildings, vol. 9, no. 7, p. 163, 2019.
[4] D. Scott, C. M. Hall, and S. Gössling, "A report on the Paris Climate Change Agreement and its implications for tourism: Why we will always have Paris," J. Sustain. Tour, vol. 24, no. 7, pp. 933–948, 2016.
[5] A. Alosaimi, "Optimising the energy performance of the residential stock of the Kingdom of Saudi Arabia by retrofit measures." University of Nottingham, 2023.
[6] M. H. Sherman, Air Infiltration in Buildings, Ph.D. thesis, University of California, Berkeley, Jan. 1980.
[7] H. T. Abd El-Hamid et al., "Detection of environmental degradation in Jazan region on the Red Sea, KSA, using mathematical treatments of remote sensing data," J. Remote. Sens., vol. 2, no. 4, pp. 183–196, 2019.
[8] A. Ucar and F. Balo, "Effect of fuel type on the optimum thickness of selected insulation materials for the four different climatic regions of Turkey," Appl. Energy, vol. 86, no. 5, pp. 730–736, 2009.
[9] F. Alrashed and M. Asif, "Trends in residential energy consumption in Saudi Arabia with particular reference to the Eastern Province," J. Sustain. Dev. Energy Water Environ. Sys., vol. 2, no. 4, pp. 376–387, 2014.
[10] A. Alaidroos and M. Krarti, "Optimal design of residential building envelope systems in the Kingdom of Saudi Arabia," Energy Build., vol. 86, pp. 104–117, 2015.
[11] M. Krarti, K. Dubey, and N. Howarth, "Evaluation of building energy efficiency investment options for the Kingdom of Saudi Arabia," Energy, vol. 134, pp. 595–610, 2017.
[12] M. Krarti, M. Aldubyan, and E. Williams, "Residential building stock model for evaluating energy retrofit programs in Saudi Arabia," Energy, vol. 195, p. 11698, 2020.
[13] S. Shaahid et al., "Techno-economic potential of retrofitting diesel power systems with hybrid wind-photovoltaic-diesel systems for off-grid electrification of remote villages of Saudi Arabia," Int. J. Green Energy, vol. 7, no. 6, pp. 632–646, 2010.
[14] H. Radhi, "Evaluating the potential impact of global warming on the UAE residential buildings–A contribution to reduce CO2 emissions. Build. Environ., vol. 44, no. 12, pp. 2451–2462, 2009.
[15] S. Ben Lasoad, A. Al-Sakkaf, and S. Baharetha, "Investigation of building envelope design for hot-humid climatic conditions in Saudi Arabia," J. Scien. Eng. Res., vol. 8, no. 4, pp. 13–29, 2021.
[16] M. Roser et al., "World population growth: Our world in data," 2013.
[17] A. Gusyachkin et al., "Effects of moisture content on thermal conductivity of thermal insulation materials," IOP Conf. Ser: Mater. Sci. Eng., IOP Publishing, 2019.
[18] PIS Arabia, "The Saudi Building Code," 2018.
[19] Y. Alsaqabi et al., "Techno-environmental assessment of insulation materials in Saudi Arabia: Integrating thermal performance and LCA. Build., vol. 13, no. 2, pp. 331, 2023.
[20] M. H. Sherman and D. J. Dickerhoff, Air-tightness of US dwellings, 1998.
[21] R. Lowe et al., "Air-tightness in masonry dwellings: Laboratory and field experience," Build Serv Eng Res Technol, vol. 15, no. 3, pp. 149–155, 1994.
[22] R. Lederle, T. Shepard, and V.D.L.V. Meza, "Comparison of methods for measuring infiltration rate of pervious concrete," Constr Build Mater, vol. 244, p. 118339, 2020.
[23] B. A. Wilcox and T.A. Weston, "Measured infiltration reduction in California production houses using housewrap," Thermal Performance of the Exterior Envelopes of Buildings VIII, 2001.
[24] H. H. R. Durschlag, Air leakage of insulated concrete from houses. Massachusetts Institute of Technology. 2012.
[25] A. Elmahdy, "Quantification of air leakage effects on the condensation resistance of windows." ASHRAE Trans, vol. 109, no. 1, pp. 600–606, 2003.
[26] M. H. Sherman, Infiltration as ventilation: Weather-induced dilution. U.S. Department of Energy, Dec. 2012.
[27] D. Fugler, Air infiltration from attached garages in Canadian houses. Canada Mortgage and Housing Corporation, 2001.
[28] Y. Du et al., "A case study of air infiltration for highly airtight buildings under the typical meteorological conditions of China," Build., vol. 14, no. 6, p. 1585, 2024.
[29] Nationwide House Energy Rating Scheme (NatHERS), "Software Accreditation Protocol," Canberra, Australia: Department of Environment and Energy, 2012.
[30] M. A. Makawi, I. M. Budaiwi, and A. A. Abdou, "Characterization of envelope air leakage behavior for centrally air-conditioned single-family detached houses," Build., vol. 13, no. 3, p. 660, 2023.

[31] A. Felimban, U. Knaack, and T. Konstantinou, "Evaluating savings potentials using energy retrofitting measures for a residential building in Jeddah, KSA," Build., vol. 13, no. 7, p. 1645, 2023.
[32] B. Jones et al., "Assessing uncertainty in housing stock infiltration rates and associated heat loss: English and UK case studies," Build. Environ., vol. 92, pp. 644–656, 2015.
[33] E. Cooper et al., "Field trialling of a pulse air-tightness tester in a range of UK homes," Int. J. Vent., vol. 18, no. 1, pp. 1–18, 2019.
[34] D. B. Crawley et al., "EnergyPlus: Creating a new-generation building energy simulation program," Energy Build., vol. 33, no. 4, pp. 319–331, 2001.
[35] A. Foucquier et al., "State of the art in building modelling and energy performances prediction: A review," Renew. Sustain. Energy Rev., vol. 23, pp. 272–288, 2013.
[36] S. B. Sadineni, S. Madala, and R. F. Boehm, "Passive building energy savings: A review of building envelope components," Renew. Sustain. Energy Rev., vol. 15, no. 8, pp. 3617–3631, 2011.

Date of publication: April 24, 2025.

Solution of Various Economic Load Dispatch Problems Using Wild Horse Optimizer

Sahar M. Abd Elazim[1], Ehab S. Ali[2], Emad S. Hassan[2]
[1]Computer Science Department, Engineering and Computer Science College, Jazan University, Jizan, KSA
[2]Electrical and Electronics Department, Engineering and Computer Science College, Jazan University, Jizan, KSA

Corresponding author: Sahar M. Abd Elazim (e-mail: sdeep@jazanu.edu.sa).

ABSTRACT This article presents a new optimization approach called the Wild Horse Optimizer (WHO). It is designed to be user-friendly, effective, and to converge rapidly when addressing economic dispatch (ED). Given that ED is a nonlinear and complex optimization problem, the primary goal of the WHO is to minimize overall generation costs while adhering to the system's equality and inequality constraints. The Combined Economic Emission Dispatch (CEED) problem is also considered, which considers the environmental impacts stemming from the emissions of gaseous pollutants produced by fossil-fueled power plants. To demonstrate the capabilities of the WHO, various networks with 3, 6, 10, 13, 15, and 40 stations have been tested and applied to resolve multiple ED scenarios, including factors such as valve point effects, losses, and prohibited operating zones. The simulation results indicate that the WHO's approach is significantly more effective than the methods found in current academic literature. This analysis highlights the strengths of the WHO's strategies compared to alternatives, suggesting they may offer better solutions to the challenges identified in previous studies.

INDEX TERMS Combined Economic Emission Dispatch, Economic Dispatch, Valve Effect, Wild Horse Optimizer.

I. INTRODUCTION

The task of running thermal units to meet a constant load request while adhering to significant physical and operational constraints is recognized as the economic dispatch (ED) issue in the electric grid [1-2]. ED is a single-goal optimization operation that minimizes power dispatch costs without exceeding limits. When an emission goal is added, ED becomes a multi-goal job, seeking to minimize jointly emissions and costs while meeting power requests and staying within constraints. This multi-objective task is called the Combined Economic Emission Dispatch (CEED) mission [3].

ED is a nonlinear, complicated, computationally bushy electric grid operations problem. Its mathematical difficulty yields that it is well-suited for optimization techniques. Various newfangled populations have addressed this challenge via metaheuristic and nature-inspired techniques. Notable optimization techniques that have been applied including: Genetic [4], Simulated Annealing (SA)[5-6], Differential Evolution (DE)[7-8], Moth Swarm (MS)[9], Spider Monkey (SM)[10], Grey Wolf Optimization (GW)[11], Fire Fly (FF)[12-13], Harmony Search (HS)[14-15], Spiral Optimization (SO)[16], Artificial Bee Colony (ABC)[17-18], Bacterial Foraging (BF)[19], Particle swarm Optimizer (PSO)[20-21], β-hill climbing optimization[22], Mine Blast (MB)[23], Flower Pollination (FP)[24], Chaotic Turbulent Flow of Water Optimization (CTFWO)[25], and Coyote Optimization (CO)[26]. The review findings demonstrate that while each technique can produce satisfactory results for specific functions, it may fail to achieve optimal solutions for others. Therefore, various techniques from different domains are required to obtain acceptable solutions for different test functions. Despite the introduction of many meta-heuristic algorithms in recent years, a continuous search remains for a more straightforward and versatile algorithm capable of solving most optimization problems.

In this work, WHO is offered to address diverse ED missions and progressed in previous studies; WHO has been utilized in numerous optimization challenges for parameter identification, demonstrating impressive results compared to existing literature [27-34]. Its success in solving diverse problems and the potential for further enhancement inspired this research [35-36].

This work is structured as follows: Section 2 summarizes the ED and CEED issues, Section 3 summarizes the mathematical formula for WHO, Section 4 offers the

simulation outcomes accompanied by statistical dissection, and Section 5 concludes the article.

II. TASK FORMATION

The CEED mission aims to diminish pair objective functions, emissions, and fuel charges while meeting specific equality and inequality constraints. The method is typically structured as follows.

A. COST FUNCTION OF ED

The fuel cost for unit output power varies noticeably with the generator's output in thermal units. Fuel costs are accounted for as a quadratic formula of product power [37], as illustrated in (1).

$$F(P) = \gamma P^2 + \beta P + \alpha \quad (1)$$

Minimize

$$F_T = \sum_{n=1}^{m} F_n(P_n) = \sum_{n=1}^{m} (\gamma_n P_n^2 + \beta_n P_n + \alpha_n) \quad (2)$$

The reduction adheres to the equate restriction that the losses plus the load must match the net generation:

$$\sum_{n=1}^{m} P_n = P_D + P_l \quad (3)$$

Net transmission losses modeled employing the formula of Kron's loss are represented by (4).

$$P_l = \sum_{n=1}^{m} \sum_{j=1}^{m} \left(P_n B_{nj} P_j\right) + \sum_{i=1}^{m} B_{0n} P_n + B_{00} \quad (4)$$

These parameters are assumed to remain constant. The units' lower and upper power boundaries constrain the inequality constraint.

$$P_n^{min} \le P_n \le P_n^{max} \quad n = 1, , \ldots\ldots, m \quad (5)$$

B. IMPACT OF VALVE POINT

The valve impact is incorporated into the units' cost formula. A significant growth in losses because of wire drawing impact as every steam admission valve begins to unlock results in a nonlinear wavy curve [38]. As illustrated in Fig. 1, the charging formula based on this curve provides a more precise layout. Hence, the fuel charge formula for each fossil fuel unit is a group of sinusoidal and quadratic functions [39].

$$F_T = \sum_{n=1}^{m} F_n(P_n) = \sum_{n=1}^{m} (\gamma_n P_n^2 + \beta_n P_n + \alpha_n + e_n * sin(f_n * (P_n^{min} - P_n))) \quad (6)$$

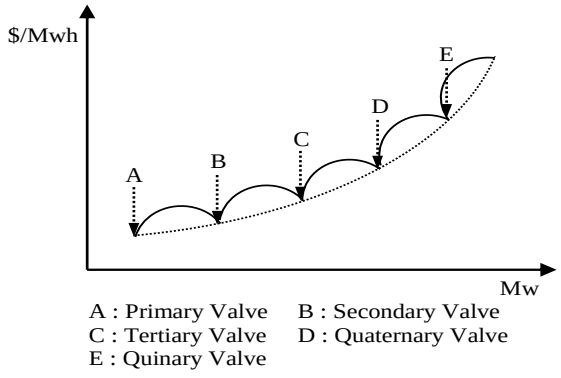

FIGURE 1. Valve point impact.

C. CEED OBJECTIVE FUNCTION

Air contaminants such as nitrogen, sulfur oxides, and carbon dioxide from fossil fuels could be represented individually [40-42]. However, for comparison, the overall emissions of these contaminants could be defined as follows [40]:

$$E_T = \sum_{n=1}^{m} E_n(P_n) = \sum_{n=1}^{m} (a_n P_n^2 + b_n P_n + c_n + \eta_n * exp(\delta_n * P_n)) \quad \text{Kg} \quad (7)$$

Unit charge optimization is based on a copycat ED with emission and line stream constraints [43].

$$\text{Min} \quad F = \sum_{n=1}^{m} \{F_n(P_n), E_n(P_n)\} \quad (8)$$

The minimum cost formula must exist according to the inequality and equality restrictions illustrated in (3) and (5). The double objective CEED task is transformed into a single one using a price penalty element g [44].

$$\text{Min} \quad F = F_T + g \times E_t \quad (9)$$

According to the restrictions of (3) and (5). The cost penalty agent g the rate of the upper fuel charge to the upper emission of the relevant generators in $/Kg [37, 43], mixes fuel with emission costs, resulting in a net operating cost of $.

$$g_n = \frac{F_T(P_n^{max})}{E_T(P_n^{max})} \quad , \quad \text{n=1,……..,m} \quad (10)$$

III. WILD HORSE OPTIMIZATION

A. DEPICTION

Horses are divided in terms of their social organization into two terrestrial and non-terrestrial groups, and they differ in terms of mating behavior, grouping, bonding, and grazing, and a hierarchy in command and control [27-28]. In this paper, we will deal with non-terrestrial horses, which consist of a barn family bunch or a bunch that includes a stallion, a harem, and one or sundry mares and breeds or single sets. Stallions are laid near the mares so that mating may take place. In the first week of Foal's life, it begins to graze and continues repeatedly as it ages. Foals depart their parents before adulthood, while males join individual groups to complete their maturation in preparation for mating. Females join other family groups [29] to suppress the mate between the father and his daughters or sisters [30]. The hierarchy in dominance and leadership is linear due to the tendency of elements within the group to react with their counterparts having the same age and degree [31]. Research [32] shows how wild horses' dominance in a flock through the dry season occurs, where the superior-ordering elements get to the watering pit as they want, and the rest look for several hours to get to the pit. Leadership comes by supremacy. The boss is the one who determines the motion tendency and velocity for the rest of the group [33]. Usually, the boss is the most dominant mare, while the remaining ones follow it with a diminishing ranking [34]. In this paper, we use collective behaviors, such as herding, dominance, driving, and mating, to design an algorithm for wild horses to solve several ED issues optimally.

B. *STEPS OF WHO*

It is composed of the following:

1. Generate a tentative population, making more sets and electing the boss.
2. Herding and horse's mate
3. Group leading by stallion;
4. Swap and election of leaders;

1) *Generating a tentative population*

The WHO algorithm, like each optimization process, begins with the primary and random population as follows:

$$(\vec{x}) = \{\vec{x}_1, \vec{x}_2, \ldots\ldots\ldots\ldots, \vec{x}_n\} \quad (11)$$

This randomized population is assessed repeatedly according to the goal function, where the goal amount is determined as follows:

$$(\vec{O}) = \{\vec{O}_1, \vec{O}_2, \ldots\ldots\ldots\ldots, \vec{O}_n\} \quad (12)$$

Since a solution cannot be guaranteed in one pull, we need improvement steps (repetition). A package of regulations represents the base of the optimization process and searches the population for the optimum.

First, the primary group is divided into various ones. If N is the horse's number in a population, then the group's number is calculated as $G = [N \times PS]$, where PS is stallions ratio of all population. So, the number of groups will be controlled by the number of leaders, G (stallion), the rest of the individuals "$N - G$" will be distributed equitably between these groups.

Fig. 2 illustrates how the group's leaders are chosen initially at the start of the process and subsequently from the group members according to their preferences.

Fig. 3 illustrates how aboriginal stallions and ponies are selected to form groups.

C. *GRAZING AND HORSE MATING*

Usually, foals consume their life grazing around their herd.

1) *Grazing behavior*

To express this behavior, it's assumed that the stallion at the middle of the grazing region, and all other foals and mares look for that middle by moving around the stallion with various radius as follows in (13):

$$\bar{X}_{i,G}^{\,j} = 2\,Z\ cos\ (2\,\pi\,R\,Y) \times \left(stallion^{\,j} - X_{i,G}^{\,j}\right) + stallion^{\,j} \quad (13)$$

Where, $X_{i,G}^{j}$ is the actual location of the steed is described by (14) where, $stallion^{j}$ is the actual location of the steed and an adaptive algorithm Y. R is a regularly varying value that lies between [-2, 2] that is responsible for various angles of horses grazing (360 degrees) around the stallion, π is equal 3.14, and the updated location of the steed at grazing is $\bar{X}_{i,G}^{\,j}$.

$$P = \vec{R}_1 < TDR; \quad IDX = (P == 0);\ Y = R_2 \Theta IDX + \vec{R}_3 \Theta(\sim IDX) \quad (14)$$

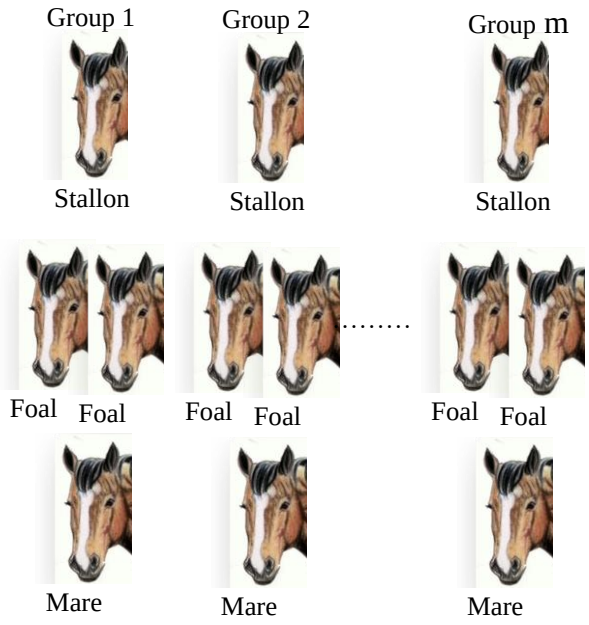

FIGURE 2. Configuration of horse collections designed for the tentative population.

Where P is a vector of zeros and ones with the same problem degree, $\vec{R}_1$ and $\vec{R}_3$ are uniformly randomized vectors with values from 0 to 1, R_2 is a uniformly randomized value from 0 to 1, IDX is $\vec{R}_1$ indexes's that achieve the rule ($P == 0$). TDR is a changeable value that initiates by 1 and lessens to 0 at the end of the execution, according to (15).

$$TDR = 1 - iter \times \left(\frac{1}{max\ iter}\right) \quad (15)$$

Where $iter$ and $max\ iter$ are the ongoing and most excellent iteration numbers.

2) *Horse mating behavior*

Foals separate themselves from the group before adulthood, where males accede a set of individual steeds, and females accede a different family set to achieve maturity and meet their mate, and this is to overcome the father/daughter and sisters mating as simulated by the following equation:

$$X_{G,K}^{P} = Crossover\left(X_{G,i}^{q}, X_{G,j}^{z}\right),\ i \neq j \neq k,\ p = q = end$$
$$Crossover = Mean \quad (16)$$

As $X_{G,K}^{P}$ represents the location of p's horse from k's group. It departed its group and exchanged its place with another horse reproduced from the mating of puberty horses, leaving groups i and j, which don't have any relationships. $X_{G,i}^{q}$ is the location of the foal from i's group, and $X_{G,j}^{y}$ is the location of y's foal from j's group.

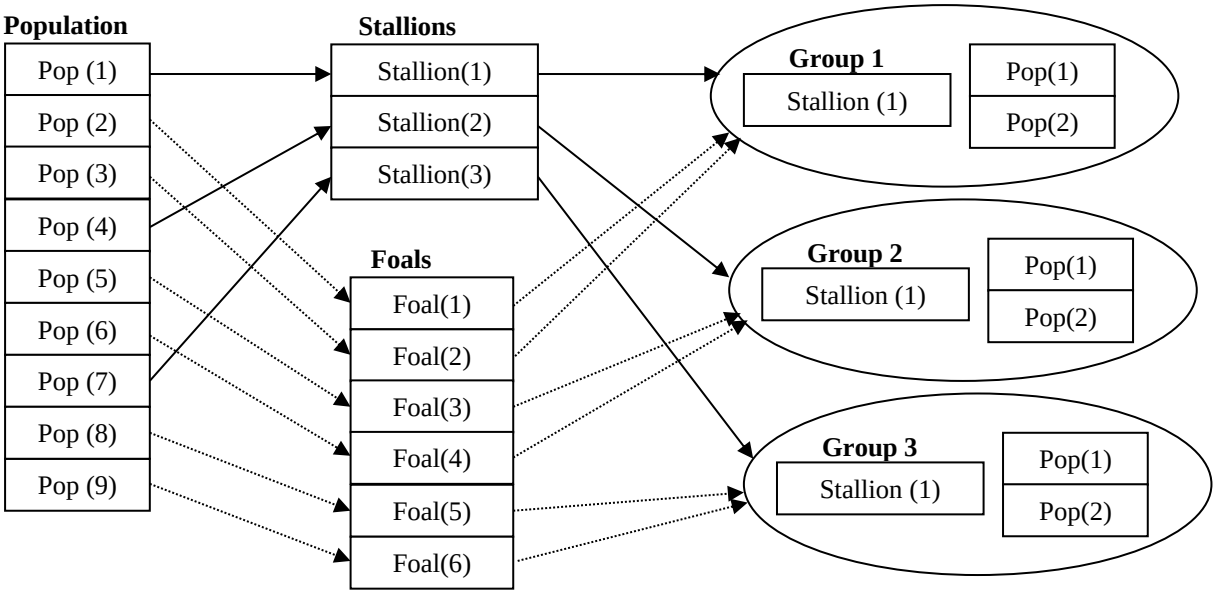

FIGURE 3. Collections shaping from native population.

D. *GROUP LEADING BY STALLION*

The group follows its leader towards the appropriate water hole, and then the leaders compete over that hole; the dominant group wins the supremacy of usage, while the others are given the right if the dominant group moves away according to dominance by the following equation:

$$\overline{Stallion_{G_i}} = \begin{cases} 2z\cos(2\pi RY) \times (WH - Stallion_{G_i}) + WH\,, & R_3 > 0.5 \\ 2z\cos(2\pi RY) \times (WH - Stallion_{G_i}) - WH\,, & R_3 \leq 0.5 \end{cases} \quad (17)$$

The boss following location for group i is $\overline{Stallion_{G_i}}$, while the ongoing one is $Stallion_{G_i}$,WH is the hole of water location, Y is calculated from (14), R_3 is a uniform random value between -2 and 2, π is 3.14.

E. *SWAP AND ELECTION OF LEADERS*

At first, the leaders are randomly selected and then selected later according to appropriateness. The most substantial element is replaced with the current leader if it exists, as illustrated in the coming formula:

$$Stallion_{G_i} = \begin{cases} X_{G,i} & if\ cos\ t(X_{G,i})\ cos\ t(Stallion_{G_i}) \\ Stallion_{G_i} & if\ cos\ t(X_{G,i})\ cos\ t(Stallion_{G_i}) \end{cases} \quad (18)$$

IV. *OUTCOMES AND DEBATING*

To demonstrate the effectiveness of WHO in solving severe ED issues, its appropriateness is evaluated in the following cases:

State 1: The required load is 850 MW via 3 generating units, including valve effects.

State 2: The required load is 2520 MW via 13 generating units.

State 3: The required load is 2630 MW via 15 generating units, considering transmission losses.

State 4: Considering the valve effects, the required load is 10500 MW via 40 generating units.

State 5: Required load of 2000 MW via 10 generating units considering valve effects and emission.

State 6: The required load is 1263 MW via 6 generating units, considering prohibited zones and transmission losses.

A. *STATE 1*

A three-unit generating system with an 850 MW demand is considered, accounting for constraints and valve-point effects but neglecting transmission losses. Data are sourced from [22]. Table 1 presents optimal generation, cost, and statistical analysis obtained by WHO, compared to other algorithms [45-52]. The lowest price is 8223.104 $/hr, showing WHO's superior performance. Fig. 4 demonstrates the effectiveness of the developed technique in reaching the lowest cost compared to other methods.

Table 1
Outcomes for 3 units.

Technique	Year	P1(MW)	P2(MW)	P3(MW)	Ptotal	Mean ($/hr)	Best ($/hr)
EP[45]	2003	300.264	400	149.736	850	8234.16	8234.07
PSO[46]	2004	300.268	400	149.732	850	8234.09	8234.07
IPSO [47]	2012	300.2655	400	149.7345	850	8346.51	8234.07
CJAYA[48]	2018	350.0254	400	99.9511	849.977	8289.41	8226.18
MPCJAYA[48]	2018	350.2464	400	99.7576	850.004	8232.06	8223.29
NGHS [49]	2018	300.2669	400	149.7331	850	8234.22	8234.07
NPHS [49]	2018	300.2669	400	149.7331	850	8234.08	8234.07
NTHS [49]	2018	300.2669	400	149.7331	850	8234.07	8234.07
NRHS [49]	2018	300.2669	400	149.7331	850	8234.07	8234.07
GWO[50]	2019	299.838	399.60	150.57	850.011	8305.91	8223.61
GWOI[50]	2019	300.618	399.60	149.803	850.021	8284.772	8223.367
HGWO[51]	2020	300.2624	400	149.7376	850	8234.83	8234.07
QOPSO[52]	2021	300.25	400	149.75	850	NA	8234.07
WHO		300.56	399.6	149.84	850	8233.567	8223.104

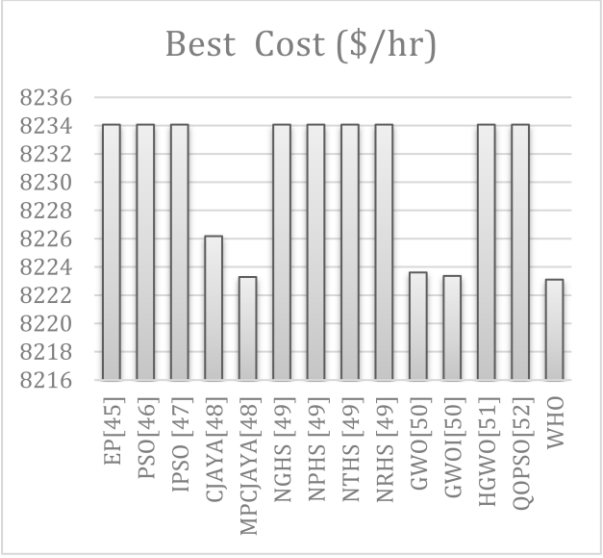

FIGURE 4. Fuel cost for distinct techniques for state 1.

B. *STATE 2*

Detailed unit data of a 13-generator system with a 2520 MW demand is taken from [53]. Table 2 shows optimal generation values and fuel costs for various algorithms [46, 48, 49, 50, 52, and 54] with WHO outperforming others, achieving a net demand cost of 24164.05$/hr. The statistical analysis is illustrated in Table 3. The mean result is close to the best, proving that the WHO is highly effective compared to other methods. Finally, Fig. 5 presents the net cost for each technique. It is clear that the developed WHO gives the most minor cost.

C. *STATE 3*

A 15-generator system with a 2630 MW demand is considered. Data and loss coefficient matrices are from [60]. The ELD problem was solved neglecting the valve-point effect. Table 4 shows the finest fuel cost via distinct approaches [60, 61, and 62]: 32,259.69 $/h using WHO, satisfying all constraints. As shown in Fig. 6, the generation cost is significantly reduced to $32,259.69 for a demand of 2,630 MW.

D. *STATE 4*

This case evaluates a large-scale power system with 40 generators to verify the effectiveness of the WHO in finding the optimal solution compared to other techniques. The analysis also considers the impact of the valve loading point [50, 63, 64, 65, 66, and 67]. Table 5 shows the output of each unit for a 10,500 MW load demand, along with the cost for each technique. The results demonstrate that the developed WHO achieves a lower cost than other techniques while meeting generation constraints, as mentioned in Fig. 7, suggesting that the different techniques may have been trapped in local minima. Thus, WHO exhibits superior performance in terms of fuel cost, even for large-scale power systems with valve loading effects. Additionally, Table 6 provides a statistical comparison between WHO and various techniques reported in [46, 65, 66, 68, 69, 70, 71, 72, 73, 74, and 75] in terms of the best, mean, and worst costs, as well as CPU time. The findings indicate that the best cost achieved by the developed WHO surpasses other techniques, and its average CPU time is the shortest.

Table 2
Outcomes of several approaches for 13 generators.

Unit	JAYA [48]	GWO[50]	SA[46]	NGHS[49]	NPHS[49]	NTHS[49]	NRHS[49]	QOPO[52]	GA[46]	CPSO[54]	**WHO**
P1(MW)	628.3185	647.3842	668.40	628.3163	628.3185	628.3185	628.3185	628.3147	627.05	628.32	**628.3185**
P2(MW)	299.2009	306.3995	359.78	299.1941	299.1984	299.1982	299.1993	359.9905	359.40	299.83	**299.1991**
P3(MW)	306.9105	309.6117	358.20	295.6601	294.4931	294.4902	294.4889	359.3237	358.95	299.17	**294.4854**
P4(MW)	159.7339	175.1400	104.28	159.7307	159.7330	159.7329	159.7325	109.8603	158.93	159.70	**159.7329**
P5(MW)	159.7337	66.8791	60.36	159.7330	159.7329	159.7329	159.7330	159.7333	159.73	159.64	**159.7331**
P6(MW)	159.7338	162.7466	110.64	159.7327	159.7321	159.7323	159.7331	159.7275	159.68	159.67	**159.7330**
P7(MW)	109.8673	174.3111	162.12	159.7311	159.7329	159.7327	159.7328	159.6924	159.53	159.64	**159.7331**
P8(MW)	159.7342	61.2250	163.03	159.7330	159.7330	159.7329	159.7326	159.7204	158.89	159.65	**159.7330**
P9(MW)	159.7340	175.1400	161.52	159.7332	159.7330	159.7330	159.7331	159.6847	110.15	159.78	**159.7330**
P10(MW)	114.8012	116.7600	117.09	77.3992	77.3994	77.3989	77.3998	40.00002	77.27	112.46	**77.3998**
P11(MW)	114.8001	116.7600	75.00	76.2539	77.3974	77.3997	77.3979	113.952	75.00	74.00	**77.3998**
P12(MW)	92.4018	99.9167	60.00	92.3916	92.3970	92.3983	92.3999	55.00017	60.00	56.50	**92.3997**
P13(MW)	55.0027	108.5598	119.58	92.3911	92.3993	92.3995	92.3986	55.00017	55.41	91.64	**92.3996**
Ptotal(MW)	2519.97	2520.83	2520	2520	2520	2520	2520	2520	2520	91.64	**2520**
Fmean($/h)	24476.254	24442.08	NA	24206.95	24208.82	24201.1	24185.61	NA	NA	NA	**24164.36**
Fbest($/h)	24220.752	24231.18	24970.91	24165.92	24164.07	24164.06	24164.06	24328.14	24418.99	24211.56	**24164.05**

Table 3
Statistic outcomes of 13 generators.

Method	**Reference**	**Best**	**Average**
NGHS	2018[49]	24165.92	24206.95
NPHS	2018[49]	24164.07	24208.82
NTHS	2018[49]	24164.06	24201.10
NRHS	2018[49]	24164.06	24185.61
ACO	2010[57]	24174.39	24211.09
FCASO-SQP	2012[55]	24190.63	NA
HCASO	2012[55]	24212.93	NA
HCPSO	2012[54]	24211.56	NA
HCPSO-SQP	2012[54]	24190.97	NA
TS	2010[57]	24180.31	24243.37
TS	2021[56]	24171.21	24184.06
HSSA	2021[56]	24164.21	24164.47
SSA	2021[56]	24168.97	24295.45
THS	2016[58]	24164.06	24195.21
TS1	2010[57]	24180.31	24243.37
TS2	2010[59]	24171.21	24184.06
WHO		**24164.05**	**24164.36**

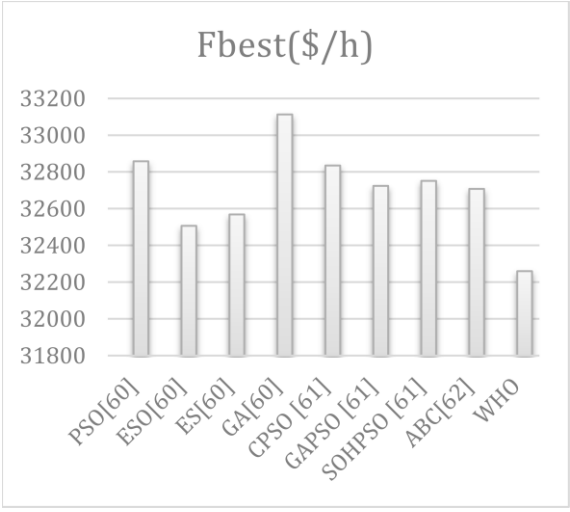

FIGURE 6. Fuel cost for distinct techniques for state 3.

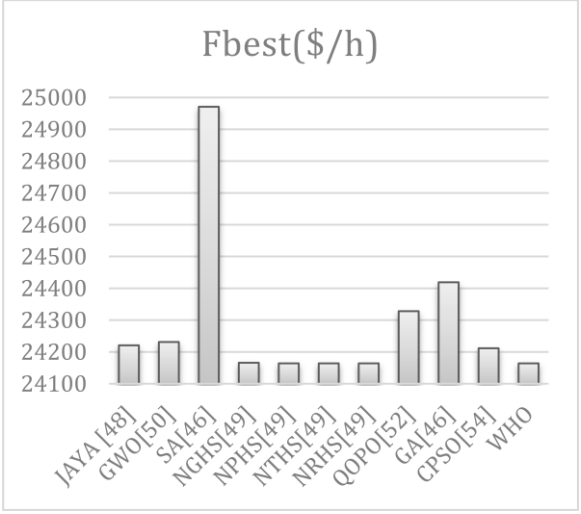

FIGURE 5. Fuel cost for distinct techniques for state 2.

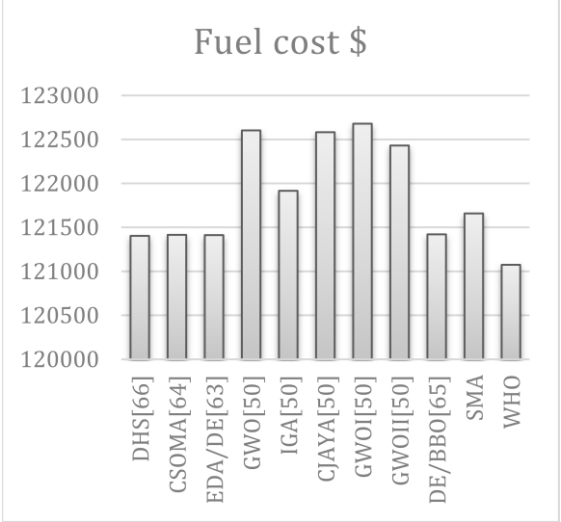

FIGURE 7. Fuel cost for distinct techniques for state 4.

Table 4
Results of diverse approaches for 15 generators.

Power(MW)	PSO[60]	ESO[60]	ES[60]	GA[60]	CPSO [61]	GAPSO [61]	SOHPSO [61]	ABC[62]	**WHO**
P1	439.12	456	455	415.31	450.05	436.8482	455	455	**455**
P2	407.97	456	380	359.72	454.04	409.6974	380	380	**454.7336**
P3	119.63	130	130	104.42	124.82	117.0074	130	130	**130**
P4	129.99	130	150	74.98	124.82	128.2705	130	130	**129.9999**
P5	151.07	304.24	168.92	380.28	151.03	153.3361	170	169.997	**288.3104**
P6	459.99	460	459.34	426.79	460	457.4078	459.96	460	**459.976**
P7	425.56	465	430	341.32	434.53	424.440	430	430	**465**
P8	98.56	60	97.42	124.79	148.41	101.1949	117.53	71.9698	**60.1935**
P9	113.49	25	30.61	133.14	63.61	116.1186	77.90	59.1798	**25**
P10	101.11	20	142.56	89.26	101.13	102.2243	119.54	159.800	**25.24209**
P11	33.91	29.15	80	60.06	28.656	35.0317	54.5	80	**20.04263**
P12	79.96	59.24	85	50	20.912	78.8482	80	80	**61.3713**
P13	25	25	15	38.77	25.001	27.1292	25	25.0024	**25.0031**
P14	41.41	17.28	15	41.94	54.418	37.1594	17.86	15.0056	**15.09977**
P15	35.61	15	15	22.64	20.625	37.0390	15	15.0014	**15.04694**
Ploss	32.42	13.79	23.85	38.28	32.1302	31.75	32.28	13	**0.01008**
Fbest($/h)	32858	32506.6	32568.5	33113	32835	32724	32751.39	32707.8	**32259.69**

Table. 5
Results of distinct techniques for state 4.

Power	DHS[66]	CSOMA[64]	EDA/DE[63]	GWO[50]	IGA[50]	GWOII[50]	DE/BBO[65]	SMA[67]	**WHO**
P1	110.7998	110.8016	111.1110	109.0947	110.97	107.6544	110.7998	112.3525	**72.4810**
P2	110.7998	110.8068	110.8299	112.0471	110.88	109.2161	110.7998	112.4688	**103.0314**
P3	97.3999	97.4007	97.4122	115.4584	98.17	94.7874	97.3999	97.4914	**83.2726**
P4	179.7331	179.7333	179.7443	179.8333	178.85	182.3441	179.7331	179.7415	**182.3106**
P5	87.7999	87.8180	88.1510	46.1649	87.78	86.9731	87.9576	93.717	**76.1669**
P6	140.0000	139.9997	139.9959	83.1571	140	109.1907	140.0000	139.9994	**126.1346**
P7	259.5997	259.6010	259.6065	261.6345	260.37	259.491	259.5997	260.4361	**258.8452**
P8	284.5997	284.6000	284.6045	292.4025	286.83	284.1803	284.5997	289.743	**297.1636**
P9	284.5997	284.6005	284.6149	284.7149	285.14	285.1526	284.5997	296.0535	**290.8899**
P10	130.0000	130.0003	130.0002	132.9049	204.86	129.35	130.0000	130.0189	**274.8232**
P11	94.0000	168.7999	168.8029	101.6726	165.98	317.4787	168.7998	168.7887	**356.9806**
P12	94.0000	168.7999	94.0000	319.8174	167.75	157.3563	94.0000	168.7212	**124.4054**
P13	214.7598	214.7599	214.7591	215.0746	214.31	300.6095	214.7598	125.0003	**493.3764**
P14	394.2794	394.2794	394.2716	394.9259	305.65	305.0848	394.2794	394.2872	**344.9029**
P15	394.2794	304.5196	304.5206	398.1829	393.66	395.3099	394.2794	304.5919	**372.3864**
P16	394.2794	394.2794	394.2834	304.1546	394.6	203.9544	394.2794	394.3118	**345.4624**
P17	489.2794	489.2796	489.2912	490.0842	489.22	489.6721	489.2794	489.2914	**422.6378**
P18	489.2794	489.2795	489.2877	493.2515	489.25	492.349	489.2794	489.8810	**434.4065**
P19	511.2794	511.2794	511.2977	511.4229	511.23	514.3882	511.2794	511.2385	**461.3107**
P20	511.2794	511.2796	511.2791	511.9422	510.69	511.7323	511.2794	511.2866	**434.3828**
P21	523.2794	523.2797	523.2958	532.3762	524.74	532.2046	523.2794	523.3004	**545.2846**
P22	523.2794	523.2798	523.2849	532.2484	525.52	527.3193	523.2794	523.2929	**490.3572**
P23	523.2794	523.2801	523.2856	530.7732	522.98	527.3193	523.2794	523.3215	**506.0639**
P24	523.2794	523.2795	523.2979	526.1112	522.22	539.9336	523.2794	523.2599	**467.3109**
P25	523.2794	523.2797	523.2799	524.4545	523.26	526.6306	523.2794	523.3046	**488.1203**
P26	523.2794	523.2799	523.2910	523.4934	523.32	524.8658	523.2794	523.2675	**486.9019**
P27	10.0000	10.0004	10.0064	11.5028	10	9.95	10.0000	10.0048	**16.8002**
P28	10.0000	10.0004	10.0018	9.9541	10	9.95	10.0000	10	**39.3475**
P29	10.0000	10.0003	10.0000	10.3272	10	9.95	10.0000	10	**23.6359**
P30	87.7999	92.7158	96.2132	91.6019	88.86	90.3385	97.0000	92.7367	**86.3295**
P31	190.0000	189.9998	189.9996	188.8475	162.3	159.6875	190.0000	189.9981	**165.9924**
P32	190.0000	189.9998	189.9998	165.2531	177.94	188.9923	190.0000	190	**174.5707**
P33	190.0000	189.9998	189.9981	188.9197	160.18	173.1974	190.0000	190	**184.0570**
P34	164.7998	164.8014	164.9126	189.2968	166.54	189.6808	164.7998	195.8292	**193.6668**
P35	200.0000	164.8015	199.9941	180.4605	164.8	192.1671	200.0000	200	**191.6152**
P36	194.3978	164.8051	200.0000	184.2698	170.68	157.5027	200.0000	200	**196.1763**
P37	110.0000	109.9998	109.9988	89.6748	108.17	104.4095	100.0000	89.8907	**90.0101**
P38	110.0000	109.9998	109.9994	90.1485	100.68	86.7413	110.0000	91.7375	**37.5421**
P39	110.0000	109.9996	109.9974	57.0464	109.34	100.297	110.0000	109.9905	**89.4239**
P40	511.2794	511.2797	511.2800	514.3622	511.28	512.4387	511.2794	511.2371	**471.4405**
cost $	**121403.5**	**121414.7**	**121412**	**122602.37**	**121915.93**	**122430.74**	**121420.8**	**121658.66**	**121074.5**

Table. 6
Statistical comparison for distinct techniques

Technique	Best*10^5 [$]	Mean*10^5 [$]	Worst*10^5 [$]	Time (Sec)
EP [46]	1.2262435	1.23382	1.25740	1167.35
DE/BBO [65]	1.2142089	1.214209	1.214209	60.00
TSAGA [68]	1.2146307	1.2292831	1.2429654	696.01
CCPSO [69]	1.21403536	1.2144532	1.2153549	19.3
CDE_SQP [70]	1.21741979	1.2229512	1.2283929	14.26
CPSO [71]	1.2186523	1.2210087	-	114.65
NPSO_LRS [72]	1.2166443	1.2220931	1.2298159	16.81
APSO [73]	1.2166352	1.2215367	1.2291239	5.05
DECDM [74]	1.2142340	1.2152673	1.2169698	44.3
FAPSO-NM [75]	1.214183	1.2141880	1.214198	40
WHO	**1.210745**	**1.2119357**	**1.2138733**	**3.27**

E. *STATE 5*

Considering valve point effects, this case examines a ten-unit thermal power generation system. The system parameters are provided in [76]. Table 7 shows the results of solving the CEED problem for a 2000 MW load demand using the WHO technique, compared to other techniques [43, 44, and 76]. The performance of the developed technique is highlighted, demonstrating that WHO achieves a lower fuel cost-$528 less than GSA, $522 less than MODE, $548 less than PDE, and $408 less than FPA while meeting all system constraints. Its emissions are also lower than those of PDE, GSA, and MODE, indicating WHO's success in finding the global minimum solution and reducing greenhouse gases. Furthermore, the CPU time is shorter than that of the other techniques, showcasing WHO's superior efficiency and effectiveness in minimizing net cost within a shorter timeframe. Finally, Fig. 8 presents the net cost for each technique.

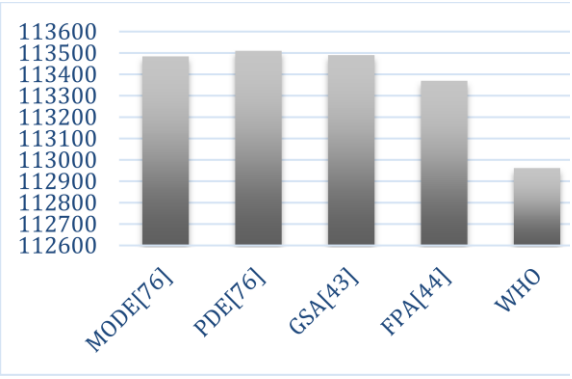

FIGURE 8. Cost function for state 5.

F. *STATE 6*

This network consists of six units with a load demand of 1263 MW, considering transmission losses, prohibited operating zones (POZ), and ramp-rate limits. The system data is sourced from [43]. Table 8 presents the optimal generation values and fuel costs obtained by various algorithms, with an optimal cost achieved at $15,443.07 per hour. Evidently, the generation values adhere to the generation limit constraints and avoid falling within the POZs. Table 9 provides a statistical comparison of the results obtained by different algorithms. In this comparison, the outcomes from WHO are evaluated against those from JAYA[48], GWO[50], PSO[46], HHO[53], NPSO-LRS[72], GA[77], TS[78], RDPSO[79], MABC[80], HCRO-DE[81], GAAPI[82], DE[83], CBA[84], and CLPSO[85]. Finally, Fig. 9 introduces the net cost for every technique.

Table 7
CEED problem for ten generating units.

Outputs (MW)	MODE[76]	PDE[76]	GSA[43]	FPA[44]	**WHO**
P1	54.9487	54.9853	54.9992	53.188	**45.5064**
P2	74.5821	79.3803	79.9586	79.975	**79.9932**
P3	79.4294	83.9842	79.4341	78.105	**105.6385**
P4	80.6875	86.5942	85.0000	97.119	**88.8318**
P5	136.8551	144.4386	142.1063	152.74	**135.2728**
P6	172.6393	165.7756	166.5670	163.08	**163.5014**
P7	283.8233	283.2122	292.8749	258.61	**261.2679**
P8	316.3407	312.7709	313.2387	302.22	**281.2322**
P9	448.5923	440.1135	441.1775	433.21	**456.4747**
P10	436.4287	432.6783	428.6306	466.07	**466.9185**
cost*$10^5$$	1.13484	1.1351	1.1349	1.1337	**1.12962**
Emission(Ib)	4124.9	4111.4	4111.4	3997.7	**4077.8**
Losses(MW)	84.33	83.9	83.9869	84.3	**84.3**
CPU(Sec)	3.82	4.23	NA	2.23	**2.15**

Table 8
Results of various algorithms for 6 units.

Power (MW)	**PSO[46]**	**JAYA[48]**	**GWO[50]**	**GA[77]**	**WHO**
P1	447.5823	457.9858	446.6281	462.0444	447.3997
P2	172.8387	176.8785	171.7686	189.4456	173.2392
P3	261.330	250.0717	264.671	254.8535	263.3163
P4	138.6812	129.3748	141.3356	127.4296	138.0006
P5	169.6781	172.8886	166.5389	151.5388	165.4104
P6	85.8963	88.4618	85.00	90.715	87.0798
Ptotal	1276.006	1275.661	1276.315	1276.027	1275.46
Ploss	13.006	12.6665	13.3099	13.0268	12.46
Fbest ($/h)	15450.14	15447.09	15450.07	15457.96	15443.07

Table 9
Statistical results of 6 units.

Algorithm	**Year**	**Best**	**Worst**	**Mean**
PSO[46]	2004	15450.14	15491.71	15465.83
JAYA[48]	2018	15477.09	15622.16	15500.11
GWO[50]	2019	15450.07	15487.14	15453.41
HHO[53]	2022	15499.78	NA	15488.41
NPSO-LRS[72]	2007	15450	15454	15452
GA[77]	1999	15457.96	15524.69	15477.71
TS[78]	2008	15454.89	15472.56	15454.89
RDPSO[79]	2017	15449.89	NA	15458.01
MABC[80]	2015	15449.899	15449.899	15449.899
HCRO-DE[81]	2014	15443.075	15443.916	15443.327
GAAPI[82]	2012	15449.78	15449.85	15449.81
DE[83]	2015	15449.582	15449.650	15449.62
CBA[84]	2016	15450.238	15454.76	15518.658
CLPSO[85]	2018	15447.72	15452.88	15449.83
WHO	-	15443.07	15443.3	15443.14

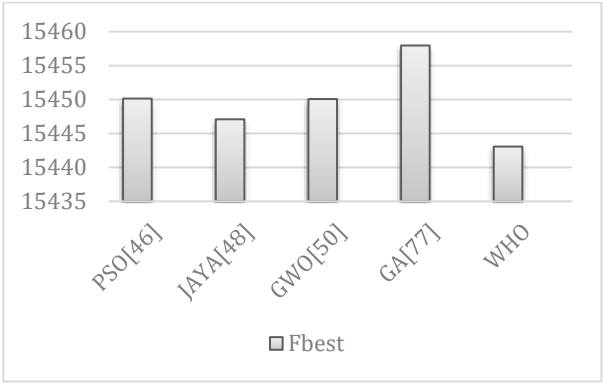

FIGURE 9. Cost function for state 6.

V. CONCLUSION

A new application of WHO has been discussed in managing ED processes in power networks. The main contributions of this article are:

1- The multi-objective function is designed to deal with ED and CEED problems.
2- The effectiveness of WHO's approach across different scenarios and comparisons to recent studies is evaluated.
3- WHO's superiority in handling both ED and CEED processes, including those involving large-scale networks with valve effects, prohibited operating zones, and losses, are highlighted.
4- Compared to other recent techniques, WHO's validity is proven through total cost, statistical analysis, and CPU.
5- The proposed WHO decreased the total cost by 0.186$/h for state 1, 0.01$/h for state 2, 246.91$/h for state 3, 329$/h for state 4, 408$/h for state 5, and 4.02$/h for state 6 compared with the best result mentioned in the literature.
6- WHO's notability as an environmentally friendly organization is confirmed since it produces fewer emissions than others.
7- WHO optimization demonstrates strong potential for solving complex power system challenges.

Future work will apply the suggested technique to multi-area electric systems, complementing wind energy and photovoltaic systems.

REFERENCES

[1] A. Chakrabarti and S. Halder, "Power System Operation and Control", PHI Learning Pvt. Ltd. 2006.
[2] D. P. Kothari and J. S. Dhillon, "Power System Optimization", PHI Learning Pvt. Ltd, 2nd Edition, 2006.
[3] A. Y. Abd-Elaziz, E. S. Ali and S. M. Abd-Elazim, "Combined Economic and Emission Dispatch Solution Using Flower Pollination Algorithm", Int. J. of Electrical Power and Energy Systems, Vol. 80 C, September 2016, pp. 264-274.
[4] A. Bakirtzis, V. Petridis, and S. Kazarlis, "Genetic Algorithm solution to the economic Dispatch Problem", IEE proceedings-generation, transmission and distribution, Vol. 141, No. 4, 1994, pp.377-382.
[5] K. P. Wong, and Y. W. Wong, "Genetic and Genetic/Simulated-Annealing Approaches to Economic Dispatch", IEE Proceedings-Generation, Transmission and Distribution, Vol. 141, No. 5, 1994, pp. 507-513.
[6] A. L. Devi, and O. V. Krishna, "Combined Economic and Emission Dispatch Using Evolutionary Algorithms-A Case Study", ARPN Journal of Engineering and Applied Sciences Vol. 3, No. 6, 2008, pp. 28-35.
[7] M. Basu, C. Jena, and C. K. Panigrahi, "Differential Evolution with Gaussian Mutation for Economic Dispatch", Journal of the Institution of Engineers (India): Series B, Vol. 97, No. 4, 2016, pp. 493-498.
[8] A. A. El Ela, M. Abido, and S. R. Spea, "Differential Evolution Algorithm for Emission Constrained Economic Power Dispatch Problem", Electric power Systems Research, Vol. 80, No. 10, 2010, pp. 1286-1292.
[9] M. Jevtic, N. Jovanovic, J. Radosavljevic, and D. Klimenta, "Moth Swarm Algorithm for Solving Combined Economic and Emission Dispatch Problem", Elektronikair Elektrotechnika, Vol. 23, No. 5, 2017, pp. 21-28.
[10] A. S. Tomar, H. M. Dubey, and M. Pandit, "Combined Economic Emission Dispatch Using Spider Monkey Optimization", In Advanced Engineering Optimization through Intelligent Techniques. Springer, 2020, Vol. 949, pp. 809-818.
[11] M. Pradhan, P. K. Roy, and T. Pal, "Grey Wolf Optimization Applied to Economic Load Dispatch Problems", Int. J. of Electrical Power & Energy Systems 83, 2016, pp. 325-334.
[12] G. Chen, and X. Ding, "Optimal Economic Dispatch with Valve Loading Effect Using Self-Adaptive Firefly Algorithm", Applied Intelligence, Vol. 42, No. 2, 2015, pp. 276-288.
[13] M. Younes, F. Khodja, and R. L. Kherfane, "Multi-Objective Economic Emission Dispatch Solution Using Hybrid FFA (Firefly Algorithm) and Considering Wind Power Penetration", Energy, Vol. 67, 2014, pp. 595-606.
[14] M. A. Al-Betar, M. A. Awadallah, A. T. Khader, A. L. Bolaji, and A. Almomani, "Economic Load Dispatch Problems with Valve-Point Loading Using Natural Updated Harmony Search", Neural Computing and Applications, Vol. 29, No. 10, 2018, pp. 767-781.
[15] H. Rezaie, M. Kazemi- Rahbar, B. Vahidi, and H. Rastegar, "Solution of Combined Economic and Emission Dispatch Problem Using A Novel Chaotic Improved Harmony Search Algorithm", Journal of Computational Design and Engineering, Vol. 6, No. 3, 2019, pp. 447-467.
[16] L. Benasla, A. Belmadani, and M. Rahli, "Spiral Optimization Algorithm for Solving Combined Economic and Emission Dispatch", Int. J. of Electrical Power & Energy Systems, Vol. 62, 2014, pp. 163-174.
[17] D. Aydin, S. Özyön, C. Yaşar, and T. Liao, "Artificial Bee Colony Algorithm with Dynamic Population Size to Combined Economic and Emission Dispatch Problem", Int. J. of Electrical Power and Energy Systems, Vol. 54, 2014, pp. 144-153.
[18] D. Aydin, G. Yavuz, S. Özyön, C. Yaşar, and T. Stützle, "Artificial Bee Colony Framework to Nonconvex Economic Dispatch Problem with Valve Point Effects: A Case Study", in: Proceedings of the Genetic and Evolutionary Computation Conference Companion 2017, pp. 1311-1318.
[19] L. Tan, H. Wang, C. Yang, and B. Niu, "A Multi-Objective Optimization Method based on Discrete Bacterial Algorithm for Environmental/Economic Power Dispatch," Natural Computing, Vol. 16, No. 4, 2017, pp. 549-565.
[20] M. Abido, "Multiobjective Particle Swarm Optimization for Environmental /Economic Dispatch Problem", Electric Power Systems Research, Vol. 79, No. 7, 2009, pp. 1105-1113.
[21] Z. L. Gaing, "Particle Swarm Optimization to Solving The Economic Dispatch Considering The Generator Constraints", IEEE Transactions on Power Systems, Vol. 18, No. 3, 2003, pp. 1187-1195.
[22] M. A. Al-Betar, M. A. Awadallah, I. A. Doush, E. Alsukhni, and H. ALkhraisat, "A Non-convex Economic Dispatch Problem with Valve Loading Effect Using a New Modified β Hill Climbing Local Search Algorithm", Arabian Journal for Science and Engineering, Vol. 43, No. 12, 2018, pp. 7439-7456.
[23] E. S. Ali, and S. M. Abd-Elazim, "Mine Blast Algorithm for Environmental Economic Load Dispatch with Valve Loading Effect", Neural Computing and Applications, Vol. 30, No. 1, July 2018, pp. 261-270.
[24] A. Y. Abd-Elaziz, E. S. Ali and S. M. Abd-Elazim, "Flower Pollination Algorithm to Solve Combined Economic and Emission Dispatch

Problems", Engineering Science and Technology: an International Journal, Vol. 19, Issue 2, June 2016, pp. 980-990.
[25] A. M. Abd-El Wahab, S. Kamel, M. H. Hassan, M. I. Mosaad, and T. A. Abdul Fattah "Optimal Reactive Power Dispatch Using a Chaotic Turbulent Flow of Water-Based Optimization Algorithm", Mathematics, MDPI, Vol. 10, No. 3, pp. 1-26, January 2022, https://doi.org/10.3390/electronics10233035.
[26] E. S. Ali, S. M. Abd-Elazim, and A.S. Balobaid, "Implementation of Coyote Optimization Algorithm for Solving Unit Commitment Problem in Power Systems", Energy, Vol. 263, pp. 1-11, January 2023.
[27] K. Carson, and D. G. M. Wood-Gush, "Equine Behaviour: I. A Review of the Literature on Social and Dam-Foal Behaviour", Applied Animal Ethology, Vol.10, May 1983, pp.165-178.
[28] K. Carson, and D. G. M. Wood-Gush, "Equine Behaviour: II. A Review of the Literature on Feeding, Eliminative and Eesting Behaviour". Applied Animal Ethology, Vol.10, May1983, pp.179-190.
[29] J. D. Feist, and D. R. McCullough, "Reproduction in Feral Horses", J Reprod Fertil Suppl., Vol. 23, October 1975, pp.13-18. PMID: 1060766
[30] H. Klingel, "Social Organization and Reproduction in Equids", J Reprod Fertil Suppl, 1975, pp. 7-11, PMID: 1060868
[31] S. M. Wells, and B. Goldschmidt-Rothschild, "Social Behaviour and Relationships in a Herd of Camargue Horses", Z Tierpsychologie, Vol.49, 1979, pp.363-380.
[32] R. Miller, and R. H. Dennisto, "Interband Dominance in Feral Horses", Z Tierpsychologie, Vol.51, 1979, pp.41-47.
[33] V. R. Squires, and G. T. Daws, "Leadership and Dominance Relationships in Merino and Border Leicester Sheep", Applied Animal Ethology, Vol.1, July 1975, pp. 263-274.
[34] D. A. Welsh, "Population, Behavioural and Grazing Ecology of the Horses of Sable Island", Nova Scotia. PhD thesis, 1975, Dalhousie University.
[35] I. Naruei, and F. Keynia. "Wild Horse Optimizer: A New Meta-Heuristic Algorithm for Solving Engineering Optimization Problems" Engineering With Computers, Springer, Vol.38,2022,ppt-3025-3056.
[36] Marliani, A. Arief, and, I. C. Gunadin, "Implementation of Wild Horse Optimization (WHO) Method for Optimal Hybrid Renewable Energy Designs", 2023 International Conference on Computer Science, Information Technology and Engineering (ICCoSITE), 16 February 2023, IEEE, Jakarta, Indonesia.
[37] A. J. Wood and B. F. Wollenberg, "Power Generation Operation and Control", 2nd Edition, John Willy and Sons, 1996.
[38] D. C. Walters and G. B. Sheble, "Genetic Algorithm Solution of Economic Dispatch with Valve Point Loading", IEEE Transaction on Power Systems, Vol. 8, No. 3, August 1993, pp. 1325-1332.
[39] K. Senthil and K. Manikandan, "Economic Thermal Power Dispatch with Emission Constraint and Valve Point Effect loading Using Improved Tabu Search Algorithm", Int. J. of Computer Applications, Vol. 3, No. 9, July 2010, pp. 6-11.
[40] P. N. Say and M. Yücel, "Energy Consumption and CO2 Emissions in Turkey: Empirical Analysis and Future Projection based on an Economic Growth", Energy Policy, Vol. 34, 2006, pp. 3870-3876.
[41] E. S. Ali, "Harris Hawks Approach for Distinct Economic Dispatch Problems", Yanbu Journal of Engineering and Science, Vol. 20, No. 1, 2023, pp.32-50.
[42] G. Aydin, "The Development and Validation of Regression Models to Predict Energy-Related CO2 Emissions in Turkey", Energy Sources Part B: Economics, Planning and Policy, 2015, Vol.10, No. 2, pp. 176-182.
[43] U. Güvenç, Y. Sonmez, S. Duman and N.Yorükeren, "Combined Economic and Emission Dispatch Solution Using Gravitational Search Algorithm", Scientia Iranica D: Computer Science, Engineering and Electrical Engineering, Vol. 19, No. 6, 2012, pp.1754-1762.
[44] A. Y. Abd-Elaziz, E. S. Ali and S. M. Abd-Elazim, "Implementation of Flower Pollination Algorithm for Solving Economic Load Dispatch and Combined Economic Emission Dispatch Problems in Power Systems", Energy, Vol. 101C, April 2016, pp. 506-518.
[45] N. Sinha, R. Chakrabarti, and P. K. Chattopadhyay, "Evolutionary Programming Techniques for Economic Load Dispatch", IEEE Trans. Evol. Comput. 2003, 7, pp. 83-94.
[46] T. A. A. Victoire, and A. E. Jeyakumar, "Hybrid PSO-SQP for Economic Dispatch with Valve-Point Effect", Electric Power System Research, 2004, 71, pp.51-59.
[47] M. N. Abdullah, A. H. A. Bakar N. A. Rahim, J. J. Jamian, and M. M. Aman, "Economic Dispatch with Valve Point Effect using Iteration Particle Swarm Optimization", 04-07 September 2012, 47th International Universities Power Engineering Conference (UPEC), Uxbridge, UK.
[48] Y. K. Wang, and X. B. Chen, "Improved Multi-Area Search and Asymptotic Convergence PSO Algorithm with Independent Local Search Mechanism", Control Decision, 2018, 33, pp.1382-1389.
[49] M. A. Al-Betar, M. A. Awadallah, A. T. Khader, A. L. Bolaji and A. Almomani, "Economic Load Dispatch Problems with Valve-Point Loading Using Natural Updated Harmony Search", Neural Computing and Applications, Vol. 29, No. 10, 2018, pp. 767-781.
[50] J. Xu, F. Yan, K. Yun, L. Su, F. Li and J. Guan, "Noninferior Solution Grey Wolf Optimizer with an Independent Local Search Mechanism for Solving Economic Load Dispatch Problems", Energies, 2019, 12, 2274; doi:10.3390/en12122274.
[51] M. A. Al-Betar, M. A. Awadallah, and M. M. Krishan, "A Non-Convex Economic Load Dispatch Problem with Valve Loading Effect Using a Hybrid Grey Wolf Optimizer", Neural Computing and Applications, Vol. 32, 2020, pp.12127-12154.
[52] V. Basetti, S. S. Rangarajan, C. K. Shiva, H. Pulluri, R. Kumar, R. E. Collins and T. Senjyu, "Economic Emission Load Dispatch Problem with Valve-Point Loading Using A Novel Quasi-Oppositional-Based Political Optimizer", Electronics 2021, 10, 2596. https://doi.org/10.3390/electronics10212596.
[53] M. A. Al-Betar, M. A. Awadallah, S. N. Makhadmeh, I. A. Doush, R. A. Zitarf, S. Alshathri, and M. A. Elaziz, "A Hybrid Harris Hawks Optimizer for Economic Load Dispatch Problems", Alexandria Engineering Journal, Vol. 64, No. 1, February 2023, pp. 365-389.
[54] J. Cai, Q. Li, L. Li, H. Peng, and Y. Yang, "A Hybrid CPSO–SQP Method for Economic Dispatch Considering the Valve-Point Effects", Energy Conversion and Management, 2012, Vol. 53, pp. 175-181.
[55] J. Cai, Q. Li, L. Li, H. Peng, and Y. Yang, "A Hybrid FCASO-SQP Method for Solving the Economic Dispatch Problems with Valve Point effects", Energy, 2012, Vol. 38, No. 1, pp.346-353.
[56] M. S. Alkoffash, M. A. Awadallah, M. Alweshah, R. A. Zitar, K. Assaleh, and M. A. Al-Betar, "A Non-Convex Economic Load Dispatch Using Hybrid Salp Swarm Algorithm", Arabian Journal for Science and Engineering, 2021, pp.1-20.
[57] S. Pothiya, I. Ngamroo, and W. Kongprawechnon, "Ant Colony Optimization for Economic Dispatch Problem with Non-smooth Cost Functions", Int. J. of Electrical Power and Energy Systems, 2010, Vol. 32, 5, pp.478-487.
[58] M.A. Al-Betar, M.A. Awadallah, A.T. Khader, and A.L. Bolaji, "Tournament-based Harmony Search Algorithm for Non-Convex Economic Load Dispatch Problem", Applied Soft Computing, Vol. 47, 2016, pp.449-459.
[59] S. Khamsawang, and S. Jiriwibhakorn, "Dspso-Tsa for Economic Dispatch Problem with Nonsmooth and Noncontinuous Cost Functions", Energy Conversion and Management, Vol.51, 2010, pp.365-375.
[60] L. D. S. Coelho, and C. S. Lee, "Solving Economic Load Dispatch Problems in Power Systems Using Chaotic and Gaussian Particle Swarm Optimization Approaches", Int. J. Electrical Power and Energy Systems, 2008, Vol. 30, pp.297-307.
[61] A. Safari, and H. Shayeghi, "Iteration Particle Swarm Optimization Procedure for Economic Load Dispatch with Generator Constraints", Expert Syst. Appl. 2011, 38, pp. 6043-6048.
[62] S. Hemamalini, and S. P. Simon, "Artificial Bee Colony Algorithm for Economic Load Dispatch Problem with Non-smooth Cost Functions", Electric Power Components and Systems 2010, Vol. 38, pp.786-803.
[63] Y. Wang, B. Li and T. Weise, "Estimation of Distribution and Differential Evolution Cooperation for Large Scale Economic Load Dispatch Optimization of Power Systems", Information Sciences, Vol. 180, No. 12, June 2010, pp. 2405-2420.
[64] L. D. S. Coelho and V. C. Mariani, "An Efficient Cultural Self-Organizing Migrating Strategy for Economic Dispatch Optimization with Valve-Point Effect", Int. J. of Energy Conversion and Management, Vol. 51, No. 12, December 2010, pp. 2580-2587.

[65] A. Bhattacharya and P. K. Chattopadhyay, "Hybrid Differential Evolution with Biogeography-Based Optimization for Solution of Economic Load Dispatch", IEEE Transactions on Power Systems, Vol. 25, No. 4, 2010, pp. 1955-1964.
[66] L. Wang and L. P. Li, "An Effective Differential Harmony Search Algorithm for the Solving Non-Convex Economic Load Dispatch Problems", Int. J. of Electrical Power and Energy Systems, Vol. 44, 2013, pp. 832-843.
[67] V. K. Kamboj, C. L. Kumari, S. K. Bath, D. Prashar, M. Rashid, S. S. Alshamrani and A. S. AlGhamdi, "A Cost-Effective Solution for Non-Convex Economic Load Dispatch Problems in Power Systems Using Slime Mould Algorithm", Sustainability 2022, 14, 2586,https://doi.org/10.3390/su14052586.
[68] P. Subbaraj, R. Rengaraj and S. Salivahanan, "Enhancement of Self-Adaptive Real Coded Genetic Algorithm Using Taguchi Method for Economic Dispatch Problem", Applied Soft Computing, Vol. 11, No. 1, January 2011, pp. 83-92.
[69] J. B. Park, Y. W. Jeong, J. R. Shin and K. Y. Lee, "An Improved Particle Swarm Optimization for Nonconvex Economic Dispatch Problems", IEEE Transactions on Power Systems, Vol. 25, No. 1, 2010, pp.156-166.
[70] L. D. S. Coelho and V. C. Mariani, "Combining of Chaotic Differential Evolution and Quadratic Programming for Economic Dispatch Optimization with Valve-Point Effect", IEEE Transactions on Power Systems, Vol. 21, No. 2, 2006, pp. 989-996.
[71] C. Jiejin, L. Qiong, L. Lixiang, P. Haipeng and Y. Yixian, "A Hybrid CPSO–SQP Method for Economic Dispatch Considering the Valve-Point Effects", Int. J. of Energy Conversion and Management, Vol. 53, No. 1, January 2012, pp. 175-181.
[72] A. I. Selvakumar, K. Thanushkodi, "A New Particle Swarm Optimization Solution to Nonconvex Economic Dispatch Problems", IEEE Transactions Power Systems, 2007, Vol. 22, No. 1, pp. 42-51.
[73] A. I. Selvakumar and K. Thanushkodi, "Anti-Predatory Particle Swarm Optimization: Solution to Nonconvex Economic Dispatch Problems", Electric Power Systems Research, Vol. 78, No. 1, January 2008, pp. 2-10.
[74] L. D. S. Coelho, R. C. T. Souza and V. C. Mariani, "Improved Differential Evolution Approach based on Cultural Algorithm and Diversity Measure Applied to Solve Economic Load Dispatch Problems", Mathematics and Computers in Simulation, Vol. 79, No. 10, June 2009, pp. 3136-3147.
[75] T. Niknam, "A New Fuzzy Adaptive Hybrid Particle Swarm Optimization Algorithm for Non-Linear, Non-Smooth and Non-Convex Economic Dispatch Problem", Applied Energy, Vol. 87, No. 1, January 2010, pp. 327-339.
[76] M. Basu, "Economic Environmental Dispatch Using Multi-objective Differential Evolution", Int. J. of Applied Soft Computing, Vol. 11, 2011, pp. 2845-2853.
[77] D. B. Das, and C. Patvardhan, "Solution of Economic Load Dispatch Using Real Coded Hybrid Stochastic Search", Int. J. Electr. Power Energy Syst. 1999, 21, pp.165-170.
[78] S. Pothiya, I. Ngamroo, and W. Kongprawechnon, "Application of Multiple Tabu Search Algorithm to Solve Dynamic Economic Dispatch Considering Generator constraints", Energy Convers Manag. 2008, 49, 506-516.
[79] W. Elsayed, Y. Hegazy, M. El-bages, and F. Bendary, "Improved Random Drift Particle Swarm Optimization with Self-Adaptive Mechanism for Solving the Power Economic Dispatch Problem", IEEE Transactions on Industrial Informatics, Vol. 13, No. 3, 2017, pp. 1017-1026.
[80] D. C. Secui, "A New Modified Artificial Bee Colony Algorithm for the Economic Dispatch Problem", Energy Conversion and Management, Vol. 89, 2015, pp. 43-62.
[81] P. K. Roy, S. Bhui, and C. Paul, "Solution of Economic Load Dispatch Using Hybrid Chemical Reaction Optimization Approach", Applied Soft Computing, vol. 24, 2014, pp. 109-125.
[82] I. Ciornei and E. Kyriakides, "A GA-API Solution for the Economic Dispatch of Generation in Power System Operation", IEEE Transactions on Power Systems, Vol. 27, No. 1, 2012, pp. 233-242.
[83] W. T. Elsayed and E. F. El-Saadany, "A Fully Decentralized Approach for Solving the Economic Dispatch Problem", IEEE Transactions on Power Systems, Vol. 30, No. 4, 2015, pp. 2179-2189.
[84] B. R. Adarsh, T. Raghunathan, T. Jayabarathi, and X.-S. Yang, "Economic Dispatch Using Chaotic Bat Algorithm", Energy, Vol. 96, 2016, pp. 666-675.
[85] X. Chen, B. Xu, and W.i Du, "An Improved Particle Swarm Optimization with Biogeography-Based Learning Strategy for Economic Dispatch Problems", Complexity, Vol. 2018, Article ID 7289674, 15 pages.

Date of publication: April 24, 2025.

Comparative Assessment of Antibacterial, Antifungal, Antimalarial, and Antioxidant Activity of Aqueous Methanolic Extracts of Common Culinary, Aromatic, and Traditional Medicinal Plants

Saleh M. Matar[1]
[1]Chemical Engineering Department, Faculty of Engineering and Computer Science, Jazan University, Jazan, 45142, Saudi Arabia.
Corresponding author: Saleh M. Matar (e-mail: sel-saidmatar@jazanu.edu.sa).

ABSTRACT Medicinal plants are fundamental sources of bioactive compounds that possess significant antimicrobial, antioxidant, and anti-inflammatory properties. They are commonly utilized in culinary, aromatic, and traditional medicine applications. This study presents a comparative analysis of the aqueous methanolic extracts of nine conventional plants—*Cinnamomum verum*, *Cuminum cyminum*, *Curcuma longa*, *Syzygium aromaticum*, *Cassia angustifolia*, *Elettaria cardamomum*, *Zingiber officinale*, *Foeniculum vulgare*, and *Ocimum basilicum*—focusing on their antimicrobial and antioxidant effects. The extracts were evaluated against various pathogenic strains, including Gram-positive bacteria, Gram-negative bacteria, fungi, and *Plasmodium chabaudi*. *Elettaria cardamomum* exhibited the strongest antibacterial activity, followed closely by *Cassia angustifolia*, *Syzygium aromaticum*, and *Zingiber officinale*, while *Cinnamomum verum* exhibited no antibacterial activity. *Curcuma longa*, *Cassia angustifolia*, and *Elettaria cardamomum* demonstrated notable antifungal properties. *Elettaria cardamomum* and *Cassia angustifolia* achieved high antimalarial activity against *Plasmodium chabaudi*, while *Foeniculum vulgare* and *Ocimum basilicum* exhibited moderate inhibition. Furthermore, the extracts displayed varying tendencies to scavenge DPPH and hydroxyl radicals, with *Cinnamomum verum* being the most effective in radical scavenging. The observed differences in biological activity are attributed to the unique phytochemical profiles of the plants, suggesting their potential as natural alternatives for managing infections and oxidative stress. Our findings highlight the significance of exploring medicinal plants for sustainable healthcare solutions, particularly in the context of rising antimicrobial resistance, while suggesting that further research into their synergistic effects and broader applications in food and health could enhance their therapeutic potential.
The study highlights the significant antimicrobial activity of various plant extracts, with *Elettaria cardamomum* and *Cassia angustifolia* showing strong antibacterial and antifungal properties, particularly against Gram-positive bacteria and certain fungi. These effects are attributed to bioactive compounds that disrupt microbial cell structures and induce oxidative stress.
Additionally, the plants demonstrated varying antioxidant activities, with *Cinnamomum verum* exhibiting strong radical scavenging capabilities, while *Curcuma longa* showed the weakest effects. The differences in antioxidant potential are linked to the unique phytochemical profiles of each plant, which include flavonoids, phenolics, and essential oils.

INDEX TERMS Antioxidants, Antimicrobial Activity, Traditional Medicine, Phytochemicals, Medicinal Plants.

I. INTRODUCTION

Commonly used traditional plants offer a wealth of therapeutic applications in cultural practices [1]. They are rich in bioactive compounds that exhibit antioxidant, anti-inflammatory, and antimicrobial properties, which make them effective for managing various diseases and promoting health [2, 3]. These plants serve as natural alternatives to synthetic drugs, with fewer side effects, and are readily available in rural areas. Moreover, their use can lead to synergistic effects and contribute to the discovery of new

pharmaceuticals, as most advanced medicines are derived from plant sources [4, 5]. Antimicrobials such as antibacterial, antiviral, antifungal, and antiparasitic drugs can be used to prevent and treat infections, assisting in the prevention of the spread of infectious diseases [6]. The emergence of antimicrobial resistance emphasizes the importance of finding advanced antimicrobial methods and suggests the use of plant-derived natural products as potential solutions.

On the other hand, free radicals are generated by the normal function of tissues in a biological system. They are involved in the control of signal transduction, gene expression, and receptor activation. However, an excess of free radicals, such as superoxide, hydrogen peroxide, hydroxyl, and nitrogen radicals, is toxic and a primary cause of oxidative stress. Oxidative stress leads to numerous diseases, including age-related disorders, neurodegenerative diseases, atherosclerosis, infections, cancer, and diabetes [7]. Antioxidants and antimicrobial agents play crucial roles in health and disease prevention. They neutralize free radicals, which can damage cells and lead to chronic diseases. By combating oxidative damage, antioxidants support overall cellular health and may enhance longevity.

Recently, interest in plants has greatly increased; therefore, most regulatory guidelines and pharmacopeia suggest a chemical analysis of plant materials, including fractions and extracts, to find natural antioxidants for human diseases linked to oxidative stress. Echinacea and goldenseal are used for immune-boosting and antibacterial effects, respectively, while ginger and turmeric are employed for their anti-inflammatory properties. Adaptogens like ashwagandha and rhodiola serve traditional applications. Many phytochemicals play a significant role in neutralizing free radicals, quenching single and triple oxygen, or decomposing peroxides. An inverse relationship has been reported between lower incidence and mortality rates for many human diseases and increased antioxidant status [8]. Plants contain free radical scavengers, such as polyphenols, flavonoids, and phenolic compounds, which inhibit the adverse effects of oxidative stress [9, 10].

Plants such as *Cinnamomum verum* (cinnamon), *Cuminum cyminum* (cumin), *Curcuma longa* (turmeric), *Syzygium aromaticum* (clove), *Cassia angustifolia* (senna), *Elettaria cardamomum* (cardamom), *Zingiber officinale* (ginger), *Foeniculum vulgare* (fennel), and *Ocimum basilicum* (basil) are commonly utilized in many countries worldwide. The selected plants have been used in traditional medicine due to their potent healing properties and contemporary holistic approaches. Various clinical studies have assessed their role in treating many diseases, such as digestive disorders, respiratory issues, and skin conditions. They possess diverse medicinal properties, culinary applications, and ecological significance and are studied for their health benefits, including anti-inflammatory, antimicrobial, and digestive properties, as well as their potential in managing chronic diseases and improving food preservation. Their rich phytochemical profiles make them beneficial for discovering new therapeutic applications. Hence, this study aims to evaluate the antimicrobial and antioxidant properties of aqueous methanolic extracts of conventional plants, including *Cinnamomum verum*, *Cuminum cyminum*, *Curcuma longa*, *Syzygium aromaticum*, *Cassia angustifolia*, *Elettaria cardamomum*, *Zingiber officinale*, *Foeniculum vulgare*, and *Ocimum basilicum*. Additionally, it aims to provide recommendations for incorporating these extracts into food, nutraceuticals, and herbal medicine, ultimately enhancing the understanding of their health benefits and potential applications in disease prevention and treatment. The study paves the way for alternatives to conventional therapy to address the growing challenge of antimicrobial resistance.

II. Materials and Methods

Selection of Plants

The dried plant materials were obtained from a local market in Saudi Arabia. The plant materials consist of *Cinnamomum verum* (cinnamon), *Cuminum cyminum* (cumin), *Curcuma longa* (turmeric), *Syzygium aromaticum* (clove), *Cassia angustifolia* (senna), *Elettaria cardamomum* (cardamom), *Zingiber officinale* (ginger), *Foeniculum vulgare* (fennel), and *Ocimum basilicum*. They are widely used because of their versatile applications, as depicted in Table 1, which shows the scientific names, family names, and traditional uses for these plants.

Table 1 List of plant materials

No	Plant name	The scientific name	Family name	Traditional uses
1	Cinnamon	*Cinnamomum verum*	Lauraceae	Aromatic
2	Cumin	*Cuminum cyminum*	Apiaceae	Culinary
3	Turmeric	*Curcuma longa*	Zingiberaceae	Culinary/Aromatic
4	Clove	*Syzygium aromaticum*	Myrtaceae	Aromatic
5	Senna	*Cassia Angustifolia*	Caesalpinaceae	Medicinal

6	Cardamomum	*Elettaria cardamomum*	Zingiberaceae	Culinary/Aromatic
7	Ginger	*Zingiber officinale*	Zingiberaceae	Culinary/Aromatic
8	Sweet Fennel	*Foeniculum vulgare*	Carrot (Apiaceae)	Culinary/Aromatic
9	Ocimum	*Ocimum basilicum*	Lamiaceae	Culinary/Aromatic

Preparation of Extracts

About 20 g of dried plant materials were soaked in 50 ml of 80% (v/v) aqueous methanol at room temperature for 3 days in a dark place. The soaked material was stirred every 18 h using a sterilized glass rod. It was then filtered and centrifuged for 20 mins to get the clear supernatant, which was evaporated to dryness for 24 h at room temperature. The remaining extract was freeze-dried and stored at -20^{o} C.

Antimicrobial Activity Assays

Inoculum preparation

Trichophyton rubrum ATCC 28189, *Candida albicans* ATCC 10231, and *Candida tropicalis ATCC* 13803 were cultivated in compliance with Clinical Laboratory and Standard Institute document M27-A3 [11]. Fungal strains were cultivated for 48 h on Sabouraud-dextrose (SD, Acumedia, USA) agar, and the isolated colonies were subsequently suspended in a 0.85% NaCl saline solution (Synth, Brazil). The density of the resultant suspension was calibrated to 106 colony-forming units (CFU)/ml, equivalent to the 0.5 McFarland standard. Subsequently, 1 ×10^3 CFU/ml of SD broth (Acumedia, USA) was utilized to dilute the fungal solution. Suspensions of Gram-negative and Gram-positive bacteria, such as *Bacillus subtilis* ATCC 6633, *Staphylococcus aureus* ATCC 24213, *Enterococcus faecalis* ATCC 51299, *Klebsiella pneumonia* ATCC 700603, *Escherichia coli* ATCC 47076, and *Pseudomonas aeruginosa* ATCC 27853, were cultured on Petri dishes containing nutrient broth (NB, HiMedia, India) for 24 h at 37°C. After the incubation period, each strain was diluted to a final concentration of 10^5 cells/ml utilizing sterile Ringer's solution. The Department of Biological Sciences at King Faisal University in Saudi Arabia kindly provided all test strains.

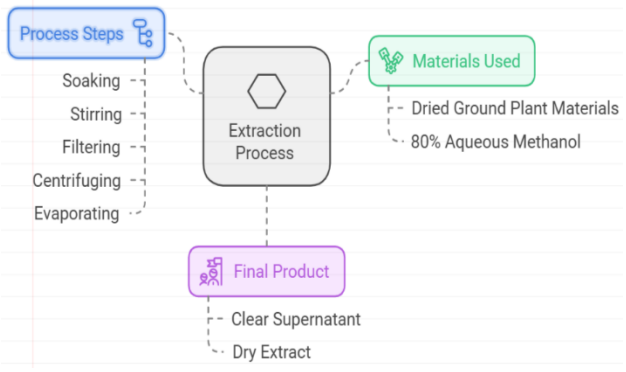

Figure 1 Preparation of extracts

Antimicrobial test

The agar well diffusion method, as detailed by [12], was used to conduct the experiment. Using a non-toxic swab, a fresh microbial culture containing 100 microliters (10^6 CFU/ml) was spread on a Muller Hilton agar plate. Using a sterile cork-borer (6 mm), four 6-mm diameter wells were created in the agar medium, and 100 µl (500 mg/ml) of each plant extract was added to each well using a micropipette while maintaining aseptic conditions. DMSO was employed as the control group. The plates were allowed to stand for one hour to allow the extract to pre-diffuse into the medium. The plates were then incubated for 24 to 48 h at 37 ± 2°C in an upright position under aerobic conditions. The inhibition zone (mm) was measured to assess the antimicrobial activity.

Minimum inhibitory concentration

The broth microdilution method was used to determine the minimum inhibitory concentration (MIC) [13, 14]. MIC values were utilized to estimate the antibacterial activity of plant extracts against pathogenic bacterial and fungal strains. In summary, the refined substance was dissolved in DMSO (1 mg/ml, Sigma-Aldrich, USA) in a 96-well plate and diluted twice to achieve concentrations of 1000–0.5 µg/ml. After injecting 100 µl of each pathogen suspension and 100 µl of the tested plant extract into each well, the combination was incubated at 37°C for 48 h. At the conclusion of the incubation period, the MIC values—the lowest concentrations of the drug that prevent microbial growth—were noted. Amphotericin B® and streptomycin (Sigma Chemical Co., St. Louis, MO, USA) were added as positive controls, and experiments were run in parallel with DMSO serving as the solvent control. Every test was performed in triplicate.

***In vitro* antiplasmodial activity**

An approach from [15] was slightly adjusted to evaluate the antimalarial activity. To summarize, 1.0 mg of each extract was diluted and dissolved in DMSO to create a (5.0 mg/mL) stock solution, which was then kept at -20°C until needed. The Department of Biological Sciences at King Faisal University in Saudi Arabia provided 200 µl of *Plasmodium chabaudi*, a malarial parasite. The parasite was grown in a 24-well culture plate at different dosages (0.01–10 mg/ml) for 48 h at 37°C. Dihydroartemisinin, a typical antimalarial medication, was utilized as a positive control in this method. Negative controls were created with 1% DMSO. Inhibition of the parasite was quantified as a percentage of the growth of the untreated (negative) control. Every investigation was conducted in triplicate.

Assay of Antioxidant Activity

Scavenging of DPPH Radical Method

DPPH radical is frequently utilized to study the free radical scavenging ability of natural candidates. It includes measuring the scavenging properties of specific substances against a stable radical. The scavenging activity was assessed as follows: 0.5 mL of the extracts (0.1–0.5 mg/mL) were mixed with 3 mL of a 0.1 mM solution of DPPH in methanol and left in a dark place for about 30 mins. The absorbance was recorded at 517 nm using a UV-Vis spectrophotometer. Blank samples were used to control the experiment, containing (DPPH and methanol instead of the sample. Vitamin C was used as a typical antioxidant. The activity of the extracts was expressed as a percentage of inhibition (% inhibition) of each free radical scavenging activity (Sanchez-Moreno et al. (1998) [16].

Hydroxyl Radical Scavenging Method

This method is estimated by an advanced Fenton-type reaction. Equal amounts of the investigated candidates were incubated with 9 mM FeSO4, 9 mM salicylic acid-ethanol, and 9 mM H_2O_2 at 37°C for one h, and absorbance was recorded at 510 nm. Distilled water was used as a control, and ascorbic acid served as a positive control. Finally, the hydroxyl radical scavenging activity was determined [17].

Statistical Analysis

The data represent the mean of three replicates ± standard error mean (SEM) using SPSS version 20.0 (Statistical Package for the Social Sciences, Inc., Chicago, IL, United States).

III. Results

Antimicrobial Activity

The antibacterial activity of the investigated plant aqueous methanolic extracts against six pathogenic bacteria is shown in Table 2. Three Gram-negative bacteria (*Pseudomonas aeruginosa*, *Escherichia coli*, and *Klebsiella pneumonia)* and three Gram-positive bacteria *(Staphylococcus aureus*, *Bacillus subtilis*, and *Enterococcus faecalis*) were employed as pathogenic bacteria. The antibacterial activity was assessed by measuring the zone of inhibition in millimeters (mm) after incubation of each bacterium with each plant extract. Among the tested extracts, *Elettaria cardamomum* exhibited the highest inhibition, revealing strong antibacterial properties, followed by *Cassia angustifolia*, *Syzygium aromaticum*, and *Zingiber officinale*, which exhibited notable inhibition. In contrast, *Ocimum basilicum* demonstrated moderate effectiveness. *Foeniculum vulgare* and *Cuminum cyminum* showed limited activity. *Curcuma longa* and *Cinnamomum verum* exhibited weaker antibacterial effects. Overall, the findings highlighted that *Elettaria cardamomum* and *Cassia angustifolia* are potent antibacterial agents.

Table 2 Antibacterial activity of investigated plant extracts against pathogenic bacteria

	Zone of inhibition (mm) of each Pathogenic bacterium					
	Pseudomonas aeruginosa	*Escherichia coli*	*Klebsiella pneumonia*	*Staphylococcus aureus*	*Bacillus subtilis*	*Enterococcus faecalis*
Cinnamomum verum	5.7±0.47	3.5±0.40	3.9±0.28	8.4±0.30	7.9±0.15	10.2±0.27
Cuminum cyminum	2.1 ± 0.41	na	3.7±0.88	6.1±0.66	13.5±0.32	11.9±0.65
Curcuma longa	na	na	na	8.9±0.22	4.2±0.45	5.8±0.81
Syzygium aromaticum	18.6±0.11	19.2±0.22	17.8±0.16	22.8±0.56	22.9±0.62	13.2±0.21
Cassia Angustifolia	14.2±0.5	19.8±0.20	11.6±0.70	29.7±0.28	24.8±0.15	28.1±0.25
Elettaria cardamomum	23.2±0.11	30.4±0.11	24.2±0.62	29.7±0.41	20.9±0.22	24.3±0.37
Zingiber officinale	20.3±0.52	15.5±0.76	13.6±0.14	14.4±0.27	21.1±0.58	25.9±0.16
Foeniculum vulgare	9.7±0.57	13.4±0.71	11.2±0.42	9.8±0.34	8.3±0.31	14.2±0.23
Ocimum basilicum	20.1±0.15	11.2±0.18	10.2±0.22	na	na	na
Streptomycin	35.3±0.85	28.8±0.48	30.0±0.87	30.2±0.77	33.9±0.49	32.6±0.33
DMSO	-	-	-	-	-	-

Growth Inhibition Zone (mm) ± SEM; na: not active
Amphotericin B as antibacterial positive control.
1% dimethyl sulfoxide (DMSO); negative control.

The antifungal action of the investigated plant aqueous methanolic extracts was assessed using three pathogenic fungal strains: *Candida tropicalis*, *Candida albicans*, and *Trichophyton rubrum*. The antifungal activity was measured by the zone of inhibition (mm), as shown in Table 3. Notably, *Cinnamomum verum* showed no activity against any of the tested fungi. In contrast, *Cuminum cyminum* demonstrated minimal effectiveness, with inhibition zones of 3.0 ± 0.92 mm against *Candida tropicalis* and 5.9 ± 0.50 mm against *Candida albicans*. *Syzygium aromaticum* showed slightly lower inhibition with 8.7 ± 0.76 mm for *Candida tropicalis* and 12.7 ± 0.52 mm for *Candida albicans*. *Curcuma longa* exhibited strong antifungal activity, particularly against *Candida tropicalis* (23.7 ± 0.22 mm) and *Trichophyton rubrum* (21.8 ± 0.96 mm). Both *Cassia angustifolia* and *Elettaria cardamomum* displayed promising antifungal properties, with *Cassia angustifolia* achieving the highest inhibition against *Candida tropicalis* (29.1 ± 0.79 mm). *Elettaria cardamomum* and *Zingiber officinale* showed the highest overall inhibition. In contrast, *Foeniculum vulgare* and *Ocimum basilicum* exhibited limited antifungal activity, with the lowest inhibition zones observed. Overall, the results indicated that several plant extracts, particularly *Cassia angustifolia* and *Elettaria cardamomum*, exhibited significant antifungal effects, highlighting their potential for therapeutic applications.

Table 3 Antifungal activity of investigated plant extracts against fungal pathogenic strains

	Zone of inhibition (mm) of each pathogenic fungus		
	Candida tropicalis	*Candida albicans*	*Trichophyton rubrum*
Cinnamomum verum	na	na	Na
Cuminum cyminum	3.0±0.92	5.9±0.50	Na
Curcuma longa	23.7 0.22	14.2±0.70	21.8±0.96
Syzygium aromaticum	8.7.3±0.76	12.7±0.52	18.4±0.21
Cassia Angustifolia	29.1±0.79	27.6±0.55	25.4±0.40
Elettaria cardamomum	28.2±0.88	29.9±0.67	31.1±0.41
Zingiber officinale	30.6±0.26	31.5±0.26	20.7±0.36
Foeniculum vulgare	12.4±0.37	13.1±0.46	6.4±0.25
Ocimum basilicum	3.8±0.72	9.4±0.29	3.5±0.12
Amphotericin B	22.2±0.97	24.8±0.40	31.1±0.80
DMSO	-	-	-

Growth Inhibition Zone (mm) ± SEM; na: not active
Streptomycin as a positive antifungal control.
1% dimethyl sulfoxide (DMSO); negative control.

The MIC values (µg/ml) of the investigated plant extracts against specific bacterial and fungal pathogens were measured and displayed in *Table 4*. It was noted that aqueous methanolic plant extracts exhibited significant variability in effectiveness. For fungal pathogens, *Candida albicans* exhibited sensitivity at 31.25 µg/ml for certain extracts, while others require higher concentrations. *Syzygium aromaticum*, *Cassia angustifolia*, *Elettaria cardamomum*, and *Zingiber officinale* demonstrated strong activity with MIC values among the other extracts, ranging from 500 to 31.25 µg/ml. In contrast, Amphotericin B, the positive antifungal control, had an MIC value of 0.5 µg/ml. Other extracts showed moderate to weak activity with MIC values ranging from 500 to >1000 µg/ml. Overall, the findings suggest the potential for certain plant extracts as alternative antimicrobial agents, warranting further investigation.

Table 4 Minimum inhibitory concentration (MIC) values (µg/ml) of some plant extracts against bacterial and fungal pathogenic strains

	Pathogen	Plant extracts (µg/ml)								
		Cinnamomum verum	*Cuminum cyminum*	*Curcuma longa*	*Syzygium aromaticum*	*Cassia Angustifolia*	*Elettaria cardamomum*	*Zingiber officinale*	*Foeniculum vulgare*	*Ocimum basilicum*
Bacteria	*Pseudomonas aeruginosa*	500	500	>1000	125	250	250	125	500	125
	Escherichia coli	500	>1000	>1000	125	250	125	250	250	500
	Klebsiella pneumonia	>1000	125	>1000	125	250	250	125	500	500
	Staphylococcus aureus	>1000	500	500	62.5	31.25	62.5	62.5	500	>1000
	Bacillus subtilis	500	125	500	62.5	31.25	250	250	500	>1000
	Enterococcus faecalis	>1000	250	250	250	31.25	125	250	250	>1000
Fungi	*Candida tropicalis*	>1000	250	125	500	31.25	31.25	31.25	500	250
	Candida albicans	>1000	250	125	500	62.5	31.25	31.25	251	250
	Trichophyton rubrum	>1000	>1000	250	125	125	62.5	31.25	250	>1000
	DMSO	–	–	–	–	–	–	–	–	–

The antimalarial activity of nine aqueous methanol plant extracts against *Plasmodium chabaudi* after a 48-hour incubation period is presented in Table 5. The activity is measured as the percentage of inhibition at different concentrations (0.01–10 mg/ml) of each plant extract. At the lowest concentration of 0.01 mg/ml, *Elettaria cardamomum* demonstrated the highest inhibition at 20.7 ± 0.8%, while *Cuminum cyminum* showed the least effect at 2.3 ± 1.6%. As the concentration increased to 0.1 mg/ml, *Cassia angustifolia* exhibited a notable rise in inhibition to 43.9 ± 2.6%, positioning it among the more effective extracts, whereas *Cuminum cyminum* remained low at 3.8 ± 3.4%. At a concentration of 1.0 mg/ml, *Cassia angustifolia* again led with 72.8 ± 4.7% inhibition, while other extracts like *Elettaria cardamomum* and *Zingiber officinale* also showed significant activity (60.7 ± 2.1% and 59.3 ± 6.8%, respectively). The highest concentration of 10 mg/ml revealed that *Elettaria cardamomum* achieved a potent 91.3 ± 3.2% inhibition, closely followed by *Cassia angustifolia* at 89.9 ± 3.2%. In comparison, the synthetic antimalarial drug dihydroartemisinin exhibited potent effects, with inhibition rates exceeding 97% across all concentrations tested. The negative control group, which received no mutagen, showed no inhibition. Overall, the results implied that *Foeniculum vulgare* and *Ocimum basilicum* exhibited moderate inhibition. Moreover, *Cassia angustifolia* and *Elettaria cardamomum* possessed significant antimalarial properties, highlighting their potential as alternative therapeutic agents.

Table 5 *In vitro* antimalarial activity of methanolic plant extracts against *P. chabaudi* after 48 h incubation period

Conc. (mg/ml)	% of inhibition									
	Cinnamomum verum	*Cuminum cyminum*	*Curcuma longa*	*Syzygium aromaticum*	*Cassia Angustifolia*	*Elettaria cardamomum*	*Zingiber officinale*	*Foeniculum vulgare*	*Ocimum basilicum*	dihydroartemisinin
0.01	9.97±0.7	2.3±1.6	8.9±5.4	1.1±2.1	15.7±4.1	20.7±0.8	12.3±5.4	10.5±2.6	13.9±0.4	95.3±2.5

0.1	11.94±1.3	3.8±3.4	10.1±6.8	1.8±0.8	43.9±2.6	25.8±2.5	28.7±6.2	16.8±4.8	14.5±1.8	97.6±3.2
1.0	14.5±1.1	6.9±1.5	10.9±4.2	2.3±1.8	72.8±4.7	60.7±2.1	59.3±6.8	24.6±3.7	50.8±1.2	97.9±1.8
10	15.2±2.2	28.7±0.9	12.5±4.2	2.5±3.3	89.9±3.2	91.3±3.2	88.7±4.3	41.9±1.9	60.2±3.7	98.1±2.7

Antioxidant activity

Antioxidant activity (DPPH free radical scavenging activity) of methanolic extracts:

The principle is that when DPPH radicals are incubated with substances that have antioxidant properties, DPPH is reduced from its characteristic violet to a yellow-colored radical, which is measured calorimetrically. The DPPH radical scavenging activity of various plant extracts is denoted in Figure 1. All the extracts displayed distinct levels of DPPH radical scavenging activity. The value of antioxidant activity with a percentage of inhibition for *Cinnamomum verum*, *Cuminum cyminum*, *Curcuma longa*, *Syzygium aromaticum*, *Cassia angustifolia*, *Elettaria cardamomum*, and *Zingiber officinale* was found to be 55.4%, 89.93%, 15.95%, 88.12%, 71.71%, 16.74%, 70.9%, 89.59%, and 90.15%, respectively. *Ocimum basilicum*, *Cuminum cyminum*, *Syzygium aromaticum*, and *Foeniculum vulgare* exhibited robust DPPH radical scavenging activity compared to other extracts, while *Curcuma longa* exhibited the weakest DPPH radical scavenging activity. The radical scavenging activity of the plant extracts was in the following order: *Ocimum basilicum* > *Cuminum cyminum* > *Foeniculum vulgare* > *Syzygium aromaticum* > *Cassia Angustifolia* > *Zingiber officinale* > *Cinnamomum verum* > *Elettaria cardamomum* > *Curcuma longa.*

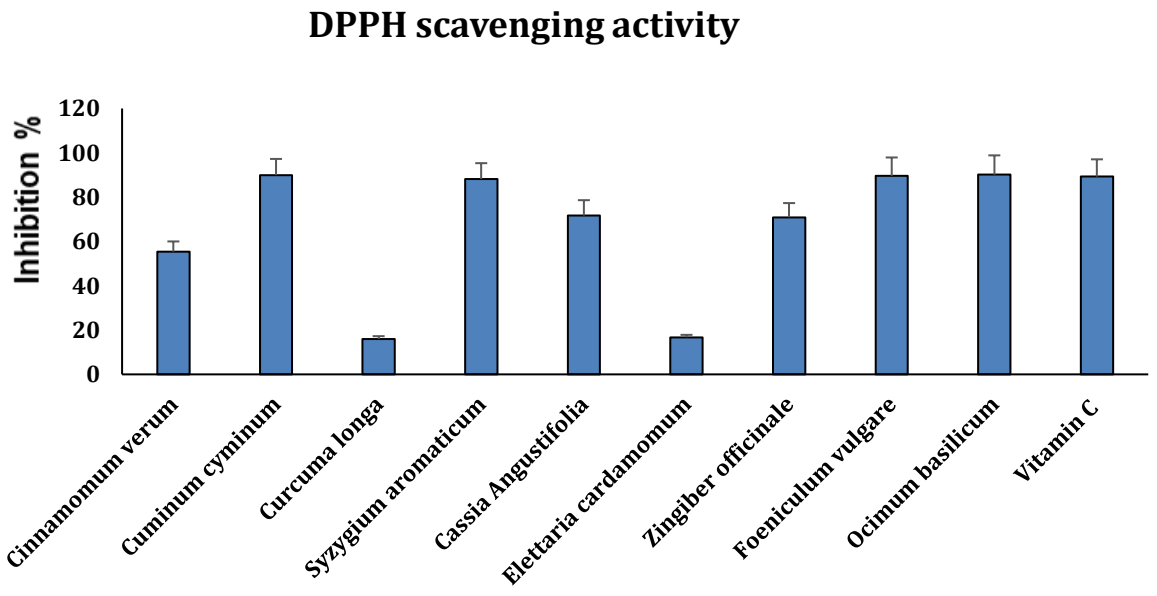

Figure 2 DPPH scavenging activity for the different plant extracts.

Antioxidant activity (Hydroxyl radical scavenging activity) of methanolic extracts

Hydroxyl radicals can easily penetrate cell membranes to interact with many biomolecules, inducing tissue injury or cellular death. Therefore, eliminating hydroxyl radicals is critical for protecting living systems [18, 19]. The plant extracts' hydroxyl radical scavenging activity of *Cinnamomum verum*, *Cuminum cyminum*, *Curcuma longa*, *Syzygium aromaticum*, *Cassia angustifolia*, *Elettaria cardamomum*, *Zingiber officinale*, *Foeniculum vulgare*, and *Ocimum basilicum* was found to be 86.1%, 5.4%, 9.55%, 19.2%, 8.3%, 31.1%, 30.8%, 16.3%, and 1.5%, respectively, as shown in Figure 3. The highest hydroxyl radical scavenging capabilities were recorded for the extract of *Cinnamomum verum*. The extracts of *Cuminum cyminum*, *Curcuma longa*, *Syzygium aromaticum*, *Cassia angustifolia*, *Elettaria cardamomum*, *Zingiber officinale*, *Foeniculum vulgare*, and *Ocimum basilicum* showed moderate to weak hydroxyl radical scavenging activity, with the extract of *Ocimum* basilicum showing the lowest scavenging activity.

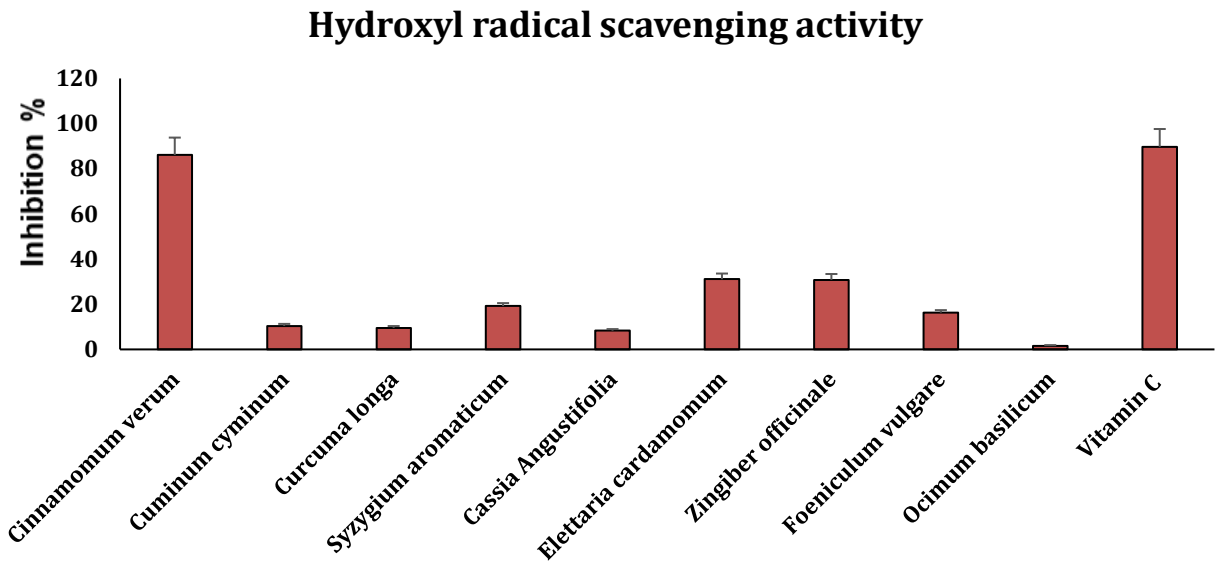

Figure 3 Hydroxyl radical scavenging activity for the different plant extracts.

IV. Discussion

Medicinal plants are crucial sources of bioactive and pharmaceutically important compounds that have antimicrobial, antioxidant, anti-inflammatory, and various other biological and medicinal applications. Some of these plants are commonly used in everyday life as medicinal, culinary, and aromatic agents. In this study, the aqueous methanolic extract of conventional plants, including *Cinnamomum verum*, *Cuminum cyminum*, *Curcuma longa*, *Syzygium aromaticum*, *Cassia angustifolia*, *Elettaria cardamomum*, *Zingiber officinale*, *Foeniculum vulgare*, and *Ocimum basilicum*, has been comparatively investigated for its antimicrobial and antioxidant properties.

Plants like *Cinnamomum verum* (cinnamon), *Cuminum cyminum* (cumin), *Curcuma longa* (turmeric), *Syzygium aromaticum* (clove), *Cassia angustifolia* (senna), *Elettaria cardamomum* (cardamom), *Zingiber officinale* (ginger), *Foeniculum vulgare* (fennel), and *Ocimum basilicum* (basil) are commonly utilized in many countries worldwide due to their diverse medicinal properties, culinary applications, and ecological significance. They are studied for their health benefits, including anti-inflammatory, antimicrobial, and digestive properties, as well as their potential in managing chronic diseases and improving food preservation. Their rich phytochemical profiles make them valuable for exploring new therapeutic applications and enhancing agricultural practices. This was in agreement with various studies that explored the biological applications of these plants [2, 3]. This is the first comparative analysis of the investigated plants.

Table 6 Key chemical compounds of investigated medicinal plants

No.	Plant	Key Chemical Compounds	References
1	*Cinnamomum verum*	Cinnamaldehyde, Eugenol, Coumarin, Myrcene and p-Cymene	[20-25]
2	*Cuminum cyminum*	Cuminaldehyde, Limonene, Thymol	[26-33]
3	*Curcuma longa*	Curcumin, Demethoxycurcumin, Bisdemethoxycurcumin	[34-42]
4	*Syzygium aromaticum*	Eugenol, Beta-caryophyllene, Acetyl eugenol	[43-52]
5	*Cassia angustifolia*	Sennosides (A and B), Anthraquinones	[53-62]
6	*Elettaria cardamomum*	1,8-Cineole, Limonene, Alpha-terpineol	[63-72]
7	*Zingiber officinale*	Gingerol, Shogaol, Zingerone	[33, 73-78]
8	*Foeniculum vulgare*	Anethole, Fenchone, Estragole	[79-87]
9	*Ocimum basilicum*	Eugenol, Linalool, Rosmarinic acid	[88-96]

The complex nature and composition of these plants indicate their potential for diverse applications based on their chemical profiles. The antibacterial, antifungal, and antimalarial activities of various plant aqueous methanolic extracts were evaluated against pathogenic strains. Three Gram-negative bacteria (*Pseudomonas aeruginosa*, *Escherichia coli*, and *Klebsiella pneumonia)* and three Gram-positive bacteria *(Staphylococcus aureus*, *Bacillus subtilis*, and *Enterococcus faecalis*) were employed as pathogenic bacteria. *Elettaria cardamomum* emerged as the most effective antibacterial agent, followed closely by *Cassia angustifolia*, *Syzygium aromaticum*, and *Zingiber officinale*, while *Cinnamomum verum* showed no

antibacterial activity. Gram-positive bacteria were more susceptible to the methanolic extracts of *Elettaria cardamomum*, which could be related to the presence of 1,8-Cineole, as suggested by previous studies [97–99], and Limonene [100, 101], as well as other active components such as Alpha-terpineol [102, 103]. Furthermore, *Syzygium aromaticum contains* Eugenol [104, 105] and Beta-caryophyllene [106], which have been reported in other studies to exhibit antimicrobial activity. The antifungal assessments of the investigated plant aqueous methanolic extracts against three pathogenic fungal strains—*Candida tropicalis*, *Candida albicans*, and *Trichophyton rubrum*—were measured by the zone of inhibition. *Curcuma longa* exhibited strong inhibition, particularly against *Candida tropicalis*, which is in agreement with previous studies showing the potential antimicrobial activities of its aqueous extract [107, 108]. Both *Cassia angustifolia* and *Elettaria cardamomum* demonstrated significant antifungal properties [60, 109, 110]. In contrast, *Foeniculum vulgare* and *Ocimum basilicum* showed limited antifungal activity, with the lowest inhibition zones observed. In the evaluation of antimalarial activity against *Plasmodium chabaudi*, Dihydroartemisinin is a drug used to treat malaria effectively through the production of free radicals that damage the essential biomolecules needed for the growth of *Plasmodium chabaudi*. The plant extracts exhibited antimalarial activities in different potencies. *Foeniculum vulgare* and *Ocimum basilicum* exhibited moderate inhibition, while *Elettaria cardamomum* and *Cassia angustifolia* achieved high inhibition rates. Specific compounds may target the metabolic pathways of Plasmodium species [111–113]. Furthermore, these extracts may enhance the host's immune response, aiding in infection clearance. Overall, the results suggest that *Cassia angustifolia* and *Elettaria cardamomum* possess considerable potential as therapeutic agents against bacterial, fungal, and malaria infections. This could be attributed to the bioactive compounds that disrupt microbial cell walls [114], inhibit protein and nucleic acid synthesis [115, 116], and alter cell membrane permeability, leading to cell lysis [117, 118]. Additionally, they may generate reactive oxygen species (ROS) that induce oxidative stress, damaging cellular components [119]. The synergistic effects of multiple phytochemicals can enhance antimicrobial efficacy [120]. Collectively, these mechanisms highlight the therapeutic potential of plant extracts as natural alternatives to conventional treatments, especially in light of increasing drug resistance. The promising antibacterial, antifungal, and antimalarial activities of these plant extracts underscore their potential as therapeutic agents in combating infectious diseases. The implications of these findings suggest a future where natural plant extracts could play a vital role in public health strategies, particularly in the context of rising antimicrobial resistance and the need for sustainable healthcare solutions.

Furthermore, the study examined the ability of various plant extracts to neutralize DPPH and hydroxyl radicals. The extracts demonstrated varying levels of DPPH and hydroxyl radical scavenging activity, with notable percentages of inhibition for *Cinnamomum verum and Cuminum cyminum*, while *Curcuma longa* showed the weakest effect. Additionally, the extracts' ability to scavenge hydroxyl radicals varied, with *Cinnamomum verum* showing the strongest activity, whereas *Ocimum basilicum* had the lowest. The variation in antioxidant actions of the plant extracts can be related to their unique phytochemical compositions, which include varying levels of flavonoids, phenolics, and essential oils that affect their ability to neutralize radicals. Each plant has developed different mechanisms for oxidative stress modification. Additionally, some extracts may contain synergistic compounds that enhance overall effectiveness. The relationship between antioxidant mechanisms and antimicrobial efficacy needs further exploration to understand their combined effects better.

V. Conclusion

The study identified significant antimicrobial and antioxidant properties of the aqueous methanolic extracts of several medicinal plants. *Elettaria cardamomum* emerged as the strongest antibacterial agent, particularly effective against Gram-positive bacteria, while *Curcuma longa* showed pronounced antifungal activity against *Candida tropicalis*. Additionally, various extracts effectively scavenged DPPH and hydroxyl radicals, with *Cinnamomum verum* exhibiting the highest antioxidant activity. These findings underscore the therapeutic potential of these plants as natural alternatives to combat infections and oxidative stress, particularly in light of increasing antimicrobial resistance. Future research could explore the synergistic effects of combinations of these plants to enhance their efficacy against resistant strains of pathogens. It is important to incorporate these extracts into food, nutraceuticals, and herbal medicine, ultimately enhancing the understanding of their health benefits and potential applications in disease prevention and treatment. Additionally, studies on the potential applications of these plants in food preservation and their role in boosting immune responses could provide insights into their broader health benefits.

Data Availability Statement: Data are available from the corresponding author upon request.

Conflicts of Interest: There are no financial or non-financial conflicts of interest or personal ties that could have influenced this study.

REFERENCES

[1] P.J. Houghton, The role of plants in traditional medicine and current therapy, The Journal of Alternative and Complementary Medicine 1(2) 1995 pp. 131-143.

[2] A. Balkrishna, N. Sharma, D. Srivastava, A. Kukreti, S. Srivastava, V. Arya, Exploring the Safety, Efficacy, and Bioactivity of Herbal Medicines: Bridging Traditional Wisdom and Modern Science in Healthcare, Future Integrative Medicine 3(1) 2024 pp. 35-49.

[3] C.-T. Che, V. George, T. Ijinu, P. Pushpangadan, K. Andrae-Marobela, Traditional medicine, Pharmacognosy, Elsevier2024, pp. 11-28.
[4] O.I. Ogidi, N.G. Emaikwu, Adoption and application of biotechnology in herbal medicine practices, Herbal medicine phytochemistry: Applications and trends, Springer2024, pp. 1601-1626.
[5] M. Fayiah, M.S. Fayiah, S. Saccoh, M.K. Kallon, Value of herbal medicine to sustainable development, Herbal Medicine Phytochemistry: Applications and Trends, Springer2024, pp. 1429-1456.
[6] D.G. Allison, P.A. Lambert, Modes of action of antibacterial agents, Molecular medical microbiology, Elsevier2024, pp. 597-614.
[7] H. Uguzlar, E. Malta, S.Z. Yildiz, SCREENING OF PHYTOCHEMICALS AND ANTIOXIDANT ACTIVITY OF ARUM DIOSCORIDIS SEEDS, Journal of Food Biochemistry 36 2012 pp. 285-291.
[8] A. Djeridane, M. Yousfi, B. Nadjemi, D. Boutassouna, P. Stocker, N. Vidal, Antioxidant activity of some algerian medicinal plants extracts containing phenolic compounds, Food Chemistry 97(4) 2006 pp. 654-660.
[9] G.A. Engwa, Free radicals and the role of plant phytochemicals as antioxidants against oxidative stress-related diseases, Phytochemicals: source of antioxidants and role in disease prevention. BoD–Books on Demand 7 2018 pp. 49-74.
[10] P. Chaudhary, P. Janmeda, A.O. Docea, B. Yeskaliyeva, A.F. Abdull Razis, B. Modu, D. Calina, J. Sharifi-Rad, Oxidative stress, free radicals and antioxidants: Potential crosstalk in the pathophysiology of human diseases, Frontiers in chemistry 11 2023 pp. 1158198.
[11] A. Standard, T. Edition, M27-A3, Wayne, PA: Clinical and Laboratory Standards Institute 2008 pp.
[12] A. Daoud, D. Malika, S. Bakari, N. Hfaiedh, K. Mnafgui, A. Kadri, N. Gharsallah, Assessment of polyphenol composition, antioxidant and antimicrobial properties of various extracts of Date Palm Pollen (DPP) from two Tunisian cultivars, Arabian Journal of Chemistry 12(8) 2019 pp. 3075-3086.
[13] O. Kayser, H. Kolodziej, Antibacterial activity of extracts and constituents of Pelargonium sidoides and Pelargonium reniforme, Planta medica 63(06) 1997 pp. 508-510.
[14] P. Masoko, D.M. Makgapeetja, Antibacterial, antifungal and antioxidant activity of Olea africana against pathogenic yeast and nosocomial pathogens, BMC complementary and alternative medicine 15 2015 pp. 1-9.
[15] A.S. Budimulja, S. Syafruddin, P. Tapchaisri, P. Wilairat, S. Marzuki, The sensitivity of Plasmodium protein synthesis to prokaryotic ribosomal inhibitors, 1997 pp.
[16] C.n. SÃ¡nchez-Moreno, J.A. Larrauri, F. Saura-Calixto, A procedure to measure the antiradical efficiency of polyphenols, Journal of the Science of Food and Agriculture 76(2) 1998 pp. 270-276.
[17] M.A. Ismail, A. Negm, R.K. Arafa, E. Abdel-Latif, W.M. El-Sayed, Anticancer activity, dual prooxidant/antioxidant effect and apoptosis induction profile of new bichalcophene-5-carboxamidines, Eur J Med Chem 169 2019 pp. 76-88.
[18] S. Di Meo, P. Venditti, Evolution of the knowledge of free radicals and other oxidants, Oxidative medicine and cellular longevity 2020(1) 2020 pp. 9829176.
[19] T.R. Kıran, O. Otlu, A.B. Karabulut, Oxidative stress and antioxidants in health and disease, Journal of Laboratory Medicine 47(1) 2023 pp. 1-11.
[20] R. Pathak, H. Sharma, A review on medicinal uses of Cinnamomum verum (Cinnamon), Journal of Drug Delivery and Therapeutics 11(6-S) 2021 pp. 161-166.
[21] N. Singh, A.S. Rao, A. Nandal, S. Kumar, S.S. Yadav, S.A. Ganaie, B. Narasimhan, Phytochemical and pharmacological review of Cinnamomum verum J. Presl-a versatile spice used in food and nutrition, Food Chemistry 338 2021 pp. 127773.
[22] H.M. Ahmed, A.M. Ramadhani, I.Y. Erwa, O.A.O. Ishag, M.B. Saeed, Phytochemical screening, chemical composition and antimicrobial activity of cinnamon verum bark, International Research Journal of Pure and Applied Chemistry 21(11) 2020 pp. 36-43.
[23] T. Liyanage, T. Madhujith, K. Wijesinghe, Comparative study on major chemical constituents in volatile oil of true cinnamon (Cinnamomum verum Presl. syn. C. zeylanicum Blum.) and five wild cinnamon species grown in Sri Lanka, 2017 pp.
[24] G.K. Jayaprakasha, L.J. Rao, K.K. Sakariah, Chemical composition of volatile oil from Cinnamomum zeylanicum buds, Zeitschrift für Naturforschung C 57(11-12) 2002 pp. 990-993.
[25] A.P.P. Farias, O.d.S. Monteiro, J.K.R. da Silva, P.L.B. Figueiredo, A.A.C. Rodrigues, I.N. Monteiro, J.G.S. Maia, Chemical composition and biological activities of two chemotype-oils from Cinnamomum verum J. Presl growing in North Brazil, Journal of Food Science and Technology 57 2020 pp. 3176-3183.
[26] A.R. Ladan Moghadam, Chemical composition and antioxidant activity Cuminum cyminum L. essential oils, International Journal of Food Properties 19(2) 2016 pp. 438-442.
[27] U. Karik, I. Demirbolat, Ö. Toluk, M. Kartal, Comparative study on yields, chemical compositions, antioxidant and antimicrobial activities of cumin (Cuminum cyminum L.) seed essential oils from different geographic origins, Journal of Essential Oil Bearing Plants 24(4) 2021 pp. 724-735.
[28] L. Gachkar, D. Yadegari, M.B. Rezaei, M. Taghizadeh, S.A. Astaneh, I. Rasooli, Chemical and biological characteristics of Cuminum cyminum and Rosmarinus officinalis essential oils, Food chemistry 102(3) 2007 pp. 898-904.
[29] H. Sowbhagya, Chemistry, technology, and nutraceutical functions of cumin (Cuminum cyminum

L): an overview, Critical reviews in food science and nutrition 53(1) 2013 pp. 1-10.
[30] H. Hajlaoui, H. Mighri, E. Noumi, M. Snoussi, N. Trabelsi, R. Ksouri, A. Bakhrouf, Chemical composition and biological activities of Tunisian Cuminum cyminum L. essential oil: A high effectiveness against Vibrio spp. strains, Food and Chemical Toxicology 48(8-9) 2010 pp. 2186-2192.
[31] J. Wanner, S. Bail, L. Jirovetz, G. Buchbauer, E. Schmidt, V. Gochev, T. Girova, T. Atanasova, A. Stoyanova, Chemical composition and antimicrobial activity of cumin oil (Cuminum cyminum, Apiaceae), Natural product communications 5(9) 2010 pp. 1934578X1000500904.
[32] K. Srinivasan, Cumin (Cuminum cyminum) and black cumin (Nigella sativa) seeds: traditional uses, chemical constituents, and nutraceutical effects, Food quality and safety 2(1) 2018 pp. 1-16.
[33] A.H. El-Ghorab, M. Nauman, F.M. Anjum, S. Hussain, M. Nadeem, A comparative study on chemical composition and antioxidant activity of ginger (Zingiber officinale) and cumin (Cuminum cyminum), Journal of agricultural and food chemistry 58(14) 2010 pp. 8231-8237.
[34] D.K. Gounder, J. Lingamallu, Comparison of chemical composition and antioxidant potential of volatile oil from fresh, dried and cured turmeric (Curcuma longa) rhizomes, Industrial crops and products 38 2012 pp. 124-131.
[35] N.T.K. LEELA, A. Tava, P.M. SHAFI, S.P. JOHN, B. CHEMPAKAM, Chemical composition of essential oil of turmeric (Curcuma longa L.), 2002 pp.
[36] J.J. Albaqami, H. Hamdi, A. Narayanankutty, N.U. Visakh, A. Sasidharan, A.M. Kuttithodi, A.C. Famurewa, B. Pathrose, Chemical composition and biological activities of the leaf essential oils of Curcuma longa, Curcuma aromatica and Curcuma angustifolia, Antibiotics 11(11) 2022 pp. 1547.
[37] A. Niranjan, S. Singh, M. Dhiman, S. Tewari, Biochemical composition of Curcuma longa L. accessions, Analytical Letters 46(7) 2013 pp. 1069-1083.
[38] A. Ikpeama, G. Onwuka, C. Nwankwo, Nutritional composition of Tumeric (Curcuma longa) and its antimicrobial properties, International Journal of Scientific and Engineering Research 5(10) 2014 pp. 1085-1089.
[39] A. Niranjan, D. Prakash, Chemical constituents and biological activities of turmeric (Curcuma longa l.)-a review, Journal of food Science and technology 45(2) 2008 pp. 109.
[40] N.S. Dosoky, W.N. Setzer, Chemical composition and biological activities of essential oils of Curcuma species, Nutrients 10(9) 2018 pp. 1196.
[41] G. Singh, I. Kapoor, P. Singh, C.S. de Heluani, M.P. de Lampasona, C.A. Catalan, Comparative study of chemical composition and antioxidant activity of fresh and dry rhizomes of turmeric (Curcuma longa Linn.), Food and chemical toxicology 48(4) 2010 pp. 1026-1031.
[42] S. Li, W. Yuan, G. Deng, P. Wang, P. Yang, B. Aggarwal, Chemical composition and product quality control of turmeric (Curcuma longa L.), 2011 pp.
[43] Q. Xue, Z. Xiang, S. Wang, Z. Cong, P. Gao, X. Liu, Recent advances in nutritional composition, phytochemistry, bioactive, and potential applications of Syzygium aromaticum L.(Myrtaceae), Frontiers in Nutrition 9 2022 pp. 1002147.
[44] G.A. Alitonou, F.P. Tchobo, F. Avlessi, B. Yehouenou, P. Yedomonhan, A.Y. Koudoro, C. Menut, D.K. Sohounhloue, Chemical and biological investigations of Syzygium aromaticum L. essential oil from Benin, International Journal of Biological and Chemical Sciences 6(3) 2012 pp. 1360-1367.
[45] K. Kaur, S. Kaushal, R. Rani, Chemical composition, antioxidant and antifungal potential of clove (Syzygium aromaticum) essential oil, its major compound and its derivatives, Journal of Essential Oil Bearing Plants 22(5) 2019 pp. 1195-1217.
[46] M.I. Nassar, A.H. Gaara, A.H. El-Ghorab, A. Farrag, H. Shen, E. Huq, T.J. Mabry, Chemical constituents of clove (Syzygium aromaticum, Fam. Myrtaceae) and their antioxidant activity, Revista Latinoamericana de Química 35(3) 2007 pp. 47.
[47] K. Chaieb, H. Hajlaoui, T. Zmantar, A.B. Kahla-Nakbi, M. Rouabhia, K. Mahdouani, A. Bakhrouf, The chemical composition and biological activity of clove essential oil, Eugenia caryophyllata (Syzigium aromaticum L. Myrtaceae): a short review, Phytotherapy Research: An International Journal Devoted to Pharmacological and Toxicological Evaluation of Natural Product Derivatives 21(6) 2007 pp. 501-506.
[48] G. El-Saber Batiha, L.M. Alkazmi, L.G. Wasef, A.M. Beshbishy, E.H. Nadwa, E.K. Rashwan, Syzygium aromaticum L.(Myrtaceae): traditional uses, bioactive chemical constituents, pharmacological and toxicological activities, Biomolecules 10(2) 2020 pp. 202.
[49] G.E.-S. Batiha, L.M. Alkazmi, L.G. Wasef, A.M. Beshbishy, E.H. Nadwa, E.K. Rashwan, Syzygium aromaticum L.(Myrtaceae): Traditional uses, bioactive chemical constituents, pharmacological and toxicological activities, Biomolecules 10(2) 2020 pp.
[50] S.M.A. Selles, M. Kouidri, B.T. Belhamiti, A. Ait Amrane, Chemical composition, in-vitro antibacterial and antioxidant activities of Syzygium aromaticum essential oil, Journal of Food Measurement and Characterization 14(4) 2020 pp. 2352-2358.
[51] K.A.K. Mohammed, H.M. Abdulkadhim, S.I. Noori, Chemical composition and anti-bacterial effects of clove (Syzygium aromaticum) flowers, International Journal of Current Microbiology and Applied Sciences 5(2) 2016 pp. 483-489.

[52] J.N. Haro-González, G.A. Castillo-Herrera, M. Martínez-Velázquez, H. Espinosa-Andrews, Clove essential oil (Syzygium aromaticum L. Myrtaceae): Extraction, chemical composition, food applications, and essential bioactivity for human health, Molecules 26(21) 2021 pp. 6387.

[53] K. Thaker, J. Patoliya, K. Rabadiya, N.R.R. Reddy, R. Joshi, Senna (Cassia angustifolia Vahl.): A Comprehensive Review of Ethnopharmacology and Phytochemistry, Pharmacological Research-Natural Products 2023 pp. 100003.

[54] S. Parveen, A. Shahzad, A. Upadhyay, V. Yadav, Gas chromatography-mass spectrometry analysis of methanolic leaf extract of Cassia angustifolia Vahl, Asian J Pharm Clin Res 9(3) 2016 pp. 111-116.

[55] A.Q. Laghari, S. Memon, A. Nelofar, A.H. Laghari, Extraction, identification and antioxidative properties of the flavonoid-rich fractions from leaves and flowers of Cassia angustifolia, American Journal of Analytical Chemistry 2(08) 2011 pp. 871.

[56] R.K. Lal, C.S. Chanotiya, A. Kumar, The prospects and potential of the horticultural and pharmacological medicinal herb senna (Cassia angustifolia Vahl.): a review, Technology in Horticulture 3(1) 2023 pp.

[57] M. Chaubey, V.P. Kapoor, Structure of a galactomannan from the seeds of Cassia angustifolia Vahl, Carbohydrate Research 332(4) 2001 pp. 439-444.

[58] E. Săvulescu, M.I. Georgescu, V. Popa, V. Luchian, Morphological and Anatomical Properties of the Senna Alexandrina Mill.(Cassia Angustifolia Vahl.), Agriculture for Life, Life for Agriculture" Conference Proceedings, 2018, pp. 305-310.

[59] S.H. Reddy, A.S. Al-Kalbani, A.S. Al-Rawahi, Studies on phytochemical screening-GC-MS characterization, antimicrobial and antioxidant assay of black cumin seeds (nigella sativa) and senna alexandria (cassia angustifolia) solvent extracts, International Journal of Pharmaceutical Sciences and Research 9(2) 2018 pp. 490-497.

[60] S.I. Ahmed, M.Q. Hayat, M. Tahir, Q. Mansoor, M. Ismail, K. Keck, R.B. Bates, Pharmacologically active flavonoids from the anticancer, antioxidant and antimicrobial extracts of Cassia angustifolia Vahl, BMC complementary and alternative medicine 16 2016 pp. 1-9.

[61] B. Müller, J. Kraus, G. Franz, Chemical structure and biological activity of water-soluble polysaccharides from Cassia angustifolia leaves, Planta medica 55(06) 1989 pp. 536-539.

[62] P.B.R. Murti, T. Seshadri, Chemical composition of Indian senna leaves (Cassia angustifolia), Proceedings of the Indian Academy of Sciences-Section A, Springer, 1939, pp. 96-103.

[63] Y. Masoumi-Ardakani, A. Mandegary, K. Esmaeilpour, H. Najafipour, F. Sharififar, M. Pakravanan, H. Ghazvini, Chemical composition, anticonvulsant activity, and toxicity of essential oil and methanolic extract of Elettaria cardamomum, Planta medica 82(17) 2016 pp. 1482-1486.

[64] F. Moulai-Hacene, M.Y. Boufadi, S. Keddari, A. Homrani, Chemical composition and antimicrobial properties of Elettaria cardamomum extract, Pharmacognosy Journal 12(5) 2020 pp.

[65] E.K. Savan, F.Z. Küçükbay, Essential oil composition of Elettaria cardamomum Maton, Journal of Applied Biological Sciences 7(3) 2013 pp. 42-45.

[66] K. Tarfaoui, N. Brhadda, R. Ziri, A. Oubihi, H. Imtara, S. Haida, O.M. Al Kamaly, A. Saleh, M.K. Parvez, S. Fettach, Chemical profile, antibacterial and antioxidant potential of Zingiber officinale Roscoe and Elettaria cardamomum (L.) maton essential oils and extracts, Plants 11(11) 2022 pp. 1487.

[67] M. Noshad, B.A. Behbahani, Identification of chemical compounds, antioxidant activity, and antimicrobial effect of Elettaria cardamomum essential oil on a number of pathogenic microorganisms in vitro, Qom University of Medical Sciences Journal 13(2) 2019 pp. 57-69.

[68] A. Alam, R.S. Majumdar, P. Alam, Systematics evaluations of morphological traits, chemical composition, and antimicrobial properties of selected varieties of Elettaria cardamomum (L.) Maton, Natural Product Communications 14(12) 2019 pp. 1934578X19892688.

[69] S. Jena, A. Ray, A. Sahoo, B.B. Champati, B.M. Padhiari, B. Dash, S. Nayak, P.C. Panda, Chemical composition and antioxidant activities of essential oil from leaf and stem of Elettaria cardamomum from eastern India, Journal of Essential Oil Bearing Plants 24(3) 2021 pp. 538-546.

[70] S. Goudarzvand Chegini, H. Abbasipour, Chemical composition and insecticidal effects of the essential oil of cardamom, Elettaria cardamomum on the tomato leaf miner, Tuta absoluta, Toxin reviews 36(1) 2017 pp. 12-17.

[71] S. Kumar, R. Kumari, Traditional, Phytochemical and Biological activities of Elettaria cardamomum (L.) Maton–A review, International Journal of Pharmaceutical Sciences and Research 12(8) 2021 pp. 4122.

[72] K. Ashokkumar, M. Murugan, M. Dhanya, T.D. Warkentin, Botany, traditional uses, phytochemistry and biological activities of cardamom [Elettaria cardamomum (L.) Maton]–A critical review, Journal of ethnopharmacology 246 2020 pp. 112244.

[73] J. Prakash, Chemical composition and antioxidant properties of ginger root (Zingiber officinale), Journal of Medicinal Plants Research 4(24) 2010 pp. 2674-2679.

[74] Y. Liu, J. Liu, Y. Zhang, Research progress on chemical constituents of Zingiber officinale Roscoe, BioMed research international 2019(1) 2019 pp. 5370823.

[75] H. Amiri, M. Mohammadi, S. Sadatmand, E. Taheri, Study the chemical composition of essential oil of ginger (zingiber officinale) and antioxidant and cell toxicity, Journal of Medicinal Plants 15(58) 2016 pp. 89-98.
[76] H.A. Hasan, A.R. Raauf, B. Razik, B.R. Hassan, Chemical composition and antimicrobial activity of the crude extracts isolated from Zingiber officinale by different solvents, Pharmaceut Anal Acta 3(9) 2012 pp. 1-5.
[77] I. Sasidharan, A.N. Menon, Comparative chemical composition and antimicrobial activity fresh & dry ginger oils (Zingiber officinale Roscoe), International Journal of Current Pharmaceutical Research 2(4) 2010 pp. 40-43.
[78] M. Mahboubi, Zingiber officinale Rosc. essential oil, a review on its composition and bioactivity, Clinical Phytoscience 5(1) 2019 pp. 1-12.
[79] A.C. Aprotosoaie, A. Spac, M. Hancianu, A. Miron, V.F. Tanasescu, V. Dorneanu, U. Stanescu, The chemical profile of essential oils obtained from fennel fruits (Foeniculum vulgare Mill.), Farmacia 58(1) 2010 pp. 46-53.
[80] W. He, B. Huang, A review of chemistry and bioactivities of a medicinal spice: Foeniculum vulgare, Journal of Medicinal Plants Research 5(16) 2011 pp. 3595-3600.
[81] A. Foroughi, P. Pournaghi, F. Najafi, A. Zangeneh, M.M. Zangeneh, R. Moradi, Medicinal plants: antibacterial effects and chemical composition of essential oil of Foeniculum vulgare, Int J Curr Pharm Rew Res 8(1) 2017 pp. 13-17.
[82] A. Ghasemian, A.-H. Al-Marzoqi, S.K.S. Mostafavi, Y.K. Alghanimi, M. Teimouri, Chemical composition and antimicrobial and cytotoxic activities of Foeniculum vulgare Mill essential oils, Journal of gastrointestinal cancer 51 2020 pp. 260-266.
[83] H.J. Hussein, M.Y. Hadi, I.H. Hameed, Study of chemical composition of Foeniculum vulgare using Fourier transform infrared spectrophotometer and gas chromatography-mass spectrometry, Journal of Pharmacognosy and Phytotherapy 8(3) 2016 pp. 60-89.
[84] F. Belabdelli, A. Piras, N. Bekhti, D. Falconieri, Z. Belmokhtar, Y. Merad, Chemical composition and antifungal activity of Foeniculum vulgare Mill, Chemistry Africa 3 2020 pp. 323-328.
[85] C. Garga, S. Khan, S. Ansari, A. Suman, M. Garg, Chemical composition, therapeutic potential and perspectives of Foeniculum vulgare, Pharmacognosy Reviews 3(6) 2009 pp. 346.
[86] M.G. Miguel, C. Cruz, L. Faleiro, M.T. Simões, A.C. Figueiredo, J.G. Barroso, L.G. Pedro, Foeniculum vulgare essential oils: chemical composition, antioxidant and antimicrobial activities, Natural product communications 5(2) 2010 pp. 1934578X1000500231.
[87] W.-R. Diao, Q.-P. Hu, H. Zhang, J.-G. Xu, Chemical composition, antibacterial activity and mechanism of action of essential oil from seeds of fennel (Foeniculum vulgare Mill.), Food control 35(1) 2014 pp. 109-116.
[88] R. Hiltunen, Chemical composition of Ocimum species, Basil, CRC Press1999, pp. 74-82.
[89] M.H. Shahrajabian, W. Sun, Q. Cheng, Chemical components and pharmacological benefits of Basil (Ocimum basilicum): A review, International Journal of Food Properties 23(1) 2020 pp. 1961-1970.
[90] D.W. Al Abbasy, N. Pathare, J.N. Al-Sabahi, S.A. Khan, Chemical composition and antibacterial activity of essential oil isolated from Omani basil (Ocimum basilicum Linn.), Asian Pacific Journal of Tropical Disease 5(8) 2015 pp. 645-649.
[91] O. Politeo, M. Jukic, M. Milos, Chemical composition and antioxidant capacity of free volatile aglycones from basil (Ocimum basilicum L.) compared with its essential oil, Food chemistry 101(1) 2007 pp. 379-385.
[92] N.H. Abou El-Soud, M. Deabes, L. Abou El-Kassem, M. Khalil, Chemical composition and antifungal activity of Ocimum basilicum L. essential oil, Open access Macedonian journal of medical sciences 3(3) 2015 pp. 374.
[93] M. Ismail, Central properties and chemical composition of Ocimum basilicum. essential oil, Pharmaceutical biology 44(8) 2006 pp. 619-626.
[94] K. Poonkodi, Chemical composition of essential oil of Ocimum basilicum L.(Basil) and its biological activities-an overview, J. Crit. Rev 3(3) 2016 pp. 56-62.
[95] L.P. Stanojevic, Z.R. Marjanovic-Balaban, V.D. Kalaba, J.S. Stanojevic, D.J. Cvetkovic, M.D. Cakic, Chemical composition, antioxidant and antimicrobial activity of basil (Ocimum basilicum L.) essential oil, Journal of Essential Oil Bearing Plants 20(6) 2017 pp. 1557-1569.
[96] A.I. Hussain, F. Anwar, S.T.H. Sherazi, R. Przybylski, Chemical composition, antioxidant and antimicrobial activities of basil (Ocimum basilicum) essential oils depends on seasonal variations, Food chemistry 108(3) 2008 pp. 986-995.
[97] Z.-M. Cai, J.-Q. Peng, Y. Chen, L. Tao, Y.-Y. Zhang, L.-Y. Fu, Q.-D. Long, X.-C. Shen, 1, 8-Cineole: A review of source, biological activities, and application, Journal of Asian natural products research 23(10) 2021 pp. 938-954.
[98] C.-L. Moo, M.A. Osman, S.-K. Yang, W.-S. Yap, S. Ismail, S.-H.-E. Lim, C.-M. Chong, K.-S. Lai, Antimicrobial activity and mode of action of 1, 8-cineol against carbapenemase-producing Klebsiella pneumoniae, Scientific reports 11(1) 2021 pp. 20824.
[99] B. YELBOĞA, S. KARAKUŞ, A study on antifungal activity of thymol, eugenol, and 1, 8-cineole against Botrytis cinerea Persoon isolated from grapevine (Vitis vinifera Linné), Journal of Central European Agriculture 24(4) 2023 pp. 888-898.

[100] A. Gupta, E. Jeyakumar, R. Lawrence, Journey of limonene as an antimicrobial agent, Journal of Pure & Applied Microbiology 15(3) 2021 pp.
[101] A. Dantas Ribeiro, M.N. Amaral Cardoso, J.C. Palhano Freire, E.C. Figueirêdo Júnior, M.M. Alexandrino Costa, P. Guimarães Silva, D.Q. de Castro Gomes, E.M. Melo de Brito, J. Vieira Pereira, Antimicrobial activity of limonene: Integrative review, Boletín Latinoamericano y del Caribe de Plantas Medicinales y Aromáticas 22(5) 2023 pp.
[102] N. Wijayati, S. Mursiti, H. Pranowo, T. Jumina, A. Utomo, Antibacterial studies of α-terpineol derived from α-pinene, Welcome to Surakarta (Solo)-Indonesia 2016 pp. 1.
[103] A. Sales, L.d.O. Felipe, J.L. Bicas, Production, properties, and applications of α-terpineol, Food and bioprocess technology 13(8) 2020 pp. 1261-1279.
[104] A. Marchese, R. Barbieri, E. Coppo, I.E. Orhan, M. Daglia, S.F. Nabavi, M. Izadi, M. Abdollahi, S.M. Nabavi, M. Ajami, Antimicrobial activity of eugenol and essential oils containing eugenol: A mechanistic viewpoint, Critical reviews in microbiology 43(6) 2017 pp. 668-689.
[105] V.V.M.A. Souza, J.M. Almeida, L.N. Barbosa, N.C.C. Silva, Citral, carvacrol, eugenol and thymol: antimicrobial activity and its application in food, Journal of Essential Oil Research 34(3) 2022 pp. 181-194.
[106] E.L. Santos, P.R. Freitas, A.C.J. Araujo, R.S. Almeida, S.R. Tintino, C.L.R. Paulo, J. Ribeiro-Filho, A.C.A. Silva, L.E. Silva, W. do Amaral, Phytochemical characterization and antibiotic potentiating effects of the essential oil of Aloysia gratissima (Gillies & Hook.) and beta-caryophyllene, South African Journal of Botany 143 2021 pp. 1-6.
[107] N. Niamsa, C. Sittiwet, Antimicrobial activity of Curcuma longa aqueous extract, 2009 pp.
[108] H. Wu, Z. Liu, Y. Zhang, B. Gao, Y. Li, X. He, J. Sun, U. Choe, P. Chen, R.A. Blaustein, Chemical Composition of Turmeric (Curcuma longa L.) Ethanol Extract and Its Antimicrobial Activities and Free Radical Scavenging Capacities, Foods 13(10) 2024 pp. 1550.
[109] V. VijayaSekhar, M.S. Prasad, D. Joshi, K. Narendra, A.K. Satya, K. Rao, Assessment of phytochemical evaluation and in-vitro antimicrobial activity of Cassia angustifolia, Int. J. Pharmacogn. Phytochem. Res 8(2) 2016 pp. 305-312.
[110] D. Khodabakhshi, G. Vaseghi, A. Mirzaee, A. Eskandarinia, A.Z. Kharazi, Antimicrobial activity and wound healing effect of a novel natural ointment: An in vitro and in vivo study, Journal of Wound Care 32(Sup6) 2023 pp. S18-S26.
[111] T. Qidwai, F. Khan, Antimalarial drugs and drug targets specific to fatty acid metabolic pathway of Plasmodium falciparum, Chemical Biology & Drug Design 80(2) 2012 pp. 155-172.
[112] E.L. Allman, H.J. Painter, J. Samra, M. Carrasquilla, M. Llinás, Metabolomic profiling of the malaria box reveals antimalarial target pathways, Antimicrobial agents and chemotherapy 60(11) 2016 pp. 6635-6649.
[113] C. Ben Mamoun, S.T. Prigge, H. Vial, Targeting the lipid metabolic pathways for the treatment of malaria, Drug development research 71(1) 2010 pp. 44-55.
[114] A.S. George, M.T. Brandl, Plant bioactive compounds as an intrinsic and sustainable tool to enhance the microbial safety of crops, Microorganisms 9(12) 2021 pp. 2485.
[115] V. Běhal, Mode of action of microbial bioactive metabolites, Folia Microbiologica 51(5) 2006 pp. 359-369.
[116] K.V. Krishna, R.S. Ulhas, A. Malaviya, Bioactive compounds from Cordyceps and their therapeutic potential, Critical reviews in biotechnology 44(5) 2024 pp. 753-773.
[117] M. Salton, Lytic agents, cell permeability, and monolayer penetrability, The Journal of general physiology 52(1) 1968 pp. 227-252.
[118] A. Bouyahya, I. Chamkhi, A. Balahbib, M. Rebezov, M.A. Shariati, P. Wilairatana, M.S. Mubarak, T. Benali, N. El Omari, Mechanisms, anti-quorum-sensing actions, and clinical trials of medicinal plant bioactive compounds against bacteria: a comprehensive review, Molecules 27(5) 2022 pp. 1484.
[119] S. Sachdev, S.A. Ansari, M.I. Ansari, M. Fujita, M. Hasanuzzaman, Abiotic stress and reactive oxygen species: Generation, signaling, and defense mechanisms, Antioxidants 10(2) 2021 pp. 277.
[120] N. Basavegowda, K.-H. Baek, Combination strategies of different antimicrobials: An efficient and alternative tool for pathogen inactivation, Biomedicines 10(9) 2022 pp. 2219.

Date of publication: April 24, 2025.

A Review of Blockchain Rewarding Strategies and Corresponding Consensus Protocols

Basem Assiri[1], Haitham Assiri[2], Shadab Alam[3], Shams Siddiqui[4], and Hussein Zangoti[5]
[1,2,3,4]Computer Science Department, Faculty of Engineering and Computer Science, Jazan, Saudi Arabia, Postal Code: 82817
[5]Department of Electrical and Electronics Engineering, Faculty of Engineering and Computer Science, Jazan, Saudi Arabia, Postal Code: 82817

Corresponding author: Basem Assiri (e-mail: babumussmar@jazanu.edu.sa).

ABSTRACT: The development of blockchain technology has facilitated its application in many areas of life due to its ability to enable decentralization in processing and storage. To support blockchain's application in various fields, its algorithms, and consensus protocols should be developed. Nowadays, there are many consensus protocols, each of which can be applied to the appropriate field, considering the cost of each protocol. Users should be motivated to use blockchain and participate in its processes. Considering the processing, communication, and storage costs, effective reward mechanisms are necessary to compensate users and encourage participation. Therefore, this study investigates and reviews a variety of blockchain consensus protocols and corresponding reward strategies. The study analyses twenty-two consensus protocols, explaining how they work, and their advantages and disadvantages. In addition, this paper discusses the types of reward strategies, their sources, limitations, and future. According to the nature of consensus protocols, they are classified into seven categories, which are computational-based, wealth-based, behavioral-based, fairness-based, fault-tolerance-based, leader-based, and transactional-based. The study aims to provide information on the future paths of blockchain consensus mechanisms, promoting a more profound understanding of their capabilities and constraints in many situations.

INDEX TERMS: Blockchain, Consensus Protocols, Rewarding Strategy.

I. INTRODUCTION

Blockchain technology has revolutionized digital transactions by introducing a decentralized, secure, and transparent ledger system. The blockchain consists of a network of nodes that share a ledger and vote on decisions. In a blockchain network, nodes verify transactions, group the valid transactions into a new block, propose the new block to other nodes, verify the new block, vote to approve it, and append it to the ledger or disapprove it. Undoubtedly, the ledger consists of a chain of all approved blocks, and every node has a consistent copy of the ledger [1]–[3]. Therefore, nodes compete for participation in such processes based on a consensus protocol.

Blockchain consensus protocols guarantee that every node in the network agrees on a single and verifiable state of the truth. Protocols are essential to the functionality and integrity of blockchain networks. For authenticating transactions, protecting the network, and preserving trust among participants, these protocols are critically important. However, the effectiveness of these protocols is influenced by two factors that have a significant impact on their success. These two factors are the nature of the application fields and the mechanisms used to reward honest participants or to punish malevolence.

Firstly, in order to support the application of blockchain in various fields, the consensus protocols should be developed and customized. There are many consensus protocols, each of which can be applied to the appropriate field. Secondly, considering the cost and to motivate proper participation, the protocols should involve reward mechanisms that compensate for the cost and motivate participants. In fact, governments need more analyses and investigations to be able to apply blockchain technologies in the areas of healthcare, education, national security, economy, and finance. For example, in 2022, the USA government required more studies and investigations to maintain its digital assets and issue the Digital Dollar [4], [5].

Therefore, in this study, a wide variety of blockchain consensus protocols have been investigated, with a particular emphasis placed on the nature of the protocol, processing cost, rewarding techniques, and punishment mechanisms employed by each protocol. In addition, the research explores the complex mechanics of reward and punishment in different consensus protocols, emphasizing their importance in preserving network integrity and trust. Indeed, the main contributions of this paper are as follows:

- **Comprehensive Analysis:** Detailed examination of the nature of various consensus protocols.
- **Rewarding Strategies:** Systematic analysis of diverse rewarding strategies to incentivize honest participation.
- **Punishment Mechanisms:** Exploration of punishment mechanisms to deter malicious behavior.
- **Efficiency:** Highlighting the main characteristics of the consensus protocols such as energy consumption, scalability, security, and fairness.

The rest of the paper is organized as follows: Section II reviews the research methodology and constraints. Section III describes various consensus protocols, advantages, disadvantages, and their rewarding strategies. Section IV presents a discussion of the implications of our findings. Finally, Section V concludes the paper and outlines some challenges and future research directions.

II. RESEARCH METHOD

This section outlines the research method used for this research work. The primary objective of this study is to provide a comprehensive review and comparative analysis of blockchain consensus protocols and their associated rewarding strategies. Given its decentralized and distributed nature, blockchain technology relies heavily on consensus mechanisms to ensure the integrity, security, and functionality of the network. These mechanisms vary widely in design and implementation, each offering distinct benefits, challenges, and efficiencies. This facilitates blockchain application in different domains. Additionally, the rewarding strategies associated with these protocols play a crucial role in motivating participants to maintain the network's stability and security. To achieve the study's objectives, the research uses a systematic and multi-faceted framework, divided into three key stages: a literature review, an analysis of the consensus protocols, and an evaluation of rewarding strategies. Each stage was meticulously planned and executed to ensure a thorough and unbiased examination of the current state of blockchain consensus mechanisms.

The first stage involves conducting a comprehensive literature review to gather the existing knowledge on blockchain consensus protocols and rewarding strategies. The review included peer-reviewed journal articles, conference papers, technical reports, and white papers published between 2018 and 2024. Databases such as IEEE Xplore, SpringerLink, and Google Scholar were extensively searched using keywords like "blockchain consensus mechanisms," "rewarding strategies," "Proof of Work," "Proof of Stake," "Protocol History," and "Byzantine Fault Tolerance." The review aimed to identify seminal works, emerging trends, and gaps in the existing literature that this study could address. This stage also helped frame the research questions and provided the theoretical foundation for the subsequent stages.

In the second stage, the research focused on a detailed analysis of various blockchain consensus protocols and their associated rewarding strategies. This study categorized the protocols based on their underlying mechanisms. For each protocol, the research examined the operational principles, security features, scalability potential, and energy efficiency. Special attention was given to how these protocols manage the trade-offs between decentralization, security, and performance. The analysis also considered the applicability of each protocol to different blockchain use cases, ranging from cryptocurrencies and smart contracts to specialized applications like supply chain management and Internet of Things (IoT) networks [6], [7].

The final stage of the research framework involved evaluating the rewarding strategies associated with each consensus protocol. Rewarding mechanisms are critical in blockchain systems because they provide incentives for participants (such as miners or validators) to engage in activities that uphold the network's integrity and security. This stage analyzed how different protocols implement rewards through transaction fees, newly minted coins, or innovative approaches like reputation- based rewards or game-theoretical models. The evaluation also considered the effectiveness of these strategies and the use of punishment in promoting honest participation, deterring malicious behavior, and ensuring long-term network sustainability.

In short, the analysis categorized and evaluated various consensus protocols and reward strategies based on their underlying mechanisms, security features, scalability, energy efficiency, and applicability to different blockchain use cases. The following consensus protocols and reward strategies were examined in detail:

1) Proof of Work
2) Proof of Exercise
3) Proof of Space or Capacity
4) Proof of Stake
5) Delegated Proof of Stake
6) Leased Proof of Stake
7) Proof of Burn
8) Proof of Transfer
9) Proof of Authority
10) Unique Node List
11) Ripple
12) Proof of Importance
13) Proof of Reputation
14) Proof of Contribution
15) Proof of Elapsed Time
16) Proof of Fairness
17) Practical Byzantine Fault Tolerance
18) Delegated Byzantine Fault Tolerance
19) Federated Byzantine Agreement
20) Proof of Quality of Service
21) Reliable, Replicated, Redundant and Fault Tolerant
22) Directed Acyclic Graph

III. CONSENSUS PROTOCOLS AND REWARDING STRATEGIES

This section provides an overview of various consensus protocols used in blockchain networks and the corresponding

rewarding strategies. For each protocol, we will discuss its background, operational principles, advantages, disadvantages, and the strategies used to reward participants based on their roles and contributions to the network.

A. PROOF OF WORK (POW)

1) HISTORY

PoW was introduced in 1993 by Cynthia Dwork and Moni Naor as a computational technique to combat spam emails and denial-of-service attacks. However, it gained significant prominence with the introduction of Bitcoin in 2008 by a group under the pseudonym Satoshi Nakamoto. The PoW consensus protocol was used as the fundamental method for reaching consensus in Bitcoin, and later on, it was also implemented in various other blockchain networks [8]–[10]. Moreover, Proof of Activity is another consensus protocol that enables the preparation of a blank block using PoW, so other miners can fill it out using other consensus protocols such as Proof of Stake.

2) POW DESCRIPTION

PoW entails miners competing with their computational skills to solve complex mathematical puzzles. A new block of transactions must be proposed by the first miner to solve the problem; this block is then validated by the remaining miners. Miners verify that the transactions of the proposed block comply with the network's rules, such as the prohibition of double-spending. This procedure is demanding in terms of resources and computation power. PoW variants that have been modified incorporate algorithms such as SHA-256 (used in Bitcoin) and Ethash (used in Ethereum) [11], [12]. Miners combine pending transactions with other data, such as the preceding block's hash, to mine a new block, using a cryptographic hashing technique. The miner adjusts the nonce to hash data repeatedly until it satisfies a network-set diffi- culty threshold. Once a miner successfully finds a valid hash, they broadcast the new block to the network. Moreover, to validate a proposed block, upon receiving the proposed block, other miners independently verify the validity by verifying transactions and proof of work. Miners accept valid blocks and extend the blockchain from this new block [13], [14].

3) ADVANTAGES AND DISADVANTAGES

Advantages

- Proven security against Sybil attacks and manipulation.
- The network is decentralized, indicating that no single entity has control over it.
- Encourages participation by providing mining rewards. Disadvantages.
- High energy consumption owing to computational de- mands.
- The network is susceptible to 51% attacks when one entity has control over the majority of the network's computational power.
- The low transaction throughput presents scalability problems.

4) POW REWARDING STRATEGIES

If a miner succeeds in adding a new block to the blockchain, they are rewarded with newly minted cryptocurrency, as well as transaction fees. There is a process known as halving that takes place at predetermined intervals, and this process is responsible for the gradual reduction of the reward over time. The purpose of this falling incentive is to both regulate the rate of inflation of the cryptocurrency and to encourage early adoption of the cryptocurrency. In addition, miners may be eligible for incentives if they participate in the governance of the network or if they support particular protocol updates [15]–[18].

B. PROOF OF EXERCISE (POX) OR (POEX)

1) HISTORY

PoeX is used as an abbreviation to differentiate between Proof of Exercise and Proof of Transfer, which are also denoted as (PoX). PoeX is a consensus mechanism that was developed by researchers in the blockchain and scientific computation fields, focusing on leveraging computational efforts to solve practical scientific problems. The concept gained traction in the late 2010s, driven by academic research and discussions within the blockchain community aimed at addressing PoW's inefficiencies [19]–[21].

2) POEX DESCRIPTION

PoeX is a consensus protocol that replaces PoW's typical hash-based puzzles with real-world matrix-based scientific computation problems. The choice of matrix-based problems is due to their composability and vast range of real-world applications, making PoeX a meaningful and long-term ap- proach to blockchain consensus. PoeX works as follows:

- **Task Proposals:** An employer (E) with a scientific computation problem (referred to as eXercise X) stores the problem in a highly available database (XDB) and generates a hash digest. The employer then creates an eXercise Transaction (XT) with the problem details and deposits a credit.
- **eXercise Bidding and Mining:** Miners (M) select eXercises from the XBoard, where eXercise Transactions are presented. Miners are allocated work at random to prevent collusion. They commit to resolving the problem by initiating a Deal Transaction (DT) and depositing credit.
- **Solving and Verifying:** Miners generate a hash digest (H(Y')) after solving the given problem and storing the solution in the database. Auditors then use a probabilistic verification scheme to confirm the solution. Verification results are submitted by auditors as Audit Transactions (AT).
- **Block Commitment:** The miner adds the block to the blockchain and appends references to all associated transactions to the block header after receiving a sufficient number of Passed Reports from auditors. Next, claims are made for the miner's deposited credits.

To propose a new block, miners select pending exercises from the XBoard and solve the given matrix-based problems. They then combine the solutions with additional data (such as the previous block's hash) to generate a new block proposal. After that, validators are selected through a random assignment of eXercises, which is done to prevent collusion and ensure fairness. Auditors, or verifiers, use a probabilistic verification scheme to verify the solutions once they have solved their assigned problem [19]–[21].

3) Advantages And Disadvantages

Advantages

- Useful computation is provided as it redirects the computational resources to solve real-world scientific challenges, making the process useful beyond the blockchain network.
- Random task assignment and transaction shuffling reduce the possibility of collusion among miners and task providers.
- Matrix-based problems enable collaborative verification, making the approach more robust.
- Focuses on relevant computations, which reduces the consumption of energy associated with standard PoW systems.

Disadvantages

- PoeX is more complicated to develop and implement because it requires sophisticated mechanisms for managing and verifying the scientific computations.
- Verifying scientific computations introduces additional complexity and overheads compared to simpler hash-based verification.
- Participation may be restricted if miners are required to possess specialist expertise or equipment to tackle particular scientific problems.

4) PoeX Rewarding Strategies

In PoeX, miners earn rewards by solving scientific problems. Once auditors have validated the solutions, rewards are credited. In which credit deposits are made by both employers and miners to demonstrate their commitment to problem's solution and verification. These credits are reclaimed after successful completion and verification. Auditors also are incentivized to provide correct verification reports. They earn credits for completed reports and are penalized for filing fake or un- successful reports. The rewards can be from transactions' fees and from other sources, such as prizes for solving some computations [19]–[21].

C. PROOF OF SPACE OR CAPACITY (POSPACE)

1) History

PoSpace was introduced in 2013 by Dziembowski and others. It allows miners to provide resources such as storage capacity or other hardware to serve the system. After that, Burstcoin, Storj, Chia, and SpaceMint have adapted PoSpace in their applications [22], [23].

2) PoSpace Description

In blockchain technology, PoSpace, capacity or usability, offers an alternate approach, where they allow miners to provide their resources, such as storage capacity or other hardware to support blockchain processes such as transactions' validation and blocks' mining. As much as miners serve the system, they are rewarded. They are also given more chances to propose or validate a new block [22]–[24].

3) Advantages and Disadvantages

Advantages

- Less power consumption.
- Enable more cooperation and decentralization.
- Having more hardware resources speeds up the mining process.

Disadvantages

- If a miner has more hardware resources, then this miner is able to control the system.
- A miner with more hardware resources, is able to attack the system and cause security threats. Additionally, if the miner soddenly withdraws the resources, the whole system may be affected and this can cause a denial-of-service issue.

4) PoSpace Rewarding Strategies

In PoSpace miners are rewarded as much as the amount of storage space that they dedicate to the system. For newly joined miners with small capabilities, the rewards are increased for encouragement [25]. In other applications, the miner is rewarded if the hash value is calculated using its resources.

D. PROOF OF STAKE (POS)

1) History

PoS has been introduced to avoid the high computation demand of PoW. In 2012, PoS was first proposed and then it was first used in Peercoin cryptocurrency [14], [15]. After that many cryptocurrencies have used PoS, mainly Ethereum, which is one of the most important and famous cryptocurrencies that recently switched to PoS [15], [16].

2) PoS Description

Using PoS, miners stake some assets to the blockchain system, and the miner who stakes the highest amount will be selected to propose a new block. Then, miners with the next highest stakes will be selected to validate the new proposed block. For example, if a miner owns 50% of the stake in the system, the chance to be selected is 50% among the other miners [17], [18], [26]–[29]. There are some versions of PoS such as Delegated Proof of Stake and Leased Proof of Stake, which will be explained later on [30].

3) Advantages and Disadvantages

Advantages

- Less power consumption.
- Less computation requirements.
- Faster than a traditional mining process.
- Solves the issue of double-spending.

Disadvantages

- If a miner has more than 50% of the system stake, this miner is able to attack the system and approve illegal blocks, which is a security threat.
- The miner with the highest stake will be a target for attackers. The failure of this miner may result in security issues such as denial of service.
- There is no chance for poor and newly joined miners as they cannot compete with rich ones, while rich miners keep competing and winning. This makes them richer. The more open and inclusive the system (that includes more validators without restrictions), the less fairness in reward distribution [31].
- It encourages money stagnation because miners try not to spend money to be able to compete.

4) PoS Rewarding Strategies

In PoS, the miner who succeeds in block creation or validation will be rewarded using transaction fees [17], [18]. There are two types of staking, active and passive. In active staking the miners stake an amount and try to participate in transaction and block validating. Thus, they are rewarded in response to each valid activity. However, in passive staking, the miners stake some amount to secure the system without participating. This works as an investment or staking money for interest. Therefore, they are rewarded with a specific percentage per month or per year. In some cryptocurrencies, the reward percentages are fixed, while in others the percentages vary from one day to another. One of the main strategies to secure the system is to punish miners who misbehave by cutting some of their stake or another systematic punishment designed to punish conspiring parties [17]. Some researchers apply game theory to introduce a fair reward-sharing strategy that suggests the number of participants and the number of pools to satisfy the Nash equilibrium, which imply efficiency, fairness, and security [32], [33].

E. DELEGATED PROOF OF STAKE (DPOS)

1) History

DPoS was first introduced by Dan Larimer in 2013. In 2015, the first application of DPoS was on the BitShares cryptocurrency, then it has been applied to many other cryptocurrencies such as Lisk, Cadano, Ark, Steem, and TRON.

2) DPoS Description

DPoS is a modified version of PoS, that enables stakeholders to elect a group of miners as delegates to propose and validate blocks. Every time, some of the delegates take on the responsibility to propose and validate a block as a group. For every cycle, other delegates are selected. In case of one miner misbehaves, the other miners vote to exclude it from the group [17], [18], [26], [27]. In addition, it is suggested to delegate the node that no one else believes in, to avoid security issues [34].

3) Advantages and Disadvantages

Advantages

- More decentralization compared to PoW and PoS.
- Solves the issue of double-spending.
- More security as it does not provide a clear target to attack. In addition, any delegate that misbehaves will be detected during the validation process and excluded.
- More efficient since it requires less computation and less power consumption, as the delegated validators group is a subset of the whole miners set.
- Faster than PoW and PoS as the delegated validators group is a subset of the whole miners' set.

Disadvantages

- If a miner has more than 50% of the system stake, or a group of miners cooperate and gather more than 50% of the system stake, they are able to attack the system and approve illegal blocks, which is a security threat.
- There is no chance for poor and newly joined miners as they cannot compete with rich ones, while the rich miners keep competing and winning. This makes them richer.
- Delegates can cooperate and form lobbies to control system decisions.
- Less scalability than PoW and PoS.

4) DPoS Rewarding Strategies

Stakeholders practice passive staking as they stake and delegate others to validate transactions and blocks. Therefore, the stakeholders should elect the delegates who bring better rewards to everyone. In DPoS, the rewards are shared among stakeholders and delegates in different and predefined percentages. The delegates, integrate their computation re- sources to perform the task efficiently and fast, so then they can earn more rewards and share them equally or according to the provided resources portions. Moreover, rewards can be in any form of liquidity such as cash (cryptocurrencies), certificates, stakes, and others.

F. LEASED PROOF OF STAKE (LPOS)

1) History

Although LPoS is less popular than other consensus algorithms, it is in use by some cryptocurrencies such as WAVES and Nix. WAVES cryptocurrency was established in 2016, and it uses LPoS. Another cryptocurrency that uses LPoS is Nix which was launched in 2018 [17].

2) LPoS Description

In LPoS, a miner can lease some cryptocurrencies from riches as an investment. Then, the miner stakes the leased cryptocurrencies to the system, so there is more chance to be selected as a validator [17]. When the miner validates transactions or blocks, the miner wins some rewards (from transaction fees). After that, the miners pay the lease amounts back to the lender. Indeed, the leasing process is conducted through transactions and smart contracts. Initially, a smart contract is executed to fulfill the leasing agreement. Accordingly, a leasing transaction is executed to hold the leasing amount, so the lessee can use it without changing the original ownership. At the end, another transaction is conducted to enable the lessee to pay part of the reward to

the lender. In case the lease contract is violated or the leasing period finishes, another transaction is conducted to cancel the leasing.

3) Advantages and Disadvantages

Advantages

- Less power consumption.
- Less computation requirement.
- Fast mining process.
- There is a chance for poor and newly joined miners to participate since they can lease, stack, compete, and win, which eventually makes them rich.
- Solves the issue of double-spending.

Disadvantages

- If a miner has more than 50% of the system stake, this miner can attack the system and approve illegal blocks, which is a security threat.
- The miner with the highest stake will be a target for attackers. The failure of these miners may result in security issues such as a denial of service, Sybil attack, and others [34].

4) LPoS Rewarding Strategies

The Lenders practice passive staking as they lend cryptocurrencies to the lessee and the lessee participates in the trans- actions' validating process. In LPoS, the rewards are the transaction fees earned by the lessee. Then the lessee pays the rent amount in the agreement to the lender.

G. PROOF OF BURN (POB)

1) History

PoB, initially conceptualized by developer Stuart Popejoy in 2012, has emerged as a persuasive alternative consensus mechanism in the middle of the dominance of PoW and PoS [35]. While Proof of Burn did not receive the same level of broad adoption as its competitors, it has garnered a significant amount of interest within the blockchain community. As a result of its ability to address issues regarding energy usage and network security, it has promoted exploration in a variety of blockchain projects and exchanges such as Slimcoin [17], [35].

2) PoB Description

PoB is a consensus mechanism used in blockchain networks to achieve agreement on the state of the distributed ledger. It operates on the principle of burning or destroying cryptocurrency tokens as a means to gain the right to mine or validate blocks within the network. PoB takes a different approach to consensus mechanisms like PoW and PoS, which need processing power or cryptocurrency stakes. PoB participants transmit their Bitcoin tokens to an "unspendable" address to burn them. The irreversible practice of burning tokens shows commitment and involvement in the blockchain ecosystem. In the beginning miners "burn" a specified quantity of cryptocurrency by exchanging it for an address from which it is impracticable to retrieve or spend. Burning tokens allows participants to propose or validate blocks and act as proof of their investment or commitment to the network. The method used to choose which blocks to validate can differ from one PoB implementation to another, but it usually considers things like the total number of tokens burned and for how long they have been burned [17], [35], [36].

3) Advantages and Disadvantages

Advantages

- Provides an alternative to energy-intensive PoW and capital-intensive PoS.
- Burning tokens promotes a long-term commitment to the network and can help with network security.
- The token supply is reduced, which could lead to an increase in scarcity and value.
- Initial token holders may have a significant advantage, as they can afford to burn tokens without affecting their overall holdings.

Disadvantages

- Lacks widespread acceptance and established precedents compared to other consensus mechanisms.
- Finding the right burning rate or criteria for participation might be challenging and susceptible to manipulation.

4) PoB Rewarding Strategies

Participants in PoB do not receive newly minted tokens as a direct reward for validating blocks. Conversely, they are granted the privilege of participating in block validation and have the potential to accrue transaction fees or other incentives produced by the network. Moreover, as a result of diminished supply and heightened scarcity, the increased value of the remaining tokens may indirectly benefit the participants [35], [36].

H. PROOF OF TRANSFER (POX)

1) History

PoX is a relatively newer concept in the realm of blockchain consensus mechanisms. Although no one individual or organization is credited with its creation, PoX has steadily gained popularity in discussions aiming at improving the efficiency and sustainability of blockchain networks. PoX has provided innovative ways to consensus that tries to solve the challenges and limitations given by existing protocols. Despite the lack of a clear debut date, PoX has emerged as a focus point of research and study within the blockchain community, indicating its potential to influence the future growth and evolution of blockchain technology [37], [38].

2) PoX Description

A blockchain network can reach consensus through the use of PoX, which is a modified version of PoB. This method requires miners to transfer cryptocurrency as collateral in order to propose a new block or to take part in the process of block validation. PoX transfers cryptocurrency to another user instead of burning it (as in PoB). The transfer process can be part of any trading or exchange process. Miners are selected based on transferred tokens, reputation, and network performance. The selection process aims to achieve a balance between computational effort (similar to PoW) and economic stake (similar to PoS) [37], [38].

3) Advantages and Disadvantages

Advantages

- Potentially more energy-efficient than PoW by reducing the computing power consumption.
- Promotes long-term network commitment through token stakes (burns) as collateral.
- Aligns the economic incentives with network security and consensus, similar to PoS.

Disadvantages

- Balancing computational effort and an economic stake through implementation complexity.
- Potential centralization if a few entities accumulate significant staked tokens.
- Limited real-world acceptance and testing compared to existing consensus mechanisms.

4) PoX Rewarding Strategies

In PoX, participants are typically rewarded with transaction fees and possibly newly minted tokens for successfully validating blocks. Depending on the particular implementation of PoX and the regulations that are established by the blockchain network, the precise strategy for rewarding may be different from one instance to another. Participants who stake tokens also have the potential to earn rewards based on their stake and participation in block validation [37], [38].

I. PROOF OF AUTHORITY (POAUTH)

1) History

The term PoAuth was first introduced and popularized by Gavin Wood, co-founder of Ethereum, around 2017. It was initially conceived as part of Ethereum's broader exploration of consensus mechanisms beyond PoW, which was seen as too energy-intensive and slow for certain types of applications [39], [40]. Nowadays, PoAuth is ideal for applications that require high throughput and quick consensus and where the integrity of validators can be reliably assured. It's commonly used in corporate environments, inter-bank settlements, sup- ply chain management, and other applications where efficiency and speed are more critical than absolute decentralization [41]–[43]. Another shape of PoAuth is Proof of Medical Trust (PoMT), which helps in finding trusted miners in healthcare systems [44].

2) PoAuth Description

PoAuth is a groundbreaking consensus mechanism that emerged as an innovative alternative to the more traditional PoW and PoS. It was specifically tailored to meet the needs of networks seeking efficient transaction processing and reduced computational overhead. PoAuth has been particularly appealing in the context of private and consortium blockchains. These are environments where all participants are known and vetted, reducing the need for a trustless system. PoAuth offers these networks a way to maintain high through- put and quick consensus without the computational waste and energy costs [39], [40]. PoAuth is a consensus mechanism used in blockchain networks where transactions and blocks are validated by approved accounts known as "validators." These validators are often chosen based on their reputation and reliability, which is crucial since the system's integrity heavily depends on their honesty and ethical behavior. The validators in a PoAuth network are pre-selected based on their reputation and trustworthiness. They are often known entities such as companies or individuals who have undergone identity verification and are considered reliable. According to this reputation, validators are ranked and so they are selected to propose or validate new blocks. Validators who have the same rank are ordered randomly or in a fixed way based on the network's configuration Since the validators are trusted entities, this process is generally quicker and does not require multiple confirmations as in other systems [36], [45]–[48].

3) Advantages and Disadvantages

Advantages

- PoAuth is more efficient than PoW and PoS, as it allows for faster transaction processing since only a few trusted validators are involved in the consensus process, eliminating the need for complex problem-solving.
- PoAuth operates with a much lower energy footprint since it relies on the authority and identity of its validators rather than mining.
- More scalability with fewer nodes required to reach consensus. PoAuth networks can handle more transactions per second compared to PoW, making it more scalable for certain applications.
- Less susceptible to 51% attacks [49], since validators are pre-selected and trusted entities, which are a significant threat in decentralized PoW and PoS systems.
- Operating a PoAuth requires significantly less capital in terms of hardware and ongoing energy costs compared to PoW, making it a cost-effective solution for many businesses and organizations.
- Suitable for permissioned blockchains, where the environment is controlled and the validators are known entities, which aligns well with organizational use cases requiring privacy and internal control.

Disadvantages

- Centralization risks as PoAuth inherently involves a smaller number of validators, which can lead to centralization, potentially undermining the decentralized ethos of blockchain technology.
- The effectiveness of PoAuth is heavily dependent on the trustworthiness of its validators. If validators act maliciously or collude, the integrity of the entire network can be compromised.

4) PoAuth Rewarding Strategies

PoAuth achieves consensus when a validator's block is accepted by other nodes in the network. Given the trust-based model, PoAuth can offer immediate finality (reward); once a block is created and accepted. It rewards authorities for certifying and ordering transactions. In PoAuth, the validators are rewarded according to the reputation and trustworthiness score, which reflects their rank in the authority group [48]. The reputation score increases and decreases based on the nodes' behaviors, which changes the nodes' ranks existence in the authorized group.

J. UNIQUE NODE LIST (UNL)

1) History

The concept of UNL is integral to Ripple's consensus mechanism, introduced by Ripple Labs during Ripple's inception. Ripple Labs and its founding members, including Jed Mc- Caleb and Chris Larsen, were instrumental in conceptualizing and deploying UNL [50], [51]. In which selected trusted nodes are listed in UNL, which process transactions. Proof of Vote is another form of UNL, where the miners who belong to different sections of the consortium blockchain are able to reach a consensus through a voting mechanism [52].

2) UNL Description

The use of UNL enhances trust by requiring validation from a trusted set of nodes. Thus, the UNL consensus mechanism ensures that transactions are accurately verified and agreed upon by a majority of nodes in UNL. In UNL validators verify transactions, group them, and send them as proposals to other validators. Then, validators compare their validated group with other groups and vote on the overlapping transactions. If a transaction receives enough votes (by 50% of the validators), it proceeds to the next round. The round continues until the transaction receives more than 80% of the votes. This process ensures that the transactions are validated by multiple trusted nodes, leading to a highly secure and reliable network

Advantages

- Fast validation, since the transactions are validated only by some of the UNL nodes.
- Low transaction fees.
- Suitable for a large-scale network.
- Strong scalability as more transactions can be validated efficiently.
- Suitable for a private or consortium blockchain.

Disadvantages

- Not realistic for public blockchain as it has less decentralization since Ripple depends on a UNL.
- High connectivity requirements.
- Security issues like the UNL can misuse the control over decisions.

3) UNL Rewarding Strategies

Since the main application of UNL is financial payment gateways, the protocol gets timeout in a few seconds as part of the secure payment, which does not require much effort in comparison to PoW for example. Therefore, transaction fee is enough to be used as a reward.

K. RIPPLE

1) History

In 2004, Fugger introduced RipplePay for digital payment and exchange. In 2014, Ripple used to produce XRP cryptocurrency [53].

2) Ripple Description

RippleNet provides many mechanisms and financial procedures such as a specific consensus ledger, transaction protocol, and structure network. The ripple network includes a large number of validators who validate transactions, then they are grouped into a candidate set. On the other hand, a group of trustworthy validators which is called Unique Node List (UNL) is elected. Each member in the UNL validates transactions, groups them into its candidate set, and sends them to all other nodes. These nodes compare their own candidate sets with others. If the transaction is validated by 80% of nodes, it is added to the new block, and the new block is linked to the ledger [26], [53].

3) Advantages and Disadvantages

Advantages

- Fast validation, since the transactions take 3 to 5 seconds to be validated.
- Low transaction fee.
- Scalable as more transactions can be validated efficiently.
- The Ripple platform supports many other currencies for exchange and cooperates with other financial bodies.

Disadvantages

- Less decentralization since Ripple depends on a UNL.
- Security issue as the UNL can misuse their control over decisions.
- The platform is affected by the process of supply and demand, which will be reflected in the price of the cryptocurrency.

4) Ripple Rewarding Strategies

Ripple is used in XRP cryptocurrency, where the system is pre-mined, so there is an amount of cryptocurrency before the system is launched. These pre-mined coins are used as financial reserves in the system. Now, each transaction has a transaction fee that is added to the system reserve. From the reserve, the system distributes rewards to truthful validators [19], [53].

L. PROOF OF IMPORTANCE (POI)

1) History

PoI is a consensus mechanism that was developed to address some of the limitations seen in other consensus models. In 2015, PoI was introduced primarily by the NEM (New Economy Movement) blockchain platform, which sought to create a more equitable and active blockchain ecosystem. NEM's developers aimed to design a platform that was not only efficient and scalable but also one that incentivized active participation and contribution to the network rather than just the passive holding of assets. The developers of NEM noticed that in PoS systems, the richest holders of the currency often have disproportionate control over the network, potentially leading to centralization issues. PoI was developed as a solution to this problem by considering not just the amount of currency held (stake) but also the activity level of the participants (im- portance) [54], [55]. PoI is most suitable for social networks, reward systems, investment, and gaming.

2) PoI Description

PoI seeks to address some of the limitations of earlier consen- sus models. It was developed to encourage not only

investment in the network but also active participation. The core of PoI is the importance score, which determines a node's ability to add new blocks to the blockchain. This score is calculated based on several factors, including:

- Vesting of coins: A certain number of coins must be held in the account for some time, transitioning them from a balance to a vested balance. The more coins a node has vested, the higher its potential importance.
- Transaction partners and volume: PoI encourages users to transact with others rather than just holding funds. It assesses the net amount transferred over time and the diversity of transactions involving different accounts. This means that transferring funds to different users in the network positively affects a user's score.
- Overall network activity: The individual's transaction activity is evaluated in the context of the total network activity, ensuring that their importance score reflects both personal and network-wide engagement [37].

Accordingly, nodes with higher importance scores are more likely to be chosen to create the next block and validate the proposed ones [54]–[56].

3) Advantages and Disadvantages

Advantages

- It encourages active participation, not just holding tokens but also conducting transactions, which helps to maintain a vibrant and healthy blockchain ecosystem.
- PoI is an energy-efficient protocol, as it does not require intensive computational work to mine new blocks.
- It reduces the wealth concentration by taking into account factors such as transaction frequency and diversity in addition to the balance held. PoI helps to mitigate the "rich-get-richer" problem which is common in PoS systems.
- It supports decentralization by valuing contributions like transaction volume and diversity. PoI supports a more decentralized network structure, reducing the risk of centralization around a few wealthy nodes.
- Enhances network security since active participation is required by PoI to contribute to network security, as a higher number of engaged users increases the network's resilience against various types of attacks, including double-spending.

Disadvantages

- PoI's effectiveness depends heavily on high levels of network activity. In quieter networks with fewer transactions, it can be harder for participants to improve their scores, which may lead to stagnation.
- New participants with lower balances and fewer network connections may find it challenging to increase their importance score, which can create an entry barrier and potentially discourage new users from joining the net- work.

4) PoI Rewarding Strategies

In PoI, nodes work to improve their importance scores, by being active in the network, processing more transactions, processing large and frequent transactions, and cooperating with other accounts. All of these operations are rewarded which increases the node's PoI score. Having a higher PoI score enables a node to issue a new block and it will be rewarded by getting all of the transaction fees for these transactions within the new block [37], [55], [56].

M. PROOF OF REPUTATION (POR)

1) History

PoR was introduced by Zhuang et al. in 2019 as part of the effort to improve consensus mechanisms by leveraging node reputation to achieve higher efficiency and security in blockchain networks [57], [58].

2) PoR Description

PoR is a way to reach consensus in blockchains using reputable nodes participating in the network. The nodes' reputations are usually calculated based on a trust score associated with each node. This score is updated, for instance, after a node generates a new block or verifies a transaction [57]. In general, a node with a high reputation score can propose a new block and the next nodes with high reputation scores can validate the block and participate in the consensus process [58]–[60].

3) Advantages and Disadvantages

Advantages

- PoR improves the transaction rates in a reputation-based environment due to the existence of trust that can expedite the verification process.
- Fairness of the miner selection process.
- Motivates nodes to be active in the network.

Disadvantages

- One significant limitation of reputation-based consensus is the necessity for a trusted or permissioned environment. This restricts the system's applicability in open, decentralized networks where trust is not pre-established.
- Enhancing throughput in permissionless blockchains remains a challenge due to the reliance on reputation systems. These systems may struggle to scale efficiently in a fully decentralized and open setting which can lead to potential bottlenecks.

4) PoR Rewarding Strategies

An example of the rewarding strategy in PoR is as follows: upon the successful creation of a new block, a fixed reward is distributed among all consensus participants where each node receives a portion of the reward proportional to its reputation [56], [60]. The rewards can be from transaction fees.

N. PROOF OF CONTRIBUTION (POC) OR (POCO)

1) History

In 2021, PoC is a consensus mechanism designed to recognize and reward various forms of participation in a blockchain net- work. PoC represents a more holistic approach to blockchain consensus mechanisms, focusing on a variety of contributions made by the network participants rather than solely on their computational power or financial stake. PoC is particularly relevant in environments where

collaborative efforts and di- verse forms of participation are key to the network's success and sustainability [61]. It is suitable for social networks, community governance platforms, collaborative development platforms, educational platforms, and academic research.

2) PoC Description

The first step in implementing PoC is to clearly define what constitutes a valuable contribution to the network. This can include code development, network maintenance, community engagement, content creation, and even active participation in governance or decision-making processes. Then, contributions must be measurable and verifiable. This often involves the implementation of systems or protocols that can automatically track and verify contributions, such as smart contracts that log activities and their outcomes. In some cases, peer review or community voting might be used to assess contributions that are not easily quantifiable. Once contributions are tracked and verified, their value needs to be calculated. This calculation can be based on predefined metrics that may weigh different types of contributions according to their perceived value to the network. For example, fixing a critical network bug might be valued more highly than writing a community blog post. For block creation and validation, participants with higher scores are more likely to be chosen to create the next block or validate it. In general case, the proposed block is broadcast to the entire network, ensuring that all network participants or nodes have an opportunity to review and validate its contents [59], [62].

3) Advantages and Disadvantages

Advantages

- Encourages diverse participation, since PoC incentivizes a wide range of contributions, not just the monetary or computational, encouraging participants to contribute in various ways such as development, governance, content creation, and community support.
- Fostering a culture of contribution can strengthen community bonds and increase the collective commitment to the network's success.
- More decentralization.
- PoC is flexible and adaptable as the criteria for valuable contributions can be adjusted based on the network needs and goals.
- Enhances network security and resilience.

Disadvantages

- Complexity in term of value measurement.
- PoC results in a high administrative overhead for monitoring, validating, and rewarding various types of contributions.
- Focusing on measurable contributions might lead participants prioritizing activities that are explicitly rewarded, potentially neglecting other important but less tangible aspects of network participation.

4) PoC Rewarding Strategies

PoC emphasizes rewarding participants based on their contributions to a blockchain network. This approach is designed to encourage a variety of valuable activities that sustain and enhance the network. The functioning of PoC can be complex, as it involves multiple dimensions of contribution and often requires sophisticated systems to assess and reward these contributions. In fact, based on the calculated value of these contributions, the participants are rewarded. These rewards can be in the form of cryptocurrency, increased voting power, reputation scores, or other benefits designed to incentivize continued participation and investment in the network. The PoC system often includes mechanisms for continuously adjusting how contributions are measured and rewarded. This adaptability helps ensure that the system remains fair and relevant as the network's needs and the external environment change [61], [62].

O. PROOF OF ELAPSED TIME (POET)

1) History

Proof of Elapsed Time (PoET) is a consensus mechanism primarily developed and popularized within the context of permissioned blockchain networks. In 2016, PoET development was closely associated with Intel, one of the world's lead- ing technology companies, which designed PoET to lever- age specific hardware features for security and efficiency in blockchain operations. PoET was introduced by Intel as part of its Sawtooth Lake blockchain platform, which is now part of the Hyperledger consortium under the Linux Foundation. This platform was designed to cater to enterprise-level blockchain applications, focusing on scalability, security, and ease of integration with any existing systems [27], [39].

2) PoET Description

The Proof of Elapsed Time (PoET) consensus mechanism is designed to provide a fair and energy-efficient method for achieving consensus within a blockchain network, particularly in permissioned or enterprise settings. It leverages trusted execution environments (TEEs) to ensure that the process is secure and resistant to manipulation. Initially, each participating node in the blockchain must have access to a TEE, such as Intel's Software Guard Extensions (SGX). The node sets up its environment within this secure enclave to initiate the PoET process. Now, inside the secure enclave, a random wait time is generated for each node. This wait time is the key element of PoET; it determines how long a node must wait before it is eligible to propose a new block. The wait time is generated in a way that ensures it cannot be predicted or influenced by external factors or the nodes themselves. Therefore, each node enters a sleeping state for the duration of its assigned wait time, consuming minimal energy. Once a node's wait time expires, it wakes up and claims the right to propose a new block. The node then creates a block and includes in it a special PoET certificate that proves it has indeed waited for the designated time. Moreover, other nodes verify the PoET certificate attached to the new block. They check that the certificate is valid and that the waiting time was adhered to, confirming that the block was proposed fairly. This process relies on the inherent

security of the TEE, which is designed to be tamper-proof [63]–[65].

3) Advantages and Disadvantages

Advantages

- PoET minimizes energy consumption by eliminating the need for extensive computational efforts and competition, relying instead on a time-based mechanism.
- Fairness in block creation is guaranteed since every participating node has an equal chance of being selected to forge the next block. Selection is based on randomly assigned wait times, promoting fairness across the network [55].
- Low resource requirement, since it does not require solving complex mathematical puzzles. PoET can be run on devices with lower computational power, making it ideal for IoT devices and networks with varied hardware capabilities.
- PoET enhances scalability as it can handle more nodes without significant impacts on performance.
- PoET reduces the possibility of centralization because PoET's random timer system does not inherently favor nodes with more powerful hardware.
- Cost-effectiveness is achieved by reducing the need for high-end hardware and energy consumption [55], [66].

Disadvantages

- Dependence on TEEs as PoET's security and effectiveness heavily rely on the integrity of secure hardware such as Intel's SGX. Any vulnerabilities in this hardware could compromise the entire network [67].
- Limited to specific hardware, since PoET operates on the premise of using trusted execution environments, it is constrained to platforms that support these environments, limiting the diversity of the hardware that can participate in the network.
- Despite reducing computational costs, the initial setup and maintenance of secure hardware environments can be costly and complex, particularly for smaller organizations and individual participants.
- Hardware failure risks, since the dependence on hardware functionality means that hardware failures could lead to significant issues within the blockchain, including downtime or a loss of consensus capability [67].

4) PoET Rewarding Strategies

PoET provides a fair chance for every node to propose and validate blocks. Therefore, the nodes are fairly rewarded. In addition, PoET gives nodes a chance according to their reputation score. The reputation score increases and decreases based on the nodes' behaviors.

P. PROOF OF FAIRNESS (POF)

1) History

PoF is a consensus protocol proposed in 2024. It applies an auction-based model within consensus protocol to maintain both the system budget and the reward system [68].

2) PoF Description

PoF is an auction-based consensus protocol, where the auctioneer system first determines the transaction's processing cost and time limit. The miners bid the rewards they expect to propose a new block of transactions according to the auctioneer's conditions. The reverse auction is applied, and the miners are ordered ascendingly according to their beds, The winner will be the one who can perform the task with minimum reward. The next x nodes in the ascending-ordered list are selected to validate the proposed block. This gives a chance to every node in the system because some tasks are doable [68].

3) Advantages and Disadvantages

Advantages

- More fairness.
- There is a chance for poor and newly joined miners to participate in the doable tasks.
- Powerful nodes participate in difficult tasks and get fair rewards.
- The miner selection process and reward system are dynamic.
- Flexible rewards maintain the system budget.

Disadvantages

- Less decentralization as the auctioneer system controls part of the mechanism.
- The security of the bidding strategy is vital.

4) PoF Rewarding Strategies

In PoF, miners are rewarded with transaction fees. The rewards should be greater than the transaction's processing cost. The miners bid the rewards they expect to propose a new block of transactions. If the miner wins proposing or validating a new block, they will be rewarded with the same amount bid. The system will not exceed the cost margin thresholds [68].

Q. PRACTICAL BYZANTINE FAULT TOLERANCE (PBFT)

1) History

PBFT is a committee-based consensus protocol that was developed in 1999 by Castro and Liskov [69]. It was designed to address the limitations of the earlier Byzantine Fault Tolerance (BFT) protocols by offering improved performance and practicality for real-world applications.

2) Description

The PBFT protocol consists of three phases to tolerate faults and commit to transactions (in a block). The phases are (PrePrepare, Prepare, and Commit). In Pre-Prepare, a node can validate transactions and broadcast a new block of the validated transaction to all network participants for voting. The next phase is Prepare, in which the nodes vote on the new block. In the Commit phase, the block is committed and added to the blockchain when the number of in-favor votes exceeds a desirable threshold (mostly two-thirds of the votes) [70], [71].

3) Advantages and Disadvantages

Advantages

- Nowadays, the PBFT consensus protocol is extensively adopted as the leading consensus protocol in blockchains.
- Enhancing security, efficiency, throughput, and reducing confirmation delays compared to other major blockchain consensus protocols.

Disadvantages

- The PBFT communication complexity (especially as the network size grows), scalability, and fault tolerance issues limit its business application [72]–[74]

4) Rewarding Strategies

The PBFT can integrate various incentive mechanisms to encourage node participation and honest behavior in the network. This can include transaction fees or external reward systems depending on the specific application [75].

R. DELEGATED BYZANTINE FAULT TOLERANCE (DBFT)

1) History

Based on the PBFT protocol, the NEO Blockchain project proposed the DBFT consensus algorithm in 2014, made by Da Hongfei and Erik Zhang [76]. The DBFT elects trusted nodes to achieve consensus which can enhance scalability and efficiency in high-volume transactions smart contracts.

2) DBFT Description

The DBFT was originally developed for the NEO Blockchain project which aims to achieve faster confirmation time for block and transactions by selecting a set of validators through real-time blockchain voting. A set of validators is delegated to validate transactions and blocks instead of all nodes. The delegates follow the same phases that are mentioned in PBFT. In March 2019, an enhanced version, DBFT 2.0, was released to improve both the robustness and safety of the blockchain by integrating a three-stage consensus process with the addition of a recovery mechanism. A third version of DBFT 3.0 was proposed which includes an additional consensus phase (totaling four phases: PrepareRequest, PrepareResponse, Pre- Commit, and Commit). In PrepareRequest, a delegated node sends a new proposed block to the other delegates. In PrepareResponse, the delegates validate the proposed block and vote. In Pre-Commit, the delegates count the votes and confirm the final decision with others. In the Commit phase, the majority confirms the final decision. Pre-Commit is added to enable rolling back before committing [76], [77].

3) Advantages and Disadvantages

Advantages

- Achieves faster block and transaction confirmation times due to its efficient validator selection process [24].
- Less power consumption and fewer computations.

Disadvantages

- Centralization risk as nodes need to establish a trust relationship between them, which may reduce blockchain decentralization.
- The centralized behaviors can result in security threats.

4) DBFT Rewarding Strategies

The DBFT employs a rewarding strategy or an incentive model that consists of transaction fees and network fees. These fees are distributed as follows: 10% for the NEO holders who have completed a transfer or voting, 10% to the committee and consensus nodes for managing and governing the Neo network, and finally 80% for voters who successfully vote [76].

S. FEDERATED BYZANTINE AGREEMENT (FBA)

1) History

FBA was introduced by Mazieres in 2015 as part of the Stellar Consensus Protocol (SCP) project to achieve worldwide con- sensus asynchronously. In addition, Ripple and UNL share similarities with FBA, in term of having a trusted list and validation process [78].

2) FBA Description

Rather than relying on global majority voting or agree- ment, each participant in the SCP identifies a list of important other participants, who are sufficient enough to validate transactions or reach an agreement. Then, the nodes accept the decision of the trusted nodes when the agreement reaches a quorum or quorum slice. A quorum is the minimum number of trusted nodes that should agree on the block to commit it. FBA also uses quorum slices, which is a subset of a quorum, that convince others to agree based on trust [78].

3) Advantages and Disadvantages

Advantages

- SCP can feature decentralized control, low latency, flexible trust, and asymptotic security.
- Avoids central authority, achieves consensus in seconds, trusts any desirable party, and applies hash and digital signatures for security.

Disadvantages

- The safety of the SCP depends on the nodes selecting sufficient quorum slices because of misconfiguration risks and unethical financial behavior by users.
- Transaction delays due to filtering where performance and latency are not optimal.
- If all nodes leave simultaneously, the system requires a consensus reset which may need central coordination.

4) FBA Rewarding Strategies

When FBA was introduced, the rewarding strategy did not exist. Hence, it was criticized for its safety and the lack of incentives [79]. In a recent work proposed by [80], they implemented a fair reward distribution based on Cooperative Game Theory (CGT) that distributes rewards based on a node's contribution. Although the paper does not specify the kind of rewards, their goal was to show that FBA is compatible with incentives.

T. PROOF OF QUALITY OF SERVICE (PROOF OF QOS)

1) History

Proof of QoS is a leader-based mechanism, that was first men- tioned in a work published in 2019 by a team of

researchers led by Bin Yu and Joseph Lui [81]. It has recently been used to integrate blockchain, cloud computing, and edge computing [81], [82].

2) Proof of QoS Description

Proof of QoS is centered around the concept of quality of service (QoS). Based on QoS, the collection of sub-regions nominates a leader. After that BFT initiates the election process. This consensus protocol enables throughput and the fairness property is considered among all participants. The system is divided into four regions, where each region has three miners. To elect the representative of a region, minors in the subregions suggest four candidate nominations. The nominated miners share the transactions and apply PBFT. Additionally, the nominated nodes send the new block to the region. The remaining nodes verify the identity of the minor and they validate the correctness of the block attach the new block to the ledger, and proceed further [81], [82].

3) Advantages and Disadvantages

Advantages

- High transaction throughput.
- Fairness among all nodes.
- Openness.

Disadvantages

- Can't deploy in high-performance infrastructures.
- It suffers from centralization and security issues as it is a leader-based mechanism.

4) Proof of QoS Rewarding Strategies

In Proof of QoS, the committee members claim rewards from proposed blocks. Nodes with similar QoS factors and probability claim the reward and provide fairness among the nodes. The rewards mechanism of the leader-based mechanism and PBFT can be applied to Proof of QoS.

U. RELIABLE, REPLICATED, REDUNDANT AND FAULT TOLERANT (RAFT)

1) History

RAFT is an alternative to the Paxos consensus algorithm that was introduced in 1989 by Leslie Lamport. The Paxos consensus algorithm enables reaching consensus within a distributed system while some participants experience periodic failure and communication issues. RAFT is a leader-based mechanism that was introduced by Diego Ongaro and John Ousterhout, in 2014 and has been used for both consortium and private blockchain. RAFT is widely used for managing replicated logs, such as databases and container orchestration systems [83], [84].

2) RAFT Description

In RAFT a group of nodes agrees upon a state or single value of the system. Indeed, RAFT is one shape of leader-based algorithms, where all nodes agree on the same sequence for the logging data. The leader has a record of logs, all nodes act to follow the same logging record of the leader. Therefore, a node is considered to be a successful validator, when the logs in the majority of nodes are replicated in its logging record. Indeed, to create a new block, the leader selects a miner to propose the new block. This miner is the one that replicates the leader's logs records the most. Then, all nodes validate the proposed block, and the leader promotes agreement based on the log replication regarding block validation [83]–[85]. This also requires to application of a secure data sharing scheme [86].

3) Advantages and Disadvantages

Advantages

- Easy to implement.
- Enhances understandability and reduces the number of states.
- Stronger degree of coherency.
- Suitable for fault tolerant systems.

Disadvantages

- Cost of additional mechanisms and complexity.
- Raft's log entries flow in only one direction, outward from the leader, which affects decentralization.

4) RAFT Rewarding Strategies

In RAFT, rewarding strategies can be implemented at a higher level in systems built on top of RAFT. Developers can design and implement their reward mechanisms based on the specific requirements of their application. For example, leaders should be rewarded according to how much they can maintain system consistency and reach consensus, while followers should be rewarded according to how much they replicate the leader and the majority [87].

V. DIRECTED ACYCLIC GRAPH (DAG)

1) History

DAG's application in cryptocurrency gained prominence with projects like the Internet of Things Application (IOTA), which debuted in 2015 on the NXT platform. The specific application of DAG to cryptocurrencies does not have a single inventor and instead evolved through multiple projects. DAG is a variant of Distributed Ledger Technology (DLT) that pro-vides enhanced decentralization, less energy consumption, and faster transactions. Compared to traditional consensus mechanisms, DAG is adopted by many projects due to its user-friendly hosting solutions. For different kinds of hierarchy, DAG has some modified forms such as BlockDAG and UL-Block [88]–[91].

2) DAG Description

DAG employs the idea of directed acyclic graphs where trans- actions are considered as graph vertices and the edges repre- sent the dependency between transactions. The transactions can be validated simultaneously and added to the graph. The dependent transactions will be connected by edges as they are validated one after the other. In DAG, the validated transac- tions are added directly to the chain (graph) in a specific order, and there is no need to compete to create a block [88], [89].

3) Advantages and Disadvantages

Advantages

- High scalability and connectivity.
- High throughput as no mining process is required.
- Low transaction fees.
- Solves the double spending issue.

Disadvantages

- Security concerns, particularly with smaller networks, as the transactions are validated and added directly to the DAG without block creation, hashing, or block validation.
- Initial phases might require a coordinator for network integrity and to arrange the validator's joining process.

4) DAG Rewarding Strategies

DAG protocols usually don't involve traditional mining; thus, they do not have direct rewarding mechanisms for transaction validation. Instead, the incentive to participate in the network comes from the utility of the system and potentially from transaction fees (which are low) in some implementations. Therefore, research introduces a reward strategy to incen- tivize miners to serve systems of public ledgers. In which, miners are rewarded with a fixed fee as they participate in transaction validation, plus the transaction fees of the valid transactions are added to an approved block [89].

IV. DISCUSSION

In a democratic electronic system, all nodes participate in system processes. So, keeping network members synchronized is achieved through a consensus mechanism. When decentralization is implemented, each network member is granted equal voting rights in system decisions. Therefore, it is essential to establish rules that allow the nodes (network members) to reach an agreement and globally execute new system updates. The consensus mechanism in a decentralized network ensures that all participating nodes have an equal opportunity to propose and validate updates. As a result, the network can collectively decide on its next update. Each node in a blockchain continuously communicates with others, as they all maintain a copy of the network's transactions. Through consensus, the nodes agree on the current state of the ledger, preserving its operational integrity and enabling decentralization without disorder. This consensus not only ensures agreement on the current state but also eliminates errors and protects the network from threats like double-spending and Sybil attacks, where malicious actors use fake nodes to manipulate the network.

As early as 2009, Bitcoin was the first widely recog- nized blockchain model that employed the PoW consensus algorithm. In this way, PoW became one of the first kinds of consensus system. However, periodic developments and implementations have led to the development of other, more innovative consensus protocols.

This section explores the nature of consensus protocols and the associated reward strategies.

TABLE 1. The Categories of Consensus Protocols

Categories	Consensus Protocols
Computational-based	PoW, PoeX and PoSpace
Wealth-based	PoS, DPoS, LPoS, PoB, and PoX
behavioral-based	PoAuth, UNL, Ripple, PoI, PoR, and PoC
Fairness-based	PoET and BoF
Fault-tolerance-based	PBFT, DBFT and FBA
Leader-based	Proof of QoS and RAFT
Transactional-based	DAG

A. *OVERVIEW OF THE NATURE OF THE CONSENSUS PROTOCOLS*

Consensus protocols can be categorized into computational-based, wealth-based, behavioral-based, fairness-based, fault-tolerance-based, leader-based, and transactional-based as shown in Table 1.

First, the computational-based consensus protocols include PoW, PoeX, and PoSpace. The fundamental consensus proto- col, PoW, is employed by Bitcoin, enabling cryptocurrency miners to resolve intensive mathematical calculations. It is used to calculate the correct hash of a block by modifying the block's nonce. The first miner to solve the problem correctly is permitted the privilege of adding a new block. PoeX also uses computational power to resolve real-world matrix-based scientific computation problems instead of a hash calculation. Both protocols are usable for systems with high computational demands. While PoSpace helps to provide hardware resources to facilitate such computations.

Second, wealth-based consensus protocols include: PoS, DPoS, LPoS, PoB, and PoX. They all move the emphasis away from computational capacity and towards economic stake. The quantity of cryptocurrency a miner possesses, stakes, leases, burns, transfers, or uses efficiently to support the system will enhance the miner's chance to contribute or validate a new block. These protocols save energy and are useful for economic systems such as cryptocurrency in-vestments and management systems in order to cope with economic matters such as currency rates, currency trading, inflation, and recession. For example, in the case of inflation, the use of PoB ensures that cryptocurrency coins are burned and permanently removed from circulation to prevent them from coming back to the money supply.

Third, behavioral-based protocols are PoAuth, UNL, Rip-ple, PoI, PoR, and PoC. All of them replace the energy and wealth capacities in a participants' behavior. They give scores and ranks to miners according to their activities, conduct, and ethics, which also enables blockchain applications in other areas. These protocols are useful for centralized or partially decentralized situations, these protocols are necessary for preserving the trustworthiness and stability of the network. In addition, they are suitable for systems that rely on one user's active interactions. Additionally, they are also useful for systems that require high-speed actions and responses.

Fourth, PoET and PoF focus on providing fair participation among users. PoET, designed for permissioned blockchains, uses trusted execution environments (TEEs) to assign random wait times to nodes, allowing them to propose blocks based on time rather than computational power, wealth, or reputation. PoET is suitable for enterprise-level blockchain applications.

Fifth, PBFT and its variations, such as DBFT and FBA, offer effective procedures for Fault Tolerance. They enable reaching consensus and continuing to function normally even while some of the nodes in the network are malfunctioning.

Sixth, leader-based protocols such as PoQoS and RAFT compromise decentralization for speed and certainty.

Notably, both RAFT and PoQoS also fall under fault-tolerance-based protocols. They can offer the added benefit of maintaining network stability and resilience whenever the possibility of faults exists.
Seventh, some applications use unique approaches such as DAG structures to rapidly validate transactions and grow without the need for traditional blocks, or by treating each transaction itself as a block. It is also a graph-based model which is suitable for graph-based blockchain applications.
Finally, some of these consensus protocols are hybrids and intersect with other categories. For example, Proof of Weight involves the features of PoS, PoI, PoR, and PoC; while Proof of Identity involves features of PoF and PoAuth. This allows them to be applied in various areas and use cases.

B. *REWARDING STRATEGIES*

This section discusses the diversity in rewarding strategies, punishment strategies, and rewarding limitations. Firstly, there is significant diversity in term of rewarding used across different protocols, as follows:

- Newly mined cryptocurrency as in PoW, PoSpace, PoB, and PoX.
- Transaction fee as in all consensus protocols that are applied to cryptocurrency systems such as PoW, PoS, and others.
- System reserves such as in PoS, Ripple and, UNL.
- Prizes for solving some computations or performing tasks such as in PoeX.
- Different forms of liquidity such as certificates, stokes, and others as used by PoS, DPoS, and PoC.
- Reputation and trust scores such as in PoAuth, PoI, PoR, PoC, and PoET.
- More privileges such as increasing voting power as in PBFT, DBFT, FBA, and QoS.

Now, we focus on the rewarding procedures. All consensus protocols give rewards when miners perform tasks correctly such as transaction validation, block creation, block validation, and other tasks. These tasks can be updating specific protocols as in PoW, providing storage space as in PoSpace, and using a passive stake as in PoS and its variants. In addition, PoET links rewards to the duration of time waiting, which is suitable for permissioned blockchain networks. PoF uses the auction-based system for miners selection and rewarding. PoeX, PoX, PoAuth, UNL, Ripple, PoI, PoR, and PoC link rewards to the miner's activities and manners. RAFT focuses on a leader and follower agreement. This paper illustrates different kinds of reward strategies that can be involved in new versions of the consensus protocols. For example, a new application that uses PoW could include a reputation score as a rewarding strategy to control the misbehaviors of miners.
Secondly, to guarantee the adequate behaviors of miners, there is a diverse range of punishments available. Unlike PoW protocols, which use the economic disincentive of wasted computational resources to discourage malicious behavior, PoS and PoB use smart contracts to cut tokens in cases of dishonest miners. PoeX, PoX, PoAuth, UNL, Ripple, PoI, PoR, and PoC use reputation scores to encourage and punish miners. Fault tolerance and leader-based protocols often employ mechanisms to identify and reject nodes that are not functioning properly, maintaining the integrity of the network [1], [3].
Thirdly, there are some limitations to the existing protocols and rewarding strategies. New kinds of tokens should be involved such as free educational courses, real estate assets, marketing products, services, IoT sensors, and art pieces (such as videos, paintings, and music) [92]–[95]. Those tokens can be transparently exchanged using blockchain applications. They can be also stored or reserved to maintain their price through supply and change management. Additionally, to enhance supply, these tokens can be produced and supplied to communities in the form of rewards, or in exchange for another product that requires to be cut [96]–[98]. Moreover, the existing systems lack soft tokens, such as human resources requirements, student attributes, and laborer skills, where some skills need to be promoted, developed, and assessed in the community.

V. CONCLUSIONS

This work explores the application of blockchain technology in many areas through exploring the nature of consensus protocols. In addition, miners are motivated by different rewarding strategies. Therefore, this work investigated a wide range of consensus protocols and their corresponding rewarding strategies. It highlights the primary contributions of comprehensive analysis, exploration of punishment mechanisms, and places an emphasis on efficiency and security. It categorizes the consensus protocol into seven categories for application. It shows the limitations of the existing rewards, suggesting the other nine types. In the future, we will work on designing customized consensus protocols and develop the existing ones for specific real-life applications. Enhancing rewarding and punishment strategies for each protocol is another area of improvement.

ACKNOWLEDGMENT

The authors gratefully acknowledge the funding of the Deanship of Graduate Studies and Scientific Research, Jazan University, Saudi Arabia, through project number: (RG24-S0149).

REFERENCES

[1] B. Assiri and W. Z. Khan, ‘‘Enhanced and lock-free tendermint blockchain protocol,’’ in 2019 IEEE International Conference on Smart Internet of Things (SmartIoT). IEEE, 2019, pp. 220–226.
[2] K. K. Vaigandla, R. Karne, M. Siluveru, and M. Kesoju, ‘‘Review on blockchain technology: architecture, characteristics, benefits, algorithms, challenges and applications,’’ Mesopotamian Journal of CyberSecurity, vol. 2023, pp. 73–84, 2023.
[3] B. Assiri and W. Z. Khan, ‘‘Fair and trustworthy: Lock-free enhanced tendermint blockchain algorithm,’’ TELKOMNIKA (Telecommunication

Computing Electronics and Control), vol. 18, no. 4, pp. 2224–2234, 2020.

[4] F. R. B. of Boston and M. I. of Technology Digital Currency Initiative, ''Project hamilton phase 1 executive summary,'' https://www.bostonfed.org/publications/one-time-pubs/project-hamilton- phase-1-executive-summary.aspx, 2022, accessed on 05-January-2025.

[5] T. W. House, ''Fact sheet: President biden to sign execu- tive order on ensuring responsible development of digital assets,'' https://www.whitehouse.gov/briefing-room/statements- releases/2022/03/09/fact-sheet-president-biden-to-sign-executive-order- on-ensuring-responsible-innovation-in-digital-assets/, 2022, accessed on 05-January-2025.

[6] A. Singh, S. C. Satapathy, A. Roy, and A. Gutub, ''Ai-based mobile edge computing for iot: Applications, challenges, and future scope,'' Arabian Journal for Science and Engineering, vol. 47, no. 8, pp. 9801–9831, 2022.

[7] N. Farooqi, A. Gutub, and M. O. Khozium, ''Smart community challenges: enabling iot/m2m technology case study,'' Life Science Journal, vol. 16, no. 7, pp. 11–17, 2019.

[8] I. G. A. K. Gemeliarana and R. F. Sari, ''Evaluation of proof of work (pow) blockchains security network on selfish mining,'' in 2018 International seminar on research of information technology and intelligent systems (ISRITI). IEEE, 2018, pp. 126–130.

[9] H. Baniata and A. Kertesz, ''Approaches to overpower proof-of-work blockchains despite minority,'' IEEE Access, vol. 11, pp. 2952–2967, 2023.

[10] A. Singh, A. Gutub, A. Nayyar, and M. K. Khan, ''Redefining food safety traceability system through blockchain: findings, challenges and open issues,'' Multimedia Tools and Applications, vol. 82, no. 14, pp. 21 243–21 277, 2023.

[11] N. T. T. Thuy, L. D. Khai et al., ''A fast approach for bitcoin blockchain cryptocurrency mining system,'' Integration, vol. 74, pp. 107–114, 2020.

[12] R. Beer and T. Sharma, ''A quick look at cryptocurrency mining: Proof of work,'' in 2022 2nd International Conference on Innovative Practices in Technology and Management (ICIPTM), vol. 2. IEEE, 2022, pp. 651– 656.

[13] A. Capponi, S. Olafsson, and H. Alsabah, ''Proof-of-work cryptocurren- cies: Does mining technology undermine decentralization?'' Management Science, vol. 69, no. 11, pp. 6455–6481, 2023.

[14] W. Zhao, S. Yang, X. Luo, and J. Zhou, ''On peercoin proof of stake for blockchain consensus,'' in Proceedings of the 2021 3rd International Conference on Blockchain Technology, 2021, pp. 129–134.

[15] C. Lepore, M. Ceria, A. Visconti, U. P. Rao, K. A. Shah, and L. Zanolini, ''A survey on blockchain consensus with a performance comparison of pow, pos and pure pos,'' Mathematics, vol. 8, no. 10, p. 1782, 2020.

[16] E. Kapengut and B. Mizrach, ''An event study of the ethereum transition to proof-of-stake,'' Commodities, vol. 2, no. 2, pp. 96–110, 2023.

[17] A. Chauhan, Rishabh, L. N. Shankar, and P. Mittal, ''A deep dive into blockchain consensus protocols,'' in Smart Trends in Computing and Com- munications: Proceedings of SmartCom 2021. Springer, 2022, pp. 571–581.

[18] A. Jain and D. S. Jat, ''A review on consensus protocol of blockchain technology,'' Intelligent Sustainable Systems: Selected Papers of WorldS4 2021, Volume 2, pp. 813–829, 2022.

[19] D. P. Oyinloye, J. S. Teh, N. Jamil, and M. Alawida, ''Blockchain con- sensus: An overview of alternative protocols,'' Symmetry, vol. 13, no. 8, p. 1363, 2021.

[20] A. Wahab and W. Mehmood, ''Survey of consensus protocols,'' arXiv preprint arXiv:1810.03357, 2018.

[21] C. Chenli, B. Li, Y. Shi, and T. Jung, ''Energy-recycling blockchain with proof-of-deep-learning,'' in 2019 IEEE International Conference on Blockchain and Cryptocurrency (ICBC). IEEE, 2019, pp. 19–23.

[22] O. A. Logachev and S. N. Fedorov, ''On a class of descrete functions for proof-of-space blockchain consensus protocols,'' International Journal of Open Information Technologies, vol. 8, no. 12, pp. 33–38, 2020.

[23] M. J. Heule, ''Proofs of unsatisfiability,'' in Handbook of Satisfiability. IOS Press, 2021, pp. 635–668.

[24] J. Xu, C. Wang, and X. Jia, ''A survey of blockchain consensus protocols,'' ACM Computing Surveys, vol. 55, no. 13s, pp. 1–35, 2023.

[25] I. Giacomelli, ''Filecoin: from proof-of-space blockchain to decentralized storage.'' CrypTorino 2021, p. 27, 2024.

[26] S. R. Chowdhary, ''A systematic analysis on blockchain consensus algo- rithms and security threats,'' International Journal of Computer Science and Mobile Computing, vol. 11, no. 7, pp. 8–17, 2022.

[27] N. Bhutani, G. K. Chadha, and V. Nehra, ''Analysis of different consensus algorithms with development of blockchain based cryptocurrency and initial coin offering,'' in 2021 9th International Conference on Reliabil- ity, Infocom Technologies and Optimization (Trends and Future Direc- tions)(ICRITO). IEEE, 2021, pp. 1–9.

[28] S. Kotha and P. Patel, ''Blockchain in depth,'' International Journal of Engineering and Computer Science, vol. 9, no. 5, pp. 25 029–25 038, 2022.

[29] M. Veinović et al., ''Comparative analysis of consensus algorithms in blockchain networks,'' in Sinteza 2021-International Scientific Conference on Information Technology and Data Related Research. Singidunum University, 2021, pp. 128–133.

[30] I. F. T. Alyaseen et al., ''Consensus algorithms blockchain: A comparative study,'' International

Journal on Perceptive and Cognitive Computing, vol. 5, no. 2, pp. 66–71, 2019.

[31] S.-N. Li, F. Spychiger, and C. J. Tessone, ‘‘Reward distribution in proof-of- stake protocols: A trade-off between inclusion and fairness,’’ IEEE Access, vol. 11, pp. 134 136–134 145, 2023.

[32] L. Brünjes, A. Kiayias, E. Koutsoupias, and A.-P. Stouka, ‘‘Reward sharing schemes for stake pools,’’ in 2020 IEEE european symposium on security and privacy (EuroS&p). IEEE, 2020, pp. 256–275.

[33] F. Saleh, ‘‘Blockchain without waste: Proof-of-stake,’’ The Review of fi- nancial studies, vol. 34, no. 3, pp. 1156–1190, 2021.

[34] A. Barhanpure, P. Belandor, and B. Das, ‘‘Proof of stack consensus for blockchain networks,’’ in Security in Computing and Communications: 6th International Symposium, SSCC 2018, Bangalore, India, September 19– 22, 2018, Revised Selected Papers 6. Springer, 2019, pp. 104–116.

[35] K. Karantias, A. Kiayias, and D. Zindros, ‘‘Proof-of-burn,’’ in Financial Cryptography and Data Security: 24th International Conference, FC 2020, Kota Kinabalu, Malaysia, February 10–14, 2020 Revised Selected Papers 24. Springer, 2020, pp. 523–540.

[36] A. A. Menon, T. Saranya, S. Sureshbabu, and A. Mahesh, ‘‘A comparatıve analysis on three consensus algorithms: proof of burn, proof of elapsed time, proof of authority,’’ in Computer Networks and Inventive Commu- nication Technologies: Proceedings of Fourth ICCNCT 2021. Springer, 2022, pp. 369–383.

[37] D. Wang, C. Jin, H. Li, and M. Perkowski, ‘‘Proof of activity consensus algorithm based on credit reward mechanism,’’ in Web Information Systems and Applications: 17th International Conference, WISA 2020, Guangzhou, China, September 23–25, 2020, Proceedings 17. Springer, 2020, pp. 618–628.

[38] Z. Ai and W. Cui, ‘‘A proof-of-transactions blockchain consensus protocol for large-scale iot,’’ IEEE Internet of Things Journal, vol. 9, no. 11, pp. 7931–7943, 2021.

[39] S. Fahim, S. K. Rahman, and S. Mahmood, ‘‘Blockchain: A comparative study of consensus algorithms pow, pos, poa, pov,’’ Int. J. Math. Sci. Comput, vol. 3, pp. 46–57, 2023.

[40] U. S. Aditya, R. Singh, P. K. Singh, and A. Kalla, ‘‘A survey on blockchain in robotics: Issues, opportunities, challenges and future directions,’’ Jour- nal of Network and Computer Applications, vol. 196, p. 103245, 2021.

[41] A. C. An, P. T. X. Diem, T. Van Toi, L. D. Q. Binh et al., ‘‘Building a product origins tracking system based on blockchain and poa consensus protocol,’’ in 2019 international conference on advanced computing and applications (ACOMP). IEEE, 2019, pp. 27–33.

[42] S. B. Wankhede and D. Patel, ‘‘The proof of authority consensus algorithm for iiot security,’’ in The International Conference on Recent Innovations in Computing. Springer, 2022, pp. 803–811.

[43] J. Yang, J. Dai, H. B. Gooi, H. D. Nguyen, and A. Paudel, ‘‘A proof-of- authority blockchain-based distributed control system for islanded micro- grids,’’ IEEE Transactions on Industrial Informatics, vol. 18, no. 11, pp. 8287–8297, 2022.

[44] S. Gopikrishnan, P. Priakanth, G. Srivastava, and C. V. Joe, ‘‘Scheisb: Design of a high efficiency iomt security model based on sharded chains using bio-inspired optimizations,’’ Computers and Electrical Engineering, vol. 111, p. 108925, 2023.

[45] G. A. F. Rebello, G. F. Camilo, L. C. Guimaraes, L. A. C. de Souza, G. A. Thomaz, and O. C. M. Duarte, ‘‘A security and performance analysis of proof-based consensus protocols,’’ Annals of Telecommunications, pp. 1– 21, 2022.

[46] M. M. Islam, M. M. Merlec, and H. P. In, ‘‘A comparative analysis of proof-of-authority consensus algorithms: Aura vs clique,’’ in 2022 IEEE International Conference on Services Computing (SCC). IEEE, 2022, pp. 327–332.

[47] Q. Wang, R. Li, Q. Wang, S. Chen, and Y. Xiang, ‘‘Exploring unfair- ness on proof of authority: Order manipulation attacks and remedies,’’ in Proceedings of the 2022 ACM on Asia Conference on Computer and Communications Security, 2022, pp. 123–137.

[48] M. A. Manolache, S. Manolache, and N. Tapus, ‘‘Decision making using the blockchain proof of authority consensus,’’ Procedia Computer Science, vol. 199, pp. 580–588, 2022.

[49] S. Altalhi and A. Gutub, ‘‘A survey on predictions of cyber-attacks utilizing real-time twitter tracing recognition,’’ Journal of Ambient Intelligence and Humanized Computing, pp. 1–13, 2021.

[50] X. Si, M. Li, Z. Yao, W. Zhu, J. Liu, and Q. Zhang, ‘‘An efficient and secure blockchain consensus protocol for internet of vehicles,’’ Electronics, vol. 12, no. 20, p. 4285, 2023.

[51] S. Pahlajani, A. Kshirsagar, and V. Pachghare, ‘‘Survey on private blockchain consensus algorithms,’’ in 2019 1st International Conference on Innovations in Information and Communication Technology (ICIICT). IEEE, 2019, pp. 1–6.

[52] K. Li, H. Li, H. Wang, H. An, P. Lu, P. Yi, and F. Zhu, ‘‘Pov: An efficient voting-based consensus algorithm for consortium blockchains,’’ Frontiers in Blockchain, vol. 3, p. 11, 2020.

[53] B. Lashkari and P. Musilek, ‘‘A comprehensive review of blockchain consensus mechanisms,’’ IEEE access, vol. 9, pp. 43 620–43 652, 2021.

[54] B. Xiao, C. Jin, Z. Li, B. Zhu, X. Li, and D. Wang, ‘‘Proof of importance: A consensus algorithm for importance based on dynamic authorization,’’ in IEEE/WIC/ACM International Conference on Web Intelligence and Intelligent Agent Technology, 2021, pp. 510–513.

[55] S. Aggarwal and N. Kumar, ‘‘Cryptographic consensus mechanisms,’’ in Advances in computers. Elsevier, 2021, vol. 121, pp. 211–226.
[56] A. O. Bada, A. Damianou, C. M. Angelopoulos, and V. Katos, ‘‘Towards a green blockchain: A review of consensus mechanisms and their energy consumption,’’ in 2021 17th international conference on distributed com- puting in sensor systems (DCOSS). IEEE, 2021, pp. 503–511.
[57] Q. Zhuang, Y. Liu, L. Chen, and Z. Ai, ‘‘Proof of reputation: A reputation- based consensus protocol for blockchain based systems,’’ in Proceedings of the 1st International Electronics Communication Conference, 2019, pp. 131–138.
[58] J. Yu, D. Kozhaya, J. Decouchant, and P. Esteves-Verissimo, ‘‘Repucoin: Your reputation is your power,’’ IEEE Transactions on Computers, vol. 68, no. 8, pp. 1225–1237, 2019.
[59] D. P. Oyinloye, J. S. Teh, N. Jamil, and J. Teh, ‘‘Sim-p—a simplified consensus protocol simulator: Applications to proof of reputation-x and proof of contribution,’’ IEEE Internet of Things Journal, vol. 10, no. 6, pp. 5083–5094, 2022.
[60] J. Yuan and L. Njilla, ‘‘Lightweight and reliable decentralized reward system using blockchain,’’ in IEEE INFOCOM 2021-IEEE Conference on Computer Communications Workshops (INFOCOM WKSHPS). IEEE, 2021, pp. 1–6.
[61] H. Song, N. Zhu, R. Xue, J. He, K. Zhang, and J. Wang, ‘‘Proof-of- contribution consensus mechanism for blockchain and its application in intellectual property protection,’’ Information processing & management, vol. 58, no. 3, p. 102507, 2021.
[62] T. Xue, Y. Yuan, Z. Ahmed, K. Moniz, G. Cao, and C. Wang, ‘‘Proof of con- tribution: A modification of proof of work to increase mining efficiency,’’ in 2018 IEEE 42nd annual computer software and applications conference (COMPSAC), vol. 1. IEEE, 2018, pp. 636–644.
[63] T. Aslam, A. Maqbool, M. Akhtar, A. Mirza, M. A. Khan, W. Z. Khan, and S. Alam, ‘‘Blockchain based enhanced erp transaction integrity archi- tecture and poet consensus,’’ Computers, Materials & Continua, vol. 70, no. 1, pp. 1089–1109, 2022.
[64] M. A. Kumar, V. Radhesyam, and B. SrinivasaRao, ‘‘Front-end iot ap- plication for the bitcoin based on proof of elapsed time (poet),’’ in 2019 Third International Conference on Inventive Systems and Control (ICISC). IEEE, 2019, pp. 646–649.
[65] M. Zouina and B. Outtai, ‘‘Towards a distributed token based payment system using blockchain technology,’’ in 2019 international conference on advanced communication technologies and networking (commnet). IEEE, 2019, pp. 1–10.
[66] N. Ramkumar, G. Sudhasadasivam, and K. Saranya, ‘‘A survey on different consensus mechanisms for the blockchain technology,’’ in 2020 Interna- tional Conference on Communication and Signal Processing (ICCSP). IEEE, 2020, pp. 0458–0464.
[67] H. Wang, G. Chen, Y. Zhang, and Z. Lin, ‘‘Multi-certificate attacks against proof-of-elapsed-time and their countermeasures.’’ in NDSS, 2022.
[68] A. Alamer and B. Assiri, ‘‘Proof of fairness: Dynamic and secure consensus protocol for blockchain,’’ Electronics, vol. 13, no. 6, p. 1056, 2024.
[69] M. Castro, B. Liskov et al., ‘‘Practical byzantine fault tolerance,’’ in OsDI, vol. 99, no. 1999, 1999, pp. 173–186.
[70] L. Yang, Y. Zou, M. Xu, Y. Xu, D. Yu, and X. Cheng, ‘‘Distributed consen- sus for blockchains in internet-of-things networks,’’ Tsinghua Science and Technology, vol. 27, no. 5, pp. 817–831, 2022.
[71] X. Qi, Z. Chen, Z. Zhang, C. Jin, A. Zhou, H. Zhuo, and Q. Xu, ‘‘A byzan- tine fault tolerant storage for permissioned blockchain,’’ in Proceedings of the 2021 International Conference on Management of Data, 2021, pp. 2770–2774.
[72] K. Venkatesan and S. B. Rahayu, ‘‘Blockchain security enhancement: an approach towards hybrid consensus algorithms and machine learning techniques,’’ Scientific Reports, vol. 14, no. 1, p. 1149, 2024.
[73] J. Yang, Z. Jia, R. Su, X. Wu, and J. Qin, ‘‘Improved fault-tolerant consen- sus based on the pbft algorithm,’’ Ieee Access, vol. 10, pp. 30 274–30 283, 2022.
[74] O. Onireti, L. Zhang, and M. A. Imran, ‘‘On the viable area of wireless practical byzantine fault tolerance (pbft) blockchain networks,’’ in 2019 IEEE global communications conference (GLOBECOM). IEEE, 2019, pp. 1–6.
[75] C. Li, J. Zhang, X. Yang, and L. Youlong, ‘‘Lightweight blockchain consensus mechanism and storage optimization for resource-constrained iot devices,’’ Information Processing & Management, vol. 58, no. 4, p. 102602, 2021.
[76] I. M. Coelho, V. N. Coelho, R. P. Araujo, W. Yong Qiang, and B. D. Rhodes, ‘‘Challenges of pbft-inspired consensus for blockchain and enhancements over neo dbft,’’ Future Internet, vol. 12, no. 8, p. 129, 2020.
[77] S. Basudan, ‘‘Ipfs-blockchain-based delegation model for internet of medi- cal robotics things telesurgery system,’’ Connection Science, vol. 36, no. 1, p. 2367549, 2024.
[78] E. W. Nugroho, ‘‘Analyzing the federated byzantine agreement blockchain network for liveness using multiple online analytical processing,’’ in 2023 7th International Conference on Information Technology (InCIT). IEEE, 2023, pp. 135–140.
[79] M. Kim, Y. Kwon, and Y. Kim, ‘‘Is stellar as secure as you think?’’ in 2019 IEEE European Symposium on Security and Privacy Workshops (EuroS&PW). IEEE, 2019, pp. 377–385.

[80] C. Ndolo, M. Florian, and F. Tschorsch, ‘‘Fair reward distribution in feder- ated byzantine agreement systems,’’ in 2023 5th Conference on Blockchain Research & Applications for Innovative Networks and Services (BRAINS). IEEE, 2023, pp. 1–8.

[81] B. Yu, J. Liu, S. Nepal, J. Yu, and P. Rimba, ‘‘Proof-of-qos: Qos based blockchain consensus protocol,’’ Computers & Security, vol. 87, p. 101580, 2019.

[82] Y. Zhang, L. Zhang, Y. Liu, and X. Luo, ‘‘Proof of service power: A blockchain consensus for cloud manufacturing,’’ Journal of Manufacturing Systems, vol. 59, pp. 1–11, 2021.

[83] X. Xu, L. Hou, Y. Li, and Y. Geng, ‘‘Weighted raft: An improved blockchain consensus mechanism for internet of things application,’’ in 2021 7th International Conference on Computer and Communications (ICCC). IEEE, 2021, pp. 1520–1525.

[84] Y. Li, Y. Fan, L. Zhang, and J. Crowcroft, ‘‘Raft consensus reliability in wireless networks: Probabilistic analysis,’’ IEEE Internet of Things Journal, vol. 10, no. 14, pp. 12 839–12 853, 2023.

[85] T. Wang, D. Huang, and S. Zhang, ‘‘Consensus algorithm analysis in blockchain: Pow and raft,’’ Wireless Blockchain: Principles, Technologies and Applications, pp. 27–72, 2021.

[86] A. M. A. Alamer, ‘‘A secure and privacy blockchain-based data sharing scheme in mobile edge caching system,’’ Expert Systems with Applications, vol. 237, p. 121572, 2024.

[87] H. Dong, W. Xiong, D. Goyal, Y. Zhang, W. Chow, R. Pan, S. Diao, J. Zhang, K. Shum, and T. Zhang, ‘‘Raft: Reward ranked finetuning for generative foundation model alignment,’’ arXiv preprint arXiv:2304.06767, 2023.

[88] Z. Hussein, M. A. Salama, and S. A. El-Rahman, ‘‘Evolution of blockchain consensus algorithms: a review on the latest milestones of blockchain consensus algorithms,’’ Cybersecurity, vol. 6, no. 1, p. 30, 2023.

[89] J. He, G. Wang, G. Zhang, and J. Zhang, ‘‘Consensus mechanism design based on structured directed acyclic graphs,’’ Blockchain: Research and Applications, vol. 2, no. 1, p. 100011, 2021.

[90] M. Revanesh, J. M. Acken, and V. Sridhar, ‘‘Dag block: Trust aware load balanced routing and lightweight authentication encryption in wsn,’’ Future Generation Computer Systems, vol. 140, pp. 402–421, 2023.

[91] A. Tokhmetov, V. Lee, and L. Tanchenko, ‘‘Development of dag blockchain model,’’ Scientific Journal of Astana IT University, 2023.

[92] Z. Zhao, ‘‘Fulfilling the right to follow: using blockchain to enforce the artist’s resale right,’’ Cardozo Arts & Ent. LJ, vol. 39, p. 239, 2021.

[93] O. Shmatko, T. Borova, S. Yevseiev, and O. Milov, ‘‘Tokenization of educa- tional assets based on blockchain technologies,’’ ScienceRise: Pedagogical Education, no. 3 (42), pp. 4–10, 2021.

[94] R. M. Garcia-Teruel, ‘‘Legal challenges and opportunities of blockchain technology in the real estate sector,’’ Journal of Property, Planning and Environmental Law, vol. 12, no. 2, pp. 129–145, 2020.

[95] B. I. Mohideen and B. Assiri, ‘‘Internet of things (iot): classification, secured architecture based on data sensitivity, security issues and their countermeasures,’’ Journal of Information & Knowledge Management, vol. 20, no. supp01, p. 2140001, 2021.

[96] T. M. Tan and S. Saraniemi, ‘‘Trust in blockchain-enabled exchanges: Future directions in blockchain marketing,’’ Journal of the Academy of marketing Science, vol. 51, no. 4, pp. 914–939, 2023.

[97] M. A. Kashem, M. Shamsuddoha, T. Nasir, and A. A. Chowdhury, ‘‘Supply chain disruption versus optimization: a review on artificial intelligence and blockchain,’’ Knowledge, vol. 3, no. 1, pp. 80–96, 2023.

[98] A. Alamer and S. Basudan, ‘‘A security and privacy-preserving accessing data protocol in vehicular crowdsensing using blockchain,’’ in Proceedings of Seventh International Congress on Information and Communication Technology: ICICT 2022, London, Volume 2. Springer, 2022, pp. 315–327.

SJAST Journal
Multidisciplinary : Open Access Journal

Date of publication: April 24, 2025.

A Secure Parking Navigation System for Autonomous Vehicles Communication

ABDULRAHMAN ALAMER[1], SULTAN BASUDAN[1]
[1]Computer Science Department, Engineering and Computer Science College, Jazan University, Jazan, KSA
Corresponding author: Sultan Basudan (e-mail: sbasudan@jazanu.edu.sa).

ABSTRACT This work suggests that sharing data about parking spaces between autonomous vehicles (Aut-Vs) will enhance parking navigation systems and congestion avoidance. For example, if a number of Aut-Vs are ready to share their parking spaces with others before leaving their spots, this will promote parking navigation services' efficiency, reduce time and energy consumption. However, sharing data will result in various challenges, including incentive and security as well as latency issues. For instance, Aut-Vs may not wish to share their data with zero benefit since doing so will incur them more computation and communication efforts and security issues. Therefore, this paper aims to propose a novel security incentive mechanism for improving the parking navigation system for the Aut-Vs paradigm. However, even with low latency and minimal cost, data sharing between Aut-Vs still has mobility issues. For this reason, the fog caching (FC) system has been created to boost data sharing effectiveness while maintaining high levels of mobility and flexibility. This paper has designed a secure incentive mechanism based on an FC network to proposed a secure parking navigation (SPN) system for the Aut-Vs paradigm. The proposed SPN combines auction methodology with attribute-based encryption algorithm to design a secure incentive mechanism which guarantees the security and privacy of sharing parking data. Security analysis shows that our work is able to achieve sharing parking with full guarantee of privacy protection. Performance evaluation also shows that the proposed scheme for the SPN system is highly feasible and scalable.

INDEX TERMS Autonomous vehicles communication, security, privacy, parking navigation system, smart application.

I. INTRODUCTION

Autonomous vehicles (Aut-Vs) are part of the artificial intelligence field that has created the potential for new intelligent driving behaviors [1]. For instance, fully Aut-Vs have the ability to improve our driving by taking the driver out of the loop by relying on navigating itself through reading traffic road data [2]. However, with the growing of vehicle numbers in our cites, Aut-Vs could be facing a serious issue related to finding a vacant parking space in a crowded area, such as malls and sport centers [3]. Due to this annoying situation, Aut-Vs are now forced to circle around parking lots or drive on the road in search of empty spots. In congested places, these vehicles account for 20% of all traffic on average [4]. Serious societal issues, including air pollution, fuel waste, vehicle accidents, and traffic congestion, are caused by this increased traffic [5]. Therefore, many studies have proposed smart parking navigation applications [6] operating on a cloud-based system. Typically, in these applications, an Aut-V that is seeking for a parking area will send a query to the cloud server to discover available parking areas in its destination. However, these studies build their parking application based on a cloud computing system, which it is not recommended for most applications that require real-time services. In fact, parking data have high sensitivity in terms of time expired, where obtaining the data in real time is the key factor for successful parking navigation systems in Aut-Vs. Thus, adopting a cloud system in an Aut-V parking navigation system could lead to the following issues:

- A latency issue. Since the communication traffic between the cloud server and the Aut-V requires a high bandwidth, this will lead to a latency issue. For example, when a number of Aut-Vs are requesting parking data at peak time, the communication between the cloud server and the Aut-Vs could be result in a significant traffic backhaul, which may result in a delay in delivering data to the requester Aut-V. Therefore, a latency issue may lead Aut-Vs to make an inappropriate decision.
- A redundancy issue. For example, the parking space data that are sent to the cloud server could be stored for a long time, by which the server may send it multiple times for

every requester Aut-V without considering the occupied situation of the parking space, especially when a large number of Aut-Vs are requesting parking navigation at a same geographic area (e.g. downtown). The cloud server may then send the same parking spot data to all requester Aut-Vs, by which this may mislead most of them.
- A privacy issue. A cloud server is considered as a not trusted entity, whereby it could be able to identify the requester Aut-V's location and its trajectory. Although numerous works have proposed privacy-preserving parking systems [7] [8] based on cryptography, these schemes require very high computation costsin terms of cryptography algorithms, which will result in a latency issue. For example, the time taken in encrypting data and sending to the cloud server, and then the time taken in requesting and decrypting the ciphertext will exceed the time in finding a vacant parking space.

In regard to the above issues, the sharing paradigm is considered the best methodology for achieving real-time data parking navigation [9]. Thus, for enhancing sharing data systems, recent studies have proved that sharing real-time data is better implemented by a fog caching (F-cache) paradigm [10] [11]. With its temporary data storage, computing, and processing features, F-cache can perform caching techniques to cache the important content data in its cache memory in order to speed up the data communication between two Aut-Vs, at the same time reducing the high bandwidth and the traffic backhaul between the requester device and the cloud server [12]. The basic idea of using F-cache techniques in the parking navigation system is to enable a provider Aut-V to upload its parking space to be cached in the F-cache node's memory in order to directly serve a requester Aut-V in real-time service. Therefore, sharing data with the F-cache system will eliminate the latency issue as well as the data redundancy issue, whereby the F-cache stores the data for just a short time period. Thus, this work exploits the F-cache paradigm in order to design a secure parking navigation (SPN) system with the attribute of a rapid sharing data (RSD) for the purpose of improving the parking navigation paradigm in the Aut-V network system. However, designing a PS with RSD features means having to cope with several challenges. First, in implementing an incentives technique for encouraging sharing data among Aut-Vs, significant investigation is needed in order to find an efficient way of inventively encouraging Aut-Vs to share their parking spaces data with other Aut-Vs. Particularly, when a provider Aut-V feels that sharing parking data with another Aut-V seeking for a parking spot without receiving any compensation is unfair. As a result, incentive mechanisms are significant and require in-depth study. The second major issue with the F-cache paradigm is that it raises issues related to security, trustworthiness, and privacy invasion during sharing data. Finally, the authorized requester Aut-V must not be able to disclose the confidential data of the provider Aut-V, such as vehicle model type, identity, etc. Therefore, significant work needs to be done to ensure that rapid parking data sharing in the designed SPS system doesn't compromise security or violate privacy. Motivated by the challenges above, an auction-based theory is exploited to model a selling parking (sp-auction) mechanism for producing advantageous proprieties such as rapid sharing data with profitability as well as designing an encryption-attribute-based homomorphic matching key (EHMK) to protect driver's privacy during sharing parking data. Based on the sp-auction mechanism and EHMK protocol, this work proposes a secure parking navigation (SPN) system for the Aut-V communication paradigm with RPD feature.

- An auction mechanism is designed as a selling parking (sp-auction) mechanism for encouraging Aut-Vs to profitably share their parking data. In the sp-auction model, the seller Aut-V will draw its strategy for selling its parking space based on its location and leaving time. In contrast, the buyer Aut-V will draw its strategy for buying the parking place based on its budget and time of arriving. Thus, both seller and buyer Aut-Vs are bidding according to their best strategies.
- An encryption-attribute-based homomorphic matching key (EHMK) scheme is designed as a privacy-preserving scheme to protect the seller and buyer Aut-Vs' privacy from being disclosed during sharing parking data. The proposed scheme enables the seller Aut-V to encrypt its parking data with a searchable keyword, which can be selected from a list of predefined searchable keywords. The parking data and keyword ciphertexts will be stored in the F-cache node. The buyer Aut-V can then search for a particular parking space using a corresponding predefined searchable keyword.
- Based on the sp-auction mechanism and EHMK protocol, a secure parking navigation (SPN) system is proposed as an efficient and secure rapid sharing parking data solution to the Aut-V communication paradigm.
- To demonstrate the proposed SPN system's efficiency, an inclusive validation is carried out through performance evaluation and security analysis to demonstrate the capabilities of the proposed sp-auction model and EHMK scheme.

The paper is arranged as follows. Related Work is demonstrated in Section II. Section III provides preliminaries required in this work. In Section IV provides a detailed description of the proposed scheme. Section V then goes with security analysis. Subsequently, the performance is assessed in terms of computational, communication overhead, and security attributes in Section VI. Finally, Section VII concludes the work.

II. RELATED WORK

Finding a parking spot is one of the road transportation activities in the Aut-V paradigm that wastes time and energy, particularly in urban areas. To the best of our knowledge, not much research has been done on the issue of parking spot search methodology in the Aut-V communication sys-

tem [13]. The majority of literature research have examined parking systems for all non-Aut-V levels.

Numerous parking guidance systems that are not Aut-V have been suggested by VANET-based systems that employ various technologies including image segmentation, deep learning, machine learning, etc. [14] [15] [16]. In addition, since the security and privacy are the key issues that must be handled with during parking navigation exchange. Nonetheless, a number of VANET-based privacy-preserving navigation systems have been put forth to help cars go where they need to go as quickly as possible by taking the right routes.

Three RSUs are able to find open parking places for cars arriving at huge parking lots thanks to a privacy-preserving parking system that proposed in [17]. This parking lot concept is a small-scale project. A VANET-based secure and privacy-preserving navigation strategy was developed by Chim et al. [18]. In this scheme, RSUs placed on highways gather real-time road data and work together to guide vehicles to destinations in a distributive manner. Sadly, because the master key is shared by all vehicles, this technique is susceptible to internal vehicle attacks. Cho et al. [19] suggested a better privacy-preserving navigation protocol to thwart this attack and do away with the need to share the master secret key. As a result, Sur et al. [20] showed that the protocols [19] and [18] are built on the firm presumption that every RSU is completely trustworthy and that the cars would not improperly communicate their credentials with other parties. Therefore the authors [20] in suggested a secure navigation protocol based on proof of knowledge and one-time credential to address these shortcomings.

Nevertheless, the techniques [19], [18] and [20] rely on the premise that a moving vehicle can complete a query with an RSU, which is actually very difficult, especially when the vehicle is traveling at a very high speed.

Thus, in light of our observations, we disprove this presumption and suggest a unique smart parking navigation system that will enable vehicles to access parking services without compromising their privacy. Therefore, in order to obtain the navigation result, we proposed a secure navigation system based on auction method that enable Aut-V to request a parking available information while en route. This approach is better than the current ones navigation systems based on VANET technology in [21] and cloud application system in [22] since it can increase the likelihood that navigation results will be retrieved.

III. PRELIMINARIES

Methodology that are needed for this work are illustrated in this section.

A. BILINEAR MAPS.

It is an admissible bilinear map such that $\hat{e} : G_1 \times G_1 \rightarrow G_2$ where G_1 is an additive cyclic group and G_2 is a multiplicative cyclic group that are generated by the same prime order p_o. The $\hat{e}$ has the various properties as illustrated below:

- Bilinear: $\forall\ g_1, g_2 \in G_1$ and $k, y \in Z^n_{p_o}$, there is $\hat{e}(kg_1, yg_2) = \hat{e}(g_1, g_2)^{ky} = \hat{e}(yg_1, kg_2)$.
- Symmertic: $\hat{e}(g_1, g_2) = \hat{e}(g_2, g_1)$.
- Non-degenerate: $\hat{e}(g_1, g_2) \neq 1_{G_2}$.
- Computable: $\hat{e}$ is computable.

B. COMPLEXITY ASSUMPTION.

The proposed cryptography scheme is designed based on following discrete logarithm problem.

Assumption 1 Computational Diffie—Hellman (CDH) Problem, which is defined as:

Definition 1: Given $(kg, yg, zg) \in G_1, \forall k, y, z \in Z^n_{p_o}$, the CDH assumption holds if an adversary $\mathcal{S}$ has a function $\mathcal{F}$ with a negligible advantage Dv^{DBDH} and a polynomial time *tim* in successfully computing $h = kyz \in Z^n_{p_o}$ and then decides the following problem:

$$Dv^{DBDH}_{\mathcal{S}}(\mathcal{F}) = \left| \begin{matrix} Pr[\mathcal{S}(kyzg = 1)] \\ -Pr[\mathcal{S}(hg = 1)] \end{matrix} \right| \geq tim \tag{1}$$

Assumption 2 Decisional Bilinear Diffie–Hellman (DBDH) Problem, which is defined as:

Definition 2: Given $(kg, yg, zg) \in G_1$, the DBDH assumption holds if an adversary $\mathcal{S}$ has a function $\mathcal{F}$ with a negligible advantage Dv^{DBDH} and a polynomial time *tim* in successfully computing $h = kyz \in Z^n_{p_o}$ and then decides the following problem:

$$Dv^{DBDH}_{\mathcal{S}}(\mathcal{F}) = \left| \begin{matrix} Pr[\mathcal{S}(\hat{e}(g, g)^{kyz} = 1)] \\ -Pr[\mathcal{S}(\hat{e}(g, g)^{h} = 1)] \end{matrix} \right| \geq tim \tag{2}$$

1) Searchable keyword mechanism

This work designed a searchable keyword (SKW) mechanism for improving parking navigation. The proposed SKW defines set of keys $\mathcal{W}$ that are used as a searchable key for each parking location in oder to enable seller Aut-V to offer its location and enable buyer Aut-V to find a particular parking spot in a secure manner. However, SKW mechanism is designed based of a polynomial fitting mechanism that is defined as below.

Definition 3: Polynomial fitting mechanism (PF). Define a set of parking locations as a list of keywords $\mathcal{W} = \{w_1, ..., w_n\}$, the PF function for each $\Gamma(w_i)$ is computed with order n, as follows:

$$\begin{aligned} \Gamma(w_i) &= \left(\frac{\sum^{n}_{0 \leq i} w_{-i} - w_{i+1}}{\sum^{n}_{0 \leq i} w_i - w_{i+1}}\right) \\ &= \tau_1 + ... + \tau_n \end{aligned} \tag{3}$$

For each $\Gamma(w_i)$ will produce a coefficient vector as $\upsilon(w_i) = [\tau_1, \tau_2, ..., \tau_n]$. Based on the SKW and PF mechanism, this work proposed a polynomial searchable keyword (PSK) protocol, which is defined below.

Definition 4: Polynomial searchable keyword (PSK) protocol. Given $\upsilon(w_i)$, vector $\mathbf{W}_i = [w_i, ..., w^n_i]$ and a query keyword $\hat{w_j}$, the PSK function $\Lambda(w_i)$ is achieved as follows:

$$\Lambda(w_i) = \hat{w}_j[\mathbf{W}_i \sum_{i=1}^{n} \upsilon(w_i)] \\ = \hat{w}_j(\tau_1 w_i) + \hat{w}_j(\tau_2 w_i^2) + ... + \hat{w}_j(\tau_n w_i^n) \quad (4)$$

Therefore, $\Lambda(w_i) = 1$ if $\hat{w}_j = w_i$. Otherwise $\hat{w}_j$ is not matching and will be rejected.

C. EHMK FRAMEWORK

In this work, we exploit an encryption-attribute-matching key with homomorphic methodology to design the encryption-attribute-based homomorphic matching key (EHMK) as a security and a privacy-preserving scheme. The proposed EHMK is used to protect seller and buyer Aut-Vs private data from being disclosed during performing s-auction model. In the proposed EHMK scheme, a keyword w_i is selected from $\mathcal{W}$ that is defined for the parking area data a dat_i. The keyword w_i will be encrypted with attributes of homomorphic function, which enable buyer Aut-v to performing a matching process between a searchable key w_i and a parking spot while they are encrypted. The proposed EHMK is implemented according to the following four algorithms.

- **KeyG($\ni$):** Given $\ni$ as a security system parameter and return a public and private key (X_i, x_i).
- **HKS ($\ni, w_i$):** Given the security system parameter $\ni$ and a parking searchable keyword w_i, return a parking location ciphertext $\mathcal{P}_i$ for w_i.
- **Searching ($x_j, \hat{w}_j$):** Given a private key x_i and a parking keyword $\hat{w}_j \in \mathcal{W}$, return a searchable keyword $\mathcal{S}_j$, where $(\hat{w}_j = w_i) \in \mathcal{W}$.
- **Matching($\mathcal{P}_i, \mathcal{S}_j$):** Given the parking location ciphertext $\mathcal{P}_i$ and the searchable keyword $\mathcal{S}_j$, return "1" if $(\hat{w}_i = w_i$ and "0" otherwise.

D. AUCTION MODEL

The auction system is a model in which a buyer can buy offers a higher price to obtain a required service from a single vendor.

In the navigation parking system, it is

Obviously, Aut-Vs are more economical vehicles, which they are not interested reservation their parking spot data to other Aut-Vs during its time checking out without any compensation.

Thus, in the effort to optimize payment system and to make Aut-Vs more interactive, this work design a parking selling auction (ps-auction) model for encourage Aut-Vs to sell their parking data before they are leaving to the other buyer Aut-Vs. The proposed ps-auction is defined as follows:

Definition 5: (ps-auction). In the ps-auction, through the auctioneer u_i, a seller Aut-V_i can reserve its a parking data dat_i to an interested buyer Aut-V_j who is offering a higher price pr_i. Indeed, each buyer Aut-V_j has n number of price strategies as $\mathcal{P}r = \{pr_1, ..., pr_n\}$. Each $pr_i \in \mathcal{P}r$ is an optimal strategy $\varphi_i(pr_i)$ for an optimal action of provided dat_i. Therefore, the action function F_a for each strategy $pr_i \in \mathcal{P}r$ guarantees that the price of buying the park data should not exceed the buyer Aut-V_j budget Bdg_j that is defined as:

$$F_a(dat_i) = \begin{cases} 1, & if pr_i \leq Bdg_i \\ 0, & otherwise \end{cases}$$

Definition 6: (Monotone Equilibrium Strategy [MES]). In the propose *system*, the auction rule F_a is designed as a MES to ensure that a buyer Aut-V_j's price pr_i is monotonically selected as its pest strategy $\varphi_i(pr_i)$.

Definition 7: (Best Strategy). The strategy $\varphi_i(pr_i)$ is called a best strategy if the buyer Aut-V_j's utility $\triangle_i$ is non-negative,

$$\triangle_i[\varphi_i(pr_i), \overline{\varphi_i}(pr_i)] \geq Bdg_i$$

where $\overline{\varphi_i}(pr_i)$ is not the Aut-V_j's best strategy.

E. THE PROPOSED PS-AUCTION ARCHITECTURE MODEL

The proposed ps-auction architecture model is consists of the following process:

- Auction process: The proposed ps-auction model is implemented as the following:
  - -- Auction entity: The F-cach node is acting as auctioneer who is responsible in initialize an auction session by publishing an available parking spot with its time availability specifications to the public through its web-platform.
  - -- Bidding entity: Each interesting buyer Aut-V_j selects its best price strategy pr_j based on its budget limitation to obtain the parking spot. Each buyer Aut-V_j sends its bidding value to the auctioneer, which includes its higher price cost to win the session of the auction.
- Selecting winner process: From a number of buyer Aut-V_j bidding values, the auctioneer will select Aut-V_j a higher claimed price pr_j as a winner.
- Payment process: The winner Aut-V_j will be demanding to pay the claimed price before obtaining the parking data.

F. PROBLEM STATEMENTS

For a full guarantee of trusted environment of parking navigation system, this work must addresses the following security issues.

Problem 1. Secure ps-auction: For a trusted auction process, the following two issues must be considered.

- Secure bidding. In the proposed ps-Auction system, the price value pr_i is considered a private data due to that if it is disclosed, it will lead to detect the player's best strategy, which enable other players to build their unfair prices' best strategies. Thus, a malicious buyer Aut-$V_j$may preforming a malicious action to bide with unfair price to win the auction session. For example, a malicious buyer Aut-V_j may eavesdrop on other buyer Aut-Vs price strategies to bide with a higher false price $\hat{pr}_i$ to win the auction session. This malicious behavior will result into non-trusted environment of the proposed ps-auction process.

- Blind Selecting Winner. Given number of buyer Aut-V_j $n = \{1, ..., n\}$, the auctioneer aims to select a winner $j \subseteq n$ without disclosing its price value.

Problem 2. While in the F-cach paradigm, the F-cach node is considered as a semi-trusted node, which can cause serious threat to the stored data in its cached memory. For example, when a seller Aut-V_i sends its parking data dat_i to the F-cach node in order to be perform auction process, the F-cach node has a full authorization to access to dat_i, hence it can easily disclose the Aut-V_i's private data as well as manipulating dat_i for a malicious miss leading buyer Aut-V_j. In addition, F-cach node can disclose the private data of the buyer Aut-V_j that request.

Note that, by solving the *SA* problem, we can ensure that there is no way for malicious Re-V to win the auction game by generating its strategy regarding the other participants player' price strategy $\overline{pr}_i$.

Therefore, the node's t_i^* and c_i^t values must be protected among nodes. Solving the *SP* problem will guarantee the confidentiality of the node's data.

G. SYSTEM ARCHITECTURE

This section will demonstrate the proposed security parking navigation system architecture, which consists of the following components:

- An Authority Server (A-server). It is a trust server that is in charge of generating a set of keywords $\mathcal{W} = \{w_1, ..., w_n\}$ as a predefined for parking areas. Each $w_i \in \mathcal{W}$ is a searchable key that describe a particular parking area for the requester Aut-V. In addition, the A-Server is also responsible for registering and initialization of parking navigation systems.
- A Seller Aut-V *i*. It is refereed to the vehicle who desire to sell its parking spot before living its spot with for Aut-V *j*. In fact, the Seller Aut-V *i* is seeking to obtain a compensation benefits from reserving its parking spot with other vehicle. However, Aut-V *i* need to register at the A-server first for receiving predefined parking area keywords $\mathcal{W}$ and being part of the parking navigation system as a seller vehicle.
- Buyer Aut-V *j*. It is refereed to one of vehicle that seeks for buying a parking spot located around its end-destination. The keywords $\mathcal{W}$ will help the buyer Aut-V *j* for better decision making on its states. Therefore, buyer Aut-V must be a part of the parking navigation system from registering at the A-server for gaining a list of predefined geographic parking keywords $\mathcal{W}$ that will be utilized to search for relevant parking area.
- F-cach node Fc_i. It is responsible for enhancing a navigation system between to vehicles through acting as an auctioneer node.

IV. THE PROPOSED SPN SYSTEM

1) System Setup

The A-server bootstraps the whole service and setups the parking navigation system parameters according to the following process

- Cryptography system parameter. The A-server chooses a security parameter $\mathbb{k}$, which ensures the security level of the system and determines the prime order p_o of the bilinear groups. It then determines an additive cyclic group G_1 of points with two generator g_1, g_2 and a bilinear map $\hat{e}$ such that $\hat{e}(G_1 \times G_1) \rightarrow G_2$, where G_2 is a multiplicative cyclic group. In addition, it determines a group $Z_{p_o}^n$ of number. Finally, the Authority-server publish the system parameter as $S_p = \{p_o, G_1, G_2, \hat{e}, g_1, g_2, Z_{p_o}^n\}$.
- Geographic regions parameter. The A-server initializes the service geographic regions for a city by pre-defining the points of parking's geographic regions of the city, as shown in Fig.2. For example, generating a set of keywords $\mathcal{W} = \{w_1, ..., w_n\}$ as a predefined for parking areas. Each $w_i \in \mathcal{W}$ is as a searchable key that describe a particular parking area for the both seller and buyer Aut-Vs.

2) Registration

According to the system public parameter S_p, the system entities are in charge to generate their public-private key pair as the following:

- Aut-V registration. Each seller Aut-V_i and buyer Aut-V_j is required to generate their public and private key pairs (pk_i, sk_i). A seller Aut-V_i picks a random $x_{s_i} \in Z_{p_o}^n$ as private key and then computes $X_{s_i} = x_i g_1$ as the public key.Also, each buyer Aut-V_j picks a random $x_{b_j} \in Z_{p_o}^n$ as private key and computes its public key as $X_{b_j} = x_{b_j} g_1$.
- F-cach node registration. Each F-cach node F_{c_i} is required to generate a public-private key pair $(pk_{F_i}, sk_i^{F_i})$ by picking a random $x_{F_i} \in Z_{p_o}^n$ as a private key and computes $X_{F_i} = x_{F_i} g_1$ as the public key. It then sends (pk_{F_i}) to the A-server. Once receive it, the A-server will issue and signs a certificate σ_{F_i} for F_{c_i}, which includes series number, pk_{F_i}, signature algorithm, etc. The certificate is allowed the Aut-Vs to check the validity of F-cach node during auction process.

3) Offering parking spot

When a seller Aut-V_i is willing to sell its parking spot data dat_i before its leaving, it will then generate a spatial parking message $SP_i = (t_i w_i)$, which t_i is a time (when parking spot will be free) and w_i is the keyword of geographic parking area (keyword of parking location). The keyword of parking geocast area $w_i \in \mathcal{W}$ is denoted as a parking searchable key from which it can help a buyer Aut-V_j to find its interested parking space.

However, sending $SP_i = (t_i w_i)$ as a plain text will definitely lead for revealing seller Aut-V_i's location and time of leaving. To prevent the exposure of $SP_i = (t_i w_i)$, seller Aut-V_i will generate a series of encrypted points of interest. It picks a random values $k_i, \gamma_i, \alpha_i, y_i \in Z_{p_o}^n$ as temperate secret keys and compute the following:

- $K_i^1 = k_i g_1$.

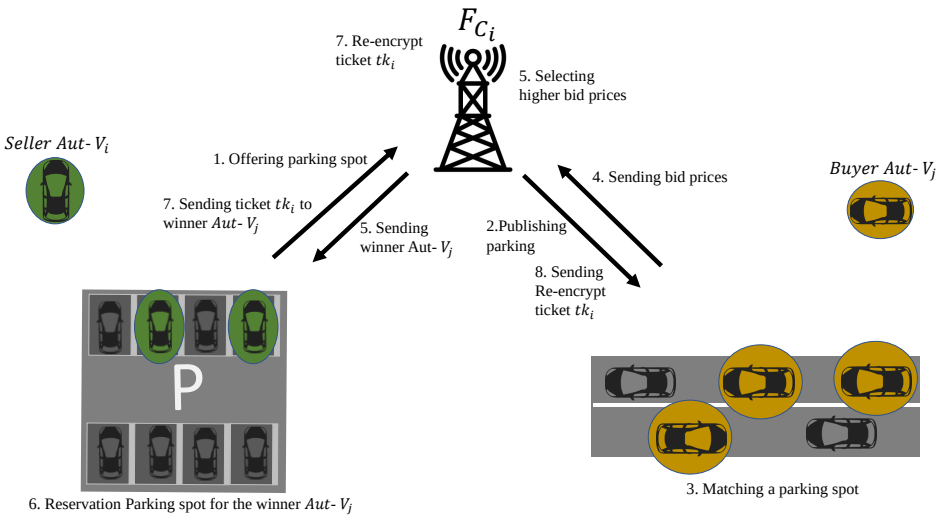

FIGURE 1. The proposed SPN system

FIGURE 2. Pre-defining the points of parking's geographic regions of the city

- $K_i^2 = \gamma_i g_1$
- $K_i^3 = \hat{e}(g_1, g_1)^{\gamma_i(k_i+w_i)+t_i y_i}$.
- $K_i^4 = [\sum_{j=1}^{n} a_j t_i^{j-1}]\gamma_i K_i^1$.
- $K_i^5 = [\sum_{j=1}^{n} a_j w_i^{j-1}] y_i g_1$.
- $K_i^6 = (K_i^2, K_i^3, K_i^4, K_i^5)$.

The seller Aut-V_i will then send (K_i^6) to the F-cach node F_{c_i}. Once receiving (K_i^6) from Aut-V_i, F_{c_i} will directly post K_i^6 to the public via the navigation parking application or website.

4) Matching a parking spot

A buyer Aut-V_j that is seeking for a parking spot in a certain area and time, it can receives a notification of the posted K_i^6 from F_{c_i}'s parking application or website. Therefore, the buyer Aut-V_j will first check if the K_i^6 is fit in its desired area w_j and time t_j by performing the following:

- $\lambda_j^1 = t_j K_i^4$
- $\lambda_j^2 = w_j K_i^5$

Then, buyer Aut-V_j verifies the following equation:

$$\lambda_j = \frac{K_i^3}{\hat{e}([\lambda_j^1 + w_j K_i^2] + t_j \lambda_j^2, g_1)} = 1$$

If the above equation is true, the buyer Aut-V_j will start sending its price pr_j strategy to the F_{c_i} for inserting pr_j into the auction game and compete with other buyer vehicles on the posted parking spot.

Lemma 1: Matching a parking spot phase is complete if the $t_j = t_i$ and $w_j = w_j$

SJAST Journal
Multidisciplinary : Open Access Journal

Proof. $\lambda_j = 1$, since:

$$\begin{aligned}
\lambda_j &= \frac{K_i^3}{\hat{e}([\lambda_j^1 + w_j K_i^2] + t_j \lambda_j^2, g_1)} \\
&= \frac{\hat{e}(g_1, g_1)^{\gamma_i(k_i+w_i)+t_i y_i}}{\hat{e}([\lambda_j^1 + w_j K_i^2] + t_j \lambda_j^2, g_1)} \\
&= \frac{\hat{e}(g_1, g_1)^{\gamma_i(k_i+w_i)+t_i y_i}}{\hat{e}([t_j K_i^4 + w_j K_i^2] + t_j w_j K_i^5, g_1)} \\
&= \frac{\hat{e}(g_1, g_1)^{\gamma_i(k_i+w_i)+t_i y_i}}{\hat{e}([t_j[\sum_{j=1}^{n} a_j t_i^{j-1}]\gamma_i K_i^1 + w_j K_i^2] + t_j w_j K_i^5, g_1)} \\
&= \frac{\hat{e}(g_1, g_1)^{\gamma_i(k_i+w_i)+t_i y_i}}{\hat{e}([\gamma_i K_i^1 + w_j K_i^2] + t_j w_j K_i^5, g_1)} \\
&= \frac{\hat{e}(g_1, g_1)^{\gamma_i(k_i+w_i)+t_i y_i}}{\hat{e}([\gamma_i K_i^1 + w_j K_i^2] + t_j w_j [\sum_{j=1}^{n} a_j w_i^{j-1}] y_i g_1, g_1)} \\
&= \frac{\hat{e}(g_1, g_1)^{\gamma_i(k_i+w_i)+t_i y_i}}{\hat{e}([\gamma_i K_i^1 + w_j K_i^2] + t_j y_i g_1, g_1)} \\
&= \frac{\hat{e}(g_1, g_1)^{\gamma_i(k_i+w_i)+t_i y_i}}{\hat{e}([\gamma_i k_i g_1 + w_j \gamma_i g_1] + t_j y_i g_1, g_1)} \\
&= \frac{\hat{e}(g_1, g_1)^{\gamma_i(k_i+w_i)+t_i y_i}}{\hat{e}([\gamma_i (k_i + w_j) g_1] + t_j y_i g_1, g_1)} \\
&= \frac{\hat{e}(g_1, g_1)^{\gamma_i(k_i+w_i)+t_i y_i}}{\hat{e}(\gamma_i (k_i + w_j) + t_j y_i g_1, g_1)} \\
&= \frac{\hat{e}(g_1, g_1)^{\gamma_i(k_i+w_i)+t_i y_i}}{\hat{e}(g_1, g_1)^{\gamma_i(k_i+w_j)+t_j y_i}} = 1
\end{aligned}$$

For protecting pr_j from being disclose, buyer Aut-V_j will generate ciphertext as

$$\rho_j = [(pr_j w_j) g_2]^{\pi_i}$$

Where π_i is the influence factor of the estimate time difference of the Aut-V_j to reach the parking spot. A lower π_i makes the time difference more important. The buyer Aut-V_j will then send ρ_j to the F_{c_i} node.

5) Winner buyer Aut-V_j

The F_{c_i} node is acting as auctioneer that is in charge to sell the parking spot to the buyer Aut-V_j with higher price ρ_j. Therefore, assume that the F_{C_i} node receives a number of $(\rho_j)_{j=1}^n$, it will then start performing an auction process by descendingly sorting $(\rho_j)_{j=1}^n$ as follows:

$$\rho_1 > \rho_2 > ... > \rho_n$$

The F_{c_i} node will select the buyer Aut-V_j with a higher price ρ_j and delete the others. The F_{c_i} node will then request from the winner Aut-V_j to make its payment according to its submitted price ρ_j and send a copy of payment receipt pr_j as a encrypted message under seller Aut-V_i's public key. Thus, the winner Aut-V_j

picks a random values $e_i \in Z_{p_o}^n$ as a temperate secret key and compute the following:

- $p_i^1 = e_i x_{b_j} X_{s_i}$
- $p_i^2 = x_{b_j} e_i g_1 \oplus pr_j \oplus \sigma_{F_i} g_1$

It then foreword the received price (p_i^1, p_i^2) to the seller Aut-V_i.

6) Parking Reservation

Once seller Aut-V_i receives (p_i^1, p_i^2), it will decrypt it using its private key, such as,

$$\begin{aligned}
pr_j^{'} &= x_{s_i}^{-1} p_i^1 \oplus \sigma_{F_i} g_1 \oplus p_i^2 \\
&= x_{s_i}^{-1} e_i x_{b_j} X_{s_i} \oplus \sigma_{F_i} g_1 \oplus p_i^2 \\
&= e_i x_{b_j} g_1 \oplus \sigma_{F_i} g_1 \oplus p_i^2 \\
&= e_i x_{b_j} g_1 \oplus \sigma_{F_i} g_1 \oplus x_{b_j} e_i g_1 \oplus pr_j \oplus \sigma_{F_i} g_1 \\
&= pr_j
\end{aligned}$$

Thus, if the pr_j is valid, seller Aut-V_i will reserve the pinking spot by buying a parking ticket tk_i from the parking center and then generate a token as a ticket parking for the winner buyer Aut-V_j. It will pick a random values $r_i, \in Z_{p_o}^n$ as the temperate secret key and perform the following:

- $E_i^1 = r_i x_{s_i} X_{b_j}$.
- $E_i^2 = x_{s_i} r_i X_{F_i} \oplus tk_i \oplus \sigma_{F_i} g_1$

The seller Aut-V_i sends (E_i^1, E_i^2) to the winner buer Aut-V_j via F_{C_i} node. Note that, the seller Aut-V_i's revenue v_i after reserving the parking spot should be satisfying the following condition:

$$v_i = pr_i - tkg_i > 0$$

7) Receiving Parking data

The F_{C_i} will re-encrypt the secret key as $\overline{E_i^1} = x_{F_i} E_i^1$ and sends $(E_i^2, \overline{E_i^1})$ to winner buyer Aut-V_j. Therefore, the buyer Aut-V_j obtains the parking ticket data detail by decrypting E_i^2 using its private key x_{b_j}, such as:

$$\begin{aligned}
tk_i^{'} &= E_i^2 \oplus x_{b_j}^{-1} \overline{E_i^1} \oplus \sigma_{F_i} g_1 \\
&= x_{s_i} r_i X_{F_i} \oplus tk_i \oplus \sigma_{F_i} g_1 \oplus x_{b_j}^{-1} \overline{E_i^1} \oplus \sigma_{F_i} g_1 \\
&= x_{s_i} r_i X_{F_i} \oplus tk_i \oplus x_{b_j}^{-1} \overline{E_i^1} \\
&= x_{s_i} r_i X_{F_i} \oplus tk_i \oplus x_{b_j}^{-1} x_{F_i} r_i x_{s_i} X_{b_j} \\
&= x_{s_i} r_i x_{F_i} g_1 \oplus tk_i \oplus x_{b_j}^{-1} x_{F_i} r_i x_{s_i} x_{b_j} g_1 \\
&= x_{s_i} r_i x_{F_i} g_1 \oplus tk_i \oplus x_{F_i} r_i x_{s_i} g_1 \\
&= tk_i
\end{aligned}$$

Once buyer Aut-V_j arrived to the parking location, it will show the ticket tk_i to the parking center in order to be allowed to park in its reservation spot.

V. SECURITY ANALYSIS

In this section, we will present the security analysis of the proposed cryptography EHMK scheme in order to illustrate the ability of the EHMK scheme in solving security and privacy Problems as descried in Subsection III-F.

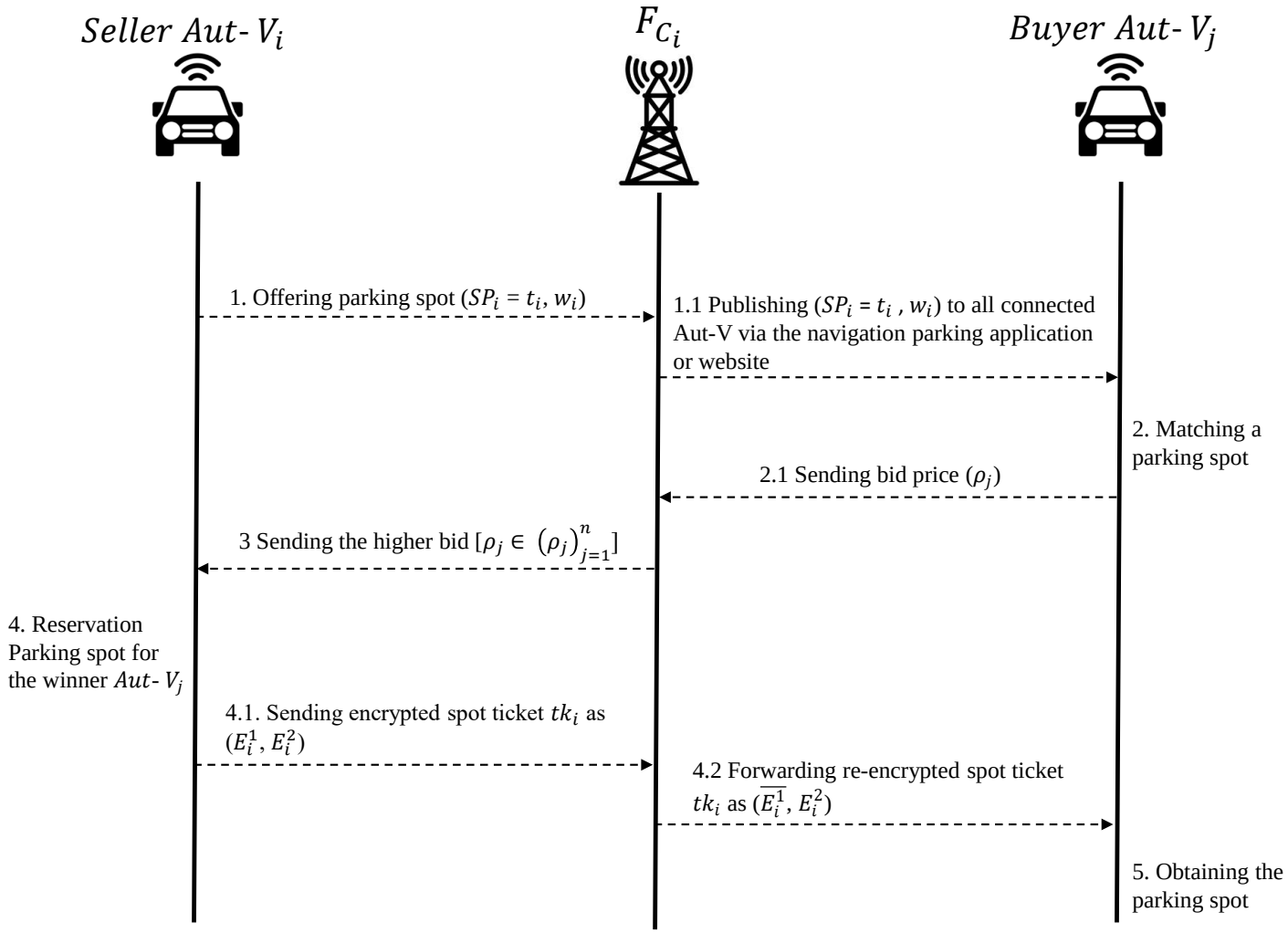

FIGURE 3. The proposed SPN system

1. Confidentiality and integrity: The proposed EHMK scheme achieves confidentiality and integrity from two perspective as descried below.

- Protecting seller Aut-V data. Before the seller Aut-V_i sending its parking spot data to the F-cach node, it will first protect it. In compliance with Definition 2, the seller Aut-V_i encrypts it spatial parking message SP_i under the *CDH* assumption, which prevents the following a malicious behavior.
  - -- A malicious F-cach node F_{C_i} will not be able to disclose or even modify the parking data SP_i. Since the sellerencrypts its SP_i under random secure $k_i, \gamma_i, \alpha_i, y_i \in Z_{p_o}^n$ to calculate $(K_{i1}, K_{i2}, K_{i3}, K_{i4}, K_{i5})$.
  - -- A malicious buyer Aut-V_j will be able to check if the seller parking's data is matching with its requirement by verifying $(K_{i2}K_{i3})$ without disclosing seller Aut-V_i's privacy. Thus, the malicious buyer Aut-V_j will have not chance to disclose or even modify the parking data SP_i.
- Protecting buyer Aut-V_j data. The buyer Aut-V_j sends it price as a ciphertext ρ_j under Definition 2. Thus, a malicious F-cach node F_{C_i} will from disclosing or modifying the real buyer Aut-V_j price pr_j without known the w_j searchable keyword.

2. Secure sorting Computation. Since the proposed EHMK is designed based on a homomorphic concept the a F-cach node F_{C_i} that is acting as an auctioneer will be able to sort bidder vehicles descendly according to their claimed prices without disclosing their real prices.

3. Authentication. The authentication phase is achieved, when the F-cach node authenticated itself by using its digital signature σ_{F_i} on the message that is generated on the p_i^2 copy of payment receipt to be sent to the seller Aut-V_i. The

receiver authenticates the source message by using the F-cach node's digital signature σ_{F_i} to obtain the parking token from decrypting $(E_i^2, \overline{E_i^1})$.

VI. PERFORMANCE EVALUATION

This section assesses the proposed SPN performance with the fog catch system. We will first demonstrate the evaluation environment parameter settings. Next, a computational cost and communication overhead analysis will be conducted to evaluate the security and privacy features of the proposed EHMK protocol. In addition, the proposed sp-auction mechanism will be evaluated based on vehicle' participation satisfaction.

A. SPN PARAMETER SETTINGS

The cryptography parameters of the proposed EHMK scheme are implemented a type A pairing with the system security parameter $\mathbb{k} = 128$ on the elliptic curve $y^2 = x^3 + x$ over the field F_p with prime $p = 3mod\ 4$. The primitives of the cryptography are implemented utilizing JPBC library[1] as well as Java on a PC that has a Microsoft Windows 10 with Intel Core i7-8700 CPU @4.6GHz, 32.00 GBRAM and 1TB of memory.

B. COMPUTATIONAL AND COMMUNICATION OVERHEAD

Any cryptography protocol's performance efficiency must be presented with limiting the assessment of computation and transmission overhead. Therefore, the focus of this part will be on assessing the computation and communication overhead efficiency performances of the suggested EHMK scheme.

1) Computation time Cost

The computational time cost is demonstrated by measuring the time consumption of performing the cryptography operations, which can be measured by counting the number of computing scalar multiplication and bilinear pairing in each system phases. Thus, lets *MG* and *PB* are used to defined the time consumption of computing scalar multiplication g_1, g_2 and bilinear pairing $\hat{e}$, respectively. The computation time cost of the proposed EHMK cryptography scheme will be evaluated based on following algorithms:

- Algorithm 1. Offering parking spot. This algorithm takes 4 multiplication operations $4(MG)$ and one bilinear pairing *PB* for generating a ciphertext K_i^6 for encrypting parking data $SP_i(t_i, Wi)$.
- Algorithm 2. Searching for a parking spot. This algorithm takes 2 number multiplication operations $2(MG)$ and 2 bilinear pairing $2(PB)$ for verifying if the offering parking spot is matching with its searching requirements. Thus, if the verification result is satisfied, the buyer Aut-V_j will continue this algorithm by generation one multiplication operation *MG* to generate a ciphertext of its offering price ρ_j.
- Algorithm 3. Winner buyer Aut-v. This algorithm takes three multiplication operation $3(MG_1)$ to send a copy of payment receipt pr_j for the winner buyer Aut-V_j to the seller Aut-V_i.
- Algorithm 4. Parking Reservation. This algorithm takes two process as follows:
  - Re-encryption process. In this process, the F_{C_i} requires to compute a multiplication operation *MG* for generating a re-encrypting the $E_i^1 \rightarrow \overline{E_i^1}$.
  - Decrypting process. In this process, the buyer Aut-V_j takes two multiplication operations $2(MG)$ for decryptying tk_i.

As a result, Table 1 shows the calculation overhead and running time expenses for each approach. It is able to determine that the parking place algorithm offering is using a low computation time cost. This encourage seller Aut-V_i to participate without concerned bout their computation and time costs. In contrast, Searching for a parking spot algorithm consumes more computation cost then algorithm 1. Thus, only the serious buyer Aut-V_j will continue to perform this algorithm.

2) Communication cost

The binary length of the ciphertext is measured to illustrate the communication cost. Therefore, each G_1 or G_2 is measured as 160 bits. In addition, each Z_{qo}^n value or $\{0, 1\}$ is equal 256 bits.

In addition, let $|G_1|$, $|G_2|$, $|Z|$ and $|M|$ demonstrate the size of elements in G_1, G_2, Z_{qo}^n and $\{0, 1\}$, respectively. Therefore, the ciphertext length size of the proposed EHMK cryptography scheme will be evaluated in each communication phase, as follows:

- Phase 1: In the Offering parking spot, the seller Aut-V_i sends the offering parking data $K_i^6 = (K_i^2, K_i^3, K_i^4, K_i^5)$ to the connected F_{C_i}. Thus, the length size of the K_i^2 is $|G_1|$, the length size of the K_i^3 is $|G_2|$, K_i^4 is $(n|G_1|)$ and the length size of the K_i^5 is $(n|G_1|)$.
- Phase 2: In the searching for a parking spot, the buyer Aut-V_j sends its calmed payment value ρ_j to the connected F_{C_i}, which cost $|G_1|$ of communication length size.
- Phase 3: In the winner buyer Aut-V_j, the F_{C_i} selects the winner buyer Aut-V_j and then sends (p_i^1, p_i^2) to the seller Aut-V_i. Thus, the length size of the p_i^1 is $|G_1|$ and the length size of the p_i^2 is $3|G_1|$.
- Phase 4: In the Parking Reservation, , the seller Aut-V_i sends (E_i^1, R_i^2) to the buyer Aut-V_j. The length size of the E_i^1 is $|G_1|$ and the length size of the E_i^2 is $3|G_1|$.

Therefore, Table 2 illustrates the communication cost for each communication phase in the proposed parking navigation network system with their length bit costs. Overall, the time cost of performing proposed scheme is more practical with stable of communication and computation cost during performing auction process.

[1] http://gas.dia.unisa.it/projects/jpbc/

TABLE 1. Computational cost

	Offering parking	Searching for parking	Winner	Parking Reservation	Receiving parking
Operations	$4MG + BP$	$3MG + PB$	$3MG$	$5MG$	$3MG$
Run Time (ms) with $n = 50$					
Max Time	352 ms	268 ms	45.7 ms	149.7 ms	44.5 ms
Min Time	298 ms	223 ms	37 ms	109 ms	34.90 ms
Avarage Time	348 ms	238 ms	41.9 ms	125.7 ms	38.7 ms

TABLE 2. Communication overhead

	Phase 1	Phase 2	Phase 3	Phase 4
Operations	$(2n+1)\|G_1\| + \|G_2\|$	$\|G_1\|$	$4\|G_2\|$	$4\|G_2\|$
Length size	$2n(160) + 320$ *bits*	160 *bits*	640 *bits*	640 *bits*

C. PERFORMANCE OF SPN SYSTEM

In this experiment, the F-cach node F_{C_i} is acting as auctioneer temporary server, which is in charge of selecting a buyer Aut-V_j for reserving a particular parking spot by considering the level location privacy of both seller and buyer Aut-V_j and the time of performing the auction process. We set up time interval A, B, which A is indicated a period time between (7 to 9) AM mooring and B is a period time between (12 to 2) PM after noon. In addition, we set a range time to performing each auction process determined as $(60ms)$. After this time, the announcement parking spot SP_i will be considered as expired spot and will be removing from the F_{C_i}'s caching memory. Thus, the experiment is contacted as the following scenarios:

- scenario 1. At the A time period, it can note that, the number of buyer Aut-*Vs* are increased compared with seller Aut-*Vs*. This is because this time most of people are going to their work place. Thus, having a parking spot is a less chance for bidders Aut-*Vs*. However, this will positively affect the seller Aut-v satisfaction as shown in Fig.**??**. This is because more buyer Aut-*Vs* will join the auction system, which in contrast, the seller Aut-V_i will obtain a satisfaction payment for reserving its parking spot, especially if the parking spot is close from most of people work place. In addition, the auctioneer F_{C_i} will be shortly find a buyer Aut-V_j with a higher claimed payment, which reducing the time of auction process as well as the time of caching parking spot in its memory.
- scenario 2. At the B time period, it can note that, the number of buyer Aut-*Vs* are decreased while the number of seller Aut-*Vs* are increased. This is because this time most of people leaving their work places. Thus, having a parking spot could be very easy. This will negatively affect the seller Aut-v satisfaction as shown in Fig.5. This is because there is a lack of buyer Aut-*Vs* will join the auction system, which in contrast, the seller Aut-V_i will obtain a less expected payment for reserving its parking spot. Moreover, the auctioneer F_{C_i} may difficultly find a buyer Aut-V_j with a fair claimed payment, which the time of auction process may increased with the time of caching parking spot in its memory.

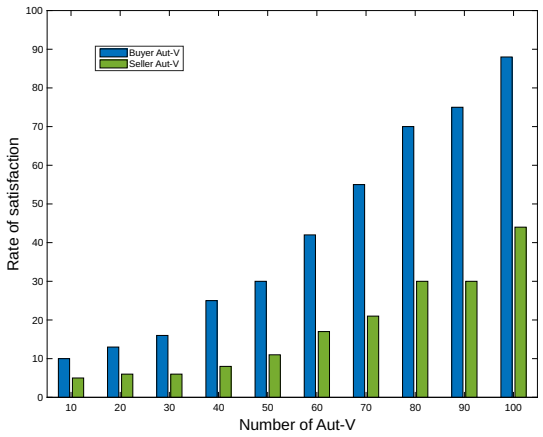

FIGURE 4. Rate of satisfaction between Seller and buyer Aut-Vs

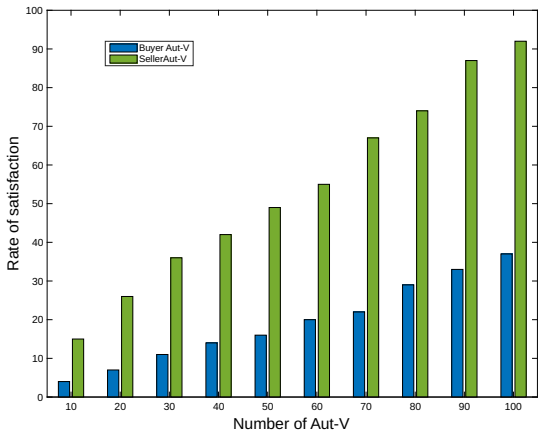

FIGURE 5. Rate of satisfaction between Seller and buyer Aut-Vs

SJAST Journal
Multidisciplinary : Open Access Journal

D. COMPARISON

From above scenarios studies, we evaluate the efficiency of the proposed system on a city traffic performance compared with navigation systems based on VANET technology in [21] and cloud application system in [22]. As shown in Fig.6, it can note that the proposed system reduce the searching time of the parking spot by 49% compared with VANET and cloud-based system. The proposed SPN system is efficiently reducing the issue of a city's traffic from helping most of Aut-V owner to find a suitable parking spot before reaching the place. In addition, the Aut-V owner is more satisfied due to save their time from searching for a parking and reducing their gas payment.

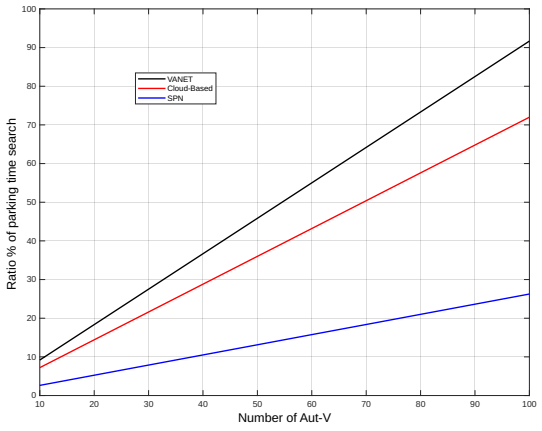

FIGURE 6. Comparison of rate of parking time search

VII. CONCLUSION AND FUTURE WORK

This paper presents a novel security incentive mechanism for improving the parking navigation system for the Aut-Vs paradigm that takes into account sharing data among Aut-Vs at low latency and minimum cost. A fog caching (FC) system has been developed to increase efficiency of data sharing with mobility of high-flexibility. In designing a secure incentive mechanism based on an FC network, we propose a secure parking navigation (SPN) system for the Aut-Vs paradigm. The proposed SPN combines auction methodology with an attribute-based encryption algorithm to design a secure incentive mechanism that guarantees the security and privacy of sharing parking data. Security analysis demonstrates that our work is able to achieve privacy protection in sharing data, and secure search and collusion resistance, while an evaluation on performance illustrates high feasibility and scalability of the SPN system's proposed scheme. Future research should focus on improving security in sharing data such as using blockchain technology taking into account low computation and communication costs.

REFERENCES

[1] M. M. Rahman and J.-C. Thill, "Impacts of connected and autonomous vehicles on urban transportation and environment: A comprehensive review," *Sustainable Cities and Society*, p. 104649, 2023.

[2] C. Ding, C. Li, Z. Xiong, Z. Li, and Q. Liang, "Intelligent identification of moving trajectory of autonomous vehicle based on friction nanogenerator," *IEEE Transactions on Intelligent Transportation Systems*, 2023.

[3] X. Xiao, Z. Peng, Y. Lin, Z. Jin, W. Shao, R. Chen, N. Cheng, and G. Mao, "Parking prediction in smart cities: A survey," *IEEE Transactions on Intelligent Transportation Systems*, 2023.

[4] B. Padmaja, C. V. Moorthy, N. Venkateswarulu, and M. M. Bala, "Exploration of issues, challenges and latest developments in autonomous cars," *Journal of Big Data*, vol. 10, no. 1, p. 61, 2023.

[5] Z. Tian, T. Feng, B. Yao, Y. Hu, and J. Zhang, "Where to park an autonomous vehicle? results of a stated choice experiment," *Transportation Research Part A: Policy and Practice*, vol. 175, p. 103763, 2023.

[6] Y. Jo, J. Ha, and S. Hwang, "Survey of technology in autonomous valet parking system," *International Journal of Automotive Technology*, vol. 24, no. 6, pp. 1577–1587, 2023.

[7] C. Huang, R. Lu, X. Lin, and X. Shen, "Secure automated valet parking: A privacy-preserving reservation scheme for autonomous vehicles," *IEEE Transactions on Vehicular Technology*, vol. 67, no. 11, pp. 11 169–11 180, 2018.

[8] S. Kim, R. Shrestha, S. Kim, and R. Shrestha, "Security and privacy in intelligent autonomous vehicles," *Automotive Cyber Security: Introduction, Challenges, and Standardization*, pp. 35–66, 2020.

[9] J. Cui, F. Ouyang, Z. Ying, L. Wei, and H. Zhong, "Secure and efficient data sharing among vehicles based on consortium blockchain," *IEEE Transactions on Intelligent Transportation Systems*, vol. 23, no. 7, pp. 8857–8867, 2021.

[10] J. Xiong, R. Bi, M. Zhao, J. Guo, and Q. Yang, "Edge-assisted privacy-preserving raw data sharing framework for connected autonomous vehicles," *IEEE Wireless Communications*, vol. 27, no. 3, pp. 24–30, 2020.

[11] A. M. A. Alamer, "A secure and privacy blockchain-based data sharing scheme in mobile edge caching system," *Expert Systems with Applications*, vol. 237, p. 121572, 2024.

[12] A. Alamer, "Security and privacy-awareness in a software-defined fog computing network for the internet of things," *Optical Switching and Networking*, vol. 41, p. 100616, 2021.

[13] B. Xia, J. Wu, J. Wang, Y. Fang, H. Shen, and J. Shen, "Sustainable renewal methods of urban public parking spaces under the scenario of shared autonomous vehicles (sav): A review and a proposal," *Sustainability*, vol. 13, no. 7, p. 3629, 2021.

[14] Y. Feng, Y. Huang, B. Li, H. Peng, J. Wang, and W. Zhou, "Connectivity enhancement of e-vanet based on ql-mrsu self-learning energy-saving algorithm," *IEEE Access*, vol. 11, pp. 3810–3825, 2023.

[15] N. I. Sarkar, F. Ahmed, and S. Gul, "Deploying a low-cost wi-fi-based vehicular ad hoc network in a shopping mall parking lot: An empirical study," *Electronics*, vol. 12, no. 22, p. 4672, 2023.

[16] A. Raj and S. D. Shetty, "Smart parking systems technologies, tools, and challenges for implementing in a smart city environment: a survey based on iot & ml perspective," *International Journal of Machine Learning and Cybernetics*, pp. 1–22, 2024.

[17] R. Lu, X. Lin, H. Zhu, and X. Shen, "An intelligent secure and privacy-preserving parking scheme through vehicular communications," *IEEE Transactions on Vehicular Technology*, vol. 59, no. 6, pp. 2772–2785, 2010.

[18] T. W. Chim, S.-M. Yiu, L. C. Hui, and V. O. Li, "Vspn: Vanet-based secure and privacy-preserving navigation," *IEEE transactions on computers*, vol. 63, no. 2, pp. 510–524, 2012.

[19] W. Cho, Y. Park, C. Sur, and K. H. Rhee, "An improved privacy-preserving navigation protocol in {VANET} s." *J. Wirel. Mob. Networks Ubiquitous Comput. Dependable Appl.*, vol. 4, no. 4, pp. 80–92, 2013.

[20] C. Sur, Y. Park, and K. H. Rhee, "An efficient and secure navigation protocol based on vehicular cloud," *International Journal of Computer Mathematics*, vol. 93, no. 2, pp. 325–344, 2016.

[21] G. Li, Q. Sun, L. Boukhatem, J. Wu, and J. Yang, "Intelligent vehicle-to-vehicle charging navigation for mobile electric vehicles via vanet-based communication," *IEEE Access*, vol. 7, pp. 170 888–170 906, 2019.

[22] D. Anand, A. Singh, K. Alsubhi, N. Goyal, A. Abdrabou, A. Vidyarthi, and J. J. Rodrigues, "A smart cloud and iovt-based kernel adaptive filtering framework for parking prediction," *IEEE Transactions on Intelligent Transportation Systems*, vol. 24, no. 3, pp. 2737–2745, 2022.

Date of publication: Apri 24, 2025.

Distribution and infestation rate of Carpomya incompleta on Sider fruit (Ziziphus spina-christi L.) in Jazan Province Saudia Arabia

Usama Abu EL-Ghiet [1,2]
[1] Department of Biology, College of Science, Jazan University, P.O. Box.114, Jazan 45142, Kingdom of Saudi Arabia.
[2] Environment and Nature Research Centre, Jazan University ،Jazan 45142, P.O. Box 114, Saudi Arabia.
Corresponding author: U. Abu El-Ghiet (e-mail: uhassan@jazanu.edu.sa)

ABSTRACT In the Middle East, people used the fruit and leaves of Sider or Ber (*Ziziphus spina-christi* L.) as food and in traditional medicine. Out of 26 sites surveyed, it was found that *Carpomya incompleta* was the dominant insect in all surveyed sites that separated from fruits in trees and fallen. In only two locations, a type of weevil was recorded on fallen fruits in a minimal number (in Khawarah, Sabia), and a different kind of Lepidoptera was recorded in (Mokhtara, Samtah) in a limited number. However, the various sites recorded Braconid wasps (parasitoids used in biological control) at the end of the fruiting season. The results pointed to no more than one larva of *C. incompleta* recorded inside the infested fruit, and no cocoons were detected inside the examined fruits. The infested fruits varied from 5 to 32% in the fruits in the investigated trees; meanwhile, it reached 4 to 80% in the fallen fruits. While the seasonal abundance was represented, a single peak of infestation occurred at the end of the fruiting season with late spring. The study introduced the surveyed sider plantations to investigate the distribution and fluctuations of the most dominant insects. It also evaluated insect infestations and their causes to determine the causes of economic losses in their fruiting yield in Jazan Province, Saudi Arabia**.**

INDEX TERMS Carpomya Incompleta, Jazan, Pest Infestation, Zizyphus Jujube.

I. INTRODUCTION

The Jazan Area is located between latitudes 16º 22´ and 17º 46´N and longitudes 41º 33´ and 43º 09´E in the southwest corner of Saudi Arabia. Jazan is considered to belong to the Afrotropical realm based on [1-3]. It is characterized by its tropical climate of high temperature (sometimes more than 50º in summer), high evaporation (with RH exceeding 60% in most months of the year), and scarce water [4]. Despite this harsh climate, it is considered one of the wealthiest areas of floral diversity in Saudi Arabia, with most species of African origin [5-6].

The genus Ziziphus belongs to the family Rhamnaceae, about 85 species. *Ziziphus spina-christi* willd. (sidr) is one of the species of *Ziziphus* found in Saudi Arabia [7]. *Ziziphus spina-christi* is one of the true native species and is very adapted to the environmental conditions of Saudia Arabia. It is locally known as ber or sider and is a multipurpose tree used for fodder, food, medicine, and desertification control in arid lands. It represents the primary source of income for a wide sector of growers and beekeepers where sider honey is produced [8-9]. Jujube fruit fly has been a limiting factor for the production of decent quality and causing crop losses [10-11-]. Tephritidae (Diptera), or the jujube fruit fly, are and economically significant [12-13]. This species is a serious pest of the fruit of Ziziphus species, including common jujube (*Z. jujuba*), distributed in Italy, Egypt, Sudan, Eritrea, and Iraq [13- 14]. A new report about the presence of the zizyphus fruit fly in Spain for the first time. This presence has been reported to the Early Warning Systems on Alien Invasive Species of the Andalusian Government (Spain)[15]. *Carpomya incompleta* causes economic losses to the crop that require management to decline their population and enhance fruit quality [16].

Balikai recorded 22 non-insect and insect species feeding on cultivated ber in Karnataka [17]. A total of 23 insect species on ber from India were observed. The species *C. incompleta* is known from Africa (Burkina Faso, Egypt, Eritrea, Ethiopia, Libya, Niger, Sudan), western Asia (Iraq, Saudi Arabia, Oman, United Arab, Emirates, Yemen) and Europe (France, Italy [including Sicily]) [16-18]. Larva Fruit fly *C. incompleta*, after hatching, enters into fruit and feeds there till larval metamorphoses is complete; the infested fruits drop down and dry off [19]. While information regarding the distribution and fluctuation of fruit flies (*Carpomya incompleta* Becker, 1903) in the Jazan region is scarce. Insect pests are a significant factor in limiting the distribution of wild and cultivated plants. One of the justifications for this study is the continuous complaints from

consumers about the presence of larvae in the jujube fruits and their unfitness for eating. Therefore, we aimed to document information about *C. incompleta* insect distribution and fluctuations in Ber fruit (*Z. spina-christi* L.) in Jazan Province. Also, seeking to help in the future in designing a successful insect management program for the pest of *Z. spina* in Saudi Arabia.

II. MATERIALS AND METHODS

Field trials were conducted in the spring months (From the beginning of February until the end of April) of 2020 and 2021 to collect samples of Sider (*Ziziphus spina-christi*) from 26 different locations in six governorates, representing most of the regions in the plain of the Jazan region (Table 1).

1-Description of study sites:

TABLE 1. shows the geographical location of the study sites and their most important features

Sampling stations	Local name	Latitude, Longitude	Remarks
Baish	Alsilaa (F)	17°14'27.9"N 42°37'25.2"E	Large and old trees, their numbers are limited
	Al Haqu (T and F)	17°27'56.5"N 42°40'38.6"E	Small, scattered trees in the valley
	Baish Alolia (F)	17°23'28.8"N 42°34'00.5"E	Large and old trees, their numbers are limited
Sabia	Aldhabyah (T)	17°07'05.5"N 42° 39'13.5"E	Small, scattered trees in the home border
	Khawarah (T and F)	17°07'24.0"N 42° 38'03.8"E	Many numbers of old and large trees
	King Abdullah Rd (T and F)	17°09'00.5"N 42° 39'11.3"E	Large, scattered trees in the valley
	East (T and F)	17°09'32.9"N 42°40'29.1"E	Small, scattered trees in the home border
	Al Husayni (T)	17°08'57.7"N 42°40'58.4"E	Small, scattered trees in the home border
	Damad Road (T and F)	17°10'40.4"N 42°45'23.5"E	Large, scattered trees in the valley
	Harub (T)	17°26'01.1"N 42°53'09.4"E	Small, scattered trees in the home border
	Hafadia (Sanba) (T and F)	17°25'56.04"N 42° 39'03.83"E	Limited numbers of trees in the middle of cultivated lands
Damad	East1 (T)	17°07'06.27"N 42° 47'51.86"E	Large, scattered trees in the valley
	East2 (T and F)	17°07'46.2"N 42° 47'10.6"E	Large, scattered trees in the valley
	East3 (T)	17°07'10.3"N 42° 48'39.0"E	Small, scattered trees in the home border
	Shokariy (T and F)	17°07'32.7"N 42° 48'52.0"E	Large, scattered trees in the valley
Abu Arish	Abo Al Nurah (F)	17°02'56.7"N 42° 52'49.7"E	Large, scattered trees in the valley
	AL Mijasas1 (T)	17°02'36.0"N 42° 52'23.9"E	Large, scattered trees in the valley
	AL Mijasas2 (T)	17°02'18.4"N 42° 52'38.7"E	Small, scattered trees in the home border
	ALkanwat Road (T and F)	17°01'20.6"N 42° 51'54.6"E	Large, scattered trees in the valley
	East (F)	17°59'36.5"N 42° 50'22.8"E	Large, scattered trees in the valley
Ahad al Masarihah	North (T)	16°43'16.0"N 42°56'08.8"E	Large, scattered trees in the valley
	West (T)	16°42'36.5"N 42°56'03.1"E	Small, scattered trees in the home border
	AL Dagharir (T and F)	16°40'59.3"N 42°57'45.7"E	Large, scattered trees in the valley
Samtah	Mokhtara (F)	16°40'14.5"N 42°56'24.4"E	Small, scattered trees in the home border
	Mokhtara (T)	16°39'44.7"N 42°56'14.5"E	Small, scattered trees in the home border
	North (T)	16°37'37.6"N 42°56'48.7"E	Large, scattered trees in the valley

- T Refers to fruits collected from trees.
- F Refers to fallen fruits collected at the bottom of the tree.
- T and F It indicates the availability of fruits above and below the tree..

2- Fruit sampling:

a. Samples of fruits from trees

Fruit ripening season begins from February to the end of April. The fruits (100 samples) were collected from each site randomly from five trees (replications) representing the site. As shown in Figure 1 (a-c), the height of the trees ranges from 3 to 4 meters. Ripe fruits were collected from the level of 1.5 meters to 2.5 meters, every 20 fruits were placed in a paper bag and transported for examination in the lab.

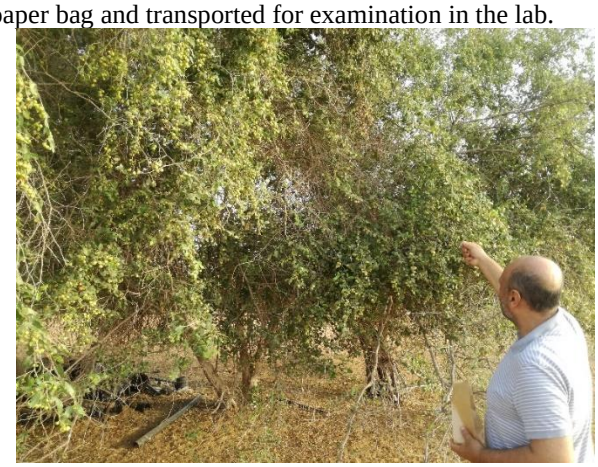

a

b

c

FIGURE 1 (A-C). Sider Trees from during sample collection in different sites (a – Fruit collection - b- High yielding trees c-Ripe fruits)

b. Samples of fallen fruits

Fallen fruits were collected from 15 sites. One hundred samples of fallen fruits were collected from each site in 5 replicates (20 * 5) to identify the pests associated with Ber fruit and compare the infestation by fruit fly in trees and fallen fruits.

a

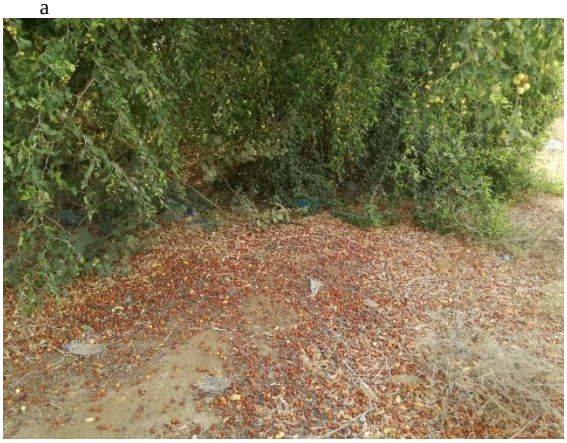

b

FIGURE 2 (A-B). The places of fruits were collected a fruit samples from tree b- fruit samples under the tree (fallen).

3- Rearing of collected larvae

As shown in Figure 3, the collected samples were transported to the lab and incubated over two weeks under laboratory conditions. Then, the emergence of adult stages was monitored, separated, and preserved in 70% alcohol until they were fully prepared and sent for identification.

4-Insect identification:

Collected insects were identified using different taxonomic keys with the help of experts Prof. Magdi El-Hawagry, Department of Entomology, Faculty of Science, Cairo University, and Giza, Egypt.

5- Statistical analysis

Data from infected trees and fallen fruit were analyzed descriptively among sites and main locations by ANOVA

followed by Tukey's HSD test ($P < 0.05$) to determine the variation in the infection across different study sites and between infection % and parasites % by SPSS (21.0 Version).

a b

FIGURE 3. Samples of *Z. spina-christi* L fruits incubated to identify the associated pests. a- Collected fruits b- Breeding containers.

III. RESULTS

The fruit of *Z. spina-christi* L roughly reached about 1.5 cm in diameter (Fig. 4a-b). Meanwhile, mature fruit falls from trees in spring and early summer. The survey collected samples from 26 sites in 6 governorates where fruitful *Z. spina-christi* trees grow.

a b

FIGURE 4. *Z. spina-christi* fruit, a- different developmental stages b-symptoms of infestation externally.

1. *Examination of Z. spina-christi fruits*

The present examination of *Z. spina-christi* fruits revealed larvae of one species namely *Carpomya incompleta* (Becker, 1903): Tephritidae as common herbivores on *Z. spina-christi* fruits in tropical and subtropical regions. The female of *C. incompleta* deposits her egg (usually one) inside the fruit while still on the tree. After hatching, the larva bores into the fruit and feeds exclusively on the contents of the fruit except the seed. The larva develops through different instars to reach the full-grown larva (5-7 mm in length). Reaching the full-grown larva, it tunnels the surface of the fruit and makes a round hole in the surface and the pericarp for emergence (Figure 5). Under the laboratory conditions (25±2 °C & 60%R.H.), the larval development within the fruit takes about 7-9 days; meanwhile, the pupal stage takes about one week. Fruits were examined internally to determine the damage caused to the fruits. Accordingly, the inspected fruits were segregated into healthy and infested ones. Throughout the study period, insect *C. incompleta* was dominant in all sites and separated from fruits in trees and fallen fruits. In only two locations, a type of weevil was recorded on fallen fruits in a minimal number (in Khawarah, Sabia). Also, another type of Lepidoptera was recorded in (Mokhtara, Samtah) in a limited number (Fig. 6a-b). During the sample's examination, important notes were observed on the 1st. More than one larva was recorded inside the infested fruit. 2nd. Also, no cocoons inside any of the examined fruits. Most of the recorded infections were in ripe fruits or those that began to ripen, characterized by a color change.

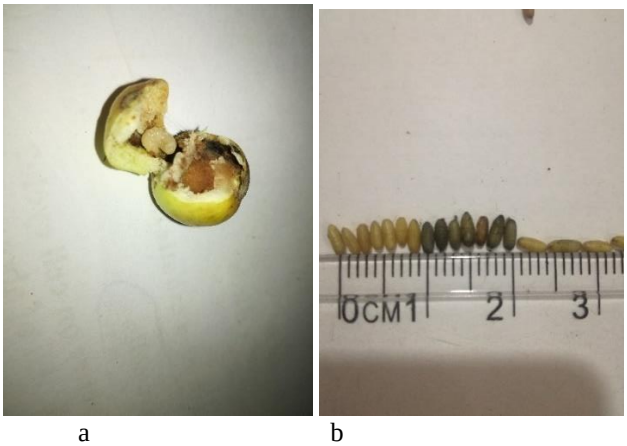

a b

FIGURE 5 (A-B). Larva of *C. incompleta* a pest on *Z. spina-christi* fruits. a- mature larva b- pupa phase.

a b

FIGURE 6. (a-b) Pests recorded in fallen fruits a- weevil recorded on fallen fruits b- cocoons outside fruits

2. *Z. spina-christi L fruit fly infestation rates in different locations in the Jazan region*

The examination during the study period (Table 2) revealed a significant difference in the infested fruit rats, where the percentage of infested fruits varied from 5% to 22.3%. The highest percentage of infestation was recorded in Samtah governorates, which represented (22.3 % infested fruit) while the lowest percentage of infested fruits was 5 % in Harub governorates (Fig. 7).

The results show the clear superiority in infestation rates for the southern governorates (Ahad al Masarihah and Samtah) over the northern governorates (Sabia and Baish). Within the governorates of the study, the lowest number of infested fruits was represented at the Harub site, where the infestation rate was 5%. In comparison, the Mokhtara site in Samtah Governorate was the highest infestation site, recording 30% infested fruit.

1. *A comparison between the rates of C. incompleta fruit fly infestation in tree and fallen fruits*

The examined fruits could be categorized according to their position of presence into two types: the 1st type was the fruit collected from the tree, while the 2nd one was collected under the tree (fallen fruit). During the study period, 15 sites were selected for trees, and fallen fruits were collected (Fig. 8). The percentage of infested fruits varied from 5 to 30 % in fruit trees; meanwhile, the percentage of infested fallen fruits varied from 4 to 80 %.

The results revealed a high percentage of the infested fruits in fallen fruits. As shown in Fig. 8, the infestation rate in fallen fruits was higher than in tree fruits in all locations except Site Aldhabyah, where the infestation rate in tree fruits was higher than in fallen fruits. Khawarah site occupied the forefront, as there was a considerable increase in the number of infested fruits, reaching 80% of the fruits. The highest significance of side effects was ($F=3.23$, $p \leq 0.04$) infected trees and ($F=48.622$, $p \leq 0.00$) fallen fruits, respectively.

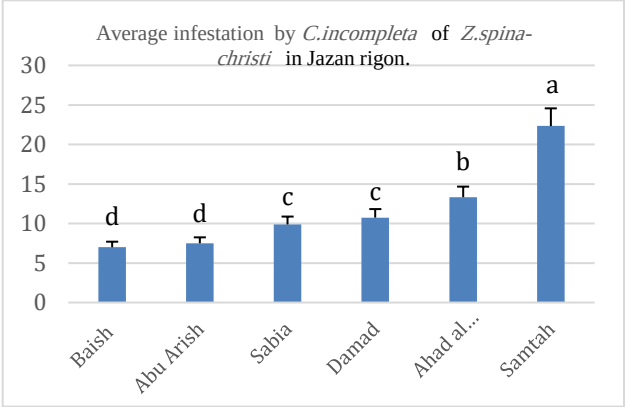

FIGURE 7. Average of Z. *spina-christi* fruit infested by *C. incompleta* in Jazan region during the spring months of 2020.

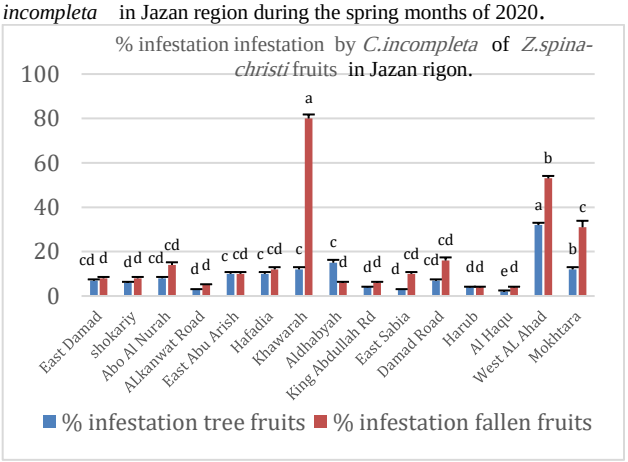

FIGURE 8. Average of Z. *spina-christi* fruit infested by C. *incompleta* (tree and fallen) in the Jazan region during the spring months of 2020

2. *Study of fluctuations of infestation by C. incompleta fruit fly during the fruiting season*

Over two successive years of study, two sites with tree-high density and fruiting rates were selected, one in the north of the Jazan region and the other in the south. The examined fruits were collected weekly to determine the fluctuation in infestation. As shown in Figure (9), the seasonal abundance of infestation was represented as a smooth wavering pattern. A single peak of infestation was observed at both study sites. It occurred at the end of the fruiting season in late spring, where the site West AL Ahad (the peak was recorded (35 % in 1st year) and (36 % in 2nd year) in the second week of April. Meanwhile, Khawarah–Sabia) site the peak was recorded (15 % in 1st year) and (20 % in 2nd year) in last week of March (Figure 10).

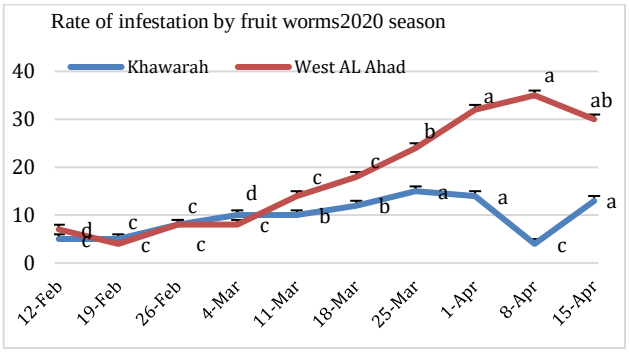

FIGURE 9. Weekly infestation for *Ziziphus spina-christi* fruits by *C. incompleta* during the period from 12 Feb. to 15 Apr. 2020.

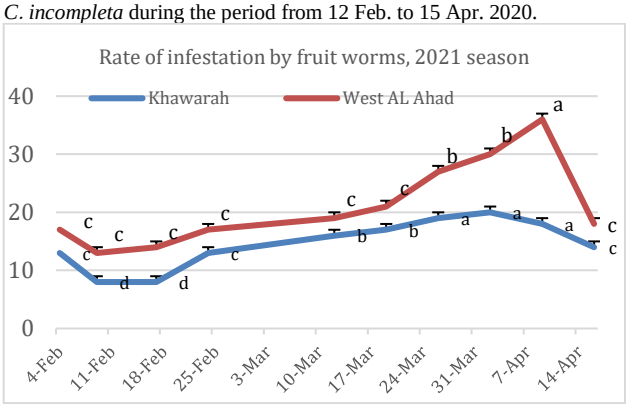

FIGURE 10. Weekly Infestation for *Ziziphus spina-christi* fruits by *C. incompleta* during the period from 9 Feb. to 16 Apr. 2021.

5- The spread of parasitoids associated with the Sidr fruit blight in the Jazan region

Table 2 and Figure 11 show insect parasitoids Braconid wasps from the order Hymenoptera were observed in the study's eight sites. Whereas, from five locations, larval parasitoids were collected from tree fruits from four locations and obtained from larvae of fallen fruits, and in one area (Samtah Mokhtara), the parasitoids were collected from both tree and fallen fruits. It could be concluded that the Sanba Hafadia site is the richest in parasite numbers, as 10 individuals were collected from the examined samples. It was noted that the largest number of parasitoids, Braconid wasps, was recorded at the end of the fruiting season at various study sites, especially in the study sites in the south of the Jazan region.

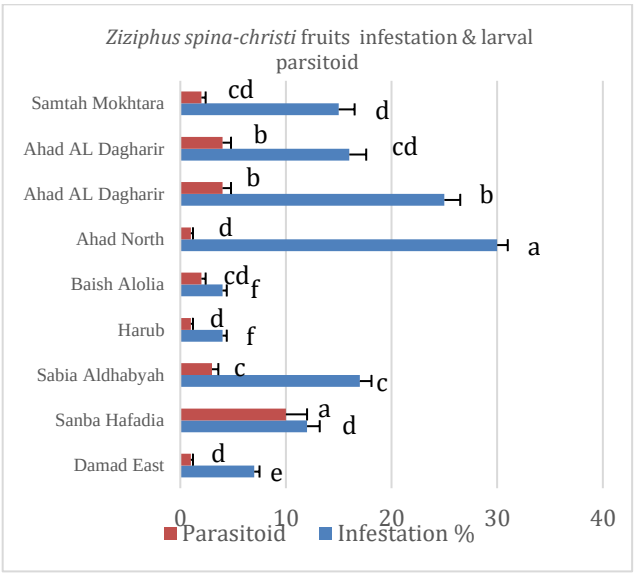

FIGURE 11. Density and spread of larval parasitoid-associated *Z.spina-christi* fruit in the Jazan region during the spring of 2020.

TABLE 2. Insect parasitoids and pest infestation percentage in the Jazan region sites.

Date	location	site	Fruits Place	Infestation %	Parasitoid
29. 2. 2020	Damad	Damad East	On tree	7	1
12. 2. 2020	Sabia	Sanba Hafadia	Fallen	12	10
21. 3. 2020	Sabia	Sabia Aldhabyah	On tree	17	3
14. 3. 2020	Harub	Harub	On tree	4	1
	Baish;	Baish Alolia	Fallen	4	2
11. 4. 2020	Ahad al Masarihah	Ahad North	On tree	30	1
	Samtah	Ahad AL Dagharir	Fallen	25	4
	Samtah	Ahad AL Dagharir	On tree	16	4
F (p value)				1.025(0.058)	

IV. DISCUSSION

Sidr is one of the most important plants in Jizan province, Saudi Arabia, as a pasture for bees to obtain the best types of honey and a basic component of balanced ecosystems in desert areas. Therefore, the study deals with sider insects and the distribution and fluctuations in Jazan. The results obtained from 26 sites representing different regions of Jazan during the study period showed one species: *Carpomya incompleta* (Becker, 1903)**:** Tephritidae as common herbivores on *Z. spina-christi* fruits. One of the critical notes we observed on the 1st. No more than one larva was recorded inside the infested fruit, and the2nd one also no cocoons were detected inside all examined fruits. Most of the recorded infestations were in ripe fruits or those that began to ripen, which are characterized by a color change. The results obtained are consistent with those **[18-21]** who reported the activity of fruit flies was very high during fruit maturity. Early harvesting of fruits at the color change stage avoids,s the over-ripening of fruits on trees and promotes fewer fruit flies' survival. Also, the study revealed a great vary from 5% to 22.3of the infested fruit rats with superiority in infestation rates in the southern governorates (Ahad al Masarihah and Samtah) over the northern governorates (Sabia and Baish); this may be due to the condition around plants and the rich fruits, as well as the accumulated and neglected fruits from the previous season. These results are consistent with the previous studies in different regions; for example, The *zizyphus* fruit fly (*C. incompleta*) is a monophagous pest of jujube (*Ziziphus* spp., Rhamnaceae), with two to five annual generations between spring and autumn [**21-24]**. Adult flies lay the eggs on fruit at the onset of ripening, and the carpophagous larvae, which go through three instars, dig a tunnel inside the fruit. They subsequently develop, with pre-pupariating third instars dropping to the soil to pupate, where enter diapause by the end of April [**22**]. Larval feeding promotes plant tissue decomposition and leads to bitter fruits, fruit rot, and drop, but sometimes, both eggs and larvae disappear inside the fruit [**12-25**]. *C. incompleta* may produce a low yield and poor quality fruits, which can often exceed 60% of infested trees **[24].** The variations among sites of collected trees and fallen fruits in infested fruits varied from 5 to 32 % in fruits in trees; meanwhile, the percent of infested fallen fruits varied from 4 to 80 %. This can be explained by several reasons, including that the pest prefers fruits in the ripening stage, and thus, they fall after that. Infested fruits are weaker in connection to the mother tree, so they fall more easily. The interaction effect of people or weather factors can increase the presence of infected fruits under the tree. In contrast, farmers collect only healthy fruits and leave the damaged fruits under the trees. As for the effect of season on inset abundance, a smooth wavering pattern of infestation was found. A single peak of infestation was observed at sites that occurred at the end of the fruiting season with late spring. It can be concluded that insects prefer ripe fruits, which is evident as the infestation rate increases with the completion of the ripening of most fruits and the forthcoming end of the season.

From eight sites, insect parasitoids Braconid wasps and order Hymenoptera were collected from trees and fallen fruits. Meanwhile, the highest rate of parasitism reached 10%, while the most significant number of parasitoids, Braconid wasps, was recorded at the end of the fruiting season, especially in the south of Jazan. The larvae bore down into the soil to a depth of 2 to 12 cm, where it pupates **[18-26]** and destroy the hibernating pupae by exposing them to bright sunlight and birds, considerably reducing the infestation. Heating of soil by burning grass and irrigation during summer also kills the pupae **[27].**

Finally, it could be concluded that *C. incompleta* is the key pest in the sider tree, and its parasitoids (Braconid wasps) are high due to the rich biodiversity in the Jazan region. However, there are no significant relationships between insect infestation and parasites ($P > 0.058$). So, this infestation needs more action to be less than the economic level to preserve this important type of plant and environment. While these results may contribute to developing suitable integrated pest control programs that meet the Jazan region's conditions, it should activate the prevention action before applying integrated pest management to protect *Z. spina-christi* trees.

V. CONCLUSION

The present study demonstrates that *C. incompleta* was the dominant insect in all surveyed sites. Braconid wasps

(parasitoids used in biological control) were recorded at various sites. In contrast, the seasonal abundance represented a single peak of infestation that occurs at the end of the fruiting season with late spring. All this data helps in designing an integrated control program for this pest, the times of activity and spread of this pest, taking advantage of the natural enemy, and considering the possibility of including it in the control program to preserve the environment.

ACKNOWLEDGMENTS

The author would like to thank Prof. Salah Abbutalb (Faculty of Science, Jazan University) for his assistance and his company during our field trips. Sincere gratitude goes to Prof. Mohamed A. Balah (Desert Research Center, Cairo, Egypt) for his valuable suggestions and critical review of the manuscript, which greatly improved this study. Thanks also exctended to Prof. Magdi El-Hawagry, Department of Entomology, Faculty of Science, Cairo University for identifiecation Collected insects.

Funding

This research received no grant from any funding institution, either public or private.

Availability of data and material

The datasets generated during and/or analyzed during the current study are available from the corresponding author upon necessary request.

DECLARATIONS

Conflict of interest

The authors declare no conflict of interest regarding this publication.

REFERENCES

[1] Corbet AS (1948) Observations on the species of *Rhopalocera* common to Madagascar and the Oriental region. Transactions of the Royal Entomological Society of London 99: 589–607. https://doi.org/10.1111/j.1365-2311.1948.tb01232.x

[2] Larsen TB (1984) Butterflies of Saudi Arabia and its neighbors. Stacy International, London, 160 pp.

[3] Burkhardt D, Mifsud D (1998) Psylloidea (Insecta: Hemiptera) of the Arabian Peninsula. Fauna of Arabia 17: 7–49.

[4] Masrahy YS, Al Turki TA, Sayed OH (2012) Geographical distribution and chorology of grasses in the Arabian Peninsula. Flora: Morphology, Distribution, Functional Ecology of Plants 207: 250–256.

[5] Hassan HM, Al-Hemaid FM (1996) Composition origin and migration trends of perennial vegetation in the Farasan El-Kabir Island (Red Sea). Saudi Journal of Biological Sciences 4: 5–15.

[6] Sayed H.Osama & Yahya S. Masrahi (2023) Climatology and phytogeography of Saudi Arabia. A review, Arid Land Research and Management, 37:3, 311-368, https://doi.org/10.1080/15324982.2023.2169846

[7] Naghmouchi S, Alsubeie M (2021) Ecological diversity of *ziziphus spina-christi* (L.) Willd. Of four provenances in Saudi Arabia: differential responses to drought stress and characterization of growth, biomass and proline contents Ann. Bot. (roma) 11: 91–104 https://doi.org/10.13133/2239-3129/16937

[8] Sudhersan C, Ashkanani JH (2009). Introduction, evaluation and propagation of *Ziziphus* in Kuwait. Acta Hortic. 840: 47-54 .https://doi.org/10.17660/ActaHortic.2009.840.4

[9] Hajer Ali Abdulla Alhmoudi1, Shaher Bano Mirza2, Fouad Lamghari Ridouane ٢٠٢٢ A Comparative Study of Nutraceutical Values of Ziziphus Spina Christi (Sidr) from the Origin of Fujairah, UAE, with Same Specie from Different Origin and Leafy Vegetables International Journal of Science and Research (IJSR) 11 (10): 517-519.

[10] Jebbar, AS.(1996) Biological, Ecological and Behavior studies of two species of ber fruit fly (*Tephritidae: Diptera*) in Basrah. Ph.D. thesis. Basrah Univ. College of Science .158 pp.(in Arabic).

[11] Al-yousuf AA, Al-Miahy MZ (2008) Effect of calcium on jujube *Ziziphus* sp. fruit growth and their resistance to jujube fruit fly *Carpomyia incomplete* .Sci. J of Kerbala Univ. 5(4):106-113.

[12] White IM, Elson-Harris MM (1992) Fruit flies of economic significance: their identification and bionomics. CAB, Wallingford, UK, 601 pp. https://doi.org/10.1079/9780851987903.0000

[13] Freidberg A, Kugler J (1989) Fauna Palaestina. Insecta IV. Diptera: Tephritidae. Israel Academy of Sciences and Humanities, Jerusalem: i- 1–212.

[14] Smith JJ, Bush GL (1999) Phylogeny of the subtribe *Carpomyina* (Trypetinae), emphasizing relationships of the genu *Rhagoletis*. In: Aluja, M., Norrbom, A. L., eds. Fruit flies (Tephritidae): Phylogeny and evolution of behavior. CRC Press, London, 187–217.

[15] Garrido-Jurado I, Quesada-Moraga E, Yousef-Yousef, M (2022) Short communication: *Zizyphus* fruit fly (*Carpomya incompleta* (Becker), Diptera: Tephritidae) is expanding its range in Europe. Spanish Journal of Agricultural Research, 20(4) 6-12. https://doi.org/10.5424/sjar/2022204-18961

[16] Ismael BF, Abd AK, Jabbar FJ (2022) Study the effect of antioxidants on the traits of the fruits of two cultivars of Jujube (*Ziziphus mauritiana* Lamk.) Al-Tufahi and Alarmouti Cultivars. Basrah Journal of Agricultural Sciences, 35(1), 1-20.

[17] Balikai RA (1999) Pest scenariao of ber (*Zizyphus mauritiana* Lamarck) in Karnataka. Pest Manage. Hort. Ecosystem 5(1):67-69.

[17] Taher M, Alyousuf A (2023) Morphological and Molecular Identification of Jujube Fruit Fly *Carpomya incompleta* (Becker, 1903) (Diptera: Tephritidae) in southeast Iraq Basrah. J. Agric. Sci., 36(1): 39-49,

[19] Kavitha Z, Savithri P, Vijayaragavan C. (2002). Insect pests of ber, *Ziziphus jujuba* in Tirupati region. Insect Environment 7(4):157-158.
[20] Mehrdad Parchami-Araghi, Ebrahim Gilasian , Farzaneh Basavand (2015) First record of jujube fruit fly *Carpomya incompleta* (Becker) (Diptera: Tephritidae) from Iran Studia dipterologica 22 (1): 163–164.
[21] Aluja MI, Norrbom AL (2001) Fruit flies (Tephritidae): phylogeny and evolution of behavior. CRC Press, Boca Raton London New York Washington, D.C. 963pp.
[22] Lakra RK (1998) Insect pests of some under-exploited fruits and their management Haryana J. Hort. Sci. 27(1):12-34.
[23] Morsy MAA (1971) Studies on certain fruit pests in Upper Egypt. M. Sc. Thesis, Fac. Agric. Assiut Univ. Egypt. 67 pp.
[24] Al-Masudey AD, Al-Yousuf AA (2013) Effect of jujube fruit cultivars on chemical control of jujabe fruit fly *Carpomyia incompleta*. Kufa J Agric Sci 5: 111-124.
[25] Rizk MM, Temerak SA, Abdel-Galil FA, Darwish DY (2014). Toxicity and persistence of Spinosad® (Conserve 0.024% and Tracer 24%) to *Zizyphus* fruit fly, *Carpomyia incompleta* Becker (Diptera: Tephritidae), under laboratory conditions. Arch Phytopathol Plant Prot 47: 1666- 1674. https://doi.org/10.1080/03235408.2013.853914.
[26] Batra HN (1953) Biology and control of *Dacus diversus* Conquillet and *Carpomyia vesuviana* Costa and important notes on other fruit flies in India. Indian J. Agric. Sci. 22:87-112.
[27] Singh MP (2008) Managing menace of insect pests on mer. Indian Hort. 53 (1):31-32.

Date of publication: April 24, 2025.

Biochemical Characterizations of Acacia mellifera Seed Extract and Evaluation of its Biological Applications

Mohamed Alawlaqi
Biology Department, Science College, Jazan University, Jazan, KSA

Corresponding author: Alawlaqi M. (e-mail: mmalawlaqi@jazanu.edu.sa).

ABSTRACT. Plant bioactive chemicals have numerous biological impacts that are vital to human health. In the present study, Acacia mellifera (*A. mellifera*) seeds were collected from Jazan in Saudi Arabia, where *A. mellifera* was extracted using 90% methanol. GC-Mass analysis of *A. mellifera* extract revealed the presence of seventeen various molecules, six of which were from different chemical classes and were the most prevalent compounds. The extract showed a significant antibacterial impact on *Klebsiella pneumonia* and *Salmonella typhi*; their minimal inhibitory levels and bactericidal impact were recoded. Testing 25, 50 and 75% of the Minimum Bactericidal Concentrations (MBC) of the extract illustrated anti-biofilm impact of *A. mellifera* extract, especially at 75% of MBC. The minimum inhibitory concentration (MIC) values of *A. mellifera* extract compared to different bacteria showed dramatic anti-hemolytic action, especially at 75% of MIC levels. *In vitro* wound scratch assay using HFB4 cells highlighted the useful role of *A. mellifera* extract in wound healing. Hence, Saudi *A. mellifera* seeds have many pharmaceutical applications to be applied on a large scale in future after verifications of these outcomes.

INDEX TERMS Acacia Mellifera, Antimicrobial, Anti-Biofilm, Anti-Hemolytic, GC-Mass, Wound Healing.

I. INTRODUCTION

Microbial infections are a major global health concern, mostly affecting individuals in the third world and affecting the digestive and respiratory systems [1]. However, several of the medications that are now being used have unfavorable adverse reactions [2,3,4]. It is vital to look for novel antibacterial compounds with little adverse effects [5,6]. Throughout the world, medicinal products are the preferred medicinal approach in rural regions and play a crucial part in conventional medicine. The plant utilized throughout conventional healthcare is among the most potential frontiers in the quest for novel biologically functional molecules [7,8,9,10].

In human and animal; healing a wound is significant but intricate, with several distinct stages controlled by interconnected, consecutive phases. A more effective therapy strategy and a growing variety of *in vitro* or *in vivo* investigations are available to support the maintenance of a controlled and coordinated inflammatory reaction during the wound healing process [11].

One significant attribute of infected wounds is the presence of biofilms [12]. In reaction to signaling substances generated by other species in the biofilm, bacteria living in a biofilm exhibit phenotypic changes that lead to modifications in the generation of virulence factors. They also have reduced rates of metabolism and more confined growth [13]. A developed biofilm provides a milieu of protection for the microbes, enhancing their resistance to traditional antibiotics and insulating them from the phagocytic action of neutrophils [14]. The difficulty in the healing of persistent ulcers may be attributed to the presence of biofilms [15].

Inflammation and discomfort are initiators of numerous degenerative illnesses. The synthetic medications employed for the treatment of these illnesses have adverse effects that are incredibly harmful. In an attempt to provide safe, inexpensive, and efficient medications, new medicinal plants are being introduced globally [16].

To discover novel remedies and create cutting-edge pharmaceuticals, ethnopharmacology conducts in-depth studies of plants [17,18]. Plants in the genus Acacia have some intriguing medicinal characteristics. The genus Acacia, which has about 1200 species and is found in nearly every type of ecosystem, is the second biggest in the Leguminosae family [19]. *Acacia mellifera* (*A. mellifera*) is one species of Acacia, a shrub or small tree that can reach a height of nine meters. With its wide-ranging root system, it

may survive in arid regions by absorbing vast amounts of dirt. Spread over arid and semi-arid areas of Africa and the Arabian Peninsula, *A. mellifera* is a drought-resistant plant. *A. mellifera* is a slow-growing, versatile tree that can be used for human respiratory infections, infertility, and stomach issues [20,21]. However, little research has been done on the potential biological uses of *A. mellifera*'s phytochemical compounds.

The present investigation designed to test various bioactive molecules in *A. mellifera* seeds grown in Saudi Arabia using GC-Mass and in vitro testing its antimicrobial, anti-biofilm, anti-hemolytic and wound healing activities of *A. mellifera* extract.

II. MATERIALS AND METHODS

A. Collection of plant specimen

A. mellifera seeds were assembled from Jazan, Saudi Arabia (16° 54' 34.8588" N and 42° 34' 4.4472" E) in August 2023. The seeds were authenticated at Jazan University Herbarium (JAZUH), Biology Department, College of Science. The gathered seeds were cleaned with flowing tap water and sterile water to remove any remaining dust. Seeds are dried in the shade for three days at room temperature and processed using an electric mixer,

B. Preparation of extract & Chemicals

The collected dried seeds (100 g) were homogenized and crushed into a fine powder using a motorized mixer. They were then macerated for eight days in a sealed bottle with two hundred milliliters of 90% methanol. The extract was then subjected to a 120-minute sonicator treatment at 45 °C for traditional extraction. To get 6.0 g of crude extract, this extract was passed through filters and then centrifuged using Rota vapor for 40 minutes at 45 °C. [22]. Investigations of its chemical composition and biological functions were conducted on the extract. Every chemical utilized in this project was bought from Sigma-Aldrich, Louis, USA.

C. GC-Mass analysis of A. mellifera extract

The GC examination was conducted using (Stabilwax-560 column (98.0 m × 0.26 mm × 0.23 µm; Stabilwax, US), auto-sampler (CHROMSERVIS, US), and flame-ionization detecting. The data was extracted from the FID using chromatography equipment (Claurs 20400, PerkinElmer, Germany). There are nine minutes in the pre-run. The equilibrium takes 0.8 minutes to attain. Two ramps were finished: ramp 1.0, which produced an end maximum temperature of 207°C at a rate of 6°C/min, and ramp 2, which produced an average temperature of 6°C/min. The temperature started at 44°C and increased to a maximum of 285°C. The tests were conducted using the systematized heat mode, which ran from 100 to 282 °C for 14.0 minutes until homogeneity was reached. A transfer flow of 1.3 ml/min was used [23].

D. Antimicrobial activity

The well agar diffusion assay was used to ascertain the in vitro anti-microbial activity of *A. mellifera* extract against a range of bacteria and fungi. For the bacteria, Mueller Hinton agar plates were employed (2.0 g. Beef infusion solids, 1.5 g. Starch, 17.5 g. Casein hydrolysate, 17.0 g. Agar, Final pH 7.3) in 1 liter of distilled water. For the fungi, malt extract media was employed (30.0 g. Malt extract, 5.0 g. Mycological peptone, 15.0 g. Agar, Final pH 5.4) in 1 liter of distilled water. A total volume of 100 µl of different suspended bacterial cells ($1.6X10^6$ colony forming units/ml) was used; for the bacteria. The assessed extract was then put into the medium-created well using a sanitized cork borer edge. Gentamicin (0.07 mg/ml) and fluconazole (0.24 µg/ml) were utilized as standards and DMSO as our control. After developing for 72 hours at 35°C for bacterial cells, 5-7 days, and 27°C for fungi, the area of inhibition was evaluated [24,25].

E. Minimal inhibitory level and minimal bactericidal action

The micro-dilution broth approach was performed to find the specimen's least inhibiting value (MIC) using the nutrient-rich broth for bacteria. The final levels of every specimen under analysis ranged from 0.98 to 1000 µg/mL and were determined by diluting the specimen twice. 200 µl of the specimen dilutions under examination in broth media have been added to prepare every hole in the 96-well micro-titrate plate. Fresh microbial cultures that met the turbidity criteria of the 1.0 McFarland standard were used to generate the inoculum. Each well received 2.0 µl of sterilized 0.9% NaCl to achieve a $3.0X\ 10^6$ CFU/ml level. Subsequently, the bacteria and fungi were cultivated at 36°C for 72 hours and 35°C for 5–7 days, respectively. To ascertain the lowest inhibiting levels (MICs) that happened when the reference strain's development was stopped entirely, Beckman DU-70 UV-Vis. was used to measure the optical density of the sample at a wavelength of 600 nanometers for each sample. On each microplate, there was a positive reference (an inoculum without the examined specimens) and a negative reference (tested specimens without an inoculum) [26, 27]. Besides, 100 milliliters of the culture of microbes from each well were sub-cultured onto plates containing media from a developmental control, the final positive specimen, and the medium with 100% growth suppression. This made it possible to calculate MBC. When it came to samples that failed to promote the development of microbes during the incubation time at the appropriate temperature, the MBC was found to be the lowest level [26, 27].

F. Anti-biofilm action

The influence of the specimens on the biofilm-forming process was evaluated using 96-well polystyrene flat-bottom trays. A final level of 10^6 CFU/mL was determined by introducing 270 µL of newly seeded trypticase soy yeast broth (TSY) to each well of a microplate. The microplate

was then cultured in MBC at the previously determined sub-lethal concentrations of 75, 50, and 25%. Wells containing medium and those containing only alcohol without any samples were used as controls. Plates were stored at 38°C for 48 hours. The floating cells in every well were thoroughly rinsed with sterile distilled water after the supernatant was discarded. The plates were left to air dry for 30 minutes, and then the formed biofilm was colored for twenty minutes at ambient conditions using a water-based solution of 0.10% crystal violet. The excess color was removed again by rinsing thrice with sterile distilled water after incubation. Following a 20-minute incubation period and adding 250 µL of 96% ethanol to each well to eventually degrade the dye adhered to the cells, absorption was assessed at 580 nm utilizing a plate reader [28].

G. Anti-hemolytic activity

Using hemolytic and phospholipase C (PLC) protocol, the hemolysis reactions in specimens in sub-MIC (25% and 50% of MIC) manipulated by bacteria were measured [29]. Centrifuged at 21,000× g for 20 minutes, tested bacteria treated with 25%, 50%, and 75% of MIC (sub-MIC) or untreated cultures have been adjusted to an OD600 of 0.4. Freshly erythrocyte solution (2%) in 0.8 mL saline was mixed with supernatants (500 µL), incubated for 2 hours at 37 °C, and then spun at 11,000× g for 10 minutes at 4 °C. By adding 0.1% Sodium Dodecyl sulfate to an erythrocyte suspension, a positive control (full hemolysis) was created. A negative control (un-hemolyzed erythrocytes) was created by incubating erythrocytes in LB broth according to the same conditions.

The experiment was run in triplicate, and the hemoglobin discharge was measured by measuring absorbance at 540 nm. Drug-induced hemolysis in sub-MIC treated cultures was expressed as mean ± standard error of percentage reduction from untreated control cultures' hemolysis. After comparing the released hemoglobin with the positive and negative controls, the following formula was used to determine the percentage of hemolysis:

[(Specimen with bacterial culture − Negative control)/ (Positive control − Negative control)] × 100

H. In vitro wound healing assay

An extracellular matrix base containing 10 µg/mL fibronectin was applied to the plate. And then two hours of incubation at 37 °C. Following its release, the unattached extracellular matrix was cleaned with phosphate-buffered saline. Trypsin was used to separate the developing cells from a tissue culture-filled dish. The cells were grown on the assay plate with scratches wounds and then incubated to allow them to proliferate and form a confluent monolayer. A pipette tip scraped the monolayer cell, incorporating the confluent monolayer. After the cell monolayer has been scraped, gently wash it to remove any detached cells. Replace with a new medium that contains the tested extract. The plate was cultured in the cell culture unit for 48 hours at 37 °C. Phosphate-buffered saline was used to wash the cell monolayer following the incubation period. The cells were then treated with 3.7% paraformaldehyde for 15 minutes. For ten minutes, the cells were stained with crystal violet (1% in ethanol). A phase-contrast microscope was then used to inspect the cell culture [30].

I. Statistical evaluation

Each experiment was run three times, and the average ±SD of the findings is shown. The *t*-test and one-way ANOVA were utilized to distinguish across means utilizing the Graph Pad Prism V5 (San Diego, CA, USA) software. Findings indicating $p < 0.05$ were designated as noteworthy modifications.

III. RESULTS

A. Detection of bioactive molecules using GC-Mass

Testing of *A. mellifera* seeds extract revealed the existence of 17 various compounds from different classes, and it could be seen that six different significant compounds present in conductive order in the extract as follows 1,2,3-Benzenetriol (35%), Hexadecane (21.53%), Isobutyl gallate (11.81%), 12-methoxy-19-n orpodocarpa-4(18),8,11,13-tetraen3-one (6.76%), Octadecane, 3-ethyl-5-(2-ethylbutyl)- (4.54%) and 4H-1-benzopyran -4-one, 2-(3,4-dimethoxyp henyl)-3,5-dihydr oxy-7-methoxy (4.49%) as shown in (Fig. 1 , Table 1)

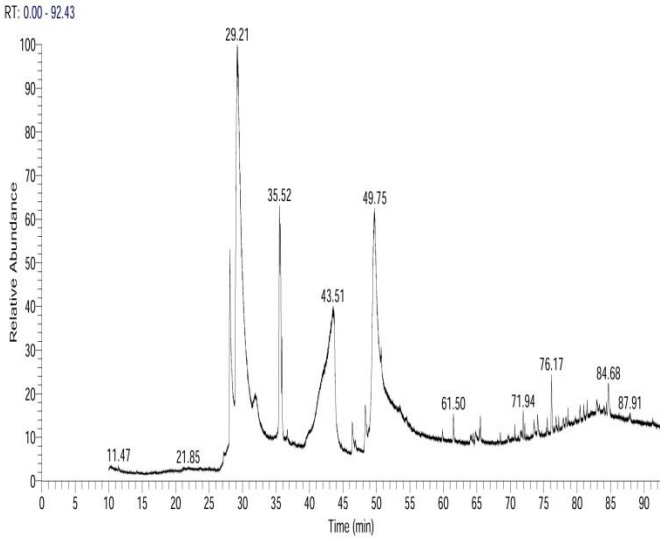

FIGURE 1. **GC-Mass testing of various compounds in *A. mellifera* extract.**

TABLE I
DIFFERENT COMPOUNDS AND THEIR PEAK AREAS AS WELL AS THEIR CLASSES IN *A. mellifera* SEEDS EXTRACT

RT Retention Time	Compound Name	Class	Peak area %	Molecular Formula	Molecular Weight
28.09	12-methoxy-19-norpodocarpa-4(18),8,11,13-tetraen3-one	Di-terpenoid	6.76	$C_{17}H_{20}O_2$	256
29.16	1,2,3-Benzenetriol	5-unsubstituted pyrrogallols	35	$C_6H_6O_3$	126
35.51	Hexadecane	Alkanes	21.53	$C_{16}H_{34}$	226
36.69	Prednisone	Corticosteroids	0.4	$C_{21}H_{26}O_5$	358
43.66	3-Methylmannoside	Oligosaccharide glycans	4.57	$C_7H_{14}O_6$	194
46.40	Dinaphtho[1,2-b:2',3'-d]furan-7,12-dione, 5-methoxy	Heterocyclic Phenol	1.09	$C_{21}H_{12}O_4$	328
48.32	Hexadecanoic acid, 1-(hydroxymethyl)-1,2-ethanediyl ester	Fatty acid ester	1.67	$C_{35}H_{68}O_5$	568
49.75	Isobutyl gallate	Galloyl esters	11.81	$C_{11}H_{14}O_5$	226
50.73	3,4,5-Triethoxybenzoic acid	Methoxybenzenes	1.71	$C_{13}H_{18}O_5$	254
61.51	Phenol, 2,2'-methylenebis[6-(1,1-dimethylethyl)-4-methyl	Dihydric phenol	1.39	$C_{23}H_{32}O_2$	340
64.81	i-Propyl 9-tetradecenoate	Unsaturated Fatty Acids	0.62	$C_{17}H_{32}O_2$	268
65.39	Allogibberic acid	Fluorenes	0.23	$C_{18}H_{20}O_3$	284
65.54	1,2-Benzenedicarboxylic acid	Dicarboxylic acid	0.77	$C_{24}H_{38}O_4$	390
71.94	4H-1-benzopyran-4-one, 2-(3,4-dimethoxyphenyl)-3,5-dihydr oxy-7-methoxy	Coumarins	4.49	$C_{18}H_{16}O_7$	344
74.08	à-Tocospiro A	Alpha-tocopheroids	1.33	$C_{29}H_{50}O_4$	462
76 .17	Octadecane, 3-ethyl-5-(2-ethylbutyl)-	Alkanes	4.54	$C_{26}H_{54}$	366
84.68	Spirost-8-en-11-one, 3-hydroxy-, (3á,5à,14á,20á,22á,25R)-	Saturated hydrocarbon	1.48	$C_{27}H_{40}O_4$	428
87.91	Lupeol	Triterpenoids.	0.62	$C_{30}H_{50}O$	426

B. Determination of Antimicrobial Activity

It could be noted that *A. mellifera* extract has inhibition zones towers *B. subtilis* (ATCC 6633) and *S. aureus* (ATCC 6538) of 20±0.1 and 21±0.2 mm which was lower relative to standard drug. While, *A. mellifera* extract showed higher inhibition zone than standard drug. The zones were measured as 24±0.2 and 23±0.2 mm towards *K. pneumoniae* (ATCC13883) and *S. typhi* (ATCC 6539), consecutively. Furthermore, *A. mellifera* extract showed no impact towards *P. glabrum* (OP694171) as well as 22±0.2 mm inhibition zone versus *C. albicans* (ATCC 10221) as shown in (Table 2 & Fig. 2).

TABLE 2
ANTIMICROBIAL IMPACT (MM) OF *A. mellifera* EXTRACT VERSUS DIFFERENT TEST MICROORGANISMS (RESULTS WERE TABULATED AS MEANS ± SD).

Specimen / Test organisms	*A. mellifera* extract	Standard
Bacillus subtilis (ATCC 6633)	20±0.1	29±0.2
Staphylococcus aureus (ATCC 6538)	21±0.2	25±0.2
Klebsiella. peregrine (ATCC13883)	24±0.2	21±0.1
Salmonella typhi (ATCC 6539)	23±0.2	20±0.2
Candida albicans (ATCC 10221)	22±0.2	30±0.2
Penicillium glabrum (OP694171)	NA	25±0.1

C. Evaluation of MIC and MBCs towards test microorganisms

It could be noticed that *A. mellifera* seeds extract had similar MIC and MBC levels for *B. subtilis* (ATCC 6633) and *S. aureus* (ATCC 6538) which were 31.25±0.1 and 62.5±0.1 µg/ml respectively. Besides, *A. mellifera* seeds extract have similar MICs and MBCs versus *K. peregrine* (ATCC13883) and *S. typhi* (ATCC 6539) which were 15.62±0.2 and 31.25±0.2 µg/ml, respectively. Finally, *A. mellifera* seeds extract had values of 15.62±0.1 and 62.5±0.1 for MIC and MBC 15.62±0.1 towards *C. albicans* (ATCC 10221) as illustrated in (Table 3).

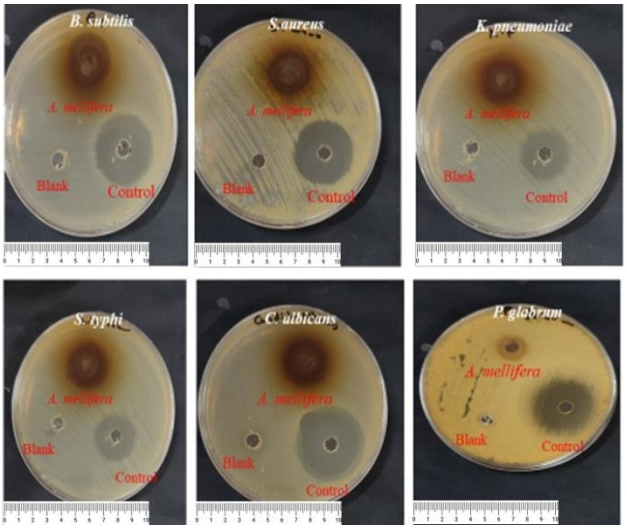

FIGURE 2. **Antimicrobial impact (mm) of *A. mellifera* seeds extract compared to standard drugs and blank in several Plates containing various test microorganisms (Results were tabulated as means ± SD).**

TABLE 3
DETERMINATION OF MIC AND MBC (µG/ML) OF *A. mellifera* SEEDS EXTRACT VERSUS DIFFERENT TEST MICROORGANISMS (RESULTS WERE TABULATED AS MEANS ± SD)

Test organisms	MIC	MBC
Bacillus subtilis (ATCC 6633)	31.25±0.1	62.5±0.1
Staphylococcus aureus (ATCC 6538)	31.25±0.2	62.5±0.2
Klebsiella. peregrine (ATCC13883)	15.62±0.2	31.25±0.2
Salmonella typhi (ATCC 6539)	15.62±0.1	31.25±0.2
Candida albicans (ATCC 10221)	15.62±0.1	62.5±0.1

D. Anti-biofilm impact of A. mellifera extract

Anti-biofilm impact (%) of *A. mellifera* extract versus *S. aureus*, *K. pneumonia*, *B. subtilis* and upon applying (25, 50 and 75%) of MBC of the extract. There is a gradual elevation of anti-biofilm impact (%) of the extract towards various tested bacteria and reaches its maximal level upon using 75% of MBC of the extract as depicted in (Fig. 3 and 4).

E. Anti-hemolytic action of A. mellifera extract

The lysed hemoglobin was evaluated upon applying 25, 50, and 75% of MICs of *A. mellifera* treated for various bacteria relative to the positive control. It could be noticed that there is a dramatic evaluation of anti-hemolytic impact of the extract, and it reached its maximal level upon using 75% of MIC. Furthermore, there is a dramatic difference in anti-hemolytic action upon using 25% of MIC of the extract relative to 75% of MIC of the extract, as shown in (Fig. 5 and 6).

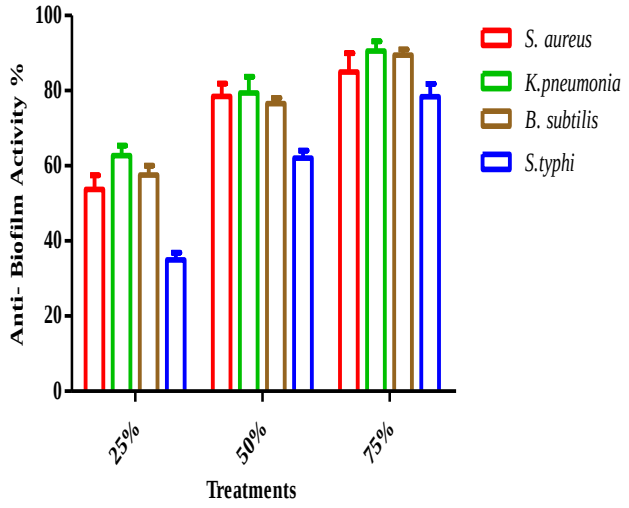

FIGURE 3. **Statistical analysis for anti-biofilm action (%) of *A. mellifera* extract versus various bacteria upon using 25, 50 and 75% of MBC (Data are drawn as means ± SD).**

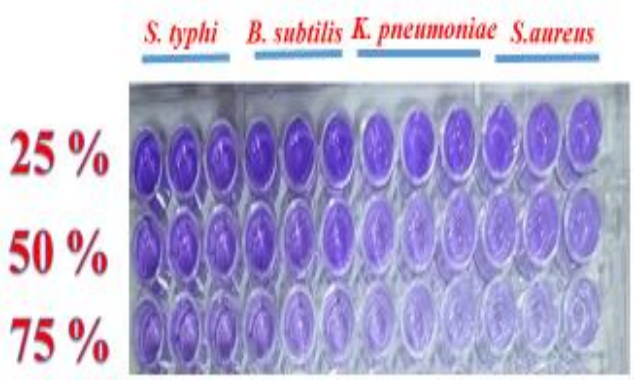

FIGURE 4. **Various in color intensities in Elisa plate upon using the tested levels for detection of anti-biofilm of the extract.**

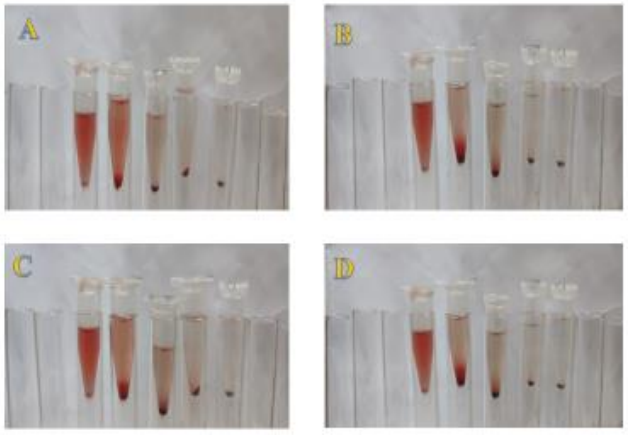

FIGURE 5. **A: Anti-hemolytic action upon using MICs for (A) *B. subtilis*, (B) *K. peregrine*, (C) *S. aureus*, and (D) *S. typhi*.**

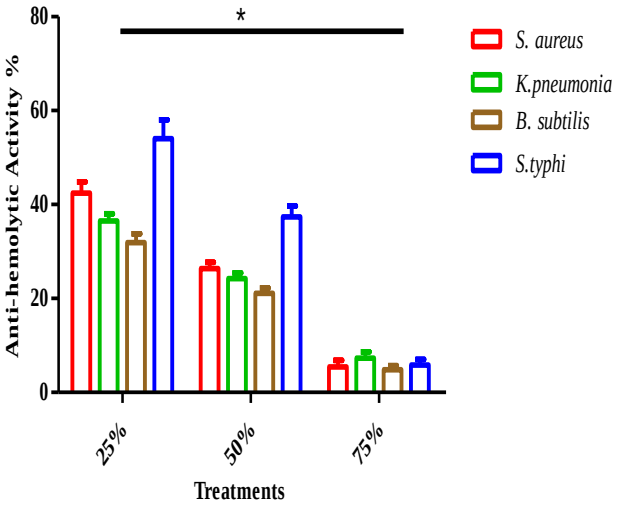

FIGURE 6. **Statistical analysis for anti-hemolytic activities of various MICs (Data are presented as means ± SD, * $P \leq 0.05$).**

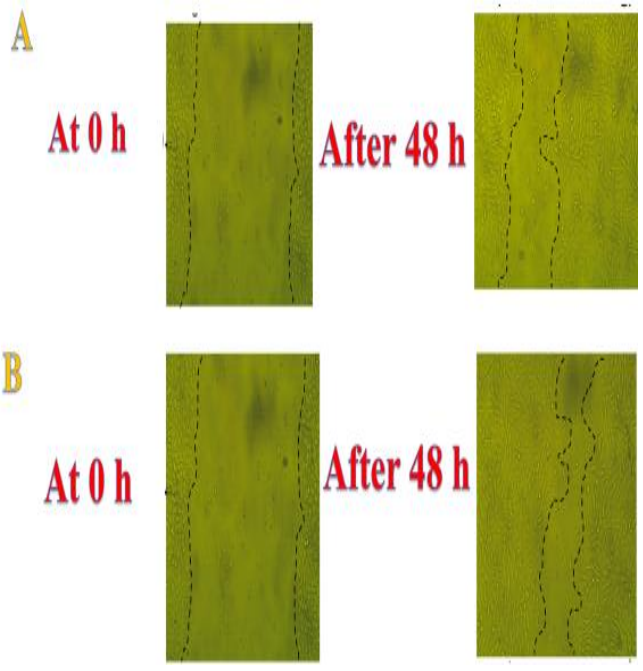

FIGURE 7. **Testing the effect of *A. mellifera* seeds extract on wound healing at 0 time and after 48 hours.**

TABLE 4
EVALUATION OF THE HEALING CHARACTERISTICS OF *A. mellifera* EXTRACT ON HFB4 CELLS (* REFER TO DRAMATIC DIFFERENCE P≤0.05).

Item	at 0 h		at 48 h	
	width	Area	width	Area
A. mellifera extract (125 µg/ml)	708.10	538187.30	246.01	186976.40
	670.03	509248.70	104.00	79044.37
	760.17	579298.20	128.06	97591.70
	684.00	519849.80	242.01	183928.70
	732.00	556322.30	244.01	185446.10
	806.00	6109480	266.12	201719.00
Mean	726.72	552309.00	205.03	155784.40
RM µm	10.87			
Wound closure % µm^2	71.79*			
Area difference	396.52*			
Control cells HFB4	708.10	538187.30	316.03	240192.30
	670.03	509248.70	238.03	180915.80
	760.17	579298.20	208.24	158692.60
	684.00	519849.80	340.01	258408.30
	732.00	556322.30	304.16	231164.60
	806.00	610948.00	318.02	241063.00
Mean	726.72	552309.00	287.42	218406.10
RM µm	9.15			
Wound closure % µm^2	60.46*			
Area difference	333.90*			

F. Determination of wound healing capabilities of A. mellifera extract

The efficacy of treatment was evaluated based on wound contraction, The simple ruler method consists of multiplying the greatest length and width of the wound to determine the surface area, *A. mellifera* seeds extract shown encouraging healing qualities for HFB4 cells; in contrast to control (cells not receiving treatment), *A. mellifera* seed extract consistently promotes healing (Table 4 and Fig. 7). The gap closing rate, which establishes the speed at which the cells move collectively, is the result of the evaluation of wound healing. Using *A. mellifera* seeds extract, the rate of migration (RM), wound closure percentage, and area difference percentage were 10.87 um, 71.79 µm^2, and 396.52%, consequently, with substantial improvement over control cells' corresponding values of 9.15 µm, 60.46 µm^2, and 333.90% (Table 4).

IV. DISCUSSION

Plants with vast distribution are exposed to ecological variations, which causes variations in the bioactive compounds that these plants generate [28, 31]. Both grassy and woody plant species accumulated triterpenoids due to soil drying [32, 33]. According to earlier research, there is an important distinction in the manufacturing of plant phytochemicals with geographic location [34, 35].

Genus *Acacia* contains many species with many therapeutic applications, including flowers, stems, and leaves [36]. In the present work, *A. mellifera* seeds collected from Jazan in Saudi Arabia were extracted, and tested by GC-Mass. *A. mellifera* contained various molecules where seven compounds were the most common. These compounds were from different chemical classes 5-unsubstituted pyrrogallols, alkanes, galloyl esters, di-terpenoids, oligosaccharide glycans, and coumarins. Australia's *A. mellifera* seeds have been found to contain vernolic acid [37]. Kenyan *A. mellifera* bark's tannin level is relatively greater [38]. Furthermore, the extraction of African *A. mellifera* using various solvents yields various bioactive fractions with multiple activities [39].

The present work illustrated that *A. mellifera* extract has antibacterial action towards *K. peregrine* and *S. typhi* nd an anti-yeast impact on *C. albicans.* In the same line, *A. ataxacantha* had antimicrobial action toward many test microbes, including *C. albicans* [5]. Also, isolation of flavanocoumarin from *Plicosepalus acacia* with antimicrobial action [40]. The antimicrobial impact of aerial parts of various species of Acacia grown in Saudi Arabia was reported [41]. Furthermore, it characterized Phenolics from *A. dealbata* with antimicrobial impacts [42].

Biofilms are intricate cellular formations made up of numerous bacterial cells encased in layers of materials the bacteria manufacture. This creates a barrier that prevents the organisms from being eliminated [43, 44]. Bacteria become resistant to antibiotics quickly, no drug can effectively treat infections linked to biofilms. The nature and form of the biofilm, the supply of oxygen and food for bacterial cells, and innate and developed resistance to antibiotics are additional factors that contribute to tolerance [45, 46]. The present work showed that A. mellifera extract showed a promising anti-biofilm towards S. aureus, K. pneumonia, B. subtilis especially upon using 75% of MBC. Following this, he anti-biofilm activity of different plant extracts was reported [47].

The cells that carry out medicine transmission the most regularly are the erythrocytes found in human tissue [48]. Hemoglobin and fatty acids, oxidizing active transporter components and erythrocyte-targeting intermediaries, are the main factors that induce triggered oxygen species in the body. Hemolysis is a disorder caused by oxidative destruction of the lipids and proteins composing the erythrocyte surface. Various variables, such as inflammatory drugs, excessive transitional metals, and deficiencies in erythrocyte antioxidant interaction, could be involved [49, 50]. In the present work, various levels of Sub-MIC values ranged from 25 to 75 % of the MIC of A. mellifera extract, which showed a promising anti-hemolytic impact, especially at 75 % of the MIC of the extract.

Free radical scavenging enzymes may disable and eliminate reactive oxygen species, which are detrimental to

wound repair due to their detrimental impact on tissue. Using molecules that can neutralize free radicals may prevent tissues from oxidative harm and increase the rate of wound healing [51]. In this study using A. mellifera extract showed a promising healing impact on HFB4 cells. In accordance with [52], who reported the role of Acaia gum in wound healing. Furthermore, [53] illustrated the healing impact of A. catechu in diabetic animals.

V. CONCLUSION

A. mellifera seeds collected from Jazan in Saudi Arabia and extracted by methanol showed promising antimicrobial, anti-biofilm, anti-hemolytic action as well as *in vitro* wound scratch assay using HFB4 cells highlighted the useful role of *A. mellifera* extract in wound healing. Hence, Saudi *A. mellifera* seeds have many pharmaceutical applications to be applied on a large scale in future after verifications of these outcomes.

ACKNOWLEDGMENT

The author thanks the Biology Department, College of Science, at Jazan University, Jazan, Saudi Arabia.

REFERENCES

[1] P. Cavazos, D. Gonzalez, J. Lanorio, and R. Ynalvez "Secondary metabolites, antibacterial and antioxidant properties of the leaf extracts of Acacia rigidula benth. And Acacia berlandieri benth" SN Applied Science, vol. 3, no. 522, April 2021, Doi: 10.1007/s42452-021-04513-8.

[2] M. I. Alghonaim, , S. A. Alsalamah, , A. Alsolami, and T. M. A. Ghany, "Characterization and Efficiency of Ganoderma lucidum Biomass as an Antimicrobial and Anticancer Agent" BioResources, vol. 18 no. 4, pp. 8037-8061, Nov. 2023, DOI: 10.15376/biores.18.4.8037-8061.

[3] M. M. Bakri, M.I. Alghonaim, S.A. Alsalamah, and T. M. Abdelghany "Impact of Moist Heat on Phytochemical Constituents, Anti-Helicobacter Pylori, Antioxidant, Anti-Diabetic, Hemolytic and Healing Properties of Rosemary Plant Extract in Vitro" Waste Biomass Valor pp. 4965–4979, April 2024, https://doi.org/10.1007/s12649-024-02490-8

[4] H. Qanash, , S. R. A. El-Fadl, N. K. Binsaleh, I. A. Aljahdali, M. A. Altayar, A. F. Khalel, S. A. Alsalamah, M. I. Alghonaim and T. M. Abdelghany "Ecofriendly extraction approach of Moringa peregrine biomass and their biological activities in vitro" Biomass Conv. Bioref., August 2024. DIO: 10.1007/s13399-024-05916-4

[5] A. M. O. Amoussa, L. Lagnika, M. Bourjot, C. Vonthron-Senecheau, and A. Sanni "Triterpenoids from Acacia ataxacantha DC: Antimicrobial and antioxidant activities" BMC Complement and Altern. Med. vol. 16, no. 284, August 2016, Doi: 10.1186/s12906-016-1266-y.

[6] A. Alsolami, , A. S. Bazaid, M. A. Alshammari, and T. M. Abdelghany "Ecofriendly fabrication of natural jojoba nanoemulsion and chitosan/jojoba nanoemulsion with studying the antimicrobial, anti-biofilm, and anti-diabetic activities in vitro" Biomass Conv. Bioref., December 2023, https://doi.org/10.1007/s13399-023-05162-0

[7] A. M. Soliman,; A. M. Younis,; T. M. Abdelgany, and S. Abdelbary "Trends in Assessment of Ganoderma lucidum Methanol Extract Against MRSA Infection In Vitro and In Vivo with Nutrition Support" J. Adv. Pharm. Res. vol. 6, no. 1, pp. 45-57, Jan. 2022, DOI: 10.21608/aprh.2022.111305.1147

[8] M. A. Tola, F. Ibrahim, H. Melak, T. Tafesse, M. Alemayehu, and G. Nigussie "Traditional Herbal Remedies in the Management of Metabolic Disorders in Ethiopia: A Systematic Review of Ethnobotanical Studies and Pharmacological Activities" Evidence-Based Complementary and Alternative Medicine, Jan. 2023, 1413038, doi:10.1155/2023/1413038.

[9] A. M. H. Al-Rajhi and Abdel T. M. A. Ghany "Nanoemulsions of some edible oils and their antimicrobial, antioxidant, and anti-hemolytic activities" BioResources vol. 18, no. 1, pp. 1465-1481, Feb. 2023, DOI:10.15376/biores.18.1.1465-1481

[10] S. A. Alsalamah, M. I. Alghonaim, M. Jusstaniah, and T. M. Abdelghany "Anti-Yeasts, Antioxidant and Healing Properties of Henna Pre-Treated by Moist Heat, and Molecular Docking of Its Major Constituents Chlorogenic and Ellagic Acids with Candida albicansand Geotrichum candidum Proteins" Life, vol. 13 no. 9:1839. Aug. 2023, https://doi.org/10.3390/life13091839

[11] M. S. Almehayawi, M. S, Almuhayawi, S. R. A. El-Fadl, M. K. Nagshabandi, M. K. Tarabulsi, S. Selim, Y. S. Alruwaili, E. M. Mostafa, S. K. Al Jaouni, and T. M. Abdelghany “Evaluating the anti-yeast, anti-diabetic, wound healing activities of Moringa oleifera extracted at different conditions of pressure via supercritical fluid extraction” BioResources vol. 19, no. 3, pp. 5961-5977, 2024, DOI: 10.15376/biores.19.3.5961-5977

[12] V. T. Anju, S. Busi, M. Imchen, R. Kumavath, M. S. Mohan, S. A. Salim, P. Subhaswaraj and M. Dyavaiah, "Polymicrobial Infections and Biofilms: Clinical Significance and Eradication Strategies" Antibiotics, vol. 11 no. 12:1731, 2022, DOI: 10.3390/antibiotics11121731.

[13] K. Kirketerp-Møller, P. S. Stewart and T. Bjarnsholt "The zone model: A conceptual model for understanding the microenvironment of chronic wound infection" Wound Repair Regen. vol.28 no. 5 pp. 593-599, June 2020, DOI: 10.1111/wrr.12841.

[14] A. Pietruczuk-Padzik, M. Śliwińska, M. Mainka, M. E. Czerwińska, W. Skowrońska and A. Bazylko "Evaluation of Antimicrobial Activity of Selected

Plant Extracts against Staphylococcus Strains Isolated from Wound Infections" Planta Med. Oct. 2024, DOI: 10.1055/a-2416-8584.

[15] C. Alihosseini, H. Kopelman, J. Lam and T. Phillips "Do Commonly Used Antimicrobial Topicals Facilitate Venous Leg Ulcer Healing?" Adv Skin Wound Care, vol. 36 no. 6, pp. 322-327, June 2023, DOI: 10.1097/01.ASW.0000926636. 51805.d5.

[16] B. Adhikari, B. Aryal and B. R. Bhattarai "A Comprehensive Review on the Chemical Composition and Pharmacological Activities of Acacia catechu (L.f.) Willd" J. Chem. :2575598. (Dec. 2021). DOI: 10.1155/2021/2575598.

[17] B. Aryal, P. Niraula, K. Khadayat, B. Adhikari, D. K. Chhetri, B. K. Sapkota, B. R. Bhattarai, N. Aryal and N. Parajuli "Antidiabetic, antimicrobial, and molecular profiling of selected medicinal plants" Evid. -Based Complement. Altern. Med., May 2021, 5510099. DOI: 10.1155/2021/5510099.

[18] M. H. Rawi, A. Abdullah, A. Ismail and S. R. Sarbini "Manipulation of Gut Microbiota Using Acacia Gum Polysaccharide" ACS Omega, vol. 6, pp. 17782–17797, July 2021, DOI: 10.1021/acsomega.1c00302.

[19] S. Elshamy, H. Handoussa, M. El-Shazly, E. D. Mohammed and N. Kuhnert "Metabolomic profiling and quantification of polyphenols from leaves of seven Acacia species by UHPLC-QTOF-ESI-MS" Fitoterapia, vol. 172, 105741, Jan. 2024, DOI: 10.1016/j.fitote.2023.105741.

[20] C. Mutai, C. Bii, G. Rukunga, J. Ondicho, P. Mwitari, D. Abatis, C. Vagias, V. Roussis, J. Kirui "Antimicrobial activity of pentacyclic triterpenes isolated from Acacia mellifera" Afr. J. Tradit. Complement Altern. Med., vol. 6 no. 1 pp. 42-48. Jan, 2009, DOI:10.4314/ajtcam. v6i1.57072

[21] L. Wadley, G. Trower, L. Backwell and F. d'Errico, "Traditional Glue, Adhesive and Poison Used for Composite Weapons by Ju/'hoan San in Nyae Nyae, Namibia. Implications for the Evolution of Hunting Equipment in Prehistory" PLoS One. Vol. 10 no. 10, e0140269, Oct. 2015. DOI: 10.1371/journal.pone.0140269.

[22] A. M. H. Al-Rajhi, S. S. Salem, A. A. Alharbi, T. M. Abdelghany "Ecofriendly synthesis of silver nanoparticles using Kei-apple Dovyalis caffra fruit and their efficacy against cancer cells and clinical pathogenic microorganisms" Arabian Journal of Chemistry, vol. 15, no. 7, Jul. 2022, 103927, https://doi.org/10.1016/j.arabjc.2022.103927

[23] T. M., Abdel Ghany, M. M. Hassan, M. A. El-Naggar, M. Abd El-Mongy (2020). "GC/MS analysis of Juniperus procera extract and its activity with Silver Nanoparticles against Aspergillus flavus growth and aflatoxins production" Biotechnology reports vol. 27, e00496, Sep. 2020, DOI: 10.1016/j.btre.2020.e00496

[24] C. Mutai, G. Rukunga, C. Vagias, and V. Roussis "In vivo screening of antimalarial activity of Acacia mellifera (Benth)(Leguminosae) on Plasmodium berghei in mice" Afr. J. Tradit. Complement. Alter. Med. Vol. 5 no, 1, pp. 46–50,. Oct. 2008, DOI:10.4314/ajtcam. v5i1.31255

[25] T. M. Abdel Ghany, M. Ganash, M. M. Alawlaqi, and A. M. H. Al-Rajhi "Antoixidant, antitumor, antimicrobial activities evaluation of Musa paradisiaca L. pseudostem exudate cultivated in Saudi Arabia" BioNanoScience vol. 9, pp. 172–178, Dec. 2018, DOI: 10.1007/s12668-018-0580-x

[26] S. Joshi, Y. P. Subedi and S. K. Paudel "Antibacterial and antifungal activity of heartwood of Acacia catechu of Nepal. Journal of Nepal Chemical Society, vol. 27, pp. 94-99, (2011). https://doi.org/10.3126/jncs.v27i1.6667.

[27] D. Adhikari, R. N. Kumar "Antimicrobial activities of Acacia genus: A review" Asian Pacific Journal of Tropical Biomedicine vol. 13, no. 2, pp. 45-59, Feb. 2023, DOI: 10.4103/2221-1691.369609

[28] S. Selim, Y. S. Alruwaili, H. Ejaz, A. E. Abdalla, M. S. Almuhayawi, M. K. Nagshabandi, T. M. Abdelghany "Estimation and Action Mechanisms of Cinnamon Bark via Oxidative Enzymes and Ultrastructures as Antimicrobial, Anti-biofilm, Antioxidant, Anti-diabetic, and Anticancer Agents" BioResources, vol. 19, no. 4, pp. 7019–7041, Aug. 2024, DOI:10.15376/biores.19.4.7019-7041

[29] G. Rossignol, A. Merieau, J. Guerillon, W. Veron, O. Lesouhaitier, M. G. Feuilloley, N. Orange "Involvement of a phospholipase C in the hemolytic activity of a clinical strain of Pseudomonas fluorescens" BMC Microbiol., vol. 8, no. 189, Oct. 2008, doi:10.1186/1471-2180-8-189

[30] S. Martinotti and E. Ranzato "Scratch Wound Healing Assay" Methods Mol Biol., vol. 2109, pp. 225-229, Aug. 2019, DOI:10.1007/7651_2019_259.

[31] T. M. Abdel Ghany, and O. M. Hakamy "Juniperus procera as Food Safe Additive, their Antioxidant, Anticancer and Antimicrobial Activity against Some Food-Borne Bacteria" J. biological and chemical research, vol. 31, no. 2, pp. 668-677, 2014.

[32] H. A. Alhaithloul, M. H. Soliman, K. L. Ameta, M. A. El-Esawi and A. Elkelish "Changes in Ecophysiology, Osmolytes, and Secondary Metabolites of the Medicinal Plants of Mentha piperita and Catharanthus roseus Subjected to Drought and Heat Stress" Biomolecules, vol. 10, no. 1:43, Dec. 2019, DOI: 10.3390/biom10010043.

[33] C. Grossiord "Having the right neighbors: how tree species diversity modulates drought impacts on forests" New Phytol., vol. 228, no. 1, pp. 42-49, 2020. DOI: 10.1111/nph.15667.

[34] S. Demasi, M. Caser, M. Lonati, P. L. Cioni, L. Pistelli, B. Najar, and V. Scariot "Latitude and Altitude Influence Secondary Metabolite Production in Peripheral Alpine Populations of the Mediterranean Species Lavandula angustifolia Mill" Front Plant Sci.,

vol. 9, no. 983, Jul. 2018, DOI: 10.3389/fpls.2018.00983.

[35] W. Y. Chen and T. Su "Asian monsoon shaped the pattern of woody dicotyledon richness in humid regions of China" Plant Divers., vol. 42 no. 3, pp. 148-154, March 2020, DOI: 10.1016/j.pld.2020.03.003.

[36] C. Sanchez, M. Nigen, V. M. Tamayo, T. Doco, P. Williams, C. Amine, D. Renard "Acacia gum: History of the future" Food Hydrocoll., vol. 78 pp. 140–160, May 2018, DOI: 10.1016/j.foodhyd.2017.04.008.

[37] A. Brown, V. Cherikoff and D. Roberts "Fatty acid composition of seeds from the Australian Acacia species" Lipids, vol. 22, pp. 490–494, July 1987, DOI: 10.1007/BF02540364.

[38] J. Z. Mugedo, P. G. Waterman "Sources of tannin: Alternatives to wattle (Acacia mearnsii) among indigenous Kenyan species" Econ. Botany, vol. 46, no. 1, pp. 55–63, Jan. 1992, DOI: 10.1007/BF02985254.

[39] C. Mutai, C. Bii, C. Vagias, D. Abatis, and V. Roussis, "Antimicrobial activity of Acacia mellifera extracts and lupane triterpenes" Journal of Ethnopharmacology, vol. 123 no. 1, pp. 143-148, May 2009, DOI:10.1016/j.jep.2009.02.007.

[40] J. M. Badr, L. A. Shaala, and D. T. Youssef "Loranthin: A new polyhydroxylated flavanocoumarin from Plicosepalus acacia with significant free radical scavenging and antimicrobial activity" Phytochem. Lett. Vol. 6 pp. 113–117, Feb. 2013, DOI: 10.1016/j.phytol.2012.11.008.

[41] M. F. Alajmi, P. Alam, S. I. Alqasoumi, N. A. Siddiqui, O. A. Basudan, A. Hussain, F. M. Husain A. A. Khan "Comparative anticancer and antimicrobial activity of aerial parts of Acacia salicina, Acacia laeta, Acacia hamulosa and Acacia tortilis grown in Saudi Arabia" Saudi Pharm. J., vol. 25, pp. 1248–1252, Sep. 2017, DOI: 10.1016/j.jsps.2017.09.010.

[42] V. Paula, S. I. Pedro, M. G. Campos, T. Delgado, L. M. Estevinho, O. Anjos, "Special Bioactivities of Phenolics from Acacia dealbata L. with Potential for Dementia, Diabetes and Antimicrobial Treatments" Appl. Sci. vol. 12, 1022, Jan. 2022, DOI: 10.3390/app12031022.

[43] C. Latasa, A. Roux, A. Toledo-Arana, J. M. Ghigo, C. Gamazo, J. R. Penadés, et al. "BapA, a large secreted protein required for bio film formation and host colonization of Salmonella enterica serovar Enteritidids" Mol Microbiol. Vol. 58, no. 5, pp. 1322–39, Oct. 2005, DOI: 10.1111/j.1365-2958.2005. 04907.x

[44] Z. Mohsenipour and M. Hassanshahian " The effects of Allium sativum extracts on biofilm formation and activities of six pathogenic bacteria" J Microb., vol. 8, no. 8, pp. E18971, Aug. 2015, DOI: 10.5812/jjm.18971v2.

[45] R. Roy, M. Tiwari, G. Donelli, and V. Tiwari "Strategies for combating bacterial biofilms: A focus on anti-biofilm agents and their mechanisms of action" Virulence vol. 9, no. 1, pp. 522–554, Feb. 2018, DOI: 10.1080/21505594.2017.1313372

[46] T. Miller, D. E. Waturangi, and Yogiara "Antibiofilm properties of bioactive compounds from Actinomycetes against foodborne and fish pathogens" Sci Rep., vol. 12, 18614, Nov. 2022, DOI: 10.1038/s41598-022-23455-8

[47] O. S. Olawuwo, I. M. Famuyide, and L. J. McGaw "Antibacterial and Antibiofilm Activity of Selected Medicinal Plant Leaf Extracts Against Pathogens Implicated in Poultry Diseases" Front. Vet. Sci., vol. 9, :820304, March 2022, DOI: 10.3389/fvets.2022.820304.

[48] M. Hamidi, and H. Tajerzadeh, "Carrier erythrocytes: an overview" Drug Deliv., vol. 10, no. 1, pp. 9–20, 2003, DOI: 10.1080/713840329.

[49] M. Ebrahimzadeh, Nabavi, S., Nabavi, S. Antioxidant activities of methanol extract of Sambucus Ebulus L. Flower" Pak J Biol Sci., vol. 12, no. 5, pp. 447-450, 2009, DOI: 10.3923/pjbs.2009.447.450.

[50] T. Afsar, S., Razak, M.R. Khan, S. Mawash, A. Almajwal, M. Shabir and I. Ul-Haq "Evaluation of antioxidant, anti-hemolytic and anticancer activity of various solvent extracts of Acacia hydaspica R. Parker aerial parts" BMC Complement Altern Med., vol. 16, 258 July 2016, DOI: 10.1186/s12906-016-1240-8

[51] E. Aliyeva, S. Umur, E. Zafer, H. Acigoz "The effect of polylactide membrane on the levels of reactive oxygen species in periodontal flaps during wound healing" Biomaterials, vol. 25, no. 19, pp. 4633–3637, Aug. 2004, DOI: 10.1016/j.biomaterials.2003.12.004

[52] C. Pagano, F. Luzi, M. Ricci, A. D. Michele, D. Puglia, M. R. Ceccarini, T. Beccari, F. Blasi, L. Cossignani, A. Schoubben, S. Primavilla, C. A. V. Iborra, and L. Perioli, "Wound Dressing: Combination of Acacia Gum/PVP/Cyclic Dextrin in Bioadhesive Patches Loaded with Grape Seed Extract" Pharmaceutics, vol. 14, no. 3, :485, Feb. 2022, DOI: 10.3390/pharmaceutics14030485.

[53] V. P. Nakhate, N. S. Akojwar, S. K. Sinha, A. D. Lomte, M. Dhobi, P. R. Itankar, and S. K. Prasad, "Wound healing potential of Acacia catechu in streptozotocin-induced diabetic mice using in vivo and in silico approach" J Tradit Complement Med., vol. 13, no. 5 pp. 489-499, Sep. 2023, DOI: 10.1016/j.jtcme.2023.05.001.

Date of publication: April 24, 2025.

Chitosan-Based Biopolymer for Efficient Cr(VI) Removal: A Thermodynamic and Adsorption Study

Isam Y. Qudsieh[1]
[1]Chemical Engineering Department, College of Engineering and Computer Sciences, Jazan University, P. O. Box 706, Jazan 45142, Saudi Arabia
Corresponding author: Isam Y. Qudsieh (e-mail: isamyq@jazanu.edu.sa).

ABSTRACT: Chitosan biopolymer was utilized without modification to separate hexavalent chromium Cr(VI) ions from liquid feed. Cr(VI) contamination in water poses a critical environmental and health concern due to its toxicity and persistence, necessitating effective and sustainable removal methods. This study investigates the use of chitosan biopolymer as an environmentally friendly adsorbent for Cr(VI) removal. Batch experiments were conducted to investigate the effects of adsorbent dose, pH, contact time, and temperature. The optimal conditions achieved were as follows: 50 mg adsorbent dose, pH 6, 70 minutes contact time, 15 mg/L Cr(VI) concentration, and 30°C, with a maximum removal capacity of 66.64 mg/g. The Langmuir isotherm Model (R^2 = 0.9981) indicated monolayer adsorption, while pseudo-first-order kinetics confirmed a physio-adsorption mechanism. Thermodynamic analysis revealed an exothermic process ($\Delta H°$ = -15.617 kJ/mol) with a negative $\Delta S°$ (kJ/mol·K), indicating a reduced randomness at the solid-liquid interface and confirming predictable adsorption behavior. The results highlight the potential of chitosan biopolymer as a sustainable solution for Cr(VI) removal, with promising applications in environmental remediation.

INDEX TERMS: Adsorption, Chitosan Biopolymer, Chromium, Isotherm, Kinetic, Thermodynamic.

I. INTRODUCTION

Hexavalent chromium Cr(VI) is a hazardous metallic element that can be released into water sources, causing serious environmental and health problems. Industrial processes such as electroplating, leather tanning, and metalworking can produce this type of pollution [1]. Cr(VI) is extremely hazardous to both humans and aquatic life [2]. Exposure to high levels of Cr(VI) can lead to numerous health complications, including respiratory issues, skin rashes, and an increased risk of cancer [3]. Contamination with Cr(VI) can adversely affect aquatic ecosystems [4], impacting species composition and reducing biodiversity [5]. It may also hinder the reproductive capabilities and overall well-being of aquatic species [6]. To protect the environment and public health, Cr(VI) and other heavy metals must be excluded from water sources. Solutions to this environmental issue must encompass sustainable industry practices, efficient wastewater treatment, and stringent regulatory enforcement [7]. Factors such as initial Cr(VI) content, co-occurring pollutants, available infrastructure, and regulatory requirements influence the choice of wastewater treatment technology [8–10]. Wastewater treatment plants often combine various methods to effectively remove Cr(VI) and other contaminants [11]. Common treatment techniques include chemical precipitation, ion exchange, adsorption, electrocoagulation, advanced oxidation processes, and membrane filtration [12–14]. Among these techniques, adsorption technology is widely applied due to its ease of use, flexibility, and high effectiveness in eliminating pollutants from wastewater [15]. Adsorption onto activated carbon or other adsorbent materials can be employed to remove Cr(VI) from wastewater [16]. Cr(VI) ions are attracted to and bound by the adsorbent material, effectively removing them from the water. Chitosan is an environmentally benign and biodegradable biopolymer deacetylated from chitin [17, 7]. It poses no harm to human health when used as a coagulant in water treatment and can also be utilized to dispose of waste generated by the seafood processing industry [19]. This study examines the efficiency of a common, inexpensive chitosan biopolymer in removing Cr(VI) ions from solutions. In batch-method investigations, the effects of interaction time, initial metal ions quantity, pH, sorbent dosage, and temperature on the rate of Cr(VI) adsorption, the kinetics, isotherms, and thermodynamics of the adsorption process were also explored.

Chitosan has been extensively studied as an adsorbent for Cr(VI) removal due to its low cost, biodegradability, and high adsorption efficiency. However, significant gaps remain in the literature. Previous studies have primarily focused on the adsorption performance of unmodified chitosan, with limited exploration of chemically or physically modified forms, such as cross-linked or grafted chitosan, which have shown potential for enhanced adsorption capacity and selectivity. Furthermore, thermodynamic and kinetic analyses of the adsorption process are often underexplored, particularly under varying temperatures and concentrations, leaving critical questions about the adsorption mechanism unanswered. Comparative studies evaluating the efficiency of chitosan relative to other adsorbents, such as activated carbon or other biosorbents, are also insufficient. Addressing these gaps is essential for optimizing the use of chitosan-based systems for Cr(VI) remediation in industrial and environmental applications.

II. MATERIALS AND METHODS

A. *Materials*

Sigma-Aldrich provided the chitosan biopolymer that was used (Figure 1). $K_2Cr_2O_7$, also sourced from Sigma Aldrich in the United States, was used to prepare the Cr(VI) feedstock. Only analytical reagent-grade chemicals and reagents were utilized in this investigation.

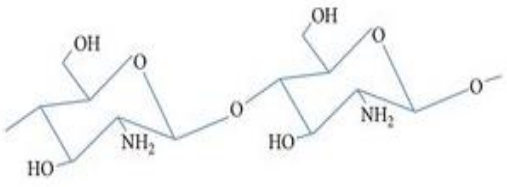

FIGURE 1. **Chitosan Cellular Structure**

B. *Preparation of Cr(VI) Stock Solution*

A 1000 mg/L Cr(VI) stock solution was prepared by dissolving 2 grams of analytical-grade $K_2Cr_2O_7$ in 2L of ionized water (Figure 2). The solution was subsequently diluted with deionized water to achieve the required concentration for the test sample. HCl and NaOH were added dropwise to adjust the pH as needed, depending on the acidity or basicity of the sample.

FIGURE 2. **Preparation of Cr(VI) Stock Solution**

C. *Methods*

Batch experiments (Figure 3) were conducted to optimize several adsorption parameters, including contact time (10–100 min), temperature (30–50°C), pH (4.5–8), sorbent dosage (5–50 mg), and initial metal concentration (5–30 mg/L). A 50 ml test sample of Cr(VI) solution with a pH ranging from 4.5 to 8 and initial concentrations between 10 and 50 mg/L was transferred to Erlenmeyer flasks containing the required amount of chitosan. The solution was agitated at 150 rpm for varying amounts of time at different temperatures in a thermostatic shaking water bath, using a UV spectrophotometer (Perkin Elmer, A 800). Chitosan's adsorption capacity (qe) was calculated using the following equation:

$$qe = \frac{C_i - C_{eq}}{D} \times V \quad (1)$$

Where:

C_i(mg/L): preliminary concentration
C_{eq}(mg/L): equilibrium Cr(VI) concentration
V(L): liquid feed of Cr(VI)
D (mg): chitosan dose (mg)

The removal percentage (Re) was determined using the following equation:

$$R_e\ (\%) = \frac{C_i - C_e}{C_i} \times 100 \quad (2)$$

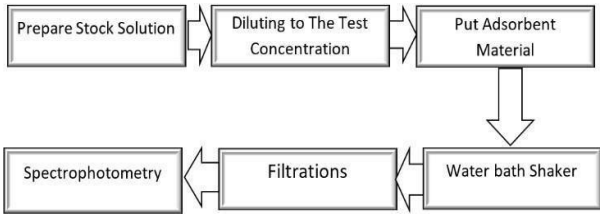

FIGURE 3. **Adsorption Process Methodology**

III. RESULTS AND DISCUSSION

A. *Adsorption Outcomes.*

1) *Impact of pH:*

The effect of pH on Cr(VI) removal efficiency was evaluated by varying the pH from 4.5 to 8 at 30°C, with a Cr(VI) concentration of 10 mg/L, 5 mg of adsorbent, and 30 minutes of contact time, as shown in Figure 4. The removal efficiency improved at pH levels between 4.5 to 6, indicating that more Cr(VI) ions were adsorbed onto the chitosan material as the pH increased. The maximum retention of Cr(VI) ions (51.23%) occurred at pH 6, demonstrating that chitosan had the highest affinity for Cr(VI) ions at this specific pH. Removal efficiency decreased at lower pH levels (below 6). This might be a result of competition between Cr(VI) ions and H^+ ions for the same adsorption sites [20]. Above pH 6, the removal efficiency declined, possibly due to the formation of negatively charged CrO_4^{2-} ions, leading to repulsion from deprotonated adsorbent surfaces and reduced

adsorption efficiency due to decreased electrostatic repulsion and potential precipitation of Cr(III) as $Cr(OH)_3$ [19].

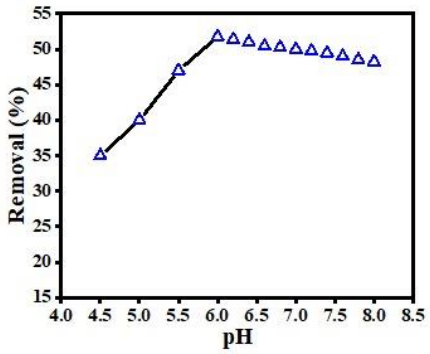

FIGURE 4. **Impact of pH (At 10 mg/L Cr(VI); 5mg;30 min; 150 rpm).**

2) Impact of Contact Time:

The duration required for chitosan to absorb the maximum Cr(VI) ions (10 mg/L) significantly depends on contact time. Longer contact times allow the adsorption process to reach completion. In our situation, the removal percentage decreased after 70 minutes, indicating that equilibrium had been reached, with a removal efficiency of 55.31% at the specified conditions (30°C, pH 6, and 5 mg adsorbent dose) (Figure 5). Initially, numerous active binding sites are accessible early on in the procedure, which causes adsorption to proceed quickly. However, as time progresses, the process slows as the metal ions occupy the active binding sites due to repulsive forces between Cr(VI) molecules [21]. Various kinetic approaches, including pseudo-first-order, pseudo-second-order, and Elovich models, were employed to better understand the adsorption procedure.

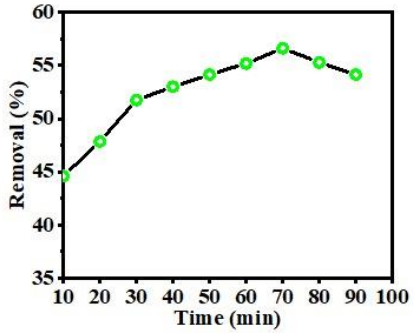

FIGURE 5. Impact of **Contact Time (30°C; 10 mg/L; pH 6; 5 mg; 150 rpm).**

The pseudo-first-order model is as follows [15,22]:

$$\log (q_e - q_t) = \log q_e - \frac{k_1}{2.303} t \quad (3)$$

The pseudo-second-order model is as follows [15, 23, 24]:

$$\frac{t}{q_t} = \frac{1}{k_2 q_e^2} + \frac{1}{q_e} t \quad (4)$$

Where K_1 and K_2 are kinetic model constants, and q_e and q_t represent the uptake capacities (mg/g) of Cr(VI) ions at optimum and at time t, respectively. Table 1 and Figure 6 indicate that the higher R^2 value demonstrates that the Cr(VI) uptake kinetics closely resemble the pseudo-first-order model (Figure 6a). Therefore, it was concluded that physical sorption is crucial to the adsorption of Cr(VI) [22].

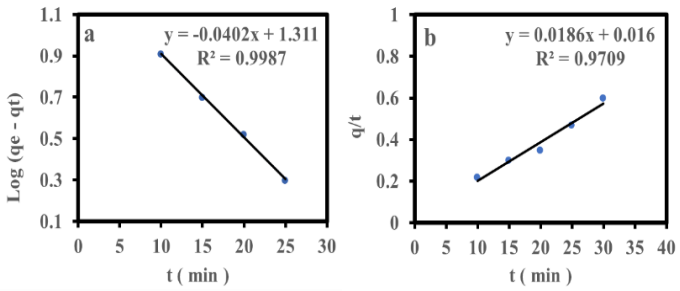

FIGURE 6. **Pseudo-first (a) and Pseudo-second (b) Order Model of the Uptake Process**

TABLE 1
ADSORPTION KINETIC MODEL CONSTANTS.

model	Parameter	Value
Pseudo-first-order	K_1 (1/min)	0.0925
	q_e (mg/g)	20.417
	R^2	0.9987
Pseudo-second-order	qe (mg/g)	44.247
	K_2 (g/mg.min)	4.9112
	R^2	0.9709

3) Impact of Initial Concentrations:

The effect of initial metal concentration on adsorption was studied within the concentration range of 5–30 mg/L, as shown in Figure 7. The adsorption uptake increased from 48.43% (24.21mg/g) to 55.57% (66.64 mg/g) as the Cr(VI) concentration rose from 5 to 15 mg/L, but decreased to 25.19% at higher concentrations. The initial removal percentage may have been influenced by the low availability of Cr(VI) ions on a number of the adsorption sites. At lower Cr(VI) concentrations, the chitosan surface has many active binding sites, allowing for efficient adsorption and achieving a maximum capacity of 66.64 mg/g. Conversely, at higher concentrations, although the adsorption capacity may increase, the removal percentage decreases due to saturation of the binding sites, resulting in a greater proportion of Cr(VI) remaining unadsorbed. These sites become saturated at higher Cr(VI) concentrations, reducing the removal efficiency. In other words, at lower concentrations, Cr(VI) ions interact more effectively with the active binding sites, leading to a higher removal percentage. The maximum adsorption capacity (66.64 mg/g) is achieved when all active binding sites are occupied [22]. The experimental results can be used to construct an adsorption isotherm. For this purpose, both the Freundlich and Langmuir isotherm models are commonly employed. These data are essential for designing

and enhancing adsorption techniques for water treatment, pollution control, and other environmental applications.

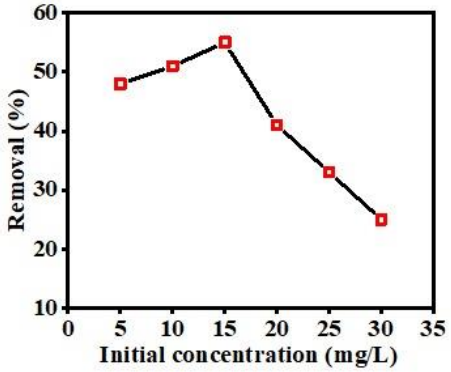

FIGURE 7. **Impact of Preliminary Cr(VI) Concentrations on the Uptake of Cr(VI) onto Chitosan (Conditions: pH 6; Adsorbent Dose 5 mg/50 mL; 70 min; Agitation Speed: 150 rpm).**

The Langmuir isotherm [24,15,26]:

$$C_e lq_e = \frac{1}{K_L Q_L} + \frac{C_e}{Q_L} \quad (5)$$

In this equation, the Langmuir constants K_L (L/mg) and Q_L (mg/g) are used.

The Freundlich isotherm [24,15,27]:

$$Logq_e = LogK_F + \frac{1}{n} LogC_e \quad (6)$$

K_F and n are Freundlich constants in this equation.

Table 2 displays the isotherm parameters derived from the Freundlich and Langmuir plots. The Langmuir isotherm is more suitable, as indicated by the higher regression coefficient (R^2) of approximatelyR^2 0.9981, as shown in Figure 8 (a). This suggests that Cr(VI) was adsorbed as a monolayer on the surface of chitosan [26].

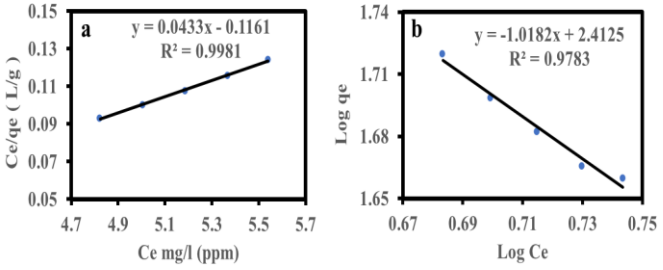

FIGURE 8. **Langmuir (a) and Freundlich (b) Isotherms of the Adsorption Process.**

TABLE 2
CONSTANTS OF THE ADSORPTION ISOTHERM

Langmuir			Freundlich		
k_L	Q_L	R^2	Kf	n	R^2
0.3729	23.094	0.9981	285.52	0.9821	0.9783

4) Effects of Chitosan Dosage:

The results of varying the chitosan dosage from 5 to 50 mg were tested. Figure 9 illustrates the effects of the chitosan dosage on adsorption. An increase in chitosan dosage resulted in a corresponding rise in the adsorption percentage. This is likely due to the increased number of adsorbent sites and a larger specific surface area with various functional groups, facilitating the entry of Cr(VI) ions into the adsorption sites more readily [23]. The highest adsorption of 63.51% was achieved at a dosage of 50 mg of chitosan.

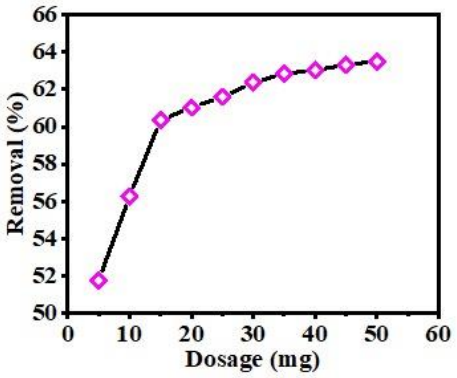

FIGURE 9. **Impact of Chitosan Dosage (At pH 6; Cr(VI) Concentration 10 mg/l;70 min; 150 rpm)**

B. *Thermodynamic Studies*

The effect of temperature on Cr(VI) ion adsorption was examined between 30 and 50°C under the following conditions: 70 min; Cr(VI) concentration: 10 mg/l; pH 6; dosage 5 mg; 150 rpm). The efficiency of Cr(VI) removal decreased as the temperature increased, indicating an exothermic process. This phenomenon can be attributed to thermodynamic factors, such as reduced spontaneity and weakened adsorbent-adsorbate interactions at higher temperatures. Increased kinetic energy and potential structural changes in the adsorbent may also hinder adsorption. Lower temperatures (around 30°C) are optimal for Cr(VI) removal, emphasizing the need for temperature control in industrial applications. The following equations were used to determine the parameters, including enthalpy (ΔH°), entropy (ΔS°), and Gibbs free energy (ΔG°), employing the distribution coefficient (K_D) [28].

$$\mathrm{Ln}K_D = \frac{\Delta S^\circ}{R} - \frac{\Delta H^\circ}{RT} \quad (7)$$

$$K_D = \frac{q}{Ce} \quad (8)$$

$$\Delta G^\circ = \Delta H^\circ - T\,\Delta S^\circ \quad (9)$$

The slope of the straight line created by plotting $\ln K_D$ vs. 1/T (Figure 10) was used to determine the values of ΔH° and ΔS°. The negative sign of ΔH° indicates the exothermic nature of the adsorption reaction [28]. The value of ΔH° provides insights into the type of adsorption. Physical and chemical adsorption are the two main types. Physical adsorption typically involves much lower heats of adsorption (between 2.1–20.9 kJ/mol) than chemisorption, which generally involves higher heats of adsorption (between 80 and 200 kJ/mol) [29]. The Cr(VI) uptake by chitosan is likely

a physio-sorption process with elements of both types, given that ΔH° has an absolute value of -15.617 kJ/mol (Table 3). The negative ΔG° indicates the spontaneous nature of the sorption process. When ΔG is negative, the process is thermodynamically favorable, meaning that no external energy is required for adsorption to occur naturally. A negative ΔS° suggests less unpredictable behavior at the solid/solution interface.

TABLE 3
THERMODYNAMIC CONSTRAINTS

ΔH° (kJ/mol)	ΔS° (kJ/mol.K)	ΔG°(kJ/mol)		
		Temperature(K)		
		303	313	323
-15.617	-0.0314	-6.1038	-5.7888	-5.4748

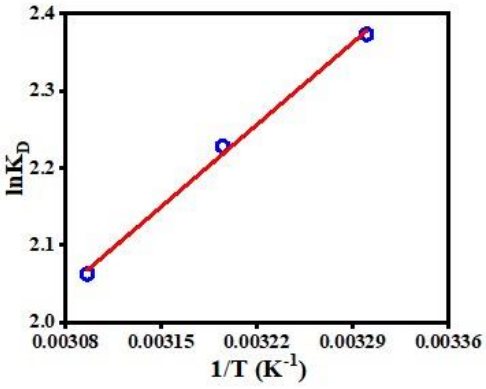

FIGURE 10. **LnK_D vs 1/T(K^{-1}) Van't Hoff plot.**

The change in energy represents the mean free energy (E) of adsorption caused by the movement of one molecule of Cr(VI) species from the fluid to the chitosan surface. The following equations provide insight into the interaction between Cr(VI) and the chitosan surface [30].

$$E = -RT\mathrm{Ln}K_D \qquad (10)$$

Where R = 8.314 J/(mol•K) and T = absolute temperature in Kelvin, respectively.

The decrease in E from 6.152 to 5.533 kJ/mol indicates a reduction in the energy barrier for Cr(VI) molecules to interact with the chitosan biopolymer surface, consistent with the exothermic nature of physical adsorption. This suggests weak, reversible interactions characteristic of van der Waals forces, where higher temperatures weaken the Cr(VI)-chitosan interactions, decreasing adsorption efficiency. This observation aligns with the exothermic nature of the process, as higher temperatures reduce the driving force for adsorption, favoring desorption instead.
The magnitude of the mean free energy can indicate the extent of interaction between Cr(VI) and the chitosan surface. The mean free energy values fluctuated with temperature, suggesting that the interactions between Cr(VI) and chitosan are temperature-dependent. Adsorption is classified as physical if E is less than 8 kJ/mol and chemical if E exceeds 8 kJ/mol [31,32]. As the temperature increased from 30°C to 50°C, E changed from 6.152 to 5.533 kJ/mol, respectively (Table 4). The physio-sorption of Cr(VI) by chitosan was confirmed by the results of the ΔH° value [33].

TABLE 4
FREE ENERGY (E) AT DIFFERENT TEMPERATURES.

Temperature °C	30	40	50
q (mg/g)	53.50	46.2	44.00
$\mathbf{K_D}$	11.50	8.58	7.85
E(KJ/mol)	-6.152	-5.593	-5.533

IV. CONCLUSION

This study demonstrates the effectiveness of the biopolymer chitosan as a biomass for the removal of Cr(V1) from liquid systems. The maximal binding capacity for Cr(VI) was found to be 66.64 mg/g. The monolayer binding of Cr(VI) to chitosan was well represented by the Langmuir model (R^2 = 0.9987). The results of the adsorption kinetics validated the pseudo-first-order model, highlighting the significance of the physical adsorption behavior. The thermodynamic analysis revealed the exothermic, feasible, and instantaneous character of the adsorption reaction. The findings suggest that unmodified chitosan is a highly effective, cost-efficient, and technically viable biosorbent for the removal of Cr(VI) from liquid media.

REFERENCES

[1] X. Zhang, M. Gao, L. Qiu, J. Sheng, W. Yang, Y. Yu, Sulfur vacancies-induced ‘‘Electron Bridge” in Ni4Mo/Sv-Zn Cd1-S regulates electron transfer for efficient H2-releasing photocatalysis, J. Energy Chem. 79 (2023) 64–71.

[2] X.-H. Yi, Y. Gao, C.-C. Wang, Y.-H. Li, H.-Y. Chu, P. Wang, Photocatalytic Cr(VI) reduction over MIL-88A(Fe) on polyurethane sponge: From batch to continuous-flow operation, Chin. Chem. Lett. 108029 (2022).

[3] K.J. Min, H.J. An, A.H. Lee, H.-G. Shin, K.Y. Park, Electrodialysis with a channeled stack for high strength cadmium removal from wastewater, Membr, Water Treat. 14 (2023) 47–54.

[4] C. Kim, S.S. Lee, A. Ghosh, J. Lee, J.D. Fortner, Cetyltrimethyl ammonium bromide – oleic acid (CTAB-OA) bilayer coated iron oxide nanocrystals for enhanced chromium (VI) photoreduction via ligand-to-metal charge transfer mechanism, Chem. Eng. J. 431 (2022) 133938.

[5] C.C. Wang, X. Ren, P. Wang, C. Chang, The state of the art review on photocatalytic Cr(VI) reduction over MOFs-based photocatalysts: from batch experiment to continuous operation, Chemosphere 303 (2022) 134949.

[6] Z. Shi, Z. Chen, Y. Zhang, X. Wang, T. Lu, Q. Wang, Z. Zhan, P. Zhang, COF TzDa/Ag/AgBr Z-scheme heterojunction photocatalyst for efficient visible light driven elimination of antibiotics tetracycline and heavy metal ion Cr(VI), Sep. Purif. Technol. 288 (2022) 120717.

[7] L. Li, H. Gao, G. Liu, S. Wang, Z. Yi, X. Wu, H. Yang, Synthesis of carnation flower-like $Bi_2O_2CO_3$ photocatalyst and its promising application for photoreduction of Cr(VI), Adv. Powder Technol. 33 (2022) 103481.

[8] S. Bao, W. Yang, Y. Wang, Y. Yu, Y. Sun, K. Li, PEI grafted amino-functionalized graphene oxide nanosheets for ultrafast and high selectivity removal of Cr(VI) from aqueous solutions by adsorption combined with reduction: behaviors and mechanisms, Chem. Eng. J. 399 (2020) 125762.

[9] C.-C. Wang, X.-D. Du, J. Li, X.-X. Guo, P. Wang, J. Zhang, Photocatalytic Cr(VI) reduction in metal-organic frameworks: a mini-review, Appl. Catal. B: Environ. 193 (2016) 198–216.

[10] Q. Zhao, X.-H. Yi, C.-C. Wang, P. Wang, W. Zheng, Photocatalytic Cr(VI) reduction over MIL-101(Fe)–NH_2 immobilized on alumina substrate: from batch test to continuous operation, Chem. Eng. J. 429 (2022) 132497.

[11] X. Ren, M. Li, L. Qiu, X. Guo, F. Tian, G. Han, W. Yang, Y. Yu, Cationic vacancies and interface engineering on crystalline– amorphous gamma-phase Ni–Co oxyhydroxides achieve ultrahigh mass/areal/volumetric energy density flexible all-solid-state asymmetric super capacitor, J. Mater. Chem. A 11 (2023) 5754–5765.

[12] S. Karthick, R. Palani, D. Sivakumar, N. Meyyappan, Biosorption of Cr(VI) ions by Ficus religiosa barks: batch and continuous study, Memb. Water Treat. 13 (2022) 209–217.

[13] P. Li, J.T. Damron, G.M. Veith, V.S. Bryant Barakatsev, S.M. Mahurin, I. Popovs, S. Jansone-Popova, Bifunctional ionic covalent organic networks for enhanced simultaneous removal of chromium(VI) and arsenic(V) oxoanions via synergetic ion exchange and redox process, Small 17 (2021) e2104703.

[14] Z.Q. Huang, W. Cai, Z. Zhang, Modification and acidification of polysulfone as effective strategies to enhance adsorptive ability of chromium(VI) and separation properties of ultrafiltration membrane, J. Appl. Polym. Sci. 139 (2022) 52127.

[15] Yogita Patil, Sanjay Attarde,, Umesh, Fegade,, Omer Y. Bakather, Syed Kashif Ali, Highly efficient removal of a toxic methylene blue dye by adsorption on CuAlMnO nanoparticles: adsorption kinetics, isotherm, and mechanism studies using statistical modelling, International Journal of Environmental Analytical Chemistry, Taylor & Francis, (2023), 1-18.

[15] C. Wang, G. Yang, W. Shi, K. Matras-Postolek, P. Yang, Construction of 2D/2D MoS_2/g-C3N4 heterostructures for photoreduction of Cr(VI), Langmuir 37 (2021) 6337–6346.

[16] A. Raja, P. Rajasekaran, B. Vishnu, K. Selvakumar, J. Yeon Do, M. Swaminathan, M. Kang, Fabrication of effective visible light-driven ternary Z-scheme ZnO-Ag-$BiVO_4$ hetero structured photocatalyst for hexavalent chromium reduction, Sep. Purif. Technol. 252 (2020) 117446.

[17] A. Shawky, N. Alahmadi, R.M. Mohamed, Z.I. Zaki, Bi_2S_3- sensitized TiO2 nanostructures prepared by solution process for highly efficient photoreduction of hexavalent chromium ions in water under visible light, Opt. Mater. 124 (2022) 111964.

[18] Y.H. Li, X.H. Yi, Y.X. Li, C.C. Wang, P. Wang, C. Zhao, W. Zheng, Robust Cr(VI) reduction over hydroxyl modified UiO-66 photocatalyst constructed from mixed ligands: Performances and mechanism insight with or without tartaric acid, Environ. Res. 201 (2021) 111596.

[19] J. Rashid, M. A. Barakat, and M.A. Alghamdi, Adsorption of Chromium (VI) from Wastewater by Anion Exchange Resin, Journal of Advanced Catalysis Science and Technology (2014) 1 26-34.

[20] N. Alias, Z. Hussain, W.K. Tan, G. Kawamura, H. Muto, A. Matsuda, Z. Lockman, Nanoporous anodic Nb_2O_5 with pore in-pore structure formation and its application for the photoreduction of Cr(VI), Chemosphere 283 (2021) 131231.

[21] B.A. Marinho, R.O. Cristo´va˜o, R. Djellabi, J.M. Loureiro, R.A. R. Boaventura, V.J.P. Vilar, Photocatalytic reduction of Cr(VI) over TiO_2-coated cellulose acetate monolithic structures using solar light, Appl. Catal. B: Environ. 203 (2017) 18–30.

[23] M.-H. Li, Y.-M. Di, Y.-W. Wang, M.-H. You, M.-J. Lin, In-situ construction of novel naphthalenediimide/metal-iodide hybrid heterostructures for enhanced photoreduction of Cr(VI), Dyes Pigm. 187 (2021) 109146.

[24] Mohamed A. Mahmoud, Kinetics and thermodynamics of aluminum oxide nanopowder as adsorbent for Fe (III) from aqueous solution, Beni-Suef University Journal of Basic and Applied Sciences, 4, 2, (2015), 142-149.

[25] Shazneen Chowdhury, Md Elias Uddin, Md Ashikur Rahaman Noyon , Md Mahmudul Hassan Mondol, Ibrahim M. Maafa, Ayman Yousef, Fabrication and performance analysis of keratin based-graphene oxide nanocomposite to remove dye from tannery wastewater, Heliyon 10 (2024) e23421.

[26] S. Luo, S. Li, S. Zhang, Z. Cheng, T.T. Nguyen, M. Guo, Visible-light-driven Z-scheme protonated g-C3N4/wood flour biochar/$BiVO_4$ photocatalyst with biochar as charge-transfer channel for enhanced RhB degradation and Cr(VI) reduction, Sci. Total Environ. 806 (2022) 150662.

[27] S. Jana, S. Pramanik, B. Show, A. Mondal, S. Mukhopadhyay, A new strategy to fabricate SnS-SnO_2

heterostructure with excellent photoresponse and charge transport properties: efficient photocatalyst for fast photoreduction of Cr(VI), Mater. Sci. Engi. B 275 (2022) 115520.
[28] Y. Pang, J. Wang, Various electron donors for biological nitrate removal: a review, Sci. Total Environ. 794 (2021) 148699.
[29] H. Shen, F. Fu, W. Xue, X. Yang, S. Ajmal, Y. Zhen, L. Guo, D. Wang, R. Chi, In situ fabrication of Bi_2MoO_6/Bi_2MoO_6-x homojunction photocatalyst for simultaneous photocatalytic phenol degradation and Cr(VI) reduction, J. Colloid. Interface Sci. 599 (2021) 741–751.
[30] A. El Barnossi, A.I. Housseini, Physico-chemical characterization of decomposing banana, pomegranate and mandarin peels in water and soil for a sustainable valorization, Ind. Crop. Prod. 193 (2023) 116207.
[31] A. El Barnossi, F. Moussaid, A. Iraqi Housseini, Tangerine, banana and pomegranate peels valorisation for sustainable environment: a review, Biotechnol. Rep. 29 (2021) e00574.
[32] J. Gu, Y. Dong, J. Zhang, Comparative study of four different flavonoid compounds-containing plant extracts functionalized waste wool for accelerating aqueous chromium(VI) reductive removal, Color. Technol. 138 (2021) 97–113.
[33] F. Bahador, R. Foroutan, H. Esmaeili, B. Ramavandi, Enhancement of the chromium removal behavior of Moringa oleifera activated carbon by chitosan and iron oxide nanoparticles from water, Carbohydr. Polym. 251 (2021) 117085.

Date of publication: April 24, 2025

Establishing a Comprehensive Spatial Data Framework to Support Road Design and Maintenance Activities Using GIS and Open Source Data

Mahmoud Abdelrahim Abdelgiom[1*]

[1]Assistant Professor, Civil and Architectural Engineering Department, College of Engineering and Computer Sciences, Jazan University, Jazan,45142, Saudi Arabia

* Corresponding author: Mahmoud Abdelrahim Abdelgiom (e-mails: mabdelmahmoud@jazanu.edu.sa.or mahmoudabdelgiom@gmail.com)

ABSTRACT This study aims to establish a Comprehensive Spatial Data Framework (CSDF) utilizing GIS and road design software to enhance road design activities in Jazan City, aligning with the Kingdom's Vision 2030. The CSDF consists of soil tests, road design, and cost estimation. AutoCAD Civil 3D is employed for road geometric design in accordance with the American Association of State Highway and Transportation Officials (AASHTO) standards and the Saudi code. The CSDF model for the Jazan road network is developed using ArcGIS 10.4. This study focuses on the Alshawajra Road, which connects University Road with Alshawajra Road. The road spans 1000 meters in length and is 28 meters wide. The methodology outlined in this paper consists of four sections: the first discusses the literature review and road design principles; the second emphasizes the survey data required; the third addresses soil collection for testing, including California Bearing Ratio (CBR), Standard Proctor, and sieve analysis. The final section covers the design of the road network and the creation of a geodatabase. The findings indicate that the third version of the proposed design is the most effective, with the total construction cost amounting to 1,233,706.17 Saudi Riyals. Additionally, the CSDF model for Jazan city roads was established, which is vital for the simplicity of data recording and updating, serving as a reference for infrastructure planning and maintenance.

INDEX TERMS Comprehensive Spatial Data Framework (CSDF), Geometric Design, Pavement Design, Geographic Information Systems (GIS), Building Geo-database, Soil Tests.

I. INTRODUCTION

A. COMPREHENSIVE SPATIAL DATA FRAMEWORK TO SUPPORT ROAD DESIGN ACTIVITIES

The primary objective of this study is to create a Comprehensive Spatial Data Framework (CSDF) to assist in the road design and maintenance efforts of Jazan City. Establishing a robust spatial data foundation for road design is essential for improving urban infrastructure and planning in Jazan City. By utilizing GIS and advanced analytical techniques, urban planners can make better judgments that enhance road safety, efficiency, and sustainability. The ongoing trend of urbanization presents unprecedented challenges for highway construction[1-2]. Constructing roads and vital connections between cities requires navigating complex terrains, coordinating various transportation modes, and managing significant land. [3].Traditional project management approaches often exacerbate coordination issues in planning, design, and construction, leading to excessive costs, information silos, and communication barriers. It is noteworthy that most existing roadway infrastructure is documented in 2D drawings, lacking 3D interactivity and advanced analytical tools, which leads to fragmented data and ineffective communication [4]. Therefore, establishing a comprehensive spatial data framework for road design and maintenance using GIS and open-source data is a critical area of research. Several studies have contributed valuable insights into how GIS technologies can enhance road infrastructure management. One notable study developed a comprehensive framework for highway maintenance planning using GIS.

This research demonstrated that spatial data visualization significantly aids decision-making processes, enabling planners to identify maintenance needs and prioritize projects effectively [5].

Another investigation integrated GIS with machine learning algorithms to optimize road maintenance strategies, highlighting the potential of combining spatial data with predictive analytics to assess road conditions and allocate resources more efficiently, ultimately improving maintenance outcomes [6]. Additionally, research by Martinez et al. (2019) [7]examined the use of open-source GIS tools for asset management in road networks, illustrating how these tools facilitate data collection and analysis, enabling better tracking of road conditions and maintenance activities. This approach supports the establishment of a more responsive and adaptive maintenance framework. Furthermore, a study conducted by Chen et al. (2022) [8] explored the application of GIS in sustainable road design, emphasizing the importance of integrating environmental considerations into road planning and maintenance. These studies collectively underscore the critical role of GIS and open-source data in developing effective frameworks for road design and maintenance, offering valuable methodologies and insights for future research and practice.

B. GEOMETRIC DESIGN AND STRUCTURAL DESIGN OF ROADS

The geometric elements of roadway design are essential for assessing traffic operational efficiency [9]. Key components of geometric design that influence traffic operations include the number and width of lanes, the presence and dimensions of shoulders and medians, as well as the horizontal and vertical alignment of the highway. Most drivers are able to travel safely at their preferred speed throughout the alignment when there is consistency in alignment. However, while the current design speed-based alignment standards allow for this, most drivers' desired speeds can vary [9]. The goal of road design is to 8. construct a safe and efficient roadway that meets the demands of its users [10,11]. Road design involves planning and laying out the physical aspects of a road, including its Width, alignment, curvature, and grade [12]. Premature road failures, manifesting as cracks, surface wear, and irreversible deformations, are common issues with flexible pavements [13]. The
main causes of these failures in asphalt concrete mixtures include increasing traffic volumes, heavy vehicle loads, high tire pressures, rising temperatures, and the use of poor-quality materials and inappropriate asphalt mix designs [14].

C. BUILDING A GEO-DATABASE OF DESCRIPTIVE DATA ABOUT JAZAN ROADS NETWORK USING ARCGIS 10.4

The geodatabase is a fundamental component of GIS. Geodatabases are typically organized using broad data types, such as land base, transportation, environment, and utility infrastructure. They utilize effective spatial indexing to continuously record an extent. Personal geodatabase datasets can represent small and medium-sized enterprises [15]. Users can dynamically model realistic network conditions, such as turn restrictions, speed limits, height restrictions, and traffic conditions at different times of the day using ArcGIS 10.4 Network Analyst [16]. ArcGIS 10.4 has proven to be one of the most efficient, productive, and time-saving tools for transportation planning and traffic engineering[17].
This study outlines the steps taken to build a geo-database of Jazan roads:

a) Choose the GIS program: ArcGIS 10.4 and QGIS 3.24.2;
b) Create a spatial database that efficiently manages and arranges the data;
c) Design the database to ensure easy access, analysis, and visualization of road information;
d) Transform collected data into common GIS-compatible formats (such shape files);
e) Integrate various information (such as environmental factors, land use, and transportation statistics) into a single GIS database; and
f) Update the Road Spatial Data Framework monthly and annually to meet the emergency tasks of the Jazan road network.

D. INTELLIGENT TRANSPORTATION SYSTEMS (ITS) AND GEOGRAPHIC INFORMATION SYSTEMS (GIS)

The intersection of Intelligent Transportation Systems (ITS) and Geographic Information Systems (GIS) represents a specialized area of research and application aimed at optimizing transportation networks through the use of spatial data and technology. This study focuses on the specializations of ITS within the CSDF using GIS and open-source data. These specializations include:

☒ **Traffic Monitoring and Control**

This area applies GIS to track and analyze traffic behavior, leveraging spatial data to understand congestion trends. Real-time monitoring facilitates adaptive traffic control measures that enhance flow and reduce delays.

☒ **Route Planning and Navigation**

GIS tools play a vital role in planning optimal routes by analyzing geographical features and current traffic conditions, enhancing navigation systems to be more responsive to real-time changes.

☒ **Smart Transportation Systems**

The integration of GIS in smart transportation initiatives enables real-time data sharing between vehicles and infrastructure, enhancing overall system responsiveness and efficiency.

☒ **Safety Analysis**

The application of GIS in analyzing accident data helps

information is crucial for developing targeted safety measures and interventions [18,19].

The primary objective of this paper is to integrate soil laboratory testing, manual design, AutoCAD Civil 3D, road geometric design, pavement design, traffic studies, cost estimation, and geodatabase establishment in Jazan City, in accordance with the requirements of the American Association of State Highway and Transportation Officials (AASHTO). Additionally, this model is utilized for maintenance. The secondary objectives are as follows: to employ engineering concepts to create a road that is both safe and efficient; to consider environmental factors in road design;

a. To establish a Comprehensive Spatial Data Framework (CSDF)was established to support road design and the geodatabase model for routine maintenance using GIS and open-source data.
b. To identify and engage relevant parties such as municipal authorities, transportation planners, civil engineers, and local communities, to gather source software (AutoCAD civil 3D);
c. To compare volume calculation methods;
d. To calculate the cost estimation of earthwork and pavement volumes;
e. To integrate the Comprehensive Spatial Data Framework (CSDF)and open source data within a Geographic Information System (GIS) environment to support road design and traffic analysis of the study area;
f. To propose Intelligent Transportation Systems (ITS) to improve traffic management.

II. MATERIALS AND METHODS

The methodology is described in the following steps:

A.THE FIELD OF STUDY

Figure 1 below illustrates the location of the study area. Jazan Road, which connects University Road and Alshawajrah Road, was selected as the route for the case study. The road is one kilometer long, twenty-eight meters wide, and has an average elevation of 9.799 meters above mean sea level (Jazan datum).

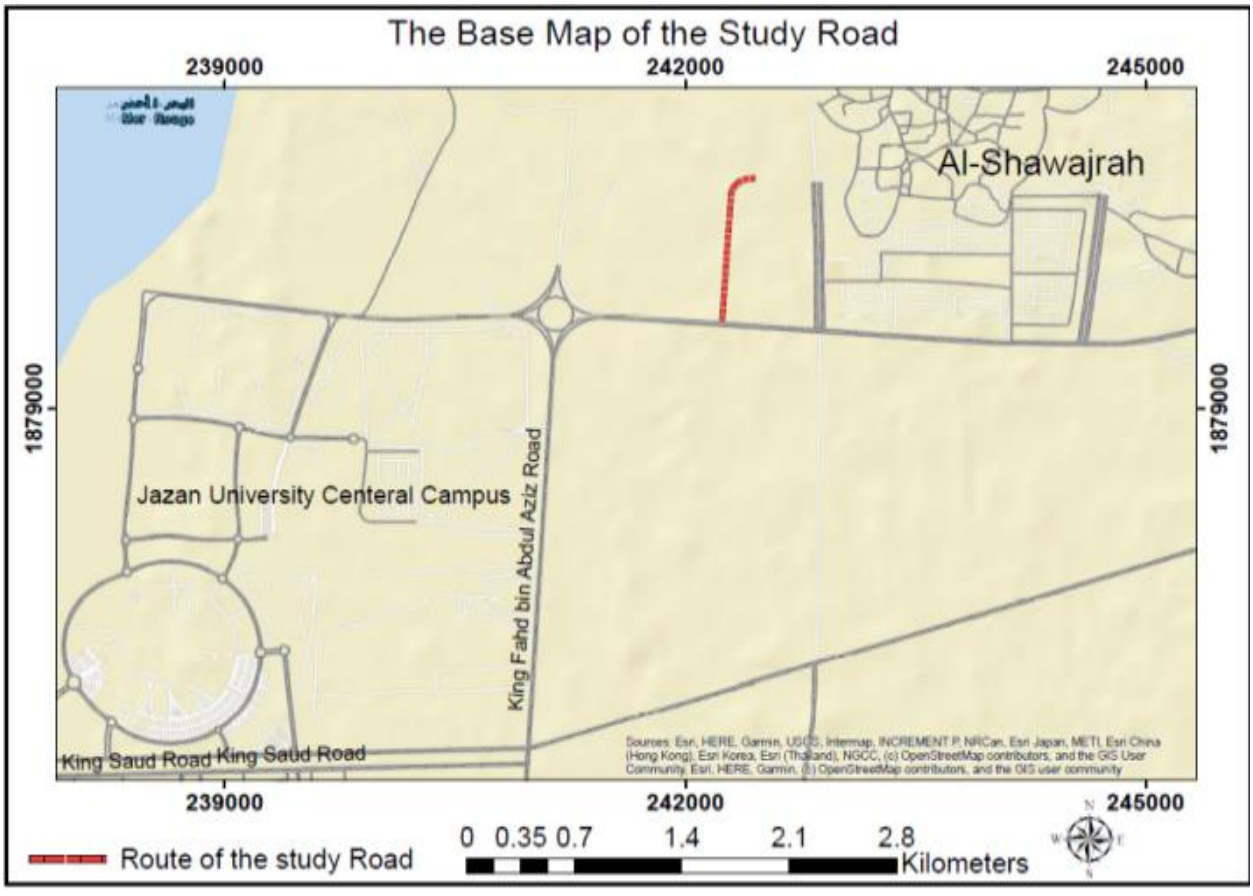

FIGURE 1. The base map of the study road

B.PAPER METHODOLOGY

Building a comprehensive road spatial data framework in Jazan City, Saudi Arabia, requires a series of systematic steps that utilize GIS and open-source data. This framework is essential for effective road design and maintenance activities. To meet these requirements, this study employed a different methodology. The main steps of the process are highlighted in **Figure 2.**

- Identify Goals and Stakeholders;
- Establish the Comprehensive Spatial Data Framework (CSDF) for the Jazan City road network;
- Focus on improving road design efficiency;
- Select the methods and techniques applied, including the study area, codes, and design and maintenance software;
- Gather data for road design and maintenance, including coordinates of the road centerline, cross-section using Topcon total station, soil data samples, traffic data, and attribute data for modeling the road network database;
- Execute the structural and geometric design using manual calculations and AutoCAD Civil 3D;
- Complete the analysis for road design and model the Jazan roads geodatabase;
- Link GIS data with engineering design software (e.g., AutoCAD, Civil 3D) to streamline the design process;
- Create the asphalt road earthwork cost estimate.

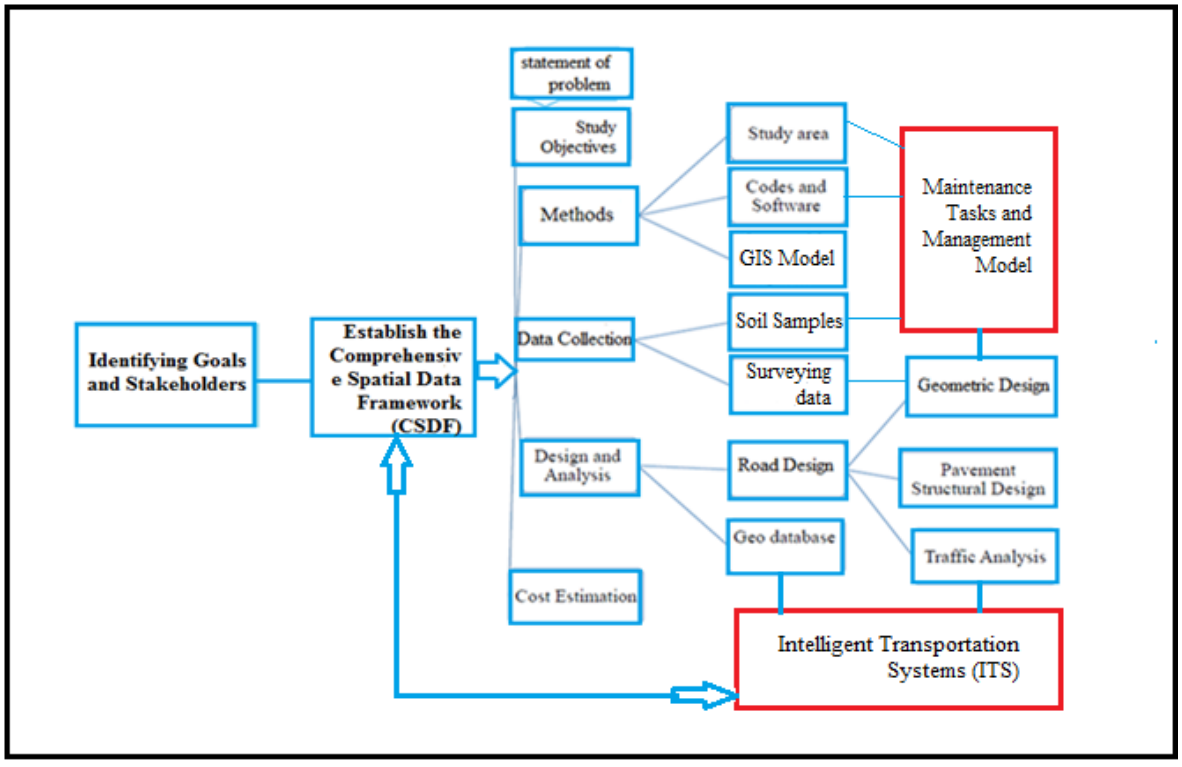

FIGURE2.Flow chart of methodology.

C. *DATA COLLECTION AND METHODS OF PROCESSING AND CALCULATIONS*

This section outlines the location data collected for the project, which was conducted on King Abdullah University Road and Alshawajrah Road, connected by this road. The information consists of several sections:

- Gathering detailed surveying data from the road site using Total Station Topcon version 7500;
- Collecting traffic data;
- Capturing Jazan roads; and
- Gathering soil samples.

1) COLLECTING DETAILED SURVEYING DATA

The 3D coordinates from surveys conducted in the field or study area of the road were collected from a baseline with known coordinates using Total Station Topcon 7500 (Table **1** shows the specifications). Moreover, survey data was collected systematically for 7. the road's geometric design, providing elevation, easting, and northing coordinates of the observed sites. These details were subsequently imported into AutoCAD Civil 3D[20].

TABLE 1
SPECIFICATIONS OF THE TOPCON GT-7500 TOTAL STATION

Items	Distance measuring Accuracy	Angle measurement accuracy	Slope distance measuring accuracy	Measuring range
accuracy	± (2 mm + 2 ppm of distance)	Horizontal Angle: ± 2" (seconds) Vertical Angle: ± 2" (seconds)	Typically ± (2 mm + 2 ppm)	With prism up to 5,000 m

In the study area (the road), 269 locations with coordinates (Easting, Northing, and Elevation) were observed using the Topcon total station from base line. The accuracy of horizontal and vertical coordinates, after checking the backsight, equals (delta E = -0.003 m, delta N =-0.002 m, and delta elevation = +0.001 m). The local datum of the collected coordinates is (Ain_el_Abd_UTM_Zone_38N). **Table 2** and **Figure 3** show the statistical summary of the detailed surveying data include the minimum, maximum, mean, and standard deviation of Easting, Northing, and height, respectively.

TABLE 2
STATISTICS OF THE ROAD SURVEY DATA COLLECTION

Statistic Expression	Easting (in meters)	Northing (in meters)	Elevations (in meters)
Minimum	**242128.268**	**1879575.569**	**7.795**
Maximum	**242407.040**	**1880501.975**	**11.132**
Mean:	**242214.788**	**1880030.400**	**9.799**
Standard Deviation:	**59.295**	**299.777**	**0.844**

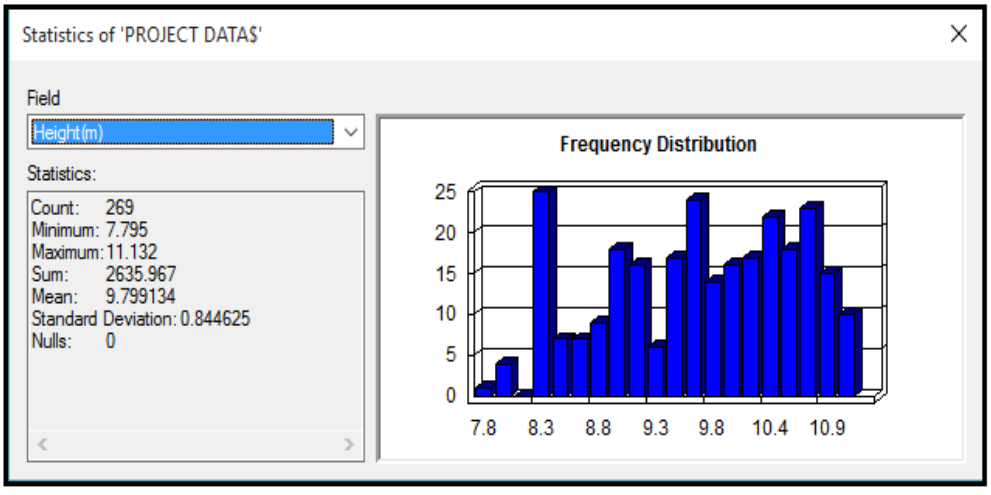

FIGURE 3. Statistics of the road's height data.

2) TRAFFIC DATA

Traffic data collection is a valuable tool that provides essential information for managing traffic and improving infrastructure. When processed in real-time, traffic data can enhance traffic flow, identify existing congestion points, and regulate urban density [21, 22]. There are various methods for gathering traffic data, including manual vehicle counts, passive and active infrared, passive magnetic, microwave radar, both passive and ultrasonic acoustics, and video image detection. In this investigation, the manual approach was employed.

3) DESCRIPTIVE DATA OF JAZAN ROADS

Before selecting a data collection approach, it is crucial to 6. determine the type of data required for the project [23]. The study area comprises 10,660 local roads, including the main thoroughfares that connect the Jazan region in four directions and pass through the neighborhoods of Jazan City. These roads also link the scheme roads both inside and outside the main thoroughfares. The most important components of the road description include the road number, length, width, direction, number of lanes, current condition of the road, and other relevant descriptive road data.

4) GATHERING SOIL SAMPLES

Soil samples were collected from the road site for this investigation and organized according to laboratory test specifications [24, 25]. Three soil samples were taken from the study road and distributed along its length. All samples were mixed in the lab before conducting tests. The following laboratory tests were performed on the road soil:

a. Particle Size Distribution (Sieve Analysis);
b. The Standard Proctor Test for compaction; and
c. California Bearing Ratio (CBR).

a. Sieve Analysis

Sieve analysis is used to weigh and allow granular materials to pass through a series of sieves with progressively smaller mesh sizes in geology, chemical engineering, and civil engineering to ascertain the material's particle size distribution or gradation. For soil particles larger than 75 microns, both dry and wet sieve examinations are conducted to quantitatively analyze the particle/grain size distribution. If the soil particles have a silt or clay coating, wet sieve analysis is also necessary. For soil particles larger than 4.75 mm and less than 75 microns, dry sieve analysis is used [26]. The following formulas are used to determine the percentages of passing and retained:

$$\text{IPR} = \frac{\text{IMR}}{\text{M}} * 100 \quad (1)$$

$$\text{PP} = \text{PCP} - \text{IPR} \quad (2)$$

$$\text{PP} = 100 - \text{CPR} \quad (3)$$

$$\text{RPP} = \text{PP} + \text{Aggregatecorrectionfactor} \quad (4)$$

Where:

IPR: Individual Percent Retained, CPR: Cumulative Percent Retained, M: Total Dry Sample mass before washing, IMR: Individual Mass Retained, CMR: Cumulative Mass Retained, PP: Calculated Percent Passing, PCP: Previously Calculated Percent Passing, and RPP: Reported Percent Passing.

b. The Standard Proctor test

The Proctor compaction test involves compacting soil samples at a predetermined water content using a standard compaction energy in a traditional mold. Compaction tests, also known as soil compaction tests, are used to determine the density and moisture content of soil, which is critical for building projects and roadways [27–29]. The following formulas are used to calculate the compaction test:

$$\gamma = \frac{w_2 - w_1}{Volumeofmold} (5)$$

$$\gamma_{dry} = \frac{\gamma}{1+\frac{w\%}{100}} (6)$$

$$w\% = \frac{weightofmoist}{dryweightofsoil} * 100 = \frac{w(can+wetsoil)-w(can+drysoil)}{w(can+drysoil)-w(can)} \quad (7)$$

$$\gamma zeroairvoid = \frac{\gamma water}{\frac{w\%}{100}+\frac{1}{Gs}} (8)$$

$$\text{Pavement Layer of mold} = \frac{\pi D^2}{4} * H = \frac{\pi 9.98^2}{4} * 12.75 = 997.381\ cm (9)$$

Where:

$\gamma: moist\ unit\ weight$, $\gamma_{dry}: dry\ unit\ weight$, w_1= weight of mold+ base plate, w_1: weight of mold + base plate + compacted moist soil in the mold, and $w\%$ moisture content(M.C).

c. California Bearing Ratio (CBR)

The California Bearing Ratio (CBR) is the percentage difference between the force required to move a standard circular piston through a mass of soil at a rate of 1.25 mm/min to a specific depth and the force required to achieve the same with a standard material. The CBR test is used to evaluate the mechanical strength and load-bearing capacity of highway sub-bases and sub-grades.CBR testing is rarely conducted as part of routine site investigations. The conversion of penetration findings to CBR values is made possible by calibration charts. Subsequently, we estimate the sub-grade surface modulus using the equation derived from CBR [30-32].

The calculation methods for CBR include the following equations:

$$\rho = \frac{m_3 - m_2}{V_m} (10)$$

$$\rho_d = \left(\frac{100}{100+w}\right)\rho \quad (11)$$

$$\rho_{ds} = \left(\frac{\rho_d}{1+\frac{A_x}{1000V_m}}\right) \quad (12)$$

Where:
m_3: The mass of soil, mold, and base plate (in g.),m_2: The mass of mold and base plate (in g.), V_m: The volume of mould (in cm^3), ρ_d: initial dry density(in kg/m^3), ρ_{ds} : The dry density (in Mg/m^3), w: the moisture content of soil (in %), A: the area of cross-section of the mold (in mm^2), x: the increase in sample height after swelling (in mm).

5. Geometric Design Using AutoCAD Civil 3D

A road that is designed and developed in accordance with regulations is deemed safe [33–36]. The following design criteria were applied to the profile, cross-section, and horizontal centerline geometry of the study road in Jazan, in accordance with AASHTO specifications, ensuring safety measures at a reasonable cost. The following criteria were used in the design of the study road:

a. The maximum super elevation rate is 4%;
b. The design speed is 100 km/h;
c. Radius of Curve: 490 m
d. Deflection angles: 3.5 degree;
e. The coefficient of friction is 0.15;
f. The minimum K for sag curves is 33 m;
g. The road's width is 20 meters;
h. For crest curves, the minimum K is 17 m; and
i. No shoulder(urban road) [37-41]. **Table 3** shows the values of the design parameters for simple curve.

The design steps in AutoCAD Civil 3D include the following:

a. Import a text format point file (Easting, Northing, and elevation) of the proposed road in Jazan City into the AutoCAD Civil 3D environment;
b. Use the alignment creation tool to create alignment (Figure 3);
c. Determine the super elevation based on the provided alignment;
d. Establish a surface and contour map for road drainage
e. system purposes (see **Figure 4**);
f. Design the existing profile of the surface and create a grade line and vertical curves (crest and sag) as highlighted in **Figure 5**;
g. Determine the thicknesses of the road layers according the requirement of design(see **Figure 6);**
h. Construct the assembly (a typical cross-section) as shown in Figure 7;
i. Construct a 3D model depiction of a corridor using a mix of horizontal, vertical, and cross-sectional features. Corridors are used to find data for construction projects, analyze sight distances, and compute the amount of earthwork needed;
j. Create a report with a volume table;
k. Create three road iterations, compare them, and select the alignment that minimizes fill volumes by adjusting the vertical alignment (crest) parameters. The calculations of crest vertical curve design parameters used in three iterations are displayed in Table 4, and Table 5 shows the vertical design parameters used in three iterations of the sag curve.

TABLE 3
VALUES OF THE SIMPLE CIRCULAR CURVE'S DESIGN PARAMETERS

Name of Curve Item	Calculated Value
Tangent (T)	46.46 m
Long Chord (L)	92.612 m
External Distance (E)	2.39 m
Middle Ordinate Distance (M)	2.37 m
Length of Circular Curve (L.C.C)	92.619 m
Degree of Curve (D)	3.88 degrees

TABLE 4
CREST VERTICAL CURVE DESIGN PARAMETERS USED IN THREE ITERATIONS

Name of Vertical Curve Item curve	Initial Grade (g_1%)	Final Grade (g_2%)	Road Elements and Formula	Design Value	Note
FCC – Algebraic difference between the two tangent grades A%(A%)	+1	-3.5	(A%) = (g2%) - (g1%) (13)	-4.5%	It.1
FCC- SSD			$\boldsymbol{SSD} = \frac{\boldsymbol{v*t}}{\boldsymbol{3.6}} + \frac{\boldsymbol{v^2}}{\boldsymbol{254*(f \pm g)}}$(m)(14)	190.233 m	It.1
L FCC (16)			$\frac{\boldsymbol{A*SSD^2}}{\boldsymbol{200(\sqrt{h1}+\sqrt{h2})^2}}$ (15)	247.490 m	It.1_SSD <L FCC (Okay, is used for design)
L FCC			$\boldsymbol{2 * SSD - \frac{200(\sqrt{h1}+\sqrt{h2})^2}{A}}$ $(\boldsymbol{m})$ (16)	234.254 m	It.1_SSD > L FCC (Not Okay)
SCC – Grade Angle (A%)	+1	-2.5	(A%)	-3.5%-3.5%	It.2
SCC - SSD (m)SCC - SSD (m)SCC - SSD (m)			$\boldsymbol{SSD}(\mathbf{m})$	184.831 m	It.2
L SCC (m)			$\frac{\boldsymbol{A * SSD^2}}{\boldsymbol{200\left(\sqrt{h1}+\sqrt{h2}\right)^2}}$	181.715 m	It.2_SSD <L SCC (Not Okay)
L SCC			$\boldsymbol{2 * SSD - \frac{200(\sqrt{h1}+\sqrt{h2})^2}{A}}$(m)	181.663 m	It.2_SSD > L SCC (Okay, is used for design)
THCC – Grade Angle (A%)	+2	-1	(A%)	-2.5%-2.5%	It.3
SCC- SSD			$\boldsymbol{SSD}$(m)	182.274 m	It.3
L THCC (m)			$\frac{\boldsymbol{A*SSD^2}}{\boldsymbol{200(\sqrt{h1}+\sqrt{h2})^2}}$(m)	151.478 m	It.2_SSD <L THCC (Not Okay)
L THCC			$\boldsymbol{2 * SSD - \frac{200(\sqrt{h1}+\sqrt{h2})^2}{A}}(\mathbf{m})$	145.216 m	It.2_SSD > L THCC (Okay, used for design)

TABLE 5
SAG VERTICAL CURVE DESIGN PARAMETERS USED IN THREE ITERATIONS (SCENARIOS)

Name of Vertical Curve Item	Initial Grade (g_1%)	Final Grade (g_2%)	Road Elements and Formula (m)	Design Value	Note
FCC – Algebraic difference between the two tangent grades(A %)	-3.5	+1	A%	+4.5%	It.1
FSC - SSD (m)			$\boldsymbol{SSD} = \frac{v*t}{3.6} + \frac{v^2}{254*(f \pm g)}$(m)	190.233 m	It.1
L FSC (m) (17)			$\frac{A*SSD\text{^}2}{200(h1+SSD*tan\beta)}$(m) (17)	207.687 m	It.1_SSD <L FSC (Okay, is used for design)
L FSC			2*SSD -$\frac{200(h1+SSD.tan.\beta)}{A}$(m) (18)	338.828 m	It.1_SSD > L FSC (Not Okay)
SSC – Grade Angle (A%)	-2.5	+1	A%	-3.5 %	It.2
SSC - SSD (m)			$\boldsymbol{SSD}$(m)	184.831 m	It.2
L SSC (m)			$\frac{A*SSD^2}{200(\sqrt{h1}+\sqrt{h2})^2}$(m)	156.248 m	It.2_SSD< L SCC (Not Okay)
L SSC			$\boldsymbol{2 * SSD - \frac{200(\sqrt{h1}+\sqrt{h2})^2}{A}}$(m)	151.020 m	It.2_SSD> L SCC (Okay, is used for design)
THSC – Grade Angle (A%)	-1	+2	A%	-2.5 %	It.3
SCC- SSD			$\boldsymbol{SSD}$(m)	182.274 m	It.3
L THSC (m)			$\boldsymbol{\frac{A * SSD^2}{200(\sqrt{h1}+\sqrt{h2})^2}}$	131.788 m	It.2_SSD< L THCC (Not Okay)
L THSC			$\boldsymbol{2 * SSD - \frac{200(\sqrt{h1}+\sqrt{h2})^2}{A}}$(m)	112.441 m	It.2_SSD> L THCC (Okay, is used for design)

Where:

Crest vertical curve

(FCC): First Crest Curve, (SSD): Stopping Sight Distance: , (A%), : Grade angle, (L FCC): Length of the First Crest Curve, (It.1): Iteration 1, (SCC): Second Crest Curve, (It.2): Iteration 2, (THCC): Third Crest Curve, (h1): driver eye height = 1.08 m, (h2): objective height = 0.60 m, (t): perception reaction time (1.5 seconds), (f): side friction = 0.3 m.

Sag vertical curve

(FSC): First Sag Curve, (SSD): Stopping Sight Distance: , (A%), : Grade angle, (L FSC): Length of the First Sag Curve, (It.1): Iteration 1, (SSC): Second Sag Curve, (It.2): Iteration 2, (THSC): Third Sag Curve, (h1): driver eye height = 1.08 m, (h2): objective height = 0.60 m, (β): 1 degree, (t): perception reaction time (1.5 seconds), side friction= 0.3 m.

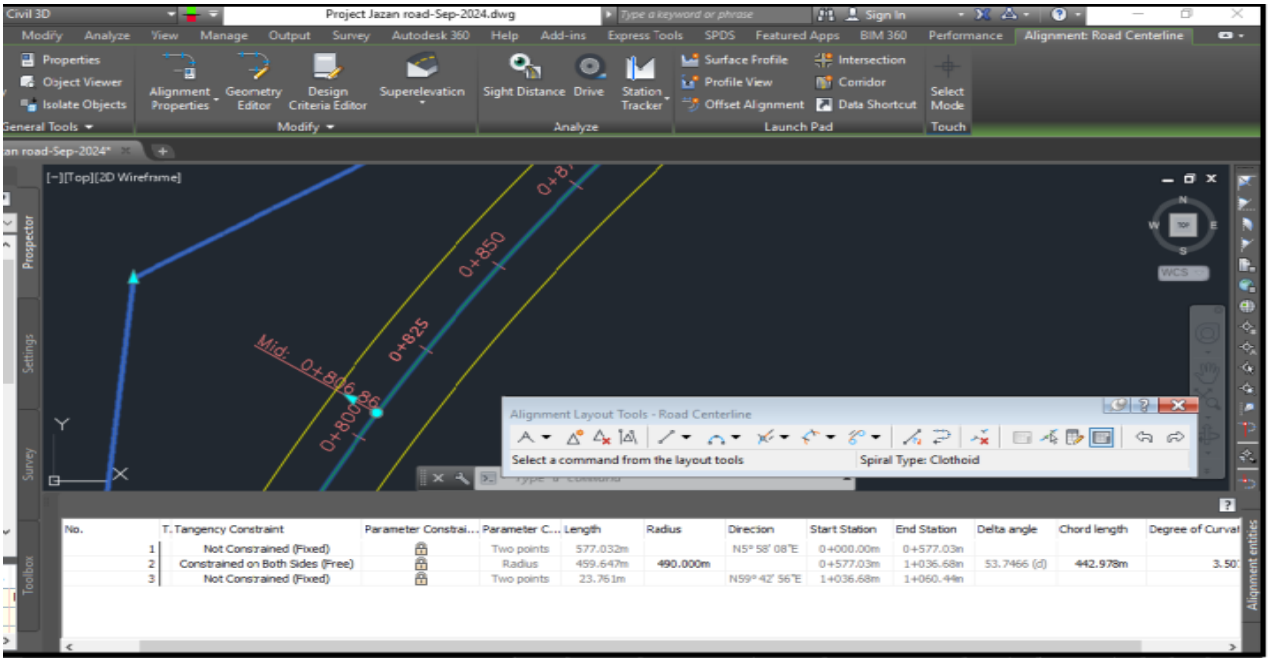

FIGURE 3.The alignment of the study road in AutoCAD Civil 3D.

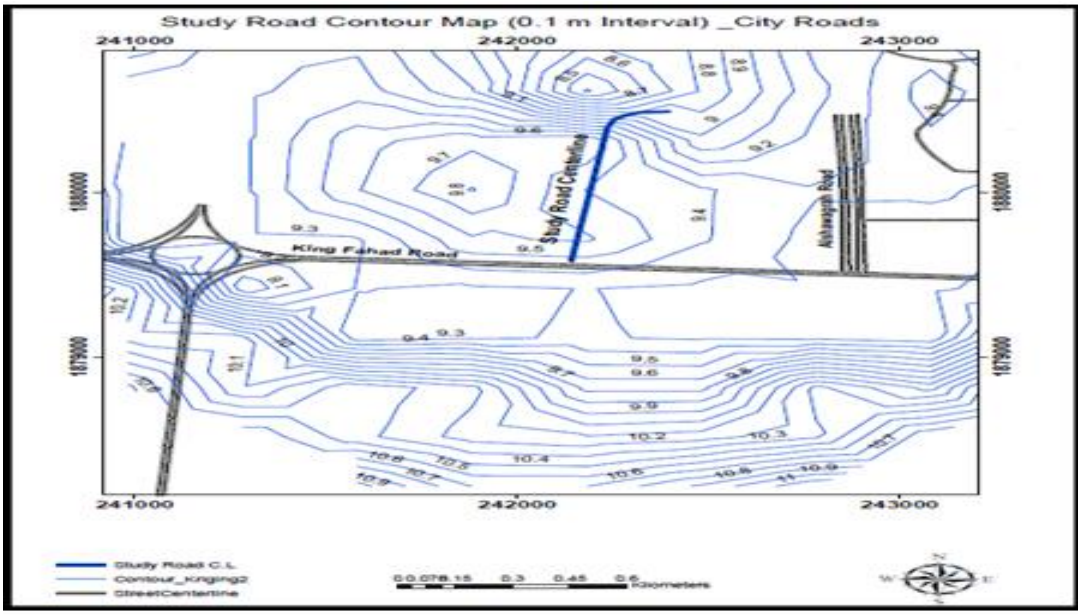

FIGURE4.Contour map of the study road's contour map (was created using ArcGIS 10.4).

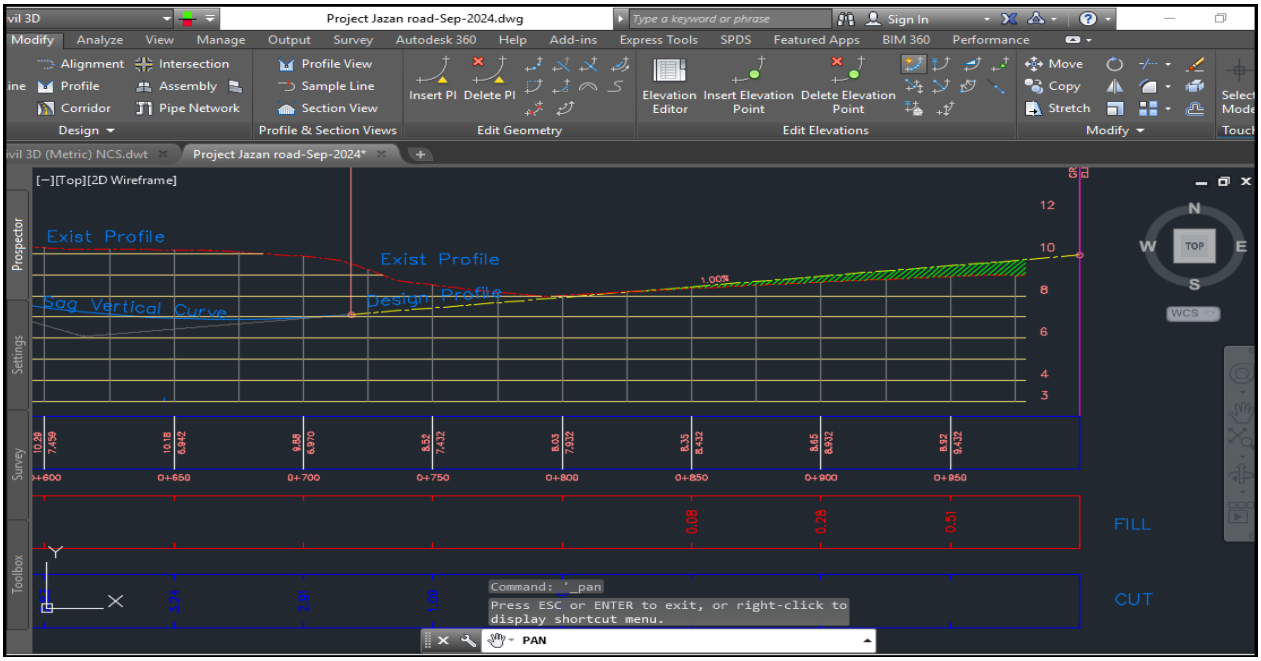

FIGURE5.Profile of natural ground level and design profile (from AutoCAD Civil 3D).

6. FLEXIBLE PAVEMENT DESIGN

The primary function of highway pavement, composed of layers of processed materials placed over a naturally existing soil sub-grade, is to distribute applied vehicle loads to the sub-grade. Flexible pavements and rigid pavements are the two types of pavement generally accepted for this purpose. This section provides an overview of pavement types, layers, and their functions, as well as pavement failures. Errors in pavement design can lead to premature failure. The designer has complete control over the paving materials and layer thickness [42–46].

a) Road Layer Thickness Calculation

The equations used for calculating road layer thickness are:

$$SN1 = a_1 D_1 \text{ inch} \quad (19)$$

$$SN2 = a_1 D_1 + a_2 D_2 m_2 \quad (20)$$

$$SN3 = a_1 D_1 + a_2 D_2 m_2 + a_3 D_3 m_3 \quad (21)$$

Where:

SN1: Asphalt Course, SN2: Base Course, SN3: Sub-Base Course, D1: layer thickness (in.), a_i: i^{th} Structural layer coefficient, SN: structural Number.

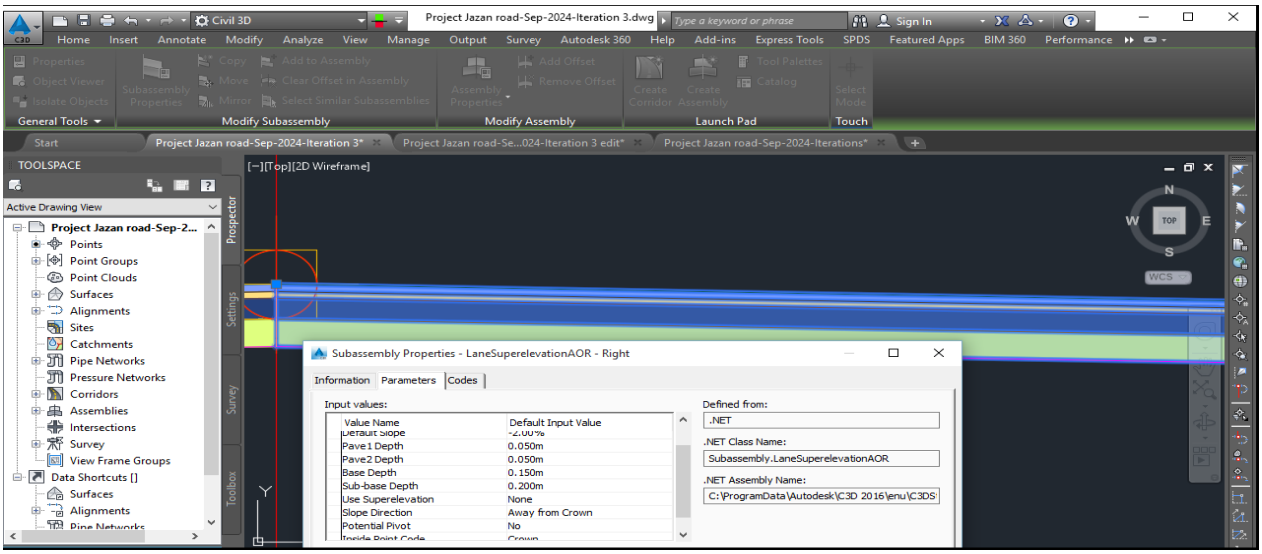

FIGURE 6.Construction assembly and design parameters inputted (derived from AutoCAD Civil 3D).

b) Calculation the traffic analysis

This study's primary traffic analysis focuses on lane computation and autonomous lane monitoring systems that maintain drivers' lanes. Roadways are divided into several cells by cell models, such as lane-changing and car-following models, with every vehicle positioned in one of these cells. The following equations are employed in this context:

Future ADT = ADT $(1+\text{Growth Rate})^n$ (22)

DDHV = ADT (or ADT) * K * D (23)

No. of Lane = DDHV/Capacity (24)

Where:

ADT: Average Daily Traffic, DDHV: Directional Design-Hour Volume, K: Peak-hour traffic, D: Peak direction generally carries.

c) Equivalent Single Axle Load (ESAL)

The conversion is frequently used to standardize a single axle load equivalent to 18,000 lb (80 kN). The AASHTO Guide to Pavement Structure (1993) states that the equivalent surface area loss (ESAL) is the ratio of the damage caused by an axle passing over pavement to the damage caused by a standard axle, typically an 80 kN single axle load passing over the same pavement. Equation 25 presents this [47,48]. The damage factor caused by Equivalent Single Axle Load (ESAL) is calculated using equation 25.

$$DF = k\left(\frac{Qi}{Qs}\right)^4 \quad (25)$$

Where:

DF: Damage Factor, Qi: Actual Load, Qs: Standard Single Axle Load 80 kN, k: 1 for single, 0.086 for tandem, and 0.053 for triaxial load.

Equivalent Single Axle Load (ESAL) is derived using equations (26) and (27).

orESAL = W_{80KN} *DD* LD *TF*365*G

ADT*TKS *DD* LD *TF*365*G(26)

$$G = \frac{(1+g)^n}{g} \quad (27)$$

Where:

W_{80KN}: Total ESAL of vehicles (ESAL) ADT: Average daily traffic, TKS: Percentage of truck traffic, DD: Directional distribution of truck traffic, LD: Lane distribution of truck traffic, TF: Average truck factor; g: Annual traffic growth factor equal 4%,

W80 KN :Total ESAL of traffic.

7. Road Cost Estimation

Since all layers will be constructed on the same formation level, the earthwork cost is calculated prior to design and is considered a constant for all three design approaches. The construction cost of each layer for each design method will depend on the projected thickness.

8. Design and Structure of Jazan Roads Geo-database Using GIS

As previously stated, the database has a direct impact on and is a major factor in a GIS's cost. A database serves as the foundation for a GIS, enabling users to develop applications, perform programming, evaluate and extract secondary data, assist with road maintenance procedures, and ultimately support decision-making [49,50]. The basis for the data placed in the database is determined by the database design. Depending on the type of data, the inventory data in this design is divided into three groups. The data in this design is derived directly from the field telemetry tool and includes tabular, spatial, and other types of data. **Table 6**and **Figure 7** show the geodatabase of the Jazan City roads network (uploaded from ArcGIS 10.4).Designing a database for roads and Intelligent Transportation Systems (ITS) using ArcGIS 10.4 requires a comprehensive approach. Here's a unique step-by-step guide to effectively structure and implement the database:

a. Establish project goals (traffic patterns, incident reports);
b. Collect stakeholder input, including urban planners, transportation officials, and emergency services, to gather insights on their data needs;
c. Plan the database framework and define tables for additional data, such as traffic statistics and maintenance logs (e.g., linking traffic volumes to specific road segments);
d. Incorporate spatial data and collect open-source spatial data through surveys, remote sensing, or existing GIS datasets. Furthermore, import the spatial datasets into the geodatabase using ArcGIS 10.4;
e. Document metadata, ensuring comprehensive metadata management tools for consistency;
f. Test database performance and Solicit user feedback during testing to identify areas for improvement; and
g. Make the database available to users and stakeholders, ensuring they are informed about its features.

TABLE 6
SAMPLE OF MANUAL INPUT OF DESCRIPTIVE DATA OF JAZAN CITY ROAD NETWORK

Object	Status	Street Name	width	No. of Lanes	Shape Length (m)
5999	Exist	Tarig bin Ziyad	13	3	267.436
6000	Exist	Tarig bin Ziyad	13	3	71.009
6001	Exist	Tarig bin Ziyad	11	2	47.385
6002	Exist	Prince Abdulaziz bin Nasser	13	2	245.107
6003	Exist	Prince Abdulaziz bin Nasser	13	2	244.137
6004	Exist	Prince Abdulaziz bin Nasser	13	2	184.578
6005	Exist	Prince Abdulaziz bin Nasser	13	2	174.411
6006	Exist	Prince Abdulaziz bin Nasser	13	2	520.963
6007	Exist	Prince Abdulaziz bin Nasser	13	2	132.817
6008	Exist	Prince Abdulaziz bin Nasser	11.5	2	172.69
6009	Exist	Prince Abdulaziz bin Nasser	11.5	2	263.193
6010	Exist	Prince Abdulaziz bin Nasser	13	2	236.746
6011	Exist	Prince Abdulaziz bin Nasser	13	2	715.910

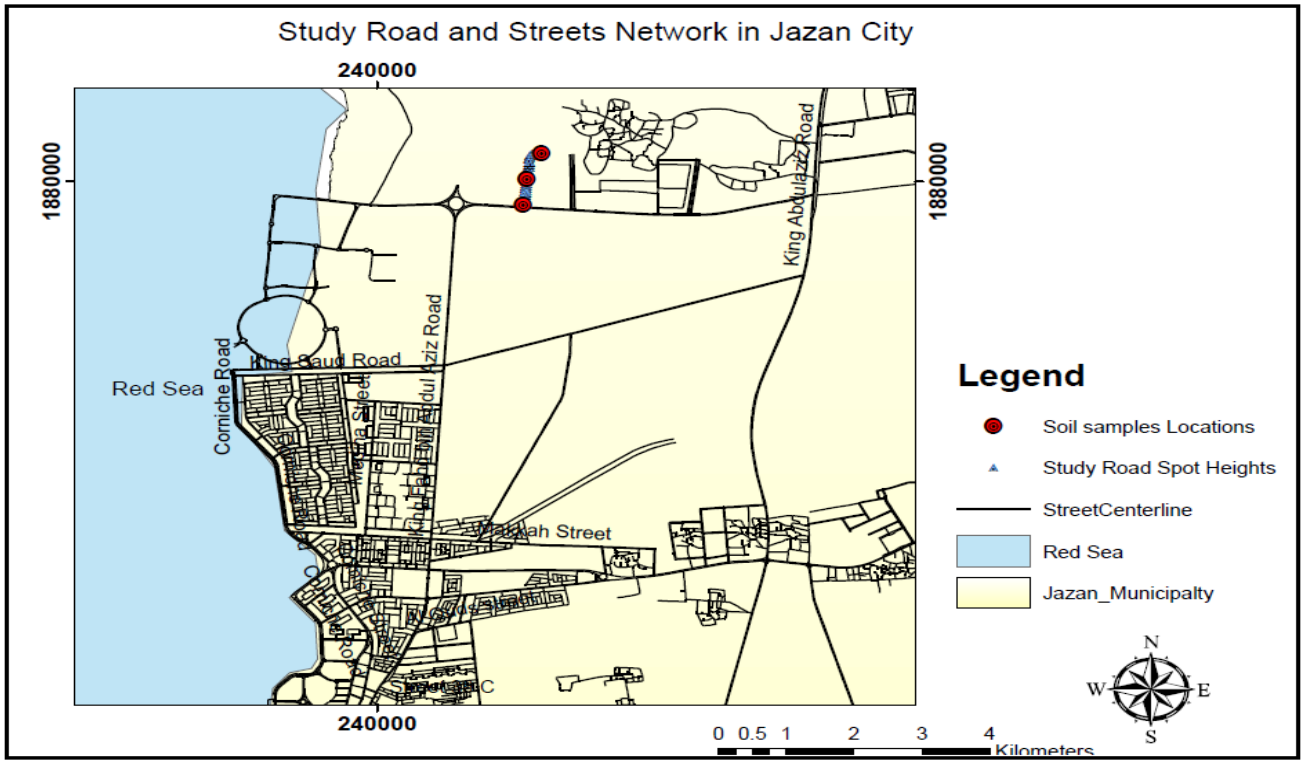

FIGURE 7. Jazan City Street network (derived from ArcGIS 10.4)

III. RESULTS

The findings of this study relate to the calculation parameters and road design in AutoCAD Civil 3D. These results include the following:

A. OPTIMUM ROUTE SELECTION FOR CONSTRUCTION

Using AutoCAD Civil 3D, the final result, as shown in **Table 7** and **Figure 8,** indicates that the third recommended road is the optimal path, with a success percentage of 1.044%. The same outcomes were achieved when applying the mini-max method to optimize the volumes according to the three iterations of design parameters calculated in **Tables4** and **5**.

TABLE 7.
THE RESULTS OF THREE SUGGESTED ROUTES OF THE STUDY ROAD

Iteration	Cumulative Cut Volume (m^3)(m^3)(m^3)(m^3)(m^3)	Cumulative Fill Volume (m^3)	Percentage of Cut Volume (%)	Percentage of Fill Volume (%)
1	**21539.32**	**422469.04**	**26.06**	**96.02**
2	**26348.78**	**12926.44**	**31.88**	**2.93%**
3	**34772.18**	**4595.200**	**42.06**	**1.044%**
Total Sum.	**82660.28**	**439990.7**	**100%**	**100%**

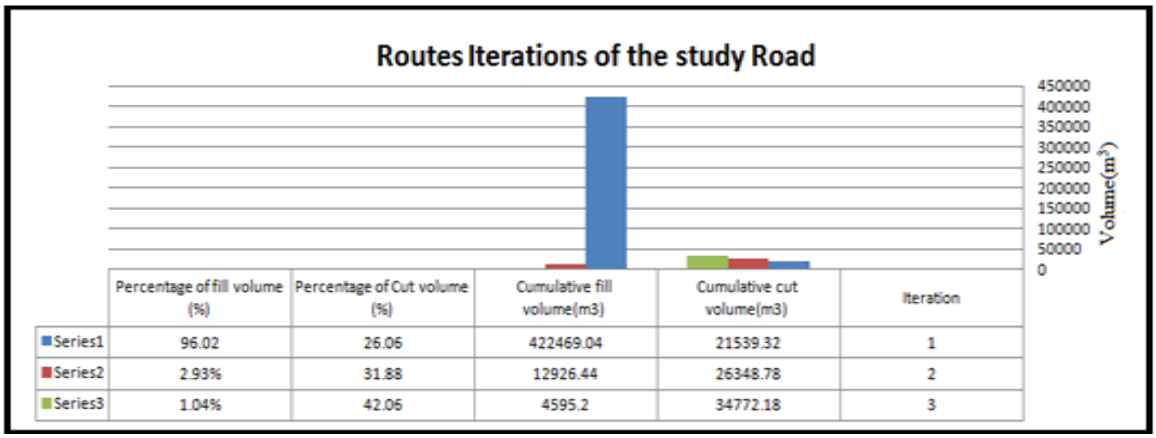

FIGURE 8. Iterations of route design using AutoCAD Civil 3D.

B. RESULTS OF SOIL TESTS

1) SIEVE ANALYSIS TEST

Equations (1-4) are used to calculate the values the percent of passing and retained. **Table 8 and Figure 9** show the results of the sieve analysis.

2) COMPACTION TEST

The compaction test demonstrated relationship between the dry density and moisture content, presenting a maximum dry density of 2.303 gm/cm³ at a moisture content of 5.1%. Equations (5-9) are used to calculate the parameters of the compaction test**. Figure 10**illustrates the results of the compaction test.

TABLE 8.
SIEVE ANALYSIS TEST

Sieve Size (mm)	50	25	11.2	4	2	0.6	0.25	0.15	0.063	Pan
Percent Finer (%)	100	69.3	52.8	46.2	40.1	32.1	29.7	16.7	3.97	0

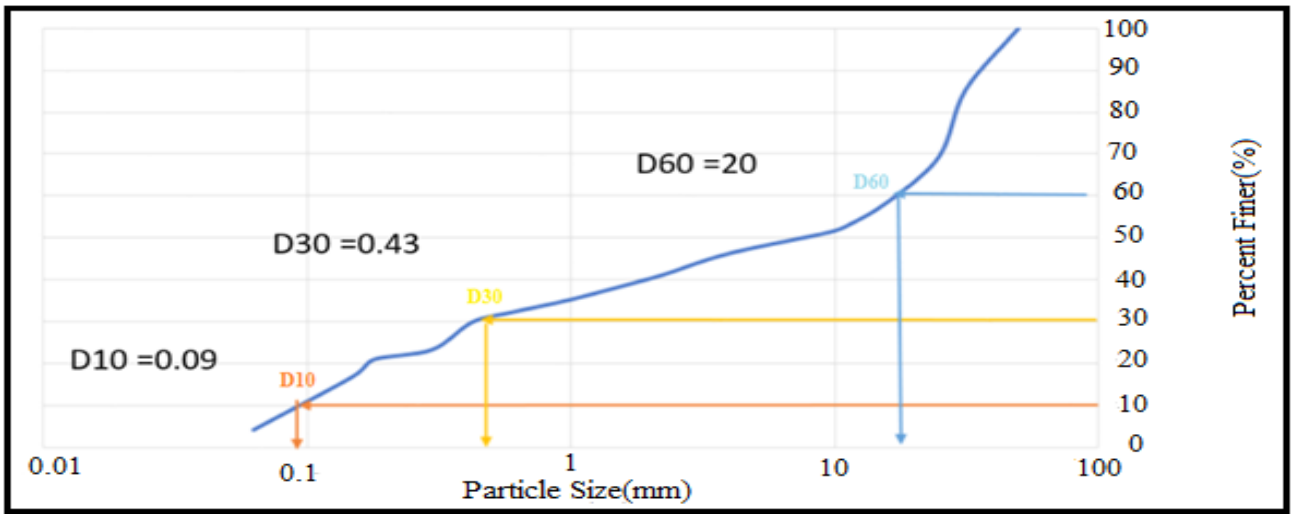

FIGURE 9. Graph of sieve analysis test of the soil sample from the road.

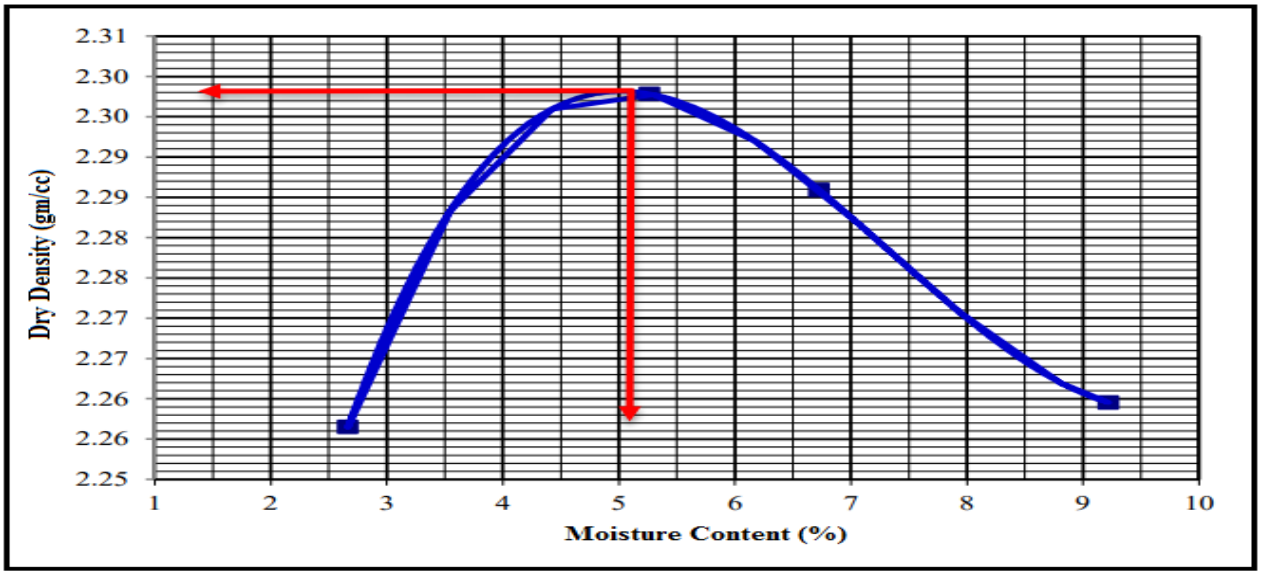

FIGURE 10. Compaction curve of dry density(gm/cc)vs. Moisture content(%)

3) California Bearing Ratio (CBR)

Using equations (10-12) to determine the parameters of the California Bearing Ratio (CBR).**Table 9 and Figure 11**show the graph of CBR of the road soil sample to determine the optimum moisture content.

TABLE 9.
CBR TEST RESULTS OF THE UN SOAKED EMBANKMENT

Compaction Effort	CBR (%)	
(blows)	2.54 mm	5.08
10	19.9	27.3
30	47.3	50.5
65	97.7	100.9

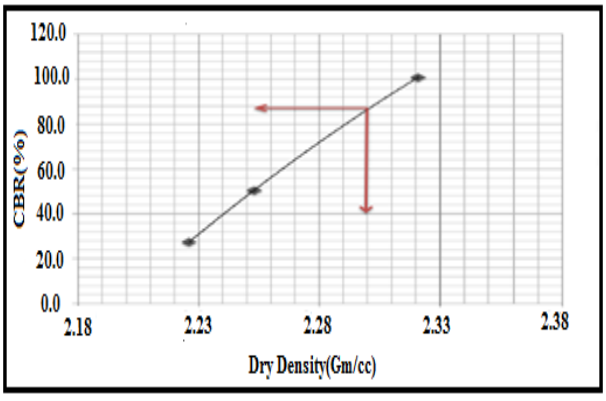

FIGURE 11. The dry density vs. the soaked CBR (%)

C. FLEXIBLE PAVEMENT DESIGN

This paper presents the main flexible pavement designs carried out, including the following**:**

1) THICKNESS OF THE ROAD LAYERS

Using equations (19-21), the thickness of the road layers was calculated according to the AASHTO pavement design of 1993 and presented in **Table 10. These values** are also used in AutoCAD Civil 3D as parameters in road design, as shown in **Figure 6**.

TABLE 10.
ROAD - AASHTO PAVEMENT DESIGN (1993) AND CALCULATED THICKNESS OF ROAD LAYERS

Data			Serial No.	Design Items				
Asphalt Layer E = 350,000 (psi)			SN	Structural Coefficient	Drainage Coefficient	Calculated Thickness (in)	Required Thickness (cm)	Design Value (cm)
			1.9	0.39	1	4.87	12.4	10
	CBR %	E (psi) from chart						
Granular Base	87	28000	2.2	0.135	1.2	1.54 use 6	15.25	15
Granular Sub Base	87	19000	3.5	0.134		7.56	19.2	20
Sub-grade	4	5000	-	-	-		-	-

2) TRAFFIC ANALYSIS

Table 11 shows the parameter data used for calculating the number of lanes in the study road in Jazan. Using formulas (22-24), the results are presented in **Table 12.** Two lanes were calculated for the study road; **Figure 13**illustrates the lanes and vehicle locations of vehicle passing.

TABLE 11.
PARAMETERS DESIGN NO. OF LANE

Design Parameter Name	The Value
Design Period	20 years
Growth rate	4%
Design Capacity of lane (pc/lane)	1300
Peak-Hour Traffic (K)	0.1
Peak Direction Generally Carries (D)	1
ADT (vehicle/day)	6468
Future ADT (pc/lane)	14172

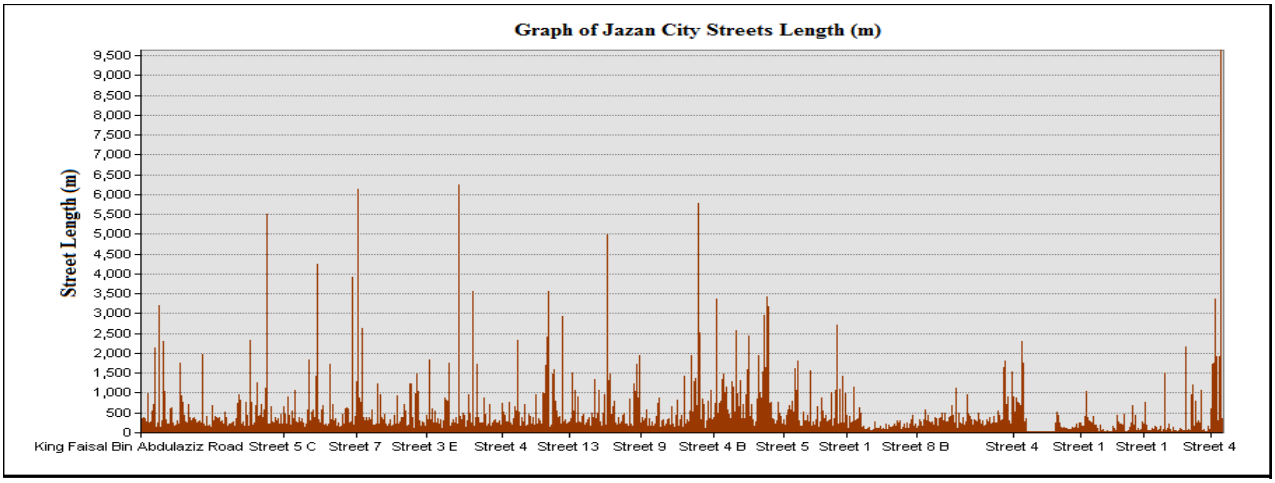

FIGURE 12.Jazan City streets graph according to length in meters

TABLE 12.
CALCULATION OF NUMBER OF LANES

Parameters	Results
ADT	$\boldsymbol{ADT} = \mathbf{646}8\ (1+0.04)^{20} = 14172$ pc/lane
DDHV	DDHV = 14172 * 0.1 * 1 =1417veh/hr
Number of Lanes	No. of lanes = 1417/1300 = 1.09 ≈ 2 lanes/direction.

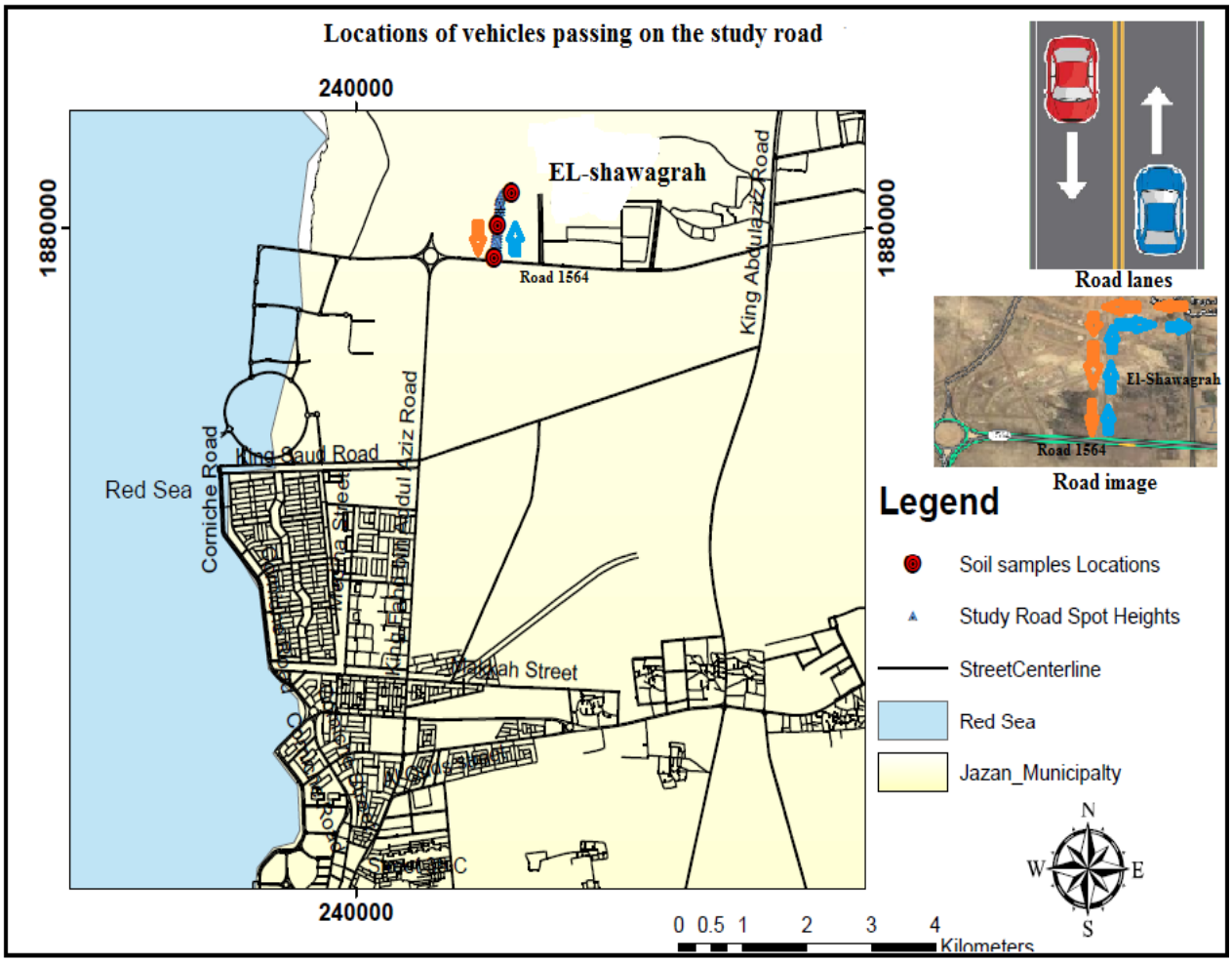

FIGURE 13. Map of lanes and locations of vehicles passing on the road (derived from ArcGIS 10.4)

3) EQUIVALENT SINGLE AXLE LOAD (ESAL)

Using equations (36-38), the traffic count was made for a two-way, two-lane highway section, with a directional distribution (DD) equal to 0.80 (80%), lane distribution (LD) equal to 0.70 (70%), and traffic factor (TF) equal to 20.2. The value of ESAL for 20 years equals 9523411.627, assuming ESAL of each axle is equal to 850.53.

$$G = \frac{(1+0.04)^{20}}{0.04} = 54.78$$

The Total ESAL = 850.53 * 0.80 *0.70*365*54.78=9523411.627

D. ANALYSIS OF GEODATABASE IN JAZAN ROAD NETWOR USING ARCGIS 10.4

This study utilized GIS tools to establish a geodatabase for the Jazan roads network to analyze traffic trends, identify congested locations, and assess road usage patterns. Furthermore, analytical models were created based on usage data and environmental factors to evaluate the current state of roads and project future maintenance needs. The digital model of the road network in Jazan, developed using the capabilities of ArcGIS 10.4, facilitated easy queries.

Table 13 provides specific descriptive statistics about the characteristics of the Jazan City roadway. The geodatabase model of the Jazan road network is designed as a flexible model capable of editing, storing, plotting maps, and analyzing. Additionally, analysis can be conducted to choose the road network graph based on the length of the roads (see **Figure 12**).

TABLE 13.
DESCRIPTIVE STATISTICS OF THE ROADS LENGTHS AND WIDTHS DATA IN THE STUDY AREA.

Statistic Expression	Road Length (km)	Road Width (m)
Minimum	0.05	3.500
Maximum	9.643018	133.50
Mean:	0.132476	11.244
Standard Deviation:	0.280151	6.944

E. RESULT OF COST ANALYSIS

In this study, the Jazan Comprehensive Road Spatial Data Framework (CRSDF) indicates that the construction costs of a road can vary significantly based on several factors, including site conditions, geography, materials used, and specific design specifications. However, in a developed nation, constructing a single kilometer of a standard paved road typically costs between one million and three million Saudi Riyals on average [51,52].**Table 14**shows the materials of the road, and the cost estimation is applied to the optimal route.

TABLE 14.
MATERIALS VOLUME CALCULATIONS USING AUTOCAD CIVIL 3D.

Iteration	Cumulative Cut Volume (m^3)	Cumulative Fill Volume (m^3)	Sub-Volume(m^3) base Layer Volume (m^3)	Base Layer Volume(m^3)	Pavement Layer Volume(m^3)
1	21539.32	422469.04			
2	26348.78	12926.44	5280.47	1977.38	960.11
3	34772.18	4595.20			

Table 15 and Figure **14** show that the third iteration is selected as the optimal path for this road because this route represents the lowest fill volume. Furthermore, the total cost of materials for iteration 3 (cut, fill, sub-base, base, and asphalt) is calculated according to the volumes and prices of the cubic meter of the volume items in Saudi Riyals.
The total basic cost of materials ($T.M_{cost}$) = 34772.18 * 1.3 * 15 + 4595.20 * 1.3 * 20 + 5280.47 * 1.3 * 30 + 1977.38 * 1.3 * 30 + 960.11 * 1.25 * 55 =**913003.793** Saudi Riyals [53].

TABLE 15. THE TOTAL COST OF MATERIALS FOR ROAD DESIGN AND CONSTRUCTION (ITERATION 3)

Iteration	**Cumulative Cut Volume (m^3)**	**Cumulative Fill Volume (m^3)**	**Sub-base Layer**	**Base Layer**	**Pavement layer**
			Volume (m^3)	**Volume (m^3)**	**Volume (m^3)**
3	**34772.18**	**4595.2**	**5280.47**	**1977.38**	**960.11**
Final Cost (Saudi Riyals)	**521582.7**	**119475.2**	**205938.33**	**77117.82**	**66007.56**

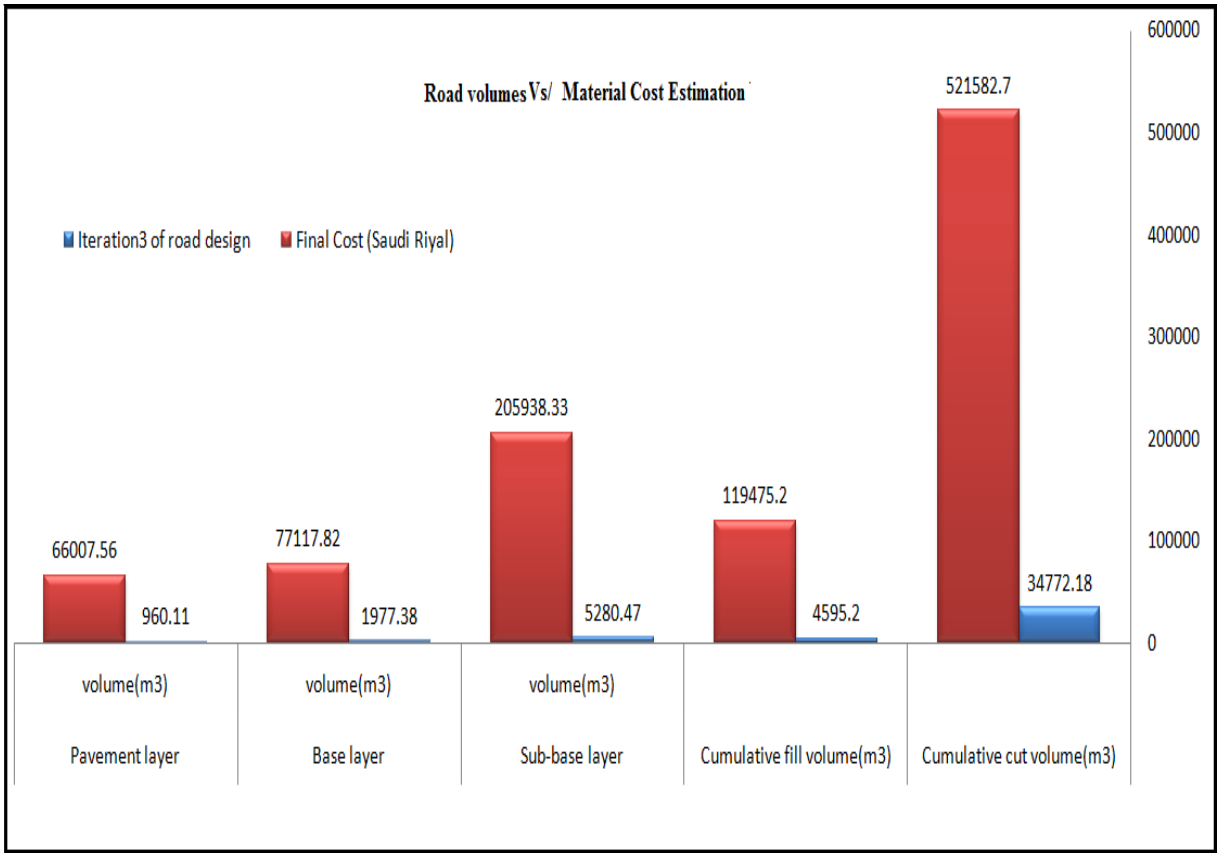

FIGURE 14. The total cost of the optimal route design per layer

This cost represents the main construction cost item for one kilometer; however, the road investigated is not one kilometer, so the projected cost for this paper is determined in **Table 16.** Material volumes include cut, fill, sub-base, base, and pavement. The price of a cubic meter, along with transportation of cut and fill with well-graded soil and asphalt, is 15, 20, 30,, 30 and 55 Saudi Riyals, respectively, according the roads contract companies in Jazan. Furthermore, the ratio of the compacted factor of well-graded soil and asphalt equals 1.3 and 1.25, respectively. For compacted layers, the computed volume increases by this ratio before determining the cost.

TABLE 16.
SUMMARY OF COST ESTIMATION OF THE STUDY ROAD

Item	Description	Actual Cost (SAR)	Costing Factor	Cost (SAR)
1	Total Materials Cost	913003.793	1.1	1,004304.17
2	Equipment Cost	186,714	1.2	224,057
3	Manpower Cost	3,650	1.1	4,015
4	Materials Testing Cost	1,330	1	1,330
	Total	1,104,697.79		,1233706.17

IV. DISCUSSIONS

This study presents a comprehensive framework for understanding the unique geographical and geological context of Jazan, established through the integration of advanced software, geographical data, and soil analysis.

The paper covers four parts and optimizes the volumes in accordance with the three design parameter iterations determined in Tables 4 and 5,which produced consistent results. Table 7 and Figure 8 demonstrate that the third suggested road is the best option.

The AASHTO classification of the Embankment Road in Jazan City is (A-1-a), with D60 = 20, D30 = 0.43, and D10 = 0.09. The soil used in this study is characterized as gravelly sand. A comparison with the Unified Classification System (USCS) indicates that the soil is coarse, retaining more than 50% (99.89 > 50) when sieved through a 0.075 mm screen. The gravelly soil can be found on road embankments and roadways, retaining over 50% (59.78 > 50) after passing through a 4.75 mm sieve.

In Figure 10 displays the results of the compaction test, illustrating the relationship between the dry density and moisture content. The highest dry density recorded was 2.303 gm/cm³ at a moisture level of 5.1%.

In **Figure 11 presents** the graph of the California Bearing Ratio (CBR) for the road soil sample, aiding in the identification of the optimal moisture level. At 100% compaction, the soaked CBR for the sub-base and base is 87%, while the sub grade equals 4%. The thickness of the road layers was estimated using equations (5–9) in accordance with the AASHTO pavement design guidelines from 1993. The results are summarized in Table 8 and are also utilized as parameters in AutoCAD Civil 3D for road design, as

This study estimates a Total Equivalent Single Axle Load (ESAL) of approximately **9,523,411.63, representing** the cumulative effect of traffic loads on the pavement over the specified duration. The significance of the Calculation

- **Road Design**: These calculations provide engineers with essential data for designing pavements capable of withstanding projected traffic loads.
- **Maintenance Planning**: Understanding Total ESAL is crucial for scheduling maintenance and repairs to ensure road safety and longevity.
- **Traffic Analysis**: The components of the equation offer a nuanced view of traffic patterns, which is vital for accurate assessments.

A geo-database model of Jazan's road network was constructed using ArcGIS 10.4. Table 7 and Figure 8 provide detailed descriptive information regarding the characteristics of the city's roads [54]. Supporting the Jazan City Road Geodatabase, **Figure 12**presents the statistical analysis of the road network using ArcGIS 10.4. Furthermore, the Kingdom of Saudi Arabia is advancing rapidly in alignment with Vision 2030, driven by the expansion of its road network in Jazan City.

Figure 13illustrates the map of lanes and locations on the road.

Volume values and construction material prices are utilized to determine the overall cost of optimal route design per layer; however, these figures vary based on topography, road centerline, and design specifications. The overall cost of one kilometer of the study road is summarized in **Table 15** and **Figure 14,** estimated at 1,233,706.17 SR, which includes the cost of materials, equipment, labor, and material testing.

V. CONCLUSIONS

The current study concludes that a Comprehensive Spatial Data Framework (CSDF) for road spatial data is essential. A spatial and descriptive data framework that effectively utilizes open-source data, direct survey measurements, and GIS tools for road construction and maintenance can be used to update Jazan City's CSDF. Ultimately, this CSDF will benefit the community by optimizing maintenance efforts, enhancing road safety, monitoring road conditions, and improving urban infrastructure planning. The study demonstrated the feasibility of compiling a comprehensive assessment of the roads in Jazan City by integrating soil test findings and design using Civil 3D and Geographic Information Systems (GIS). Additionally, similar objectives were achieved in studies conducted by [55-57]. Furthermore, the numerous models created for highways will support future infrastructure research.

The challenges faced in this study were addressed, leading to the following conclusions:

a. A comprehensive Spatial Data Framework (CSDF) to support road design and a geo-database model for routine (periodic) maintenance using GIS and open-source data.
b. The CSDF was utilized to emphasize traffic management optimization, improve maintenance efficiency, and enhance road safety.
c. Collaboration with municipal authorities, transportation planners, civil engineers, and local communities to gather data; was identified;
d. By combining open-source software such as AutoCAD Civil 3D,QGIS, a geodatabase of the road network, site visits, GPS data, traffic data, soil data, and experienced staff, the CSDF will be developed and updated.
e. Volume calculation methods were compared to minimize the costs of road construction and maintenance in Jazan City.
f. A holistic approach to the Comprehensive Spatial Data Framework (CSDF) was established by integrating advanced software, geographical data, and soil analysis, providing a thorough framework

for understanding the distinct geographical and geological context of Jazan is provided,

g. Optimized Road Design: With the aid of accurate modeling facilitated by Civil 3D, the road design was improved, enhancing road longevity and safety.
h. The cost of the study road in Jazan City was calculated and estimated at 1,233,706.17 SAR per kilometer, accounting for the total costs of materials, equipment, labor, and material testing.

VI. SUGGESTIONS FOR FUTURE WORK

Figure 15 outlines the suggestion of Intelligent Transportation Systems (ITS). This system comprises eight components: a control center, a monitor screen, traffic information, data message transmission, data storage and analysis devices, traffic dispatch, and traffic signal adjustments. The author recommends establishing the ITS to support the Comprehensive Spatial Data Framework (CSDF) in the Jazan road network to enhance traffic management, safety, and transportation efficiency. Moreover, numerous benefits can be gained from ITS:

a. Dynamic Lane Management
b. Connected Vehicle Technologies
c. Smart Traffic Signs
d. Comprehensive Incident Detection Systems
e. Mobile Ticketing and Fare Collection
f. Predictive Traffic Modeling
g. Bicycle and Pedestrian Safety Systems
h. Freight Traffic Management Solutions
i. Enhanced Public Transport Real-Time Tracking
j. Integrated Emergency Management Systems

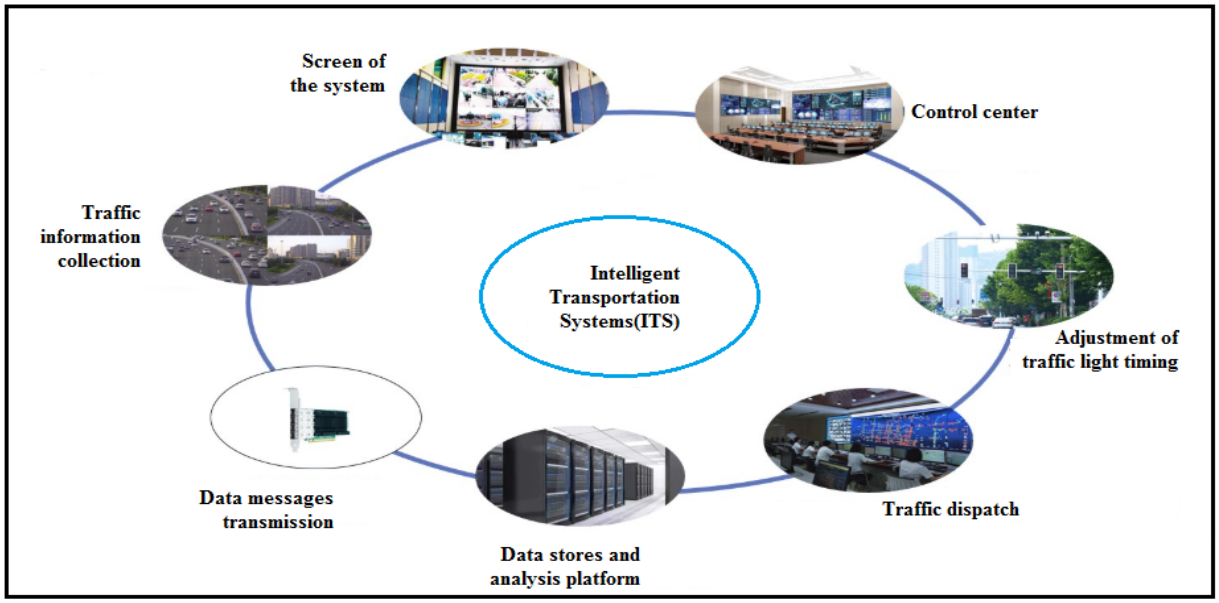

FIGURE 15. Components of Intelligent Transportation Systems (ITS) in Jazan City.

REFERENCES

[1] L. Zhao, Q. Wang, B.-G. Hwang, How to Promote Urban Intelligent Transportation: A Fuzzy Cognitive Map Study, Front. Neurosci. 16 (2022). https://doi.org/10.3389/fnins.2022.919914.
[2] H. Lv, G. Wu, J. Song, C. Mo, G. Yao, X. He, Data Management Framework for Highways: An Unreal Engine-Based Digital Sandbox Platform, Buildings 14 (2024). https://doi.org/10.3390/buildings14071961.
[3] W.Y. Yan, S. Morsy, A. Shaker, M. Tulloch, Automatic extraction of highway light poles and towers from mobile LiDAR data, Opt. Laser Technol. 77 (2016) 162–168. https://doi.org/10.1016/j.optlastec.2015.09.017.
[4] L. Liu, M. Zhang, T. Xu, A conceptual framework and implementation tool for land use planning for corridor transit-oriented development, Cities 107 (2020) 102939. https://doi.org/10.1016/j.cities.2020.102939.
[5] France-Mensah, J., O'Brien, W.J., Khwaja, N. et al. GIS-based visualization of integrated highway maintenance and construction planning: a case study of Fort Worth, Texas. Vis. in Eng. 5, 7 (2017). https://doi.org/10.1186/s40327-017-0046-1.
[6] Mohamed, A.G., Alqahtani, F.K., Ismail, E.R. et al. Synergizing GIS and genetic algorithms to enhance road management and fund allocation with

a comprehensive case study approach. Sci Rep 15, 4634 (2025). https://doi.org/10.1038/s41598-025-88760-4.

[7] Martinez, A., Smith, J., & Taylor, R. "Leveraging Open-Source GIS Tools for Effective Asset Management in Road Networks." Journal of Transportation Engineering, 145(3), 04019004.(2019). doi:10.1061/(ASCE)TE.1943-5436.0001094.

[8] Chen, L., Zhang, Y., & Huang, X. "Integrating GIS for Sustainable Road Design: Assessing Environmental Impacts and Planning Mitigation Strategies." Sustainable Cities and Society, 75, 103420. (2022).doi:10.1016/j.scs.2021.103420.

[9] K. Vasu, P. Murahari Krishna, A.V. Kumar, G. Veeraswamy, Upgrading Pavements for Nh-18 (New Nh-40), 18 (2018). www.ijtrs.com.

[10] M.A. Abdelgiom, M. Mubaraki, Evaluating Settlement on King Faisal Road Using GIS Analysis Techniques, in: Sustain. Civ. Infrastructures, (2019). pp. 96–109. https://doi.org/10.1007/978-3-319-96241-2_8.

[11] G. Valença, F. Moura, A. Morais de Sá, Main challenges and opportunities for dynamic road space allocation: From static to dynamic urban designs, J. Urban Mobil. 1 (2021). https://doi.org/10.1016/j.urbmob.2021.100008.

[12] O. Tengilimoglu, O. Carsten, Z. Wadud, Implications of automated vehicles for the physical road environment: A comprehensive review, Transp. Res. Part E Logist. Transp. Rev. 169 (2023) 102989. https://doi.org/10.1016/j.tre.2022.102989.

[13] T. Zhu, T. Ma, X. Huang, S. Wang, Evaluating the rutting resistance of asphalt mixtures using a simplified triaxial repeated load test, Constr. Build. Mater. 116 (2016) 72–78. https://doi.org/10.1016/j.conbuildmat.2016.04.102.

[14] S. Ullah, A. Qabur, A. Ullah, K. Aati, Mahmoud Abdelrahim Abdelgiom, Enhancing High-Temperature Performance of Flexible Pavement with Plastic-Modified Asphalt, (2024) 1–20.

[15] A.T.G.A.A.N.Z. Nasioula, Building a Geo-Database for Urban Road Network Environmental Quality, 3rd Int. Conf. Cartogr. GIS (2010).

[16] Network Analysis using GIS Techniques: A Case of Chandigarh City, Int. J. Sci. Res. 5 (2016) 409–411. https://doi.org/10.21275/v5i2.NOV161143.

[17] D. Das, A.K. Ojha, H. Kramsapi, P.P. Baruah, M.K. Dutta, Road network analysis of Guwahati city using GIS, SN Appl. Sci. 1 (2019) 1–11. https://doi.org/10.1007/s42452-019-0907-4.

[18]Zhao, J., & Zhang, Y. "Dynamic route optimization based on GIS and real-time traffic data." Journal of Transport Geography, (2019). 75, 184-195. doi:10.1016/j.jtrangeo.2018.12.006.

[19] Alhajyaseen, W., et al. "Smart transportation systems: Integrating GIS with IoT." *Transportation Research Part C: Emerging Technologies*, 124, 102946 (2021). doi:10.1016/j.trc.2021.102946.

[20] Vivek Gajanan Sukalkar, Kunal Pawar, Dr. P. L. Naktode, A Study and Design of Two Lane with Paved Shoulder in Green Field Corridor, By Using Civil 3D, Int. J. Sci. Res. Sci. Eng. Technol. 4099 (2022) 202–211. https://doi.org/10.32628/ijsrset229347.

[21] G. Del Serrone, G. Cantisani, P. Peluso, Speed data collection methods: a review, Transp. Res. Procedia 69 (2023) 512–519. https://doi.org/10.1016/j.trpro.2023.02.202.

[22] A.A. Obiri-Yeboah, M.S. Gbeckor-Kove, Y. Oliver-Commey, Overview and Recommendations for Road Traffic Data Collection Methods and Applications in Ghana, Int. J. Eng. Res. Appl. Www.Ijera.Com 11 (2021) 1–09. https://doi.org/10.9790/9622-1102010109.

[23] M.S. Tehrany, B. Pradhan, M.N. Jebur, Flood susceptibility analysis and its verification using a novel ensemble support vector machine and frequency ratio method, Stoch. Environ. Res. Risk Assess. 29 (2015) 1149–1165. https://doi.org/10.1007/s00477-015-1021-9.

[24] B.A. Mir, Manual of Geotechnical Laboratory Soil Testing, 2021. https://doi.org/10.1201/9781003200260.

[25] Manual of Geotechnical Laboratory Soil Testing (Laboratory-I&II) Dept. of Civil Engg. By, n.d.

[26] S.A. Khattak, A. Qadir, H. Daud, K. Shehzad, M. Yasir, M. Abubakar, Terrace Soil Suitability for Highway Construction: Case Study in Lesser Himalaya (CPEC Project E-35), North Pakistan, Int. J. Econ. Environ. Geol. 12 (2021) 54–59. https://doi.org/10.46660/ijeeg.vol12.iss3.2021.622.

[27] J. Kodikara, T. Islam, A. Sounthararajah, Review of soil compaction: History and recent developments, Transp. Geotech. 17 (2018) 24–34. https://doi.org/10.1016/j.trgeo.2018.09.006.

[28] G. Spagnoli, S. Shimobe, An overview of the compaction characteristics of soils through laboratory tests, Eng. Geol. 278 (2020) 105830. https://doi.org/10.1016/j.enggeo.2020.105830.

[29] T. Batey, Soil compaction and soil management - A review, Soil Use Manag. 25 (2009) 335–345. https://doi.org/10.1111/j.1475-2743.2009.00236.x.

[30] S.T. Ahmed, M.U. Kabir, C.Z. Bin Zahid, T. Tareque, S. Mirmotalebi, Improvement of subgrade California Bearing Ratio (CBR) using recycled concrete aggregate and fly ash, Hybrid Adv. 5

(2024) 100153. https://doi.org/10.1016/j.hybadv.2024.100153.
[31] A. Bardhan, C. Gokceoglu, A. Burman, P. Samui, P.G. Asteris, Efficient computational techniques for predicting the California Bearing Ratio of soil in soaked conditions, Eng. Geol. 291 (2021) 106239. https://doi.org/10.1016/j.enggeo.2021.106239.
[32] V.S. Landge, S. Gupta, S. Patni, P. Shahare, Relationship between field CBR and dynamic deflection modulus for BC soil, Int. J. Civ. Eng. Technol. 8 (2017) 546–553.
[33] M. Rizqi, A.I. Rifai, S.K. Bhakti, Design of Road Geometry with AutoCAD® Civil 3D: A Case Study of Jalan Kertawangunan–Kadugede, Kuningan-Indonesia, Citiz. J. Ilm. Multidisiplin Indones. 2 (2022) 879–887. https://doi.org/10.53866/jimi.v2i5.205.
[34] A.I. Rifai, E.J. Purviyanto, J. Prasetijo, The implementation of AutoCAD® Civil 3D for highway geometric redesign: a case of an Indonesian toll road, IOP Conf. Ser. Earth Environ. Sci. 1347 (2024) 012060. https://doi.org/10.1088/1755-1315/1347/1/012060.
[35] A. Megarestya, A.I. Rifai, M. Isradi, The Horizontal Curved Geometric Design with AutoCAD® Civil 3D on Jalan Muara Wahau, East Kalimantan, Indones. J. Multidiscip. Sci. 1 (2023) 237–250. https://doi.org/10.55324/ijoms.v1i1.386.
[36] A.I. Rifai, J. Prasetijo, M. Pasha, S. Handayani, The Implementation of AutoCAD® Civil 3D for Road Geometric Redesign in Educational Areas: A Case Study of Leumah Neundet Bandung, E3S Web Conf. 517 (2024). https://doi.org/10.1051/e3sconf/202451705003.
[37] H. Chakole, D. JWadhai, A. Info, A Review on the Comparison of Geometric Design Using Civil 3D Software and Manual Method, Int. J. Mod. Trends Sci. Technol. 8 (2022) 115–122. https://doi.org/10.46501/IJMTST0806017.
[38] J.N. Ivan, N.W. Garrick, G. Hanson, Designing Roads That Guide Drivers to Choose Safer Speeds, (2009) 115.
[39] E. Kurakina, S. Evtyukov, Results of Studying Road Construction Parameters' Condition, Archit. Eng. (2018) 29–37. https://doi.org/10.23968/2500-0055-2018-3-1-29-37.
[40] F.J. Camacho-Torregrosa, A.M. Pérez-Zuriaga, J.M. Campoy-Ungría, A. García-García, New geometric design consistency model based on operating speed profiles for road safety evaluation, Accid. Anal. Prev. 61 (2013) 33–42. https://doi.org/10.1016/j.aap.2012.10.001.
[41] C. Jurewicz, P. Aumann, C. Bradshaw, R. Beesley, A. Lim, Road geometry study for improved rural safety, 2015. https://doi.org/10.13140/RG.2.1.4144.3605.
[42] P. Pereira, J. Pais, Main flexible pavement and mix design methods in Europe and challenges for the development of a European method, J. Traffic Transp. Eng. (English Ed. 4 (2017) 316–346. https://doi.org/10.1016/j.jtte.2017.06.001.
[43] S. Sreenatha, M. Vasudeva, S. Madan, Comparative Study on Analysis and Design of Flexible and Rigid Pavements, Int. J. Innov. Technol. Res. (2016) 3797–3802. http://www.ijitr.com.
[44] A. Demir, J. Santos, S. Miller, R. Diele, G. Naarding, Multi-objective optimization of flexible pavement design from an environmental and economic perspective, J. Clean. Prod. 430 (2023) 139441. https://doi.org/10.1016/j.jclepro.2023.139441.
[45] U.C. Sahoo, K.S. Reddy, Effect of nonlinearity in granular layer on critical pavement responses of low volume roads, Int. J. Pavement Res. Technol. 3 (2010) 320–325.
[46] A. Parvini, M. Keymanesh, Analysis of Traffic Based on Drivers' Lane Change Separation Models to Calculate the Appropriate Position for Vehicle Movement on the Highway, in: Proc. 5th Int. Conf. Civ. Eng. Archit. Urban Plan. Elit., Acavent, 2018. https://doi.org/10.33422/5th-caue.2018.02.45.
[47] P.B. Shahi, B.B. Nepali, Impact of Overloaded Vehicles on Flexible Pavement: Case Study of Belhiya-Butwal Road in Nepal, IOSR J. Mech. Civ. Eng. e-ISSN 17 (2020) 49–61. https://doi.org/10.9790/1684-1705034961.
[48] J. Jihanny, B.S. Subagio, E.S. Hariyadi, The Analysis of overloaded trucks in Indonesia Based on weigh in motion data (east of Sumatera National Road Case Study), MATEC Web Conf. 147 (2018) 1–6. https://doi.org/10.1051/matecconf/201814702006.
[49] B. Istiyanto, Y.E.R.D. Unzilatirrizqi, M. De Rizka Dewantoro, R. Ahmad, Geographic Information System (GIS-T) Database Design for Transportation Safety System (Case Study: Spatial Database for road transportation system in Indonesia), IOP Conf. Ser. Earth Environ. Sci. 1117 (2022) 0–6. https://doi.org/10.1088/1755-1315/1117/1/012023.
[50] I. Mahamid, Early Cost Estimating for Road Construction Projects Using Multiple Regression Techniques, Australas. J. Constr. Econ. Build. 11 (2011) 87–101. https://doi.org/10.5130/ajceb.v11i4.2195.
[51] A.M. Alsugair, Cost Deviation Model of Construction Projects in Saudi Arabia Using PLS-SEM, Sustain. 14 (2022). https://doi.org/10.3390/su142416391.

[52] G. Specifications, Kingdom of Saudi Arabia Ministry of Communications General Specifications for Table of Contents, (1998).
[53] M. Barakchi, O. Torp, A.M. Belay, Cost Estimation Methods for Transport Infrastructure: A Systematic Literature Review, Procedia Eng. 196 (2017) 270–277. https://doi.org/10.1016/j.proeng.2017.07.199.
[54] N.H. Maerz, A.M. Youssef, B. Pradhan, A. Bulkhi, Remediation and Mitigation Strategies for Rock Fall Hazards Along the Highways of Fayfa Mountain, Jazan Region, Kingdom of Saudi Arabia, Arab. J. Geosci. 8 (2015) 2633–2651. https://doi.org/10.1007/s12517-014-1423-x.
[55] M.E. Nicoară, I. Haidu, Creation of the Roads Network as a Network Dataset within a Geodatabase, Geogr. Tech. (2011) 81–86.
[56] M.A. Abdelgiom, M. Mubaraki, Evaluating Settlement on King Faisal Road Using GIS Analysis Techniques, in: Sustain. Civ. Infrastructures, 2019: pp. 96–109. https://doi.org/10.1007/978-3-319-96241-2_8.
[57] Mahmoud Abdelrahim Abdelgiom, Ali Yahiya Almalki, and Gar Al-nabi Ibrahim Mohamed. Pavement Maintenance Management System of Jazan City Roads Using Geographic Information Systems, Journal of Jazan University for Applied Sciences, Supplement to Volume 11, Issue 1, 2019: pp. 160-177.